Tânia Isabel da Silva Carvalho

Mestre em Biotecnologia

Development of Ion Jelly thin films for electrochemical devices

Dissertação para obtenção do Grau de Doutor em Química Sustentável

Orientador: Prof. Doutora Susana Barreiros, Professora Associada com Agregação da Faculdade de Ciência e Tecnologia da Universidade Nova de Lisboa

Co-orientador: Prof. Doutora Madalena Dionísio, Professora Auxiliar da Faculdade de Ciência e Tecnologia da Universidade Nova de Lisboa

Co-orientador: Doutor Pedro Vidinha, Investigador Convidado do REQUIMTE, Faculdade de Ciência e Tecnologia da Universidade Nova de Lisboa

Júri:

Presidente: Prof. Doutora Maria Paula Pires dos Santos Diogo

Arguentes: Prof. Doutor Joaquim José de Azevedo Moura Ramos

Doutor Pedro Miguel Pimenta Góis

Vogais: Prof. Doutora Maria Gabriela Machado de Almeida

FACULDADE DE CIÊNCIAS E TECNOLOGIA
UNIVERSIDADE NOVA DE LISBOA

Julho 2013

Universidade Nova de Lisboa

Tânia Isabel da Silva Carvalho
Mestre em Biotecnologia

Development of Ion Jelly thin films for electrochemical devices

Orientador: Prof. Doutora Susana Barreiros, Professora Associada com Agregação da Faculdade de Ciência e Tecnologia da Universidade Nova de Lisboa

Co-orientador: Prof. Doutora Madalena Dionísio, Professora Auxiliar da Faculdade de Ciência e Tecnologia da Universidade Nova de Lisboa

Co-orientador: Doutor Pedro Vidinha, Investigador Convidado do REQUIMTE, Faculdade de Ciência e Tecnologia da Universidade Nova de Lisboa

Júri:

Presidente: Prof. Doutora Maria Paula Pires dos Santos Diogo

Arguentes: Prof. Doutor Joaquim José de Azevedo Moura Ramos

Doutor Pedro Miguel Pimenta Góis

Vogais: Prof. Doutora Maria Gabriela Machado de Almeida

FACULDADE DE CIÊNCIAS E TECNOLOGIA
UNIVERSIDADE NOVA DE LISBOA

Julho 2013

À memória do meu pai,

à minha mãe,

à minha mana,

ao António.

"O homem bom tira coisas boas do bom tesouro que está em seu coração, e o homem mau tira coisas más do mal que está em seu coração, porque a sua boca fala do que está cheio o coração."

Lucas 6:45

DEVELOPMENT OF ION JELLY THIN FILMS FOR ELECTROCHEMICAL DEVICES

ACKNOWLEGEMENTS

À minha querida Vera Augusto que me calculou as difusões de todos os IJs possíveis e imaginários, mais os ILs…..obrigada pelo teu esforço e paciência.

Ao Ângelo Rocha e ao Nuno Lourenço pela síntese dos líquidos iónicos! Sem eles esta tese teria ficado muito mais pobre.

À minha Dianinha, tudo o que partilhamos foi muito bom, desde os tempos de laboratório, aos tempos do Cambrigde e as skype sessions ☺

À Gabriela que atravessou o Atlântico para vir conhecer o incrível mundo do DRS/DSC! Muito obrigada pelo teu trabalho, o capítulo 5 desta tese é inteirinho dedicado a ti.

À minha mana, não de sangue mas de coração, Ana Pina. Estás sempre presente na minha vida e, claro está, também tinhas que ter estado ao meu lado nesta corrida contra o tempo!! Muito obrigada!!!! Mas só aceitei a tua ajuda porque já não fazias noitadas há muito tempo! ☺

Á D. Idalina e à D. Conceição, por todo o carinho e disponibilidade. Quantas vezes andámos a pedir coisas….muito obrigada!

À minha mãe, que esteve sempre ao meu lado, apoiando-me, acarinhando-me. Esta tese reflecte muito do teu trabalho e do teu amor na minha vida. E não foi nada pouco…és a melhor mãe do mundo. Amo-te muito.

Á minha mana, cujos testes psicotécnicos lhe deram Química Aplicada!!! Tu não te metas nisto! ☺ muito obrigada pelo teu carinho, amizade, cumplicidade…amo-te muito!

Ao António, és muito mais do que um namorado. Tens sido o meu braço direito… e o esquerdo…obrigada por toda a tua paciência, pelo teu amor, pelo teu apoio. És uma bênção maravilhosa de Deus para mim. Amo-te muito!

Por último, agradeço ao Criador de tudo, Deus por me ter permitido estar 4 anos a fazer algo que adoro e pelo privilégio de vos ter conhecido a todos.

ABSTRACT

Ionic liquids (ILs) are promising materials which have been used in a wide range of applications. However, their major limitation is their physical state. In order to address this challenge, a self-supported IL-based material was developed by combining gelatine with an IL, originating a quasi-solid material named Ion Jelly (IJ). This is a light flexible material, dimensionally stable, with promising properties to develop safe and highly conductive electrolytes. This thesis is focused on the characterization of IJ films based on different ILs. The conductive mechanisms of IJ materials were studied using dielectric relaxation spectroscopy (DRS) in the frequency range 10^{-1}−10^{6} Hz. The study was complemented by differential scanning calorimetry (DSC) and pulsed field gradient nuclear magnetic resonance (PFG NMR) spectroscopy.

A glass transition was detected by DSC for all materials allowing to classify them as glass formers. From dielectric measurements, transport properties such as mobility and diffusion coefficients were extracted. Moreover, it was found that the diffusion coefficients and mobility are similar for the IL and IJ, especially for the IL EMIMDCA.

Since for BMIMDCA, those properties significantly change upon hydration, the influence of water content [0.4 - 30% (w/w)] was also studied for the ILs. In particular for BMPyrDCA with 30% water, it was analyzed the reorientational polarization by the complex permittivity and electric modulus, from which three different processes were identified: a secondary relaxation with Arrhenian temperature dependence, the process that is believed to be behind the dynamic glass transition and the mobility of charge carriers.

An application of the IJs was successfully explored with a chemoresistive gas sensor made up by different IJs as active layer, which is an electronic nose formed by an array of such sensors. The performance of this e-nose revealed its ability to correctly detect eight common volatile solvents.

Keywords: Ionic liquids, Ion Jelly, Dielectric Relaxation Spectroscopy, Differential Scanning Calorimetry, PFG – nuclear magnetic resonance.

RESUMO

Os líquidos iónicos (LIs) são materiais promissores utilizados numa vasta gama de aplicações. No entanto, a sua maior limitação é o seu estado físico. A fim de enfrentar este desafio, foi desenvolvido um novo material baseado em LIs, o qual resultou da combinação de gelatina com um LI, originando um material quase sólido denominado Ion Jelly (IJ). Este é um dispositivo flexível, leve, dimensionalmente estável com propriedades promissores para desenvolver electrólitos seguros e condutores. Esta tese está focada na caracterização de IJs baseados em diferentes LIs. Para a caracterização dos IJs foi utilizada espectroscopia de relaxação dieléctrica (ERD) na gama de frequências 10^{-1}-10^{6} Hz. O estudo foi complementado por calorimetria de varrimento diferencial (CVD) e gradiente de espectroscopia de ressonância nuclear magnética de campo pulsado (GE RMN).

Por CVD detectou-se uma transição vítrea para todos os materiais, o que permite classificá-los como materiais formadores de vidro. Das medidas dieléctricas, foram obtidas propriedades de transporte como a mobilidade e coeficientes de difusão. Para além disso, verificou-se que os coeficientes de difusão e mobilidade são semelhantes para o LI e IJ, especialmente para o LI EMIMDCA.

Uma vez que para o LI BMIMDCA essas propriedades alteraram significativamente após hidratação, a influência do teor em água [0.4-30% (w / w)] do LI foi também estudada. Em particular, para o LI BMPyrDCA com 30% de água, foi analisada a polarização de reorientação pela permitividade e módulo eléctrico, a partir do qual são identificados três processos diferentes: relaxamento com dependência Arrheniana da temperatura, o processo que acreditamos estar envolvido na origem da transição vítrea e a mobilidade dos portadores de carga.

O IJ foi aplicado com sucesso num sensor de gases quimioresistivo, um nariz electrónico, composto por um conjunto de diferentes IJs que actuam como sensores. O desempenho deste nariz electrónico revelou grande capacidade para detectar correctamente oito solventes voláteis comuns.

Palavra-chave: Líquidos iónicos, Ion Jelly, Espectroscopia de Relaxação Dieléctrica, Calorimetria de Varrimento Diferencial, gradiente de espectroscopia de ressonância nuclear magnética de campo pulsado.

Table of Contents

TABLES INDEX

INDEX OF SCHEMES

ABBREVIATIONS, SYMBOLS AND CONSTANTS

BDS: Broadband dielectric spectroscopy

BMIMBr: 1-butyl-3-methyl imidazolium bromide

BMIMDCA : 1-butyl-3-methyl imidazolium dicyanamide

BMIMDCA$_{1.9\%water}$: 1-butyl-3-methyl imidazolium dicyanamide with 1.9% water amount

BMIMDCA$_{6.6\%water}$: 1-butyl-3-methyl imidazolium dicyanamide with 6.6% water amount

BMPyrDCA: 1-butyl-1-Methyl Pyrrolidinium Dicyanamide

BNN: Barton–Nakajima–Namikawa

BPyDCA: 1-buthyl pyridinium dicyanamide

BPyrDCA: 1-buthyl pyrrolidinium dicyanamide

CCP: Composite Conductive Polymers

CA: Cluster Analysis

DCA: Dicyanamide

DFA: Discriminant Function Analysis

DFT: Density Functional Theory

DRS: Dielectric Relaxation Spectroscopy

DSC: Differential Scanning Calorimetry

EMIMDCA: 1-ethyl-3-methyl imidazolium dicyanamide

EMIMEtSO4: 1-ethyl-3-methyl imidazolium ethylsulfate

E-nose: Electronic nose

EP: Electrode polarization

FRA: Frequency Response Analyzer

FTIR: Fourier Transform Infrared Spectroscopy

Gelatin$_{22\%water}$: Gelatin with 22% water content

H-Bonds: Hydrogen Bonds

IJ: Ion Jelly

IJ1: Ion Jelly with a ratio 1:1 (gelatin/ionic liquid)

IJ3: Ion Jelly with a ratio 1:3 (gelatin/ionic liquid)

IL: Ionic Liquid

LNCS: Liquid Nitrogen Cooling System

MLR: Multiple Linear Regressions

MOS: Metal oxide semi conductors

NMR: Nuclear Magnetic Resonance

PCA: Principal components analysis

PCL: Poly (ε-caprolactone)

PED: Printed electrochemical devices

PFG: Pulse Field Gradient

PLS: Partial Least Squares

PM-IRRAS: polarization-modulation infrared reflection absorption spectroscopy

Ra:	Relative responses
RTIL:	Room temperature Ionic Liquid
SD:	Region of sub-diffusive conductivity
SPEs:	Solid polymer electrolytes
SOS:	Poly (styrene-block-ethylene oxide-block-styrene)
T_c:	Crystallization temperature
TFB:	Thin film battery
T_g:	Glass Transition Temperature
T_m:	Melting temperature
UHF:	Ultra high frequency
VHF:	Very high frequency
VHOC:	Volatile halogenated organic compounds
VFT:	Vogel Fülcher Tammann-Hesse
VFTH:	Vogel-Fulcher-Tamman-Hesse

Chapter 1

INTRODUCTION

1. INTRODUCTION

1.1. Electrochemical Devices

Electrochemistry was born as a science at the end of the 18th century when, for the first time, Alessandro Volta, an Italian Physicists, announced to the scientific community, based on Galvani's experiments (Luigi Galvani, an Italian Physicists too, who had also studied medicine), the invention of the electric battery, a device which would later revolutionize the concept of energy production having a large potential application [1-2]. This invention had such a huge impact in the scientific world, that currently it is considered as the birth of Electrochemistry [3]. Nonetheless, it is very interesting to note that, despite the fact that Galvani's conclusions about his experiments were not exactly correct, the same experiments gave rise to an exhaustive work made by Alessandro Volta, who is considered the "Father of the Electrochemistry". However, his work is based on Galvani´s observations and, for that reason, the importance of Luigi Galvani cannot be disregarded. It is noticeable that Galvani was the first to discover the current flow in an electrochemical system. However he did not realize it. The recognition of his notable work in this area is related to the battery name: galvanic cell [1].

Nowadays, electrochemistry is one of the main pathways of chemistry giving rise to a wide range of technological advances due to the combination of many different materials in electrochemical cells. Consequently, new electroactive polymeric materials are produced every day, with very different properties, for instance, electroluminescence [4], semiconductor [5], electronic and ionic properties [6] or electrochromism [7]. From the arrangement between different polymers with several components, arises new opportunities of creating high performance electrochemical devices for commercial purposes. New polymers have been developed with multiple applications such as active electrodes in electronically conducting polymers, solid electrolytes in ionic conducting polymers and as transparent substrates (optically transparent plastic electrodes) [3].

The conductivity associated to a given material is based on the free mobility of ions which transport the current known as ionic conductors. The first ionic conductors were aqueous electrolytes. Later on, polymer and solid electrolytes appeared as a great innovation to fill some gaps related with liquid electrolytes.

The main characteristics sought in electrolyte solutions are nonvolatility and high ion conductivity, i. e., the ability to perform ion transfer between two electrodes of an electrochemical device, e.g. thin films batteries (TFBs), lithium ion batteries, photoelectrochemical cells, fuel cells and double layer capacitors. These are the crucial properties of advanced and safe electrolyte solutions that are needed for this kind of energy devices put in outdoor use. Nowadays, for these types of applications, safety is more an issue than performance and has to be taken into account in future material developments.

Electrolyte solutions are essential for electrochemical devices. Until recently, most of the batteries available in the market used liquid electrolytes. Nevertheless, these devices present crucial drawbacks, such as leakage of the (flammable) electrolyte, gas production upon charge/over-discharge, thermal runway reactions and the volatility of the electrolyte. The use of solid electrolytes

can avoid many of these problems. Nevertheless, solid electrolytes still have low conductivity at room temperature, when compared with liquid electrolytes, low biodegradability and high cost. However, a new solid electrolyte, Ion Jelly (IJ), was developed showing, in some cases, very competitive conductivities when compared with the conductivity of the pure IL (see section 1.1.2 and chapter IV).

There is a wide range of liquid electrolytes [8], ILs being a the suitable solution for electrochemical devices due to their unique properties.

1.1.1. ILs

ILs are also called molten salts; however, molten salts are normally solid salts whereas the IL can be liquid at room temperature. ILs are called room temperature ionic liquids (RTILs). The relationship between ILs and molten salts has been discussed for decades.

> *Michael Faraday in the 1830s was the first to investigate systematically, the electrolysis of molten salts and used his results to assist and establishing the fundamental law of electrolysis which bears his name.*
> *It is now accepted that pure molten salts consist predominantly of ions. They differ, therefore, from all other classes of liquids in that they are the only group of pure liquids in which positively and negatively charged particles coexist and could therefore logically be called "liquid electrolytes" or "ionic liquids" (*Harry Bloom, Liverpool 1961, from the Eleventh Spires Memorial Lecture in *The Structure and Properties of Ionic Melts: A General Discussion of the Faraday Society).*

Molten salts imply a salt that is normally solid in a standard state of 298 K (25 ºC) and 1 bar, while a RTIL implies a liquid. Nevertheless, both are only composed of ions. Ideally, an IL should have a freezing point below 100 ºC. However, this is not a rule without exception, otherwise, what should we call pyridinium chloride (mp 144 ºC) or pyridinium ethanoate (mp < 25 ºC)? Therefore a suitable description of an IL is a liquid composed of ions and ion pairs (or parent molecules), dominant forces being ion-ion interactions [8].

The earliest IL referred in the literature is believed to be ethylammonium nitrate $[EtNH_3][NO_3]$, which was described by Paul Walden in 1914 [9]. Many ILs were discovered since then. For instance, in the late 40s, the first RTIL based on chloroaluminate anion was patented[10-11] and in the 60s a similar system was introduced, based on chlorocuprate anion, $CuCl_2^-$, and tetraalkylammonium cation [12], one of the most important families of ILs. In 1967 the application of tetra-*n*-hexylammonium benzoate as a solvent was published [13]. In the 90s, the major event in this area was the discovery of a new type of ILs based on the 1-ethyl-3-methylimidazolium cation and the tetrafluoroborate anion [14-17]. Nevertheless, novel combinations of cations and anions have been proposed, giving rise to new ILs with very different and interesting properties and applications. One of the most remarkable properties for this work is undoubtedly their conductivity. A system containing both anions and cations that are free to move, will conduct electricity.

In the table below we can see a selection of electric conductivities, σ, of some liquids, at different temperatures (T):

Table 1.1 - A selection of Electrical Conductivities of Liquids[18]

Electrolyte	Solvent	σ/S.cm^{-1}	T/K
H_2SO_4 (30 wt. %)	H_2O	0.730	298
KOH (29.4 wt. %)	H_2O	0.540	298
NH_4Cl (25 wt. %)	H_2O	0.400	298
$[Et_4N]^+[BF_4]^-$ (1 mol/dm^3)	AN	0.060	298
$LiN(CF_3SO_2)_2$ (1 mol/dm^3)	EC + DME (1:1)	0.0133	298
$LiN(CF_3SO_2)_2$ (1 mol/dm^3)	EC + DC (1:1)	6.5×10^{-3}	298
$LiCF_3SO_3$ (1 mol/dm^3)	EC + DME (1:1)	8.3×10^{-3}	298
$LiPF_6$ (1 mol/dm^3)	EC + DME (1:1)	0.016	298
$[Et_4N]^+[BF_4]^-$ (0.65 mol/dm^3)	PC	0.0106	298
$[EMim]^+[BF_4]^-$ (2 mol/dm^3)	AN	0.047	298
$[EMIm]^+[BF_4]^-$ (2 mol/dm^3)	PC	0.016	298

In table 1.2 it is possible to observe the electrical conductivities of several ILs and compare them with the liquid electrolytes above. Some ILs show very promising conductivities.

Table 1.2 - A selection of Electrical Conductivities of Ionic Liquids[18]**.**

System	σ/S.cm^{-1}	T/K
$[Bu_3HexN][CF_3SO_2)_2N]$	1.60×10^{-4}	298
$[MPPip][CF_3SO_2)_2N]$	1.51×10^{-3}	298
$[BPy][BF_4]$	1.94×10^{-3}	298
$[BMPyr][PF_6]$	7.65×10^{-3}	368
$[EMIM][(CF_3SO_2)_2N]$	7.73×10^{-3}	298
$[EMIM][DCA]$	9.53×10^{-3}	298
$[BMIM][DCA]$	9.54×10^{-3}	298
$[BMPyr][DCA]$	9.83×10^{-3}	298
$[EMIM][BF_4]$	0.01305	298
$[EMPyr][(CF_3SO_2)_2N]$	0.0172	365
$[BMPy][DCA]$	0.0174	298
$[P_{6,6,6,14}][DCA]$	0.156	368
$[P_{6,6,6,14}][C_9H_{19}CO_2]$	0.740	378

ILs have a broad range of conductivities from 0.1 – 740 mS/cm. Higher conductivities are associated to the cations 1-butyl-3-methylpyridinium [BMPy]$^+$ and trihexyl (tetradecyl) phosphonium [P$_{6,6,6,14}$]$^+$ whereas lower conductivities are associated to the ILs based on tributyl (hexyl) ammonium [Bu$_3$HexN]$^+$, 1-butyl-pyridinium [BPy]$^+$ and piperidinium [PMPip]$^+$ cations (0.1 to 2 mS/cm).

Due to this essential property, the main application of ILs is as electrolytes [19-23]. Classical electrolytes are obtained by dissolution of salts in molecular solvents, which consist of solvated ions, their charged or neutral combinations, and solvent molecules. However, ILs, which are formed entirely by anions and cations, have a great advantage, since they are free of any solvent.

ILs are probably one of the most studied chemical compounds in the past decade. In addition to conductivity, a very useful property of ILs is the negligible vapour pressure, which is probably their "greenest" property. It should also be mentioned high thermal, chemical, and electrochemical stability [18], [24-25]. But are ILs really green? In April 2002, Albrecht Salzer asked the scientific community this question (*Chemical and Engineering News*, 2002, 80 [April 29], 4-6). Different opinions arose and Robin Rogers, a Chemist and distinguished scientist, gave his important contribution:

"Salzer has not fully realized the magnitude of the number of potential of ionic liquid solvents. However, by letting the principles of green chemistry drive this research field, we can ensure that the ionic liquids and ionic liquid processes developed are in fact green […] but there is a need for further work to demonstrate the credibility of ionic liquid-based processes as viable green technology. In particular, comprehensive toxicity studies, physical and chemical property collation and dissemination, and realistic comparisons to traditional systems are needed" [26].

It is important to analyze those properties based on the twelve principles of Green Chemistry, proposed by Paul Anastas and John Warner in 1998 [27]. Table 1.3 shows those twelve principles in detail.

Table 1.3 - The twelve principles of Green Chemistry (retrieved from reference [27])

Prevention	It is better to prevent waste than to treat or clean up waste after it is formed.
Atom Economy	Synthetic methods should be designed to maximize the incorporation of all materials used in the process into the final product.
Less Hazardous Chemical Synthesis	Whenever practicable, synthetic methodologies should be designed to use and generate substances that pose little or no toxicity to human health and the environment.
Designing Safer Chemicals	Chemical products should be designed to preserve efficacy of the function while reducing toxicity.
Safer Solvents and Auxiliaries	The use of auxiliary substances (e. g. solvents, separation solvents, etc.) should be made unnecessary whenever possible and, when used, innocuous.
Design of Energy Efficiency	Energy requirements of chemical processes should be recognized for their environmental and economic impacts and should be minimized. If possible, synthetic methods should be conducted at ambient temperature and pressure.
Use of Renewable Feedstock	A raw material or feedstock should be renewable rather than depleting whenever technically and economically practicable.
Reduce Derivatives	Unnecessary derivation (use of blocking groups, protection/deprotection, and temporary modification of physical/chemical processes) should be minimized or avoided if possible, because such steps require additional reagents and can generate waste.
Catalysis	Catalytic reagents (as selective as possible) are superior to stoichiometric reagents.
Design for Degradation	Chemical products should be designed so that at the end of their function they break down into innocuous degradation products and do not persist in the environment.
Real-Time Analysis for Pollution Prevention	Analytical methodologies need to be further developed to allow for real-time, in-process monitoring and control prior to the formation of hazardous substances.
Inherently Safer Chemistry for Accident Prevention	Substances and the form of a substance used in a chemical process should be chosen to minimize the potential for chemical accidents, including releases, explosions, and fires.

When ILs are used as electrolytes, the principle Safer Solvents and Auxiliaries strongly applies, unlike what happens with common liquid electrolytes, ILs are free from solvents, which means that it is possible to achieve a substantial reduction of both environmental and economic impact. When thinking of liquid electrolytes in a battery, a main drawback is the possible leakage of the (flammable) liquid, as mentioned earlier. Since most ILs are non-flammable, the principle of Inherently Safer Chemistry for Accident Prevention applies. For that reason, ILs are one of the main pillars of Green Chemistry. Nevertheless, Green Chemistry is favoured not only by the use of ILs, but also by solvents such as super critical fluids [28-29].

Nonetheless, it should be pointed out that some ILs have vapour pressure that allow to distil the previously believed "undistilled" [30-31].   Due to their negligible volatility, ILs were taken as non-toxic, but this common accepted notion as shown to be incorrect being proven that several ILs, commonly used to date are toxic to a wide range of organisms (Dongbin Zhao *et al*. Toxicity of Ionic Liquids). In fact, the tailor-made design of ILs to meet a particular application is probably the most fascinating and creative domain in IL research. The type of molecular interaction between cation and anion is determinant for physical-chemical properties such as melting temperature, glass transition temperature, T_g, or conductivity [32-33]. These are relevant parameters in applications of ILs as novel electrolytes for electrochemical devices, such as dye synthesized solar cells, double layer capacitors, fuel cells, electrochemical windows and lithium secondary batteries [24-25].

The actual trend in electrochemical devices, point to ILs as the most promising approach to develop safe and highly conductive electrolytes. Nevertheless, the large scale production of the above electrochemical devices is following the printing trend due to large scale production impositions. To address this issue, different authors have tried to develop solid/polymeric/composite-based ILs [34-37] and some of these systems seem very competitive in terms of ionic conductivity [35-36].

One of the most simple and efficient approaches is based on gelation, which is a simple method that allows a good compromise between the retention of IL and its fluidity inside the polymeric network. This strategy is quite different from the traditional solid polymer electrolytes that results either from the doping of a given polymer matrix with an IL or from the introduction of polymerizable groups on IL structures. These so-called ion gels are in a way simpler than solid polymer electrolytes and exhibit improved conductivities. For instance, MacFarlane and co-workers [35] have shown the potential of an ion gel formed by gelation of poly(styrene-block-ethylene oxide-block-styrene) (SOS) triblock copolymer in 1-butyl-3-methylimidazolium hexafluorophosphate. This system has shown interesting conductivity values at room temperature (above 10^{-3} S cm^{-1}). Such IL-based materials can work as electrolytes in different electrochemical devices and be used either as printer substrates or printable inks.

1.1.2. IJ

Aiming to obtain a material exhibiting such properties, the combination of an IL and a biopolymer was tested, which properties were recently reported [38]. The initial line of work focused on the immobilization of an enzyme using sol-gel procedure and an IL. The idea was to combine the ability that ILs have to modulate enzymatic properties with the advantages of enzyme immobilization.

Nevertheless, the IL did not have a positive impact on the activity of the enzyme tested. Therefore, the mentors of the idea, P. Vidinha and N. Lourenço, started to think of different approaches. Since ILs can be used as templates for sol-gel matrices, they tried to add different materials to accomplish the immobilization of the ILs. The materials they first used were alginate and gelatine, in order to create a polymeric bead containing the IL. Of the two polymers used, gelatine was the one that allowed to produce a material with the desired conductive properties, which synthesis and applications are register in a patent [39]. The attractive values of the conductivity of IJ materials led to their use as electrolyte. The vision was to seek new applications in the area of sensors [40-41], electrospinning [42] and electrochemistry [38]. This thesis mainly results from the questions that arose from this article, namely: "Can we improve the IJ electrochemical window? Is it possible to increase IJ conductivity?". "In what way does gelatine interact with the IL?". The crucial question seemed to be, "Can we apply this simple combination of gelatine and IL to a battery? Can we solve the effective problems related to batteries? Can we produce an electrolyte that is conductive enough?". These topics will be discussed along this thesis.

IJ is a light and flexible electrolyte. It is an extremely versatile conductive material that can be molded into different shapes, using several techniques, and can be adapted to multiple surfaces. Moreover, on cooling, IJ can undergo a liquid-gel transition near room temperature (near 308 K), which could make it a promising solution to develop electrolyte inks for printed electrochemical devices (PED) [38].

Going back to Table 1.3, there are some features that apply to IJ. *Safer solvents and auxiliaries*, for example, since in the preparation of IJ the only solvent that is used, is water, an innocuous solvent; *reduce derivatives*, since there is no need for blocking groups or protection/deprotection groups; *design of energy efficiency*, due to the fact that IJ is produced at relatively low temperature (35ºC) and ambient pressure; and *inherently safer chemistry for accident prevention*, since IJ is a solid polymer, which contains water and an IL, non-hazardous substances, and in its applications there is no danger of the occurrence of accidents such as leakage, explosions or fires.

Polymer electrolytes are an important component of many electrochemical devices, and due to this fact, the scientific community has made an extraordinary effort in the development of this kind of system. There is a wide range of polymer electrolytes using aqueous and nonaqueous-based natural polymers, such as, solid polymer electrolytes (SPEs) [44], which arises from the necessity to fill some gaps on the search for new architectures for electrochemical devices, given that more and more devices, such as solid-state batteries, sensors, and portable electrochemical units require increasingly smaller and safer electrolytes. In this regard, the best candidates for this type of applications can be materials such as ceramics, polymers, hybrids and gels. One of the most applied systems are SPEs due to their huge advantages when compared with liquid electrolytes, related to the possibility of higher temperatures of operation, no flowing and corrosion after damage, and ease of application to electrochemical devices. One of the major drawbacks of the majority of SPEs is their low ionic conductivity. In this respect, IJ has a very competitive conductivity. Any polymer that goes with an IL will form, in theory, an ion gel, as discussed by Hiroyuki Ohno, one of the most cited authors in this research field [45].

The evaluation of basic thermophysical properties is vital to the design of IJs and to conceive new applications. For that purpose, it is essential to understand the physicochemical behaviour of ILs in an IJ matrix. To accomplish this goal, we have performed a dielectric relaxation spectroscopy (DRS) characterization, whose basic principles are described in the next section.

The main IJ system chosen for this study is based on 1-butyl-3-methyl imidazolium dicyanamide (BMIMDCA). The dicyanamide (DCA) compounds are liquid at room temperature and characterized by their low viscosity, water miscibility, and high thermo (over 373 K) and electrochemical stability (over 3.5 V) [46-47]. Moreover, the DCA ion is an anionic bridge ligand that has Lewis base attributes, which makes it particularly attractive to synthesize ILs with very specific properties. Compared to common anions such PF_6 or BF_4, DCA has a permanent dipole and thus facilitates the research on IL dynamics through dielectric spectroscopy [47-48]. Other IJ systems were made based on different ILs. However, since dicyanamide was found to be the most suitable anion for the preparation of IJ films, the chosen ILs are composed by this anion, changing the type of cation. Three ILs were used, in addition to BMIMDCA: 1-ethyl-3-methyl imidazolium dicyanamide (EMIMDCA), 1-butyl-1-methyl pyrrolidinium dicyanamide (BMPyrDCA) and 1-butyl pyridinium dicyanamide (BPyDCA). The next figure shows the structure of each IL:
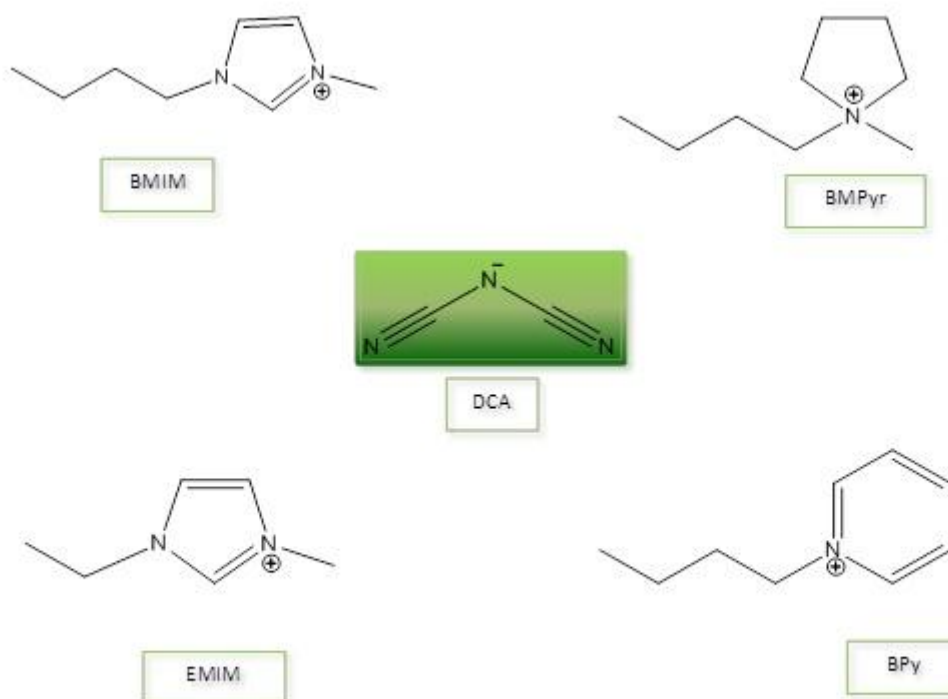
Figure 1.1 – Ionic liquid structures: 1-butyl-3-methyl imidazolium dicyanamide (BMIMDCA), 1-ethyl-3-methyl imidazolium dicyanamide (EMIMDCA), 1-butyl-1-methyl pyrrolidinium dicyanamide (BMPyrDCA) and 1-butyl pyridinium dicyanamide (BPyDCA).

On the basis of the analysis of the thermal behaviour, charge transporters, ion mobility, and conductivity, we are able to obtain useful information to clarify the impact of gelatine on IL

physicochemical properties, which are ultimately implicated on IJ conductivity and consequently on its application to PEDs.

1.2. Polarization and Dielectric Relaxation Spectroscopy (DRS)

DRS was used to gain a better insight into the mechanism of charge transport that determines conductivity in the IJ and it precursors, and also to better understand the polarization effects that manifest in these materials. Basically dielectric relaxation occurs when a material, which is the dielectric, is submitted to a periodically alternating electrical field between two electrodes. This is the main phenomenon of DRS, which is a very well established experimental method and highly used in order to study the structure and the molecular dynamics in manifold systems, providing a powerful tool for the molecular dynamical study in confined spaces at both mesoscopic and molecular level.

The application of an oscillating electric field induces a polarization in the sample whose mechanisms will be next described.

1.2.1. Polarization Mechanisms

A pre-requisite for DRS is the presence of molecular dipoles in the material structure.

Fundamentally, matter is composed by a distribution of electrical charges, positive (protons) and negative (electrons). Accordingly, when an electric field is applied to a certain material, the atomic and molecular charges present within the material will respond to the presence of this field through a modification or distortion of these charges, i.e., a displacement from their equilibrium positions. This phenomenon is called polarization and describes the dielectric displacement which originates from the response of a material to an external field only. There are two main polarization mechanisms in the different materials [49]:

1)   Induced Polarization that results from induced dipoles comprehending three different types of polarization: *electronic polarization*, which arises from the displacement of the electric cloud distribution with respect to the atomic nucleus, corresponding to electronic spectroscopy in ultra-violet and visible region of the spectrum of electromagnetic waves (figure 1.2); *atomic polarization*, which is observed when the atomic nucleus is reoriented in response to the electric field, which is intrinsic to the nature of the atom in a polar covalent bond, corresponding to vibrational spectroscopy in the infra-red domain; and *ionic polarization*, which is due to relative displacements between cations and anions in ionic crystals, for example, sodium chloride.

Both atomic and electronic polarizations are described as resonant mechanisms, where polarization build-up almost instantaneously being detected by optical spectroscopies. This kind of response to electromagnetic radiation is so fast that it could not be analyzed by dielectric relaxation, which is essentially studied in the radio and microwaves range of the electromagnetic spectrum (see figure 1.2).
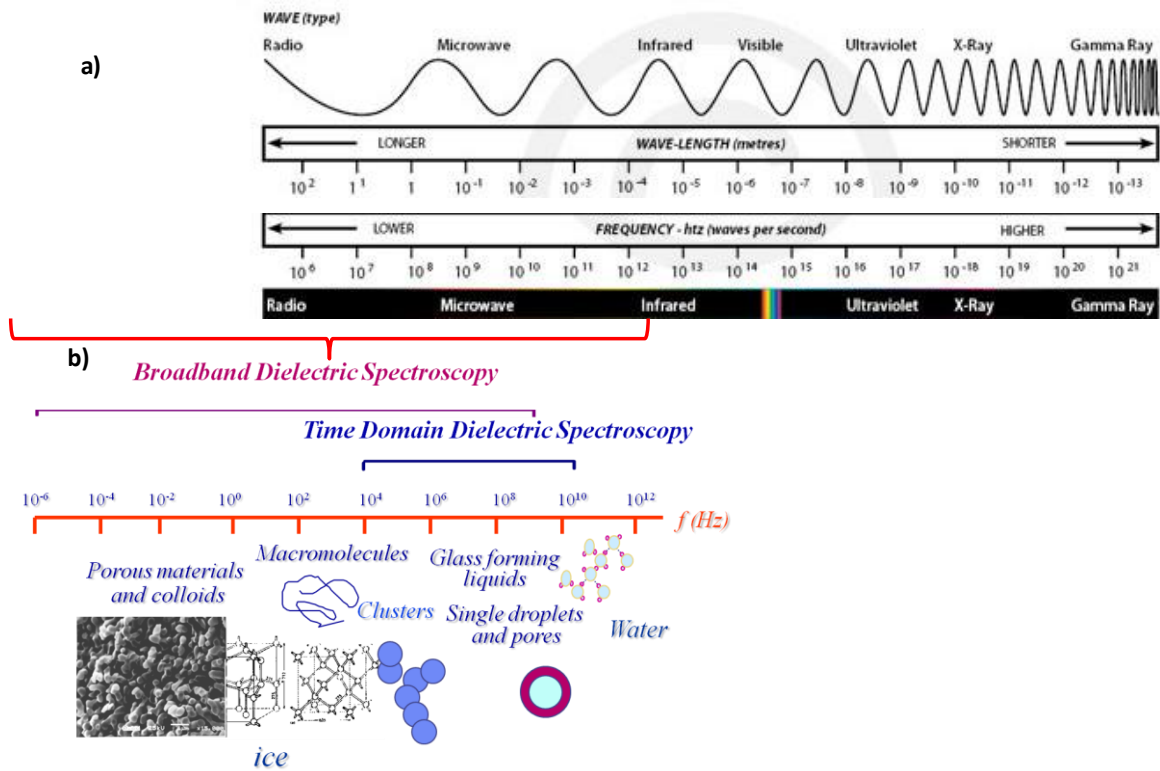
Figure 1.2 – (a) - Electro Magnetic Spectrum; (b) – Time domain dielectric spectroscopy (adapted from: http://www.colourtherapyhealing.com/colour/electromagnetic_spectrum.php; Y. Feldman, "The Physics of dielectrics", lecture 1, in http://aph.huji.ac.il/courses/2008_9/83887/index.html, accessed in March 2013).

2)   Orientational or Dipolar Polarization, due to alignment of permanent dipoles. This type of polarization is originated from permanent ionic or molecular dipoles only, resulting in the alignment of dipoles with the applied electric field giving rise to orientational polarization. The orientation of permanent dipoles is driven by molecular motions that can be very local in nature or by cooperative motions of molecular segments in a viscous medium with times scales measurable by dielectric spectroscopy. However, there is a difference between ionic and molecular dipoles: in the later, the charge density is unequally shared by the covalently bounded nuclei of a molecule and therefore no significant differences on the dipolar moment are observed upon temperature changes, while the temperature increase highly shortens the lifetime of ionic dipoles which are maintained by electrostatic interactions.

The orientational polarization occurs only at low frequencies, and therefore it is the slowest mechanism.

It is important to note that both induced and orientational polarizations have very different times response: around 10^{-17} and 10^{-14} s for electronic polarization, 10^{-13} and 10^{-12} s for atomic polarization and between 10^{-12} and 10^{-6} s for orientational polarization (see Figure 1.2).

Figure 1.3 shows the frequency dependent dielectric permittivity upon application of a time varying electric field. Here we can see different processes involved in the polarization and the respective differences in the intensity of each mechanism. While the atomic and electronic polarization may follow

the changes in the electric field instantaneously, as already mentioned, orientational polarization response it is not immediate due to the resistance imposed to the dipole's motion. The opposite is also true, whereas atomic and electronic polarizations disappear immediately upon removal the electric field, orientational polarization decreases slowly owing to the internal friction of the material which depends on viscosity [50]. The relaxation phenomenon is the delayed response to a variant stimulus; therefore, the time-dependent loss of orientation of dipoles upon removal the oscillating electric field is called dipolar relaxation.

The parameter that describes the polarization loss upon electric field removal is designated by relaxation time, i. e., it describes the time required for the dipolar polarization to decay $1/e$ of its initial value, where e is the Neper number (see equation 1.8 later on text). At low frequencies the dipoles can follow the changes in the electric field and the permittivity value has its highest value. With the frequency increase the dipoles do not have enough time to follow the changes in the field direction losing the ability to align with the applied electric field, resulting in a decrease in the dielectric permittivity, ε' (see figure 1.3). It should be noted that the figure illustrates the behaviour of a molten liquid, highly mobile, which is not the case of the materials studied in this thesis, in which the dipolar response is shifted to lower frequencies. Relaxation processes are characterized by a peak in the imaginary part of permittivity ε'' and a marked decrease of the real part ε' of the complex dielectric function with increasing frequency. Above this range of frequencies, the dipolar polarization does not contribute to the total polarization, and only induced polarization remains.
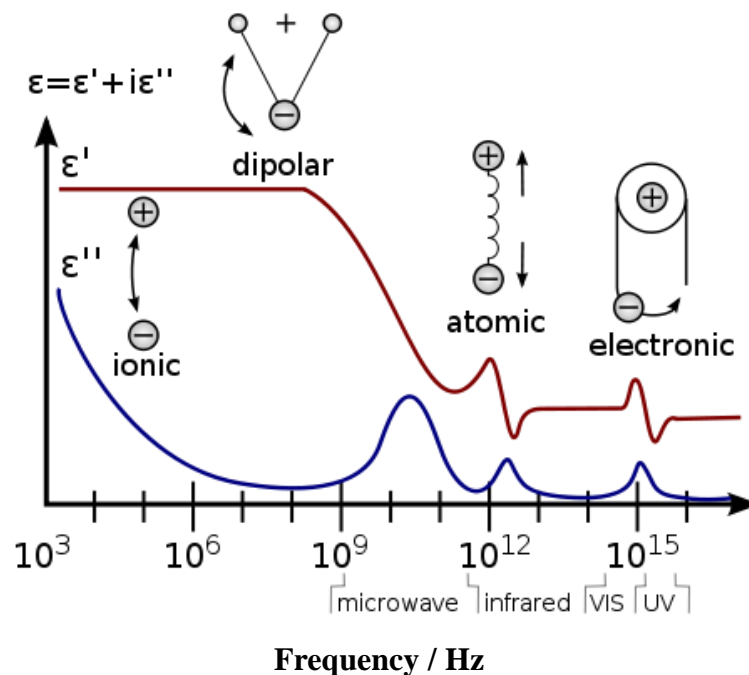
Frequency / Hz

Figure 1.3 - A dielectric permittivity spectrum over a wide range of frequencies. ε' and ε'' denote the real and the imaginary part of the permittivity, respectively. Various processes are labelled on the image: ionic and dipolar relaxation, and atomic and electronic resonances at higher energies (Redrawn from reference [51])

The permittivity due to these induced dipoles is known as the unrelaxed or permittivity at infinite frequency, ε_∞. The difference between the permittivity at low frequencies, ε_s, and at high

frequencies is the dielectric strength, and establishes the relation between the applied electrical field, *E*, and the resulting orientational polarization, P, according to the following equation:

$$P_{or} = \varepsilon_0(\varepsilon_s - \varepsilon_\infty)E \qquad (1.1)$$

$$P(v) = P_T = \varepsilon_0(\varepsilon_s - 1)E(v) \quad (1.1 - a) \qquad P(\infty) = P_{ind}\varepsilon_0(\varepsilon_\infty - 1)E(\infty) \quad (1.1 - b)$$

where ε_0 is the vacuum permittivity. For the low frequencies, equation 1.1 reduces to 1.1 – a), while for high frequencies the equation reduces to 1.1 – b).

Additionally to the two polarization mechanisms described above, conductivity can also contribute to the dielectric response of the material due to propagation of mobile charge carriers that is due to translational diffusion of the electrons, holes and ions.

Migration of charges gives rise to conductivity that comes from this continuous movement of charges. Conductivity comprehends both types of intrinsic (e.g., proton transfer along hydrogen bonds) and extrinsic (e.g., ionic impurities) migrating charges. The last one describes conductivity as inversely proportional to viscosity, according to the viscous model of charge transfer (Stokes law). This means that a material with zero conductivity is obtained, if the viscosity is infinitely high. Nevertheless, this is only a theoretical situation meaning that the conductivity exhibited by a cross-linked-polymer network could be partially explained in association with intrinsic migrating charge [52].

The separation of charges at interfaces originates an additional polarization. This process arises from the build-up of charges at the inner dielectric boundary layers, or in the interphases between components in heterogeneous systems, known as interfacial, space charge, or Maxwell-Wagner-Sillars polarization. The accumulation of ions at the material-electrode-interface gives rise to electrode polarization. The latter mechanism is observed in the systems tested in this thesis (see chapters 3, 4 and 5).

1.2.2. Dielectric Spectroscopy

Since Debye, in 1927, established the relationship between dielectric relaxation and the molecular motions of molecular dipoles, the technique of dielectric spectroscopy has been gaining the attention of many research groups with around forty thousand articles published (according to search on IsiWeb visualized in March 2013).

Current methods were used for very low frequencies (f < 1Hz), and alternating current (a. c) for higher frequencies (1 a 10^7 Hz) in applications such as power, audio, ultra high frequency (UHF) and very high frequency (VHF). Methods for microwaves frequency (10^8 to 10^{11} Hz) were developed in the decade of 1940s, and in the decade of 1970s new advances were made in order to improve the spectroscopic methods for infrared frequencies (3×10^{11} to 3×10^{12} Hz) [53].

Nowadays, dielectric measurement techniques were developed in many different materials such as molecular liquids, solids and semi-conductors [54-59] giving very useful information about electrical conductivity and, hence, giving rise to knowledge about the effective mobility of charge carriers.

Furthermore, depending on the particular polymer system, ranging from simple amorphous or semi-crystalline polymers [60-62] to more complex systems such as miscible [63-66] and immiscible systems [66-69] polymer blends, liquid crystalline polymers [70-71], supramolecular polymers[72-73], nanocomposites [74] and ILs with low molecular weight materials [102], one or more characteristic dielectric relaxation processes are detected, which can be assigned to, e. g., the primary relaxation (usually designated as α-process) associated with the dynamic glass transition[69].

In this work, Broadband Dielectric Spectroscopy (BDS) data were extracted from the range between 10^{-1} to 10^6 Hz since the aim of our work is to study the conductive properties of some ILs and the respective IJs based on these ILs.

Basically, DRS spectra reproduce the set of molecular motions of all dipolar species present in the media. In ILs, these motions are highly correlated with the multiplicity of interactions between the different charged species present in the media, which makes it impossible to address a specific motion to a well-defined dipole.

In fact, in ILs, the molecular motions reflect the kinetics of the network rearrangement [46-47]. However, the IJ network is settled by the interaction between two polyelectrolyte molecules (gelatine and IL) creating in such way a complex network with multiple interaction sites that can lead to a great variety of dipolar aggregates. Moreover, since these materials have some degree of hydration, the role of water needs also to be evaluated (see chapter 5). Thus, a comprehensive and detailed analysis of IL relaxation behaviour inside a hydrated gelatine matrix can result in important data about the crucial mechanisms implicated in the IJ conductivity.

1.2.3. Theoretical Principles of Dielectric Relaxation

Since matter is composed by electrical charges, it becomes predictable to infer that there is an interaction between electric and magnetic fields with matter.

The linear interaction of electromagnetic fields with matter is described by two Maxwell's equations [53]:

$$\nabla . E = -\frac{\partial}{\partial t} B \qquad (1.2)$$

$$\nabla . H = j + \frac{\partial}{\partial t} D \qquad (1.3)$$

Where E (Vm^{-1}) and H (Am^{-1}) describe the electric field and magnetic field, respectively, B (Vs m^{-2}) the magnetic induction, D (As m^{-2}) the dielectric displacement and j (A m^{-2}) the current density. For weak electric fields D can be expressed by:

$$D = \varepsilon * \varepsilon_0 E \qquad (1.4)$$

Where ε_0 is the dielectric permittivity of vacuum (ε_0=8.854x10^{-12} Fm^{-1}). $\varepsilon *$ is the complex dielectric function or dielectric permittivity. In general, time dependent processes within a material lead to a

difference of the time dependencies of the outer electrical field E(t) and the resulting dielectric displacement D(t). For a periodic electrical field $E(t) = E_0 \exp(-i\omega t)$ (ω is the angular frequency, in rad.s^{-1}; $i = \sqrt{-1}$) the complex dielectric function, $\varepsilon *$ is defined by:

$$\varepsilon * (\omega) = \varepsilon'(\omega) - i\varepsilon'' \qquad (1.5)$$

Where $\varepsilon'(\omega)$ is the real part of permittivity which is related with the energy storage inside the material, and $\varepsilon''(\omega)$ is the imaginary part of the complex dielectric function related with the energy dissipation (loss) inside the material, due to the interaction between the applied field and dipoles.

Equation 1.4 is similar to Ohms law:

$$j = \sigma * E \qquad (1.6)$$

Giving the relationship between the electric field and the current density j where:

$$\sigma * (\omega) = \sigma'(\omega) - i\sigma''(\omega) \qquad (1.7)$$

$\sigma * (\omega)$ is the complex electric conductivity. σ' and σ'' are the corresponding real and imaginary parts. $\varepsilon * (\omega)$ and $\sigma * (\omega)$ are time dependent empirical functions of molecular properties that give information about both reorientational and translational movements of molecules and charge transport properties in solids and molecular liquids. The dielectric function and the conductivity are complex because the excitation due to the external electrical field and the response of the system under study are not in phase with each other. Because the current density and the time derivative of the dielectric displacement are equivalent quantities according to equations 1.3 and 1.4 it holds:

$$\sigma *= i\omega\varepsilon_0\varepsilon * \qquad (1.8)$$

1.2.4. Debye Behaviour

In the model of Debye to calculate the time dependence of dielectric behaviour it is assumed a change of the polarization where the time variation is proportional to the equilibrium value, following a first order differential equation [53], [75-76]:

$$\frac{dP(t)}{d(t)} = -\frac{1}{\tau_D}P(t) \qquad (1.9)$$

Where τ_D is the characteristic relaxation time. Therefore, upon removing the electric field at $t = 0$, the orientation polarization will be given by $P(t) = P_0 \exp(-t/\tau)$, where P_0 is the value of the polarization at the moment of electric field removal. Consequently, in the Debye model, the response material to external electric fields has an exponential nature, i. e., $\phi(t) = \exp(-t/\tau)$.

The model of dipole orientation is due to Debye [76] and assumes a single relaxation time for all molecular species. The Debye model for the frequency dependence of $\varepsilon * (\omega)$, gives rise to the following equation (eq. 1.10), which can be decomposed by the real and imaginary components of permittivity (equations 1.10 – (a-b)), accounting for a new parameter, the ionic conductivity[77]:

$$\varepsilon * (\omega) = \varepsilon_{\infty} + \frac{\varepsilon_s - \varepsilon_{\infty}}{1 + i\omega\tau} \qquad (1.10)$$

$$\varepsilon'(\omega) = \varepsilon_{\infty} + \frac{\varepsilon_s - \varepsilon_{\infty}}{1 + \omega^2\tau^2} \quad (1.10-a) \qquad \varepsilon''(\omega) = \frac{\sigma}{\omega\varepsilon_0} + \frac{\varepsilon_s - \varepsilon_{\infty}}{1 + \omega^2\tau^2}\omega\tau \quad (1.10-b)$$

Figure 1.4 illustrates the frequency dependence of $\varepsilon'(\log f)$ and $\varepsilon''(\log f)$ for equations 1.10 – (a) and (b), where f is the frequency in Hertz, whereas the frequency of the applied outer electric field is given by $f = \omega/2\pi$. The corresponding plots for ε'' are more complex owing to the relative contribution of conductivity and the dipole loss. The simplest case is shown in figure 1.4 by the symmetrical peak associated to ε'', when $\sigma = 0$. Here it is possible to see the characteristic dipolar loss peak which presents a maximum value that occurs at $\omega_{max}.\tau = 1$ and has an amplitude of $\varepsilon''_{max} = (\varepsilon_s - \varepsilon_{\infty})/2$. The mean relaxation time of the process, τ, is defined as $\tau = 1/(2\pi f_{max})$. However, when the conductivity is different from zero, this curve is distorted from ideal Debye peak, meaning that, as conductivity increases, it becomes more difficult to discern the dipole peak. Basically, for $\sigma/\omega\varepsilon_0$ greater than about three times ε_s, the observed ε'' is completely dominated by the conductivity [77]. Ideally, even when the conductivity dominates the dipolar contribution to ε'', it should still be possible to observe the dipolar contribution to ε'. Nevertheless, when the conductivity contribution is large enough, there is another factor which will influence ε' measurements, which is the electrode polarization (see section *1.2.5*).
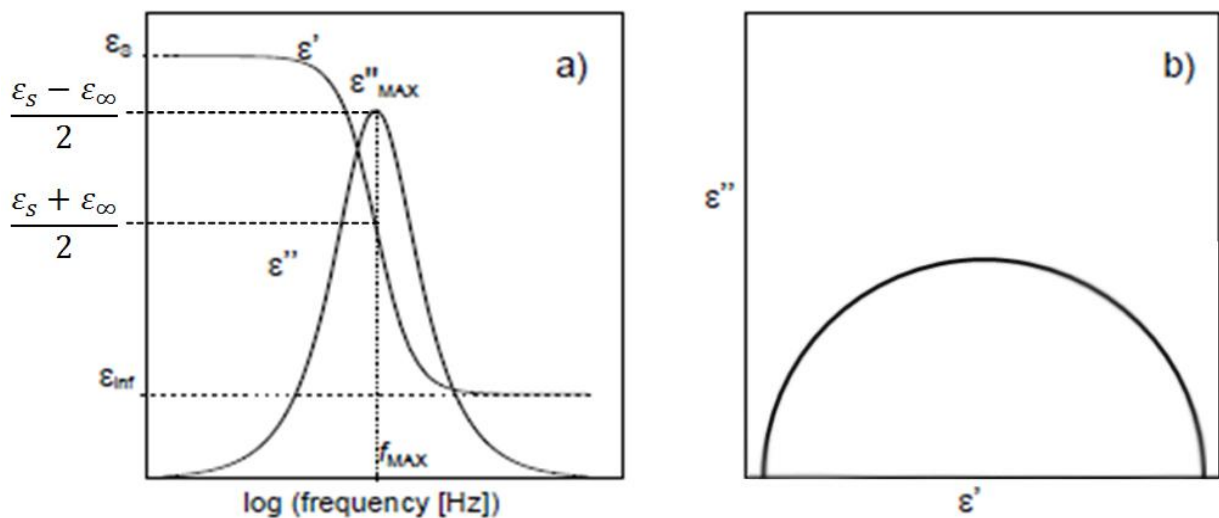
Figure 1.4 – Debye single relaxation time model for dipole orientation showing a (a) frequency dependence of the real, ε', and imaginary, ε'', permittivities and (b) Imaginary part *vs.* real part of permittivity, $\varepsilon *$.

An alternative method to present the ε' and ε'' frequency dependencies is in a Cole-Cole plot [78], where ε'' is plotted against ε'. Figure 1.4 – (b) shows the Cole-Cole diagram for the ideal case when the Debye model is obeyed, yielding a symmetric semicircle, i. e., when $\sigma = 0$.

In real systems, the Cole-Cole diagram differ from the one shown above in two distinct phenomena: *i)* electrode polarization and *ii)* some distribution of relaxation times, since the dipolar mechanisms are not characterized by one single relaxation time, τ. This distribution of relaxation times has a probability density function of $\rho(\ln \tau)$ [75]:

$$\phi(t) = \int_{-\infty}^{+\infty} e^{-\frac{t}{\tau}} \rho(\ln \tau) d \ln \tau \qquad (1.11)$$

In the frequency domain, the existence of this distribution, converts equation 1.11 (ε*) into a new equation:

$$\frac{\varepsilon^*(\omega) - \varepsilon_\infty}{\varepsilon_s - \varepsilon_\infty} = \int_{-\infty}^{+\infty} \frac{\rho(\ln \tau)}{1 + i\omega\tau} d \ln \tau \qquad (1.12)$$

The calculation of $\rho(\ln \tau)$ it is not an easy process to obtain from the experimental data. Accordingly, in order to fit the $\varepsilon^*(\omega)$ data directly, several empirical models were developed enabling essential information to be extracted. The main equations obtained can be written in the following form:

$$\varepsilon^*(\omega) = \varepsilon_\infty + \frac{\varepsilon_s - \varepsilon_\infty}{[1 + (i\omega\tau)^x]^y} \qquad (1.13)$$

With:

$x = \alpha; y = 1 \ (0 < \alpha \leq 1)$ Cole-Cole[79]

$x = 1; y = \beta \ (0 \leq \beta < 1)$ Cole-Davidson [80]

$x = \alpha; y = \beta \ (0 < \alpha \leq 1)$ Havriliak-Negami [81]

Where α is the value related to the broadness of the distribution of relaxation times and β describes its asymmetry, which means that when $x = y = 1$ the ideal Debye case is reached. Since the Havriliak-Negami (HN) equation has two adjustable parameters it is relatively easy to describe a single relaxation process. However, when a system presents more than a relaxation process, the experimental data is fitted with a sum of HN equations, one for each relaxation process.

No further development is given here for the different models since, in the majority of the materials tested in this work, the orientational polarization becomes submerged by conductivity. This impairs the analysis of relaxational processes through those models; only in one system - (BMPyrDCA) – was the HN equation fitted to the dielectric data (see chapter 5). An alternative process

to analyze the dielectric response due to reorientational motion of dipoles is through the modulus (see chapter 5 for a more detailed description).

In the next section the charge transport mechanism is analyzed in more detail.

1.2.5. Transport Properties

As previously mentioned, in addition to reorientational dipolar motions, the propagation of mobile charge carriers also contributes to the dielectric response. In order to extract transport properties, the dielectric spectra are better analyzed through the complex conductivity, $\sigma^*(\omega) = \sigma'(\omega) + i\sigma''(\omega)$. The later is related with the complex permittivity by [82]: $\sigma^*(\omega) = i\omega\varepsilon_0\varepsilon^*(\omega)$.

It is quite remarkable that the frequency dependence of the complex conductivity for a variety of disordered conductive systems obeys a common pattern. In all cases, it is observed a plateau at the lowest frequencies where the conductivity is frequency independent being identical to dc conductivity (σ_0), bending off at higher frequencies into a dispersive regime, with a pronounced increase of the conductivity with increasing frequency [83]; the frequency at which the plateau bends off to the frequency dependent region separating the two regimes, is called the crossover frequency, ν_{cross}.

The ionic conductivity arises from ion transport which corresponds to "hopping movements of mobile ions between different positions in a solid or supercooled liquid matrix" [84]. Depending on whether measurements are being made over short or large time scales, the corresponding mean-square displacement, $<\Delta r^2(t)>$ which is of the order of the distance that a particle can jump when diffusing in a time $t^* = 1/\nu_{cross}$ [85], exhibits different time dependencies. At long times or low frequencies (and high temperatures), where $\omega < \omega_{cross}$, ($\omega_{cross=}2.\pi.\nu_{cross}$) the mean square displacement of ions during charge transport, varies linearly with time ($<\Delta r^2(t)> \alpha$ t) [86] and the conductivity is frequency independent, all σ' values falling in a plateau. Therefore, the conductivity properties are governed by diffusive movements of ions. On the other hand, for short time scales, i.e., at high frequencies where $\omega > \omega_{cross}$, the movement of ions is sub-diffusive which means that the mean square displacement increases sublinearly with time [87] , ($<\Delta r^2(t)> \alpha$ $t^{0.35}$ [84] and the conductivity increases with frequency.

The overall conductivity behaviour follows a power law dependence (a. c. conductivity) against the angular frequency ω as proposed by Jonscher [88].

$$\sigma'(\omega) = \sigma_0 \left[1 + \left(\frac{\omega}{\omega_{cross}} \right)^s \right] \qquad (1.14)$$

Where s is a material and temperature dependent parameter, which allows to obtain ω_{cross}, and is used to take into account a low frequency tail that is influenced by both electrode or interfacial polarization. When the conductivity is not pure, $s < 1$, normally, $0.5 \leq s < 1$ [89].

For the description of the charge transport mechanism, the hopping of charge carriers is conceptualized in a random spatially varying potential landscape; unlike crystals, the potential-energy

landscape experienced by an ion in a disordered solid is irregular and contains a distribution of depths and barrier heights. Basically, the transport process is governed by the ability of charge carriers to overcome the randomly distributed barriers. On short time scales where the conduction regime is sub-diffusive only the smallest barriers overcome, which is a fast process, the main event being the back-and-forth jump between near energy minima.

As time passes, higher and higher barriers are overcome, and eventually the highest barriers too, achieving an infinite cluster of hopping sites, that determines the onset of dc conductivity and thus, of the diffusive regime. The frequency, ν, which characterizes this onset of the dc conductivity, is related to it by the empirical relation known as the Barton–Nakajima–Namikawa (BNN) relation, $\sigma_0 \sim 1/\tau_e$ [83], where , τ_e, is the attempt rate of the charge carriers to overcome the highest energy barrier. Therefore similar temperature dependencies for σ_0 and τ_e^{-1} are expected. To test this, the value of the attempt rate can be derived from the crossover frequency [90], $1/\tau_e = \omega_{cross} = 2\pi\nu_{cross}$; Figure 1.5 illustrates these features.
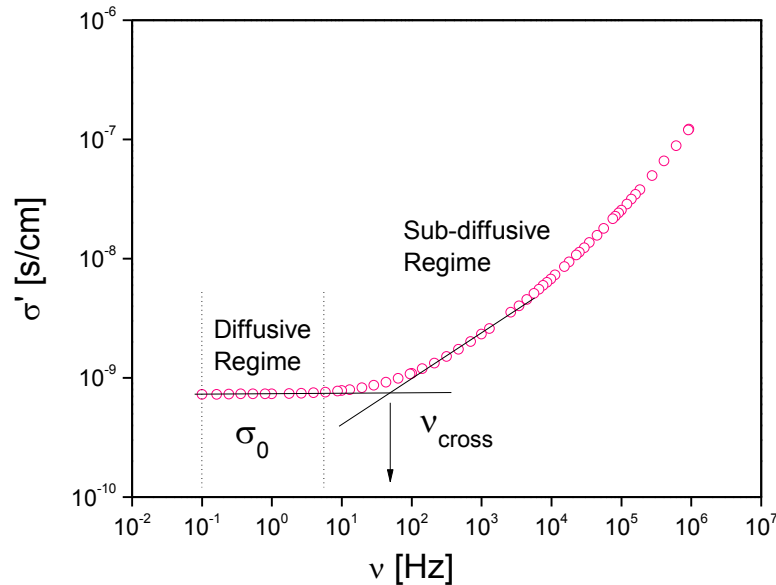
Figure 1.5 - Illustrative representation of frequency dependence of real conductivity at 193 K for IJ3.

The plot of $\sigma_0(T)$ versus $-\log\tau_e(T)$ gives a straight line with a slope equal to 1 being reported for a variety of ion conducting disordered systems [48], [91], confirming that the BNN relation is obeyed.

If it is demonstrated that the BNN relationship is followed , it is possible to separate the mobility, μ, and the effective number density, n, of charge carriers from σ_0 obtained from the dielectric measurements [48]:

$$\sigma_0 = nq\mu \qquad\qquad (1.15 - a)$$

This allows relating dc conductivity and the diffusion coefficient of migrating charges, D, considering the Nernst-Einstein equation

$$\mu = \frac{qD}{k_B T}$$ (1.15 - b)

as

$$\sigma_0 = \frac{nq^2}{k_B T} D$$ (1.15 - c)

Where q is the elementary charge of an electron and K_B the Boltzman constant.

By applying the fluctuation-dissipation theorem, Dyre $et\ al.$ [92] proposed the following expression to account for the relationship between σ_0 and n:

$$\sigma_0 = \frac{nq^2}{6k_B T} \frac{\langle \Delta r^2(t^*) \rangle}{\gamma H} v_{cross}$$ (1.16)

Where $\langle \Delta r^2(t^*) \rangle$ is the mean-square displacement as previously defined assuming similar jump rates for all ions, $\gamma \approx 2$ is a numerical factor reflecting the conductivity spectrum at the onset of ac conduction and H is an in principle time-scale-dependent Haven ratio [93], which accounts for cross correlations between the movements of different types of ions that for ILs can be approximated 1.5 [94] (see details on the deduction of the equation in ref. 23). The value predicted for the BMIM cation is in very good agreement with the literature [95].

The factor 6 in eq. 1.16 comes from 2d where d is the number of dimensions of the particle trajectory in the absence of electrical field; therefore, $d = 3$ since a tridimensional motion occurs in this type of disordered material.

Equations 1.16 and 1.15 - c give:

$$D = \frac{\langle \Delta r^2(t^*) \rangle}{6\gamma} v_{cross}$$ (1.17)

Since the tested systems comprise both cations and anions, the overall diffusion coefficients, obtained from dielectric data, can be decomposed into their individual components, i.e., D$_+$ and D$_-$ diffusion coefficients, and therefore, eq. 1.15 - c can be rewritten as:

$$\sigma_0 = \frac{q^2}{6.k_B T H}(n_+ D_+ + n_- D_-)$$ (1.18)

From equations 1.17 and 1.18 and considering that the number density of cations equals the number density of anions, i. e., $n_+ = n_- = n$, it is possible to obtain:

$$\sigma_0 = \frac{q^2 n}{k_B T} \cdot \frac{v_{cross}}{6\gamma H} (\langle \Delta r_+^2(t*) \rangle + \langle \Delta r_-^2(t*) \rangle) \qquad (1.19)$$

meaning that

$$D_+ = \frac{\langle \Delta r_+^2(t*) \rangle}{6\gamma} v_{cross} \qquad (1.20\text{-}a) \qquad\qquad D_- = \frac{\langle \Delta r_-^2(t*) \rangle}{6\gamma} v_{cross} \qquad (1.20\text{-}b)$$

and

where $\langle \Delta r_+^2(t*) \rangle$ and $\langle \Delta r_-^2(t*) \rangle$ are the mean-square displacements for the cation and anion, respectively.

Equations 1.15 – a) to 1.20 – a) and 1.20 – b) will be used to extract the transport properties of the ILs under study. This data treatment will be presented in chapters 3, 4 and 5.

1.3. Differential Scanning Calorimetry

The technique of Differential Scanning Calorimetry, DSC, was described by Emmett S. Watson and Michael J. O´Neill in 1962 [96]. Many physical and chemical transformations occur with absorption or release of heat. This is relevant for many different materials used in a wide range of applications, covering nanosciences [97], polymers [98], biomolecules [99], macromolecules [100] and the pharmaceutical field [101]. DSC will measure, as a function of temperature, the difference between the amount of heat required to increase the temperature of a sample and an inert reference material, which should have a well-defined heat capacity over the range of temperatures to which the samples are submitted to. Both sample and the reference material are maintained at nearly the same temperature during the control heating program. Depending on the amount of heat that must flow to the sample, the observed process can be energy-emitting (exothermic) or energy-absorbing (endothermic). For example, if a solid sample melts to the liquid state, which is an endothermic process, higher heat flow to the sample will be required in order to maintain its temperature constant during the transformation. On the other hand, in an exothermic process, such as crystallization, a lower heat flow is required in order to reach the sample temperature. DSC is a reliable technique to monitor phase changes and measure the amount of heat absorbed and released as those transitions take place.

First order transitions, such as melting and crystallization, characterized by a melting temperature (T_m) and crystallization temperature (T_c), respectively, have associated latent heats, i.e. at the temperature of the transition there are two phases present, each with its enthalpy. These transitions occur at constant temperature and thus the heat capacity of the system goes to infinity at T_m or T_c. In DSC, they appear as peaks. On the other hand, a second order transition, such as a glass

transition, characterized by a glass transition temperature (T_g), has no latent heat. In DSC, it appears as a step transition, as the sample structure changes from a glassy-like state to a rubber-like state, or vice-versa, reflecting a jump in the heat capacity of the sample at T_g. These phenomena and the way to obtain each one are presented in Figure 1.5.
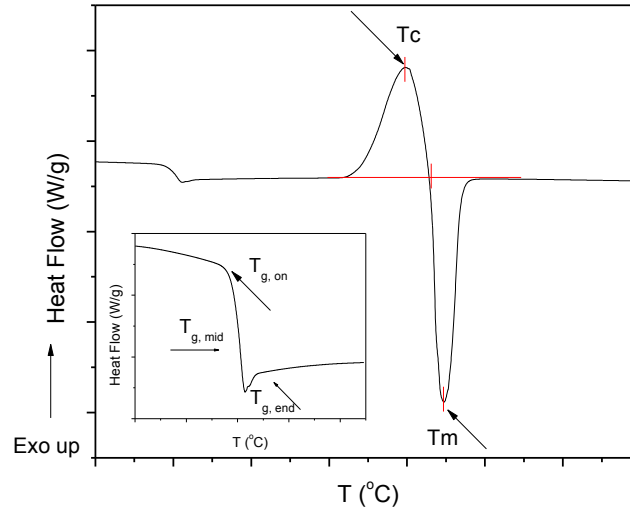
Figure 1.5 – A schematic DSC curve showing the crystallization temperature (T_c), the melting temperature (Tm) and the glass transition temperature (T_g) at the onset ($T_{g, on}$), midpoint ($T_{g, mid}$) and endset ($T_{g, end}$).

In some cases, T_g is not very well defined. Despite the fact that DSC assumes that the heat flow effect happens over a narrow range of temperatures, if the interval temperature where T_g is located is very broad, it becomes difficult to measure its value. Nevertheless, in this work, a different method will be used to determine T_g, namely the DRS technique. The discussion on the combination of techniques is presented in chapters 3, 4 and 5.

1.4. Bibliography

[1]   S. Trasatti, "1786-1986: Bicentennial of Luigi Galvani, Luigi most famous experiments," *Journal of Electroanalytical Chemistry and Interfacial Electrochemistry*, vol. 197, no. 1–2, pp. 1–4, 1986.

[2]   S. Trasatti, "1799 – 1999 : Alessandro Volta's ' Electric Pile' Two hundred years , but it doesn ' t seem like it," *Journal of Ectroanalytical Chemistry and Interfacial Electrochemistry*, vol. 460, no. 1–2, pp. 1–4, 1999.

[3]   M. A. De Paoli and W. a. Gazotti, "Electrochemistry, polymers and opto-electronic devices: a combination with a future," *Journal of the Brazilian Chemical Society*, vol. 13, no. 4, pp. 410–424, Aug. 2002.

[4]   E. I. Mal'tsev, D. A. Lypenko, O. M. Perelygina, V. F. Ivanov, O. L. Gribkova, M. A. Brusentseva, and A. V. Vannikov, "Molecular nanocrystals in polyaniline-based light-emitting diode structures," *Protection of Metals*, vol. 44, no. 5, pp. 443–446, Sep. 2008.

[5]   T. Carvalho, V. Augusto, A. R. Brás, N. M. T. Lourenço, C. A. M. Afonso, S. Barreiros, N. T. Correia, P. Vidinha, E. J. Cabrita, C. J. Dias, M. Dionísio, and B. Roling, "Understanding the ion jelly conductivity mechanism.," *The journal of physical chemistry. B*, vol. 116, no. 9, pp. 2664–76, Mar. 2012.

[6]   R. Shankar, T. K. Ghosh, and R. J. Spontak, "Dielectric elastomers as next-generation polymeric actuators," *Soft Matter*, vol. 3, no. 9, p. 1116, 2007.

[7]   H. J. Yen, H. Y. Lin, and G. S. Liou, "Novel Starburst Triarylamine-Containing Electroactive Aramids with Highly Stable Electrochromism in Near-Infrared and Visible Light Regions," *Chemistry of Materials*, vol. 23, no. 7, pp. 1874–1882, Apr. 2011.

[8]   J. Keith, "Liquid Electrolytes: Their Characterisation, Investigation, and Diverse Applications," in in *Molten Salts and Ionic Liquids Never the Twain?*, M. Gaune-Escard and K. R. Seddon, Eds. 2010.

[9]   T. M. Letcher, *Chemical Thermodynamics for Industry*. Royal Society of Chemistry, 2004, p. 82.

[10]   F. H. Hurley, U. S. Patent 4,446,331, 1948.

[11]   T. P. Wier Jr. and F. H. Hurley, U. S. Patent 4,446,350, 1948.

[12]   J. Yoke, J. Weiss, and G. Tollin, "Reactions of Triethylamine with Copper(I) and Copper(II) Halides," *Inorganic Chemistry*, vol. 2, no. 6, pp. 1210–1216, 1962.

[13]   C. G. Swain, A. Ohno, D. K. Roe, R. Brown, and T. Maugh, "Tetrahexylammonium Benzoate, a Liquid Salt at 25°C, a Solvent for Kinetics and Electrochemistry," *Journal of the American Chemical Society*, vol. 4492, no. 1964, pp. 2648–2649, 1967.

[14]   P. Wasserscheid and W. Keim, "Ionic Liquids-New 'Solutions' for Transition Metal Catalysis," *Angewandte Chemie (International ed. in English)*, vol. 39, no. 21, pp. 3772–3789, Nov. 2000.

[15]   J. Fuller, "The Room Temperature Ionic Liquid 1-Ethyl-3-methylimidazolium Tetrafluoroborate: Electrochemical Couples and Physical Properties," *Journal of The Electrochemical Society*, vol. 144, no. 11, p. 3881, 1997.

[16]   T. Frank, U. States, and A. Force, "Air and Water Stable I-Ethyl-3-methylimidazolium Based Ionic Liquids," *Journal of the Chemical Society, Chemical Communications*, no. 13, pp. 965–967, 1992.

[17]   Y. Zhou, J. H. Schattka, and M. Antonietti, "Room-Temperature Ionic Liquids as Template to Monolithic Mesoporous Silica with Wormlike Pores via a Sol−Gel Nanocasting Technique," *Nano Letters*, vol. 4, no. 3, pp. 477–481, Mar. 2004.

[18]   M. Galiński, A. Lewandowski, and I. Stępniak, "Ionic liquids as electrolytes," *Electrochimica Acta*, vol. 51, no. 26, pp. 5567–5580, Aug. 2006.

[19]   W. Lu, A. Goering, L. Qu, and L. Dai, "Lithium-ion batteries based on vertically-aligned carbon nanotube electrodes and ionic liquid electrolytes.," *Physical chemistry chemical physics : PCCP*, vol. 14, no. 35, pp. 12099–104, Sep. 2012.

[20]   H. Wang, S. Liu, N. Wang, and Y. Liu, "Vinylene Carbonate Modified 1-Butyl-3-Methyle-Imidazolium Tetrafluoroborate Ionic Liquid Mixture as Electrolyte," *International Journal of Electrochemical Science*, vol. 7, pp. 7579–7586, 2012.

[21]   T. Welton, "Room-temperature ionic liquids: solvents for synthesis and catalysis.," *Chemical reviews*, vol. 99, pp. 2071–2083, May 1999.

[22]   M. Hagen, S. Dörfler, H. Althues, J. Tübke, M. J. Hoffmann, S. Kaskel, and K. Pinkwart, "Lithium–sulphur batteries – binder free carbon nanotubes electrode examined with various electrolytes," *Journal of Power Sources*, vol. 213, pp. 239–248, Sep. 2012.

[23]   T. E. Sutto and T. T. Duncan, "Electrochemical and structural characterization of Mg ion intercalation into RuO2 using an ionic liquid electrolyte," *Electrochimica Acta*, vol. 79, pp. 170–174, Sep. 2012.

[24] W. Lu, A. G. Fadeev, B. Qi, E. Smela, B. R. Mattes, J. Ding, G. M. Spinks, J. Mazurkiewicz, D. Zhou, G. G. Wallace, D. R. MacFarlane, S. A. Forsyth, and M. Forsyth, "Use of ionic liquids for pi-conjugated polymer electrochemical devices," *Science (New York, N.Y.),* vol. 297, no. 5583, pp. 983–7, 2002.

[25] A. Fernicola, B. Scrosati, and H. Ohno, "Potentialities of ionic liquids as new electrolyte media in advanced electrochemical devices," *Ionics*, vol. 12, no. 2, pp. 95–102, 2006.

[26] P. Wasserscheid and T. Welton, *Ionic Liquids in Synthesis*. Wiley-VCH, 2002.

[27] P. Anastas and N. Eghbali, "Green chemistry: principles and practice," *Chemical Society Reviews*, vol. 39, no. 1, pp. 301–12, 2010.

[28] J. Yan, J. Liu, P. Jing, C. Xu, J. Wu, D. Gao, and Y. Fang, "Cholesterol-based low-molecular mass gelators towards smart ionogels.pdf," *Soft Matter*, vol. 8, pp. 11697–11703, 2012.

[29] S. Mekki, C. M. Wai, I. Billard, G. Moutiers, J. Burt, B. Yoon, J. S. Wang, C. Gaillard, A. Ouadi, and P. Hesemann, "Extraction of lanthanides from aqueous solution by using room-temperature ionic liquid and supercritical carbon dioxide in conjunction.," *Chemistry (Weinheim an der Bergstrasse, Germany)*, vol. 12, no. 6, pp. 1760–6, 2006.

[30] M. J. Earle, J. M. S. S. Esperança, M. a Gilea, J. N. C. Lopes, L. P. N. Rebelo, J. W. Magee, K. R. Seddon, and J. a Widegren, "The distillation and volatility of ionic liquids.," *Nature*, vol. 439, no. 7078, pp. 831–4, 2006.

[31] D. R. MacFarlane and K. R. Seddon, "Ionic Liquids — Progress on the Fundamental Issues," *ChemInform*, vol. 38, no. 23, pp. 3–5, 2007.

[32] W. Ogihara, S. Washiro, H. Nakajima, and H. Ohno, "Effect of cation structure on the electrochemical and thermal properties of ion conductive polymers obtained from polymerizable ionic liquids," *Electrochimica Acta*, vol. 51, no. 13, pp. 2614–2619, 2006.

[33] Y. Yoshida, O. Baba, and G. Saito, "Ionic Liquids Based on Dicyanamide Anion : Influence of Structural Variations in Cationic," *Journal of Physical Chemistry B*, vol. 111, pp. 4742–4749, 2007.

[34] J. Leys, M. Wübbenhorst, C. Preethy Menon, R. Rajesh, J. Thoen, C. Glorieux, P. Nockemann, B. Thijs, K. Binnemans, and S. Longuemart, "Temperature dependence of the electrical conductivity of imidazolium ionic liquids.," *The Journal of chemical physics*, vol. 128, no. 6, p. 064509, 2008.

[35]   O. Winther-Jensen, R. Vijayaraghavan, J. Sun, B. Winther-Jensen, and D. R. MacFarlane, "Self polymerising ionic liquid gel.," *Chemical communications (Cambridge, England)*, no. 21, pp. 3041–3, 2009.

[36]   Y. He, P. G. Boswell, P. Bühlmann, and T. P. Lodge, "Ion gels by self-assembly of a triblock copolymer in an ionic liquid.," *The journal of physical chemistry. B*, vol. 111, no. 18, pp. 4645–52, 2007.

[37]   C. Tiyapiboonchaiya, J. M. Pringle, D. R. MacFarlane, M. Forsyth, and J. Sun, "Polyelectrolyte-in-Ionic-Liquid Electrolytes," *Macromolecular Chemistry and Physics*, vol. 204, no. 17, pp. 2147–2154, 2003.

[38]   P. Vidinha, N. M. T. Lourenço, C. Pinheiro, A. R. Brás, T. Carvalho, T. Santos-Silva, A. Mukhopadhyay, M. J. Romão, J. Parola, M. Dionisio, J. M. S. Cabral, C. a M. Afonso, and S. Barreiros, "Ion jelly: a tailor-made conducting material for smart electrochemical devices.," *Chemical communications (Cambridge, England)*, no. 44, pp. 5842–4, 2008.

[39]   P. Vidinha, N. M. T. Lourenco, J. Cabral, I. Ribeiro, and C. Afonso, "Synthesis and application of a family of new materials resulting from the chemical cross-linking between gelatine and organic salts," 2008.

[40]   N. M. T. Lourenço, J. Österreicher, P. Vidinha, S. Barreiros, C. a. M. Afonso, J. M. S. Cabral, and L. P. Fonseca, "Effect of gelatin–ionic liquid functional polymers on glucose oxidase and horseradish peroxidase kinetics," *Reactive and Functional Polymers*, vol. 71, no. 4, pp. 489–495, 2011.

[41]   C. Cordas, N. M. T. Lourenço, P. Vidinha, C. Afonso, S. Barreiros, and L. Fonseca, "New conducting biomaterial based on Ion Jelly® technology for development of a new generation of biosensors," *New Biotechnology*, vol. 25, no. September, pp. S138–S139, 2009.

[42]   A. F. R. Pimenta, A. C. Baptista, T. Carvalho, P. Brogueira, N. M. T. Lourenço, C. A. M. Afonso, S. Barreiros, P. Vidinha, and J. P. Borges, "Electrospinning of Ion Jelly fibers," *Materials Letters*, vol. 83, pp. 161–164, 2012.

[44]   P. K. Varshney and S. Gupta, "Natural polymer-based electrolytes for electrochemical devices : a review," *Ionics*, vol. 17, no. 6, pp. 479–483, 2011.

[45]   H. Ohno, *Electrochemical Aspects of Ionic Liquids.* Hoboken, NJ, USA: John Wiley & Sons, Inc., 2011.

[46]   D. R. MacFarlane, J. Golding, S. Forsyth, M. Forsyth, and G. B. Deacon, "Low viscosity ionic liquids based on organic salts of the dicyanamide anion," *Chemical Communications*, no. 16, pp. 1430–1431, 2001.

[47]   C. Aliaga and S. Baldelli, "Sum frequency generation spectroscopy of dicyanamide based room-temperature ionic liquids. Orientation of the cation and the anion at the gas-liquid interface.," *The journal of physical chemistry. B*, vol. 111, no. 33, pp. 9733–40, 2007.

[48]   J. R. Sangoro, A. Serghei, S. Naumov, P. Galvosas, J. Kärger, C. Wespe, F. Bordusa, and F. Kremer, "Charge transport and mass transport in imidazolium-based ionic liquids," *Physical Review E*, vol. 77, no. 5, pp. 4–7, 2008.

[49]   K. Friedrich and S. Andreas, "Dielectric Spectroscopy of Reactive Network-Forming Polymers," in in *Broadband Dielectric Spectroscopy*, 2003.

[50]   M. Teresa and V. Plaza, "Molecular mobility of n-ethylene glycol dimethacrylate glass formers upon free radical polymerization," Universidade Nova de Lisboa/Faculdade de Ciências e Tecnologia, 2007.

[51]   "Application note 1217-1, (1992) 'Basics of measuring the dielectric properties of materials,' Hewlett Packard Literature Number 5091-3300E."

[52]   G. Gallone, J. Levita, S. Mijovic, S. Andjelic, and P. A. Rolla, "Anomalous trends in conductivity during epoxy-amine reactions," *Polymer*, vol. 39, no. 11, pp. 2095–2102, 1998.

[53]   A. Schonhals and F. Kremer, "Theory of Dielectric Relaxation," in in *Broadband Dielectric Spectroscopy*, 2003, p. chpater 1.

[54]   P. Salamon, N. Éber, J. Seltmann, M. Lehmann, J. Gleeson, S. Sprunt, and a. Jákli, "Dielectric technique to measure the twist elastic constant of liquid crystals: The case of a bent-core material," *Physical Review E*, vol. 85, no. 6, pp. 1–9, 2012.

[55]   Y. Du, Y. Lv, C. Li, M. Chen, Y. Zhong, J. Zhou, X. Li, and Y. Zhou, "Effect of Semiconductive Nanoparticles on Insulating Performances of Transformer Oil," no. March, pp. 770–776, 2012.

[56]   K. Adrjanowicz, D. Zakowiecki, K. Kaminski, L. Hawelek, K. Grzybowska, M. Tarnacka, M. Paluch, and K. Cal, "Molecular dynamics in supercooled liquid and glassy states of antibiotics: azithromycin, clarithromycin and roxithromycin studied by dielectric spectroscopy. Advantages given by the amorphous state.," *Molecular pharmaceutics*, vol. 9, no. 6, pp. 1748–63, 2012.

[57]   J. R. Sangoro and F. Kremer, "Liquids," *Accounts of Chemical Research*, vol. 45, no. 4, pp. 525–532, 2012.

[58] K. S. Patel, P. A. Kohl, and S. Bidstrup-allen, "Three-Dimensional Dielectric Characterization of Polymer Films," pp. 2328–2334, 2001.

[59] R. Rai and K. B. Varma, "Thermal and dielectric studies on binary organic system: benzil–m-nitroaniline," *Materials Letters*, vol. 48, no. 6, pp. 356–361, May 2001.

[60] A. M. Castagna, D. Fragiadakis, H. Lee, T. Choi, and J. Runt, "The Role of Hard Segment Content on the Molecular Dynamics of Poly (tetramethylene oxide) -Based Polyurethane Copolymers," pp. 7831–7836, 2011.

[61] E. Laredo, D. Newman, A. Bello, and A. J. Müller, "Primary and secondary dielectric relaxations in semi-crystalline and amorphous starch," *European Polymer Journal*, vol. 45, no. 5, pp. 1506–1515, 2009.

[62] A. Kahouli, A. Sylvestre, F. Jomni, E. André, J. L. Garden, B. Berge, and J. Legrand, "Dielectric properties of parylene AF4 as low-k material for microelectronic applications," *Thin Solid Films*, vol. 520, no. 7, pp. 2493–2497, 2012.

[63] H. Watanabe, Q. Chen, Y. Kawasaki, Y. Matsumiya, T. Inoue, and O. Urakawa, "Entanglement Dynamics in Miscible Polyisoprene/Poly(p - tert -butylstyrene) Blends," *Macromolecules*, p. 110218184831037, 2011.

[64] Q. Chen, Y. Matsumiya, and H. Watanabe, "Dynamics in miscible blends of polyisoprene and poly(p-tert-butyl styrene): thermo–rheological behavior of components," *Polymer Journal*, vol. 44, no. 1, pp. 102–114, 2011.

[65] R. R. Mocellini, O. A. Lambri, C. L. Matteo, and P. A. Sorichetti, "Dielectric properties and viscoelastic response in two-phase polymers," *IEEE Transactions on Dielectrics and Electrical Insulation*, vol. 15, no. 4, pp. 982–993, 2008.

[66] A. Zetsche and E. N. Fischer, "Dielectric Studies of the Alpha - Relaxation in Miscible Polymer Blends and its Relaxation to Concentration Flutuations," *Acta Polymerica*, vol. 45, no. 3, pp. 168–175, 1994.

[67] M. C. Herna, E. Laredo, A. Bello, P. Carrizales, L. Marcano, V. Balsamo, M. Grimau, and A. J. Mu, "From Miscible to Immiscible Polycarbonate / Poly (-caprolactone) Blends," pp. 7301–7313, 2002.

[68] M. M. Pradas and J. M. M. Duenas, "Conformational Motions in Immiscible Blends of Po I," *Polymer Engineering and Science*, vol. 39, no. 4, pp. 688–698, 1999.

[69]   W. G. F. Sengers, O. van den Berg, M. Wübbenhorst, A. D. Gotsis, and S. J. Picken, "Dielectric spectroscopy using dielectric probes: a new approach to study glass transition dynamics in immiscible apolar polymer blends," *Polymer*, vol. 46, no. 16, pp. 6064–6074, 2005.

[70]   A. Boersma, J. Van Turnhout, and M. Wu, "Dielectric Characterization of a Thermotropic Liquid Crystalline Copolyesteramide: 1. Relaxation Peak Assignment," *Macromolecules*, vol. 31, pp. 7453–7460, 1998.

[71]   J. J. M. Correia, N. T. Ramos, "Dipolar Motions and Phase Transitions in a Side-Chain Polysiloxane Liquid Crystal . A Study by Thermally Stimulated Depolarization Currents," *Journal of Polymer Science: Part B: Polymer Physics*, vol. 37, pp. 227–235, 1998.

[72]   A. Dimopoulos, J. L. Wietor, M. Wübbenhorst, S. Napolitano, R. A. T. M. van Benthem, G. de With, and R. P. Sijbesma, "Enhanced Mechanical Relaxation below the Glass Transition Temperature in Partially Supramolecular Networks," *Macromolecules*, vol. 43, no. 20, pp. 8664–8669, 2010.

[73]   S. Polymers, M. Wubbenhorst, and J. Van Turnhout, "Complex Dynamics of Hydrogen Bonded," *IEEE Transactions on Dielectrics and Electrical Insulation*, vol. 8, no. 3, 2001.

[74]   S. Choudhary and R. J. Sengwa, "Dielectric spectroscopy and confirmation of ion conduction mechanism in direct melt compounded hot-press polymer nanocomposite electrolytes," *Ionics*, vol. 17, no. 9, pp. 811–819, 2011.

[75]   M. Dionisio and J. F. Mano, "Electrical Techniques," in in *Handbook of Thermal Analysis and Calorimetry*, 5th ed., Elsevier, 2008, pp. 209–268.

[76]   P. Debye, "Polar Molecules. Chemical Catalog, reprinted by Dover." 1929.

[77]   S. D. Senturia and N. F. Sheppard Jr, "Dielectric Analysis of Thermoset Cure," *Advances in Polymer Science*, vol. 80, pp. 1–47, 1986.

[78]   K. S. Cole and R. H. Cole, "Dispersion and Absorption in Dielectrics I. Alternating Current Characteristics," *The Journal of Chemical Physics*, vol. 9, no. 4, p. 341, 1941.

[79]   K. S. Cole and R. H. Cole, "Dispersion and Absorption in Dielectrics I. Alternating Current Characteristics," *The Journal of Chemical Physics*, vol. 9, no. 4, p. 341, 1941.

[80]   D. W. Davidson and R. H. Cole, "Dielectric Relaxation in Glycerine," *The Journal of Chemical Physics*, vol. 18, no. 10, p. 1417, 1950.

[81]   S. Havriliak and S. Negami, "A complex plane analysis of alpha-dispersion in some polymer systems," *Jounal of Polymer Science*, no. 14PC, p. 99–&, 1966.

[82] A. Schonhals and F. Kremer, "Analysis of Dielectric Spectra," in in *Broadband Dielectric Spectroscopy*, 2002, pp. 59 – 96.

[83] F. Kremer and S. A. Rozanski, "The Dielectric Properties of Semiconducting Disordered Materials," in in *Broadband Dielectric Spectroscopy*, 2002, pp. 475 – 493.

[84] B. Roling, "Conductivity spectra of disordered ionic conductors : Calculating the time-dependent mean square displacement of the mobile ions introduction," *Dielectrics Newsletter*, no. November, pp. 1–8, 2002.

[85] T. Carvalho, V. Augusto, a R. Brás, N. M. T. Lourenço, C. a M. Afonso, S. Barreiros, N. T. Correia, P. Vidinha, E. J. Cabrita, C. J. Dias, M. Dionísio, and B. Roling, "Understanding the ion jelly conductivity mechanism.," *The journal of physical chemistry. B*, vol. 116, no. 9, pp. 2664–76, 2012.

[86] J. Dyre and J. Jacobsen, "Universal time dependence of the mean-square displacement in extremely rugged energy landscapes with equal minima.," *Physical review. E, Statistical physics, plasmas, fluids, and related interdisciplinary topics*, vol. 52, no. 3, pp. 2429–2433, 1995.

[87] B. Roling, *Charge Transport in Disordered Solids with Applications in Electronics*. John Wiley & Sons, 2006, 2006, p. 382.

[88] A. K. Jonscher, "Universal Dielectric Response," *Nature*, vol. 267, no. 5613, pp. 673–679, 1977.

[89] F. Kremer and S. A. Rozanski, "The Dielectric Properties of Semiconducting Disordered Materials," in in *Broadband Dielectric Spectroscopy*, Springer-V., Berlin, Germany, 2003, pp. 475–494.

[90] J. Sangoro, C. Iacob, a Serghei, S. Naumov, P. Galvosas, J. Kärger, C. Wespe, F. Bordusa, a Stoppa, J. Hunger, R. Buchner, and F. Kremer, "Electrical conductivity and translational diffusion in the 1-butyl-3-methylimidazolium tetrafluoroborate ionic liquid.," *The Journal of chemical physics*, vol. 128, no. 21, p. 214509, 2008.

[91] J. Sangoro, C. Iacob, a Serghei, S. Naumov, P. Galvosas, J. Kärger, C. Wespe, F. Bordusa, a Stoppa, J. Hunger, R. Buchner, and F. Kremer, "Electrical conductivity and translational diffusion in the 1-butyl-3-methylimidazolium tetrafluoroborate ionic liquid.," *The Journal of chemical physics*, vol. 128, no. 21, p. 214509, 2008.

[92]   J. C. Dyre, P. Maass, B. Roling, and D. L. Sidebottom, "Fundamental questions relating to ion conduction in disordered solids," *Reports on Progress in Physics*, vol. 72, no. 4, p. 046501, 2009.

[93]   B. Roling, C. Martiny, and S. Murugavel, "Ionic Conduction in Glass: New Information on the Interrelation between the 'Jonscher Behavior' and the 'Nearly Constant-Loss Behavior' from Broadband Conductivity Spectra," *Physical Review Letters*, vol. 87, no. 8, pp. 1–4, 2001.

[94]   T. Frömling, M. Kunze, M. Schönhoff, J. Sundermeyer, and B. Roling, "Enhanced lithium transference numbers in ionic liquid electrolytes.," *The journal of physical chemistry. B*, vol. 112, no. 41, pp. 12985–90, 2008.

[95]   J. R. Sangoro, C. Iacob, S. Naumov, R. Valiullin, H. Rexhausen, J. Hunger, R. Buchner, V. Strehmel, J. Kärger, and F. Kremer, "Diffusion in ionic liquids: the interplay between molecular structure and dynamics," *Soft Matter*, vol. 7, no. 5, p. 1678, 2011.

[96]   E. S. Watson and M. J. O'Neill, "Differential Microcalorimeter," 1962.

[97]   P. Gill, T. T. Moghadam, and B. Ranjbar, "Differential scanning calorimetry techniques: applications in biology and nanoscience.," *Journal of biomolecular techniques : JBT*, vol. 21, no. 4, pp. 167–93, Dec. 2010.

[98]   C. Schick, "Differential scanning calorimetry (DSC) of semicrystalline polymers.," *Analytical and bioanalytical chemistry*, vol. 395, no. 6, pp. 1589–611, Dec. 2009.

[99]   G. Bruylants, J. Wouters, and C. Michaux, "Differential scanning calorimetry in life science: thermodynamics, stability, molecular recognition and application in drug design.," *Current medicinal chemistry*, vol. 12, no. 17, pp. 2011–20, Jan. 2005.

[100]   M. H. Chiu and E. J. Prenner, "Differential scanning calorimetry: An invaluable tool for a detailed thermodynamic characterization of macromolecules and their interactions.," *Journal of pharmacy & bioallied sciences*, vol. 3, no. 1, pp. 39–59, Jan. 2011.

[101]   S. Mathkar, S. Kumar, a Bystol, K. Olawoore, D. Min, R. Markovich, and a Rustum, "The use of differential scanning calorimetry for the purity verification of pharmaceutical reference standards.," *Journal of pharmaceutical and biomedical analysis*, vol. 49, no. 3, pp. 627–31, May 2009.

Chapter 2

EXPERIMENTAL SECTION

2. EXPERIMENTAL SECTION

2.1 Materials

The RTILs BMIMDCA (IL-0010-HP), $C_{10}H_{15}N_5$ (MW, 205.26; density$_{298\ K}$[1]=1.058 g cm^{-3}, purity >98%), EMIMDCA (IL-0003-HP), $C_8H_{11}N_5$ (MW, 177.21; density$_{298\ K}$=1.110 g cm^{-3}, purity >98%), BMPyrDCA (IL-0041-HP), $C_{11}H_{20}N_4$ (MW, 208.30; density$_{298\ K}$=1.013 g cm^{-3}, purity >98%) and 1-ethyl-3-methyl imidazolium ethylsulfate (EMIMEtSO$_4$) (IL-0033-HP), $C_8H_{16}N_2O_4S$ (MW 236.29; density$_{298\ K}$=1.240 g cm^{-3}, purity >98%) were provided by Iolitec. The RTIL 1-butyl-3-methyl imidazolium bromide (BMIMBr) (64133), $C_8H_{15}BrN_2$ (MW, 219.12; density$_{298\ K}$=1.300 g cm^{-3}, 97%) was provided by Sigma-Aldrich. The RTIL BPyDCA was kindly provided by Ângelo Rocha (*Instituto Superior Técnico, Portugal)*.

Ethyl acetate (109623), $C_4H_8O_2$ (MW, 88.11; density$_{293\ K}$=0.900 g cm^{-3}), Acetone (100014), C_3H_6O (MW, 58.08; density$_{293\ K}$=0.790 g cm^{-3}), Chloroform (102445), CHCl$_3$ (MW, 119.38; density$_{293\ K}$=1.480 g cm^{-3}), Ethanol (100983), C_2H_6O (MW, 46.07; density$_{293\ K}$=0.790 – 0.793 g cm^{-3}), Hexane (104374), C_6H_{14} (MW, 86.18; density$_{293\ K}$=0.660 g cm^{-3}), Methanol (106009), CH$_4$O (MW, 32.04; density$_{293\ K}$=0.792 g cm^{-3}) and Toluene (108325), C_7H_8 (MW, 92.14; density$_{293\ K}$=0.870 g cm^{-3}) were provided by Merck. All materials were used as received. Gelatine (403 902) was purchased from Panreac. All materials were used as received.

2.2. Ion Jelly preparation

To prepare IJ1 (IJ3), 100 µL (300 µL) of IL was heated to 313 K under magnetic stirring, followed by the addition of 120 mg of gelatine; the designation 1 and 3 in the IJ materials gives the ratio of BMIMDCA/gelatine in the starting mixture. In order to obtain a homogeneous mixture, 206 µL (75 µL) of water was added dropwise. The mixtures were kept stirring at 313 K until the gelatine was completely solubilized (approximately 15 min). The solutions were then spread over a glass surface in order to form thin films. Jellification occurs at room temperature.

To have a blank for comparison on the influence of gelatine, a gelatine film was prepared by adding 120 mg of gelatine to 1012 µL of water at 313 K under magnetic stirring in order to obtain a homogeneous mixture. The solution was also spread over a glass surface at room temperature to form a film.

2.3. Techniques

2.3.1. Karl Fischer titration

Karl Fischer titration was used to determine the water content in each final material, of chapters 3, 4 and 5, as IJ1-12.2%, IJ3-6.6%, BMIMDCA-1.9% as received (w/w), ILs 0.4% as received (w/w), ILs 9%, ILs 12%, ILs 30% and IJs 9%; the water content in the gelatin film was determined to be 22%

(w/w). No lower water amounts were possible to achieve gelatine films; otherwise, no self-supported films are obtained.

To evaluate the effluence of water in conductive and transport properties, water was added to the received IL until a final content of 6.6% (w/w) (chapter 3), 9% (w/w) (chapter 4) and 9%, 12% and 30% (w/w) (chapter 5) was achieved (quantified by Karl Fischer titration) having the same water amount as IJ3; For the IJ materials it was achieved a final content of 6.6% (w/w) (chapter 3) and 9% (w/w) (chapter 4).

The final composition of the IJ materials is thus IJ1-IL/gelatin/water=41.1/46.7/12.2% (w/w) and IJ3-IL/gelatin/water=67.8/25.6/6.6% (w/w).

In chapter 4 the water content was determined for all the twelve systems, as we can see in table 2.1.

Table 2.1 – Water content on the neat IL, aqueous solutions and respective IJs (chapter 4).

IL	H_2O %	Average (%)
BMIMDCA	0.40%	0.35±0.09
	9%	8.72±0.05
EMIMDCA	0.40%	0.38±0.02
	9%	8.58
BPyDCA	0.40%	0.44±0.10
	9%	9.66±0.11
BMPryDCA	0.40%	0.39±0.08
	9%	9.65±0.12

IJ	H_2O %	Average (%)
BMIMDCA	9%	8.88±0.18
EMIMDCA	9%	10.4
BPyDCA	9%	9.45±0.44
BMPyrDCA	9%	9.54±0.07

For chapter 5, the water content on the neat IL and the aqueous solutions, were also determined:

Table 2.2 – Water content on the neat IL and the aqueous solutions (chapter 5).

IL	H_2O %	Average (%)
BMIMDCA	0.40%	0.50±0.10
	9%	9.25±0.32
	12%	12.66±0.58
	30%	29.70±0.61
EMIMDCA	0.40%	0.51±0.17
	9%	9.15±0.44

	12%	12.58±0.62
	30%	29.90±0.97
EMIMEtSO$_4$	0.40%	0.44±0.10
	9%	9.28±0.58
	12%	12.30±0.83
	30%	30.73±1.45
BMPryDCA	0.40%	0.39±0.08
	9%	9.48±0.16
	12%	12.43±0.51
	30%	30.67±2.70

2.3.2 Van der Waals radii

The van der Waals radii were estimated by the using an Hartree−Fock ab initio method provided by the Spartan Student (V4.1.2) commercially available software and molecular volumes were estimated (the following table presents the estimated values).

Table 2.3 – Van de Waals radii and cation volumes for the ILs tested in the present work (chapters 4 and 5).

cation	vdW radius[a] /Å	Cation volume[b]/Å^3	Molecular volume[c] cm^3.mol^{-1}
EMIM	2.9	134.6	184.5
BMIM	3.3	171.8	206.9
BMPyr	3.7	169.5	205.5
BPy	3.8	184.3	214.5

[a] estimated by Spartan Student (V4.1.2)

2.3.3 Dielectric Relaxation Spectroscopy

This section describes the equipment used to perform the analysis used in DRS, DSC and NMR, being DRS the main technique employed in this work. The used impedance analyzer was the Alpha-N analyzer from Novocontrol GmbH, available in the laboratory 122 of Chemical Department of *Faculdade de Ciências e Tecnologia* from *Universidade Nova de Lisboa*. For the DSC measurements two devices were used: *i*) SETARAM DSC 131 available in the Chemical Department of the same university; *ii*) DSC Q2000 from TA Instruments Inc. (Tzero™ DSC technology) available in the laboratory 122 of Chemical Department too.

Equivalent Circuits on DRS:

In order to obtain the dielectric information of a given material, it is used an electric circuit with several components which simulate the response of the material. This model circuit is known as *equivalent circuit.* The loss part of dielectric response is represented by a resistance $R(x)$, while the introduction of a capacitance $C(x)$ plays the role of the storage material, i. e., the ability to store the electric field. In such a way, the overall admittance $Y(x)$ and impedance $Z(x)$ in a resistor - capacitor (RC) circuit is given by the sum of the contributions of both elements:

$$Y(\omega) = \frac{1}{Z(\omega)} = \frac{1}{R_p(\omega)} + i\omega C_p(\omega) = \frac{1}{R_s(\omega) + \frac{1}{i\omega C_s(\omega)}}$$

Equation 2.1

Where sub index *P* and *S* correspond to parallel and series circuit respectively, i is $\sqrt{-1}$ and ω is the angular frequency (this equivalence does not apply to d.c. step function experiments[2]). The measured values will depend on the geometry of the sample. As that is localized between a parallel capacitor, the factors to be considered are the plate area A and separation d (with $A \gg d$). In order to avoid this influence, the dielectric properties of the material are expressed in terms of dielectric permittivity (sometimes with conductivity) using the relation $\varepsilon * (\omega) = C * (\omega)/C_0$. Here, $C_0 = A\varepsilon_0/d$ is the vacuum capacitance of the parallel plate capacitor and $C *$ is the complex capacitance of the same capacitor filled with the material under study. If a sinusoidal electric field is applied, the complex permittivity relates to the impedance through:

$$\varepsilon * (\omega) = \frac{1}{i\omega Z(\omega) C_0}$$

Equation 2.2

When one is in the presence of a material with a Debye response, i. e. with a relaxation process with a single relation time, the simplest equivalent circuit consists in one resistance R_1 associated in series with the capacitance C_1. For describing this instantaneous polarization due to atomic and electronic contributions, a capacitance, C_∞ associated in parallel with those components must be included[3] (see Figure 2.1). To describe this situation, equation 2.3 (for series elements) must be introduced in equation above:

$$\varepsilon * (\omega) = \frac{C_\infty}{C_0} + \frac{1}{i\omega C_0 \left[R_s(\omega) + \frac{1}{i\omega C_s(\omega)} \right]} = \varepsilon_\infty + \frac{1}{i\omega C_0 R_s(\omega) + \frac{C_0}{C_s(\omega)}}$$

$$= \varepsilon_\infty + \frac{\frac{C_s(\omega)}{C_0}}{i\omega C_s(\omega) R_s(\omega) + 1}$$

Equation 2.3

(a)   (b)   (c)
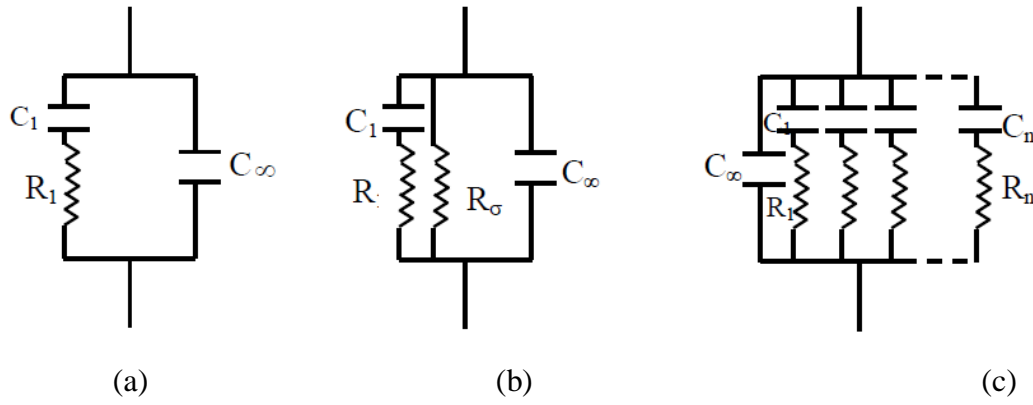
Figure 2.1– Circuit diagrams for a material exhibiting: (a) a relaxation process with a single relaxation time and induced polarization, (b) a relaxation process with a single relaxation time, conduction and induced polarization and (c) a distribution of relaxation times and induced polarization (reproduced from reference[4].

where ε_∞ denotes the quotient C_∞/C_0. In the last expression the relaxation time of the equivalent RC circuit as $\tau_{RC} = R_s C_s$ and $\varepsilon_0 - \varepsilon_\infty$ as the fraction C_∞/C_0 can be identified, rewriting equation 2.3, we obtain:

$$\varepsilon * (\omega) = \varepsilon_\infty + \frac{\varepsilon_0 - \varepsilon_\infty}{1 + i\omega\tau_{RC}}$$ **Equation 2.3**

which is a typical representation of complex permittivity for a material that responds according the Debye function.

Additionally, if a translational diffusion of mobile charges occurs, i. e. if the material exhibits conductions, like the materials study in this work, the term $1/R_\sigma$ must be introduced in the overall impedance leading to a complex permittivity as:

$$\varepsilon *= \frac{C_\infty}{C_0} + \frac{1}{i\omega C_0 \left[R_s(\omega) + \frac{1}{i\omega C_s(\omega)} + \frac{1}{R_\sigma} \right]} = \varepsilon_\infty + \frac{\varepsilon_0 - \varepsilon_\infty}{1 + i\omega\tau_{RC}} - \frac{i}{\omega C_0 R_\sigma}$$ **Equation 2.5**

The conduction process appears as a low frequency tail in the plot of ε'', giving a value for $C_0 R_\sigma = \varepsilon_0/\sigma_0$, being σ_0 the frequency independent specific conductivity. The equivalent circuit is presented in figure 2.1 (b).

2.3.3.1 Impedance Analyzers

Samples were prepared in parallel plate geometry between two gold and stainless steel-plated electrodes with diameter of 10 mm in the frequency range from 10^{-1} to 10^6 Hz.

2.3.3.2 Alpha High Resolution Impedance Analyzer and Temperature Control

The Alpha-N Analyzer measures the impedance or complex permittivity function of materials at frequencies between 3 µHz and 10 MHz with high precision.

It is possible to distinguish two main parts in this analyzer:

1. A frequency response analyzer with a sine wave and two a. c. voltage input channels. Each input channel measures the a. c. voltage amplitude of an applied sine wave, i. e. they measure the amplitude and phase angle of the harmonic base wave component of the signal. The phase shift between the sine waves applied to the both inputs is also detected.

2. A dielectric (or impedance) converter with a wide dynamic range current to voltage converter and a set of precision reference capacitors. This dielectric converter is mounted inside the Alpha analyzer mainframe.

For electric material measurements and additional dielectric sample cell is required. The BDS1200 sample cell from Novocontrol was employed for the measurements. It is suitable for low frequency DC to 10 MHz. It includes PT100 temperature sensor localized inside the inferior electrode. It can work in the temperature range from 113 K (-160 °C) to 723K (450 °C). This cell is connected to the Alpha-N analyzer by two wires BNC. These BNC cables have the disadvantage of limiting the performance at high frequencies (up to MHz).

Principles of operation

The Alpha-N analyzer is used with both frequency response analyzer (FRA) a dielectric converter. This component measures the response of a system to a harmonic (sinusoidal) excitation. Both excitation and the response signals are voltages. The response signal is analyzed by Fourier transform, being of special interest the amplitude and phase angle of the sinusoidal base wave with respect to the excitation signal.

The basic principle of measurement of the internal Alpha current to voltage converter used for impedance measurements is show in Figure 2.2.
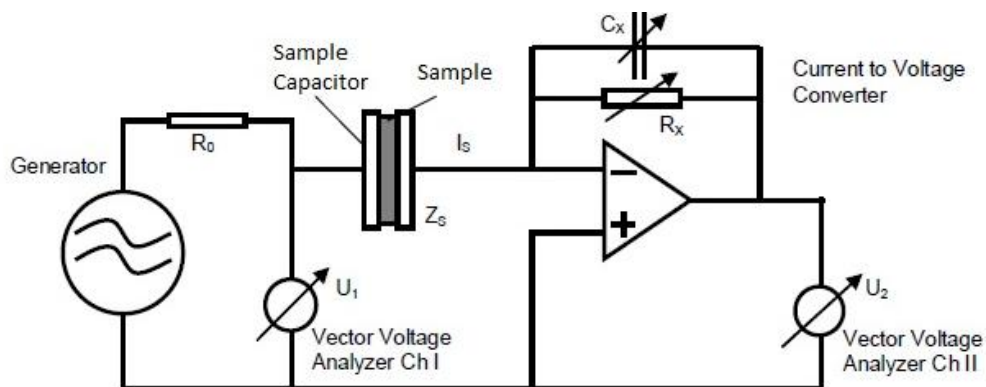
Figure 2.2– Principle of the impedance measurement (reproduced from reference [5]).

The a. c. voltage from the generator is applied to the sample and measured in amplitude and phase as U_1. The resistor R_0 (50 Ω) limits the sample current if the sample impedance becomes too low. The sample current I_S feeds in the inverting input of an operational amplifier which as the variable capacity C_x (100-470 pF) and the resistor R_x (it switches 30 Ω, 100 Ω and 1T Ω) in its feedback loop. The Alpha analyzer selects a combination of C_x and R_x in such a way that the output voltage U_2 is in good measurable range of the voltage input channels (3 V – 30 mV). For ideal components, U_2 is related to the sample current I_S by:

$$I_S = -\frac{U_2}{Z_x}$$

Where $Z_x = (R_x - 1 + i\omega C_x)^{-1}$ and $\omega = 2\pi f$. For an ideal operational amplifier, the voltage at the input is 0 V with respect to ground and therefore U_1 to the voltage over the sample capacitor. By this way, the sample impedance Z_S

$$Z_S = \frac{U_1}{I_S} = -\frac{U_1}{U_2} Z_x$$

The impedance Z_S relates to the complex dielectric permittivity through the equation 2.2.

Temperature Control

The temperature control was made by the QUATRO modulus from Novocontrol. This temperature controller is connected to the Alpha-N analyzer as schematized in Figure 2.3.
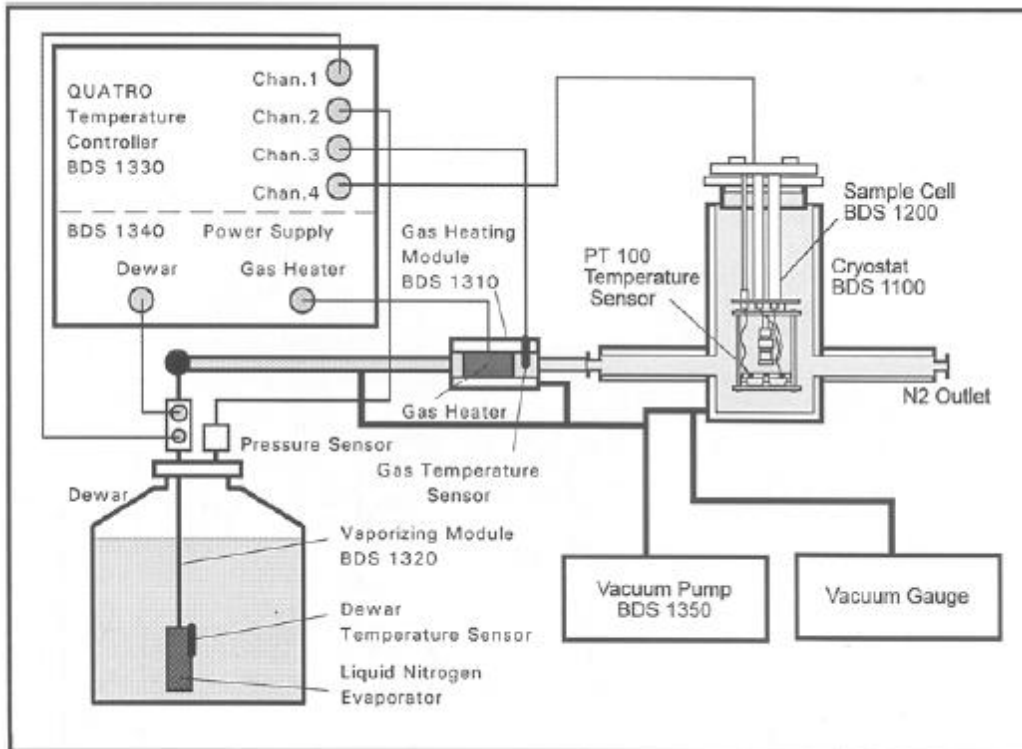
Figure 2.3 – Temperature control device and its connection to the sample cell (reproduced from reference [5]).

The QUATRO controller has four circuits controlling the sample temperature, the gas temperature, the temperature of the liquid nitrogen in the dewar and the pressure in the dewar. The sample temperature is reached by heating the nitrogen gas with a precision that can be of $\pm$ 0.01K. All the nitrogen passing circuit is isolated by a vacuum chamber whose pressure is measured.

Both the acquisition data and temperature control are carried out by the software WinDETA also from Novocontrol.

The data treatment was carried out by the software origin considering the VFT and Jonscher fitting functions [6].

For the dielectric relaxation spectroscopy measurements, films were cut into disks of about 10 10 mm in diameter. The films thickness was 0.5 and 0.7 mm, respectively, for IJ1 and IJ3; no thinner films were possible to obtain being the thickness limited by the formation of a self-supported gelatin film. For BMIMDCA samples, two silica spacers of 0.05 mm thickness were used. The samples were placed between two gold plated electrodes (10 mm diameter) in a parallel plate capacitor, BDS 1200. The sample cell was mounted on a cryostat, BDS 1100, and exposed to a heated gas stream being evaporated from liquid nitrogen in a Dewar. The temperature control was assured by the Quatro Cryosystem and performed within ±0.5 K (all modules supplied by Novocontrol). Measurements were carried out using as Alpha N analyzer also from Novocontrol GmbH, covering a frequency range from 10^{-1} Hz to 1 MHz. After a first cooling ramp from room temperature to 163 K, isothermal spectra were collected in steps of 5 K up to 248 K (IJ1) and 303 K (IJ3). Both BMIMDCA were isothermally measured from 143 K up to 213 K; from 143 K to 153 K in steps of 5 K and from 153 K to 213 K in steps of 2 K.

The dielectric relaxation data obtained were deconvoluted using a sum of the model function introduced by Havriliak-Negami[7]

$$\varepsilon^*(\omega) = \varepsilon_\infty + \sum_j \frac{\Delta\varepsilon_j}{\left[1 + \left(i\omega\tau_j\right)^{\alpha_{HNj}}\right]^{\beta_{HNj}}}$$

where j is the number of relaxation process, $\Delta\varepsilon = \varepsilon_s - \varepsilon_\infty$ is the dielectric strength, i. e., the difference between the real permittivity values at, respectively, the low and high frequency values, τ_{HN} is the relaxation time, and α_{HN} and β_{HN} are the shape parameters (0<α_{HN}<1; 0<$\alpha_{HN}\beta_{HN}$<1). Since date are strongly influenced by the low frequency conductivity contribution, an additional term $i\sigma/\omega^c\varepsilon_0$ was added to the dielectric loss, where ε_0 is the vacuum permittivity; σ and *c* are fitting parameters: σ is related to the dc conductivity of the sample, and the parameter *c* (0 < *c* ≤ 1) reflects conductivity of ions for *c* = 1 and for *c* < 1 interfacial polarizations, including electrode polarization.

2.3.4 Differential Scanning Calorimetry

The calorimetric experiments were carried out with a DSC Q2000 from TA Instruments Inc. (Tzero™ DSC technology) operating in the Heat Flow T4P option (details can be found in reference

[8]. The melting heat of indium was used for calibrating heat flow. Sample ~26 mg were placed in open aluminum pans; an empty aluminum pan was used as reference. Dry high purity N_2 gas was purged through the samples during the measurements. The two IJ and gelatin were analyzed. Thermograms were collected, after a previous cooling run down to 123 K, upom heating to 363 K at a rate of 20 K min^{-1}. This relatively high heating rate was chosen to enhance the heat capacity step in the IJ materials, mainly in IJ1 for which the jump is quite broad;

Measurements were realized under dry high purity helium at flow rate of 50 mL·min^{-1}; a liquid nitrogen cooling system (LNCS) was used in order to reach temperatures as low as 123 K. DSC Tzero calibration was carried out in the temperature range from 108 K to 573 K. It requires two experiments: the first run with the empty cell (baseline) and the second run with equal weight sapphire disks on the sample and reference platforms (without pans). This procedure allows for cell resistance and capacitance calibration which compensates for subtle differences in thermal resistance and capacitance between the reference and sample platforms in the DSC sensor. Enthalpy (cell constant) and temperature calibration were based on the melting peak of indium standard (T_m = 429.75 K) supplied by TA Instruments (Lot #E10W029). Small amount of samples (less than 5 mg) were encapsulated in Tzero (aluminium) hermetic pans with a Tzero hermetic lid with a pinhole;

The thermal stability of the samples during the measurement was *a priori* not considered as a problem, since the used ILs and the respective based Ion Jellies, are known to rather stable and the temperature range was limited to 40ºC. The samples were visually inspected after each measurement aiming the possibility to see some color change or other effect of degradation. The DSC apparatus is presented in Figure 2.4.

Figure 2.4 – DSC apparatus.

2.3.5. Nuclear Magnetic Resonance

NMR spectra were recorded on a Bruker Avance III 400 spectrometer, operating at 400.15 MHz, equipped with pulse gradient units, capable of producing magnetic field pulsed gradients in the z direction of 0.54 T m^{-1}. Diffusion measurements were performed using the stimulated echo sequence using bipolar sine gradient pulses and eddy current delay before the detection.[9] The signal attenuation is given by

$$S = S_0 \exp\left(-\gamma^2 g^2 D \delta^2 \left(\Delta - \frac{2\delta}{3} - \frac{\tau_g}{2} \right) \right)$$

where D denotes the self-diffusion coefficient, γ the gyromagnetic ratio, δ the gradient pulse width, Δ the diffusion time, τ$_g$ the gradient recovery delay, and g the gradient strength corrected according to the shape of the gradient pulse.

Before all NMR experiments, the temperature was equilibrated and maintained constant within ±0.1 K, as measured using the spectrometer thermocouple system. Experiments were performed at 298.15 K, 288.15 K, 278.15 K, 273.15 K, 268.15 K, 258.15 K, 253.15 K, and 248.15 K.

The spectra were recorded in 5 mm NMR tubes with an air flow of 535 L h^{-1}. Typically, in each experiment, a number of 32 spectra of 32 K data points were collected, with values for the duration of the magnetic field pulse gradient (δ) of 2.5 to 3.5 ms, diffusion times (Δ) of 400 to 200 ms, and an eddy current delay set to 5 ms, the gradient recovery time (τ$_g$) was 20 μs. The sine shaped pulse gradient (g) was incremented from 5 to 95% of the maximum gradient strength in a linear ramp. The spectra were first processed in the F2 dimension by standard Fourier transform and baseline correction with the Bruker Topspin software package (version 2.1). The diffusion coefficients are calculated by exponential fitting of the data belonging to individual columns of the 2D matrix. The diffusion coefficients (D) were obtained by measuring the signal intensity at more than one place in the spectra. At least two different measurements were done for the determination of each diffusion coefficient.

2.3.6. Electronic Nose

Preparation of the sensors: While still warm (40 ºC), 40 μL of an ion-jelly solution was spin-coated (1000 rpm, 30 s) onto an interdigitated electrode, forming a uniform jellified transparent film. This procedure was repeated for all the IJs (Figure 2.5).
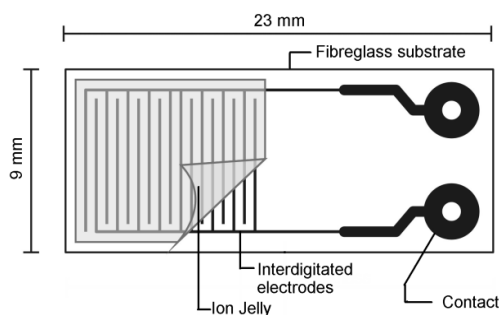
Figure 2.5. Ion jelly gas sensor.

E-nose measurements: A pneumatic assembly for dynamic sampling, as show in Figure 6.4, was used for the measurements. Thus, the sensors were exposed to the headspace of each volatile sample, kept at 30 ºC, for 5 s (exposure period; valves 1 and 2 open, valve 3 closed), then to dry air for 65 s (recovery time; valves 1 and 2 closed, valve 3 open). The airflow was maintained constant at 0.5 Lmin^{-1}. The tests were repeated fifteen times for each of the eight samples. The conductance of the sensors was continuously monitored with accurate conductivity meters, operating with an 80 mV peak-to-peak 2 KHz triangle wave AC voltage connected *via* 10 bits analog to digital converter to a personal computer.

Chemometrics. Principal component analysis (PCA) was performed using Statgraphics Centurion XV. Leave-one-out analysis was performed using DimReduction (GNU) [10]. The analyses were carried out using, separately, the relative responses $Ra = (G2 - G1)/G1$, where G1 is the maximum conductance and G1 the initial conductance of the sensors values (see Figure 2.6).
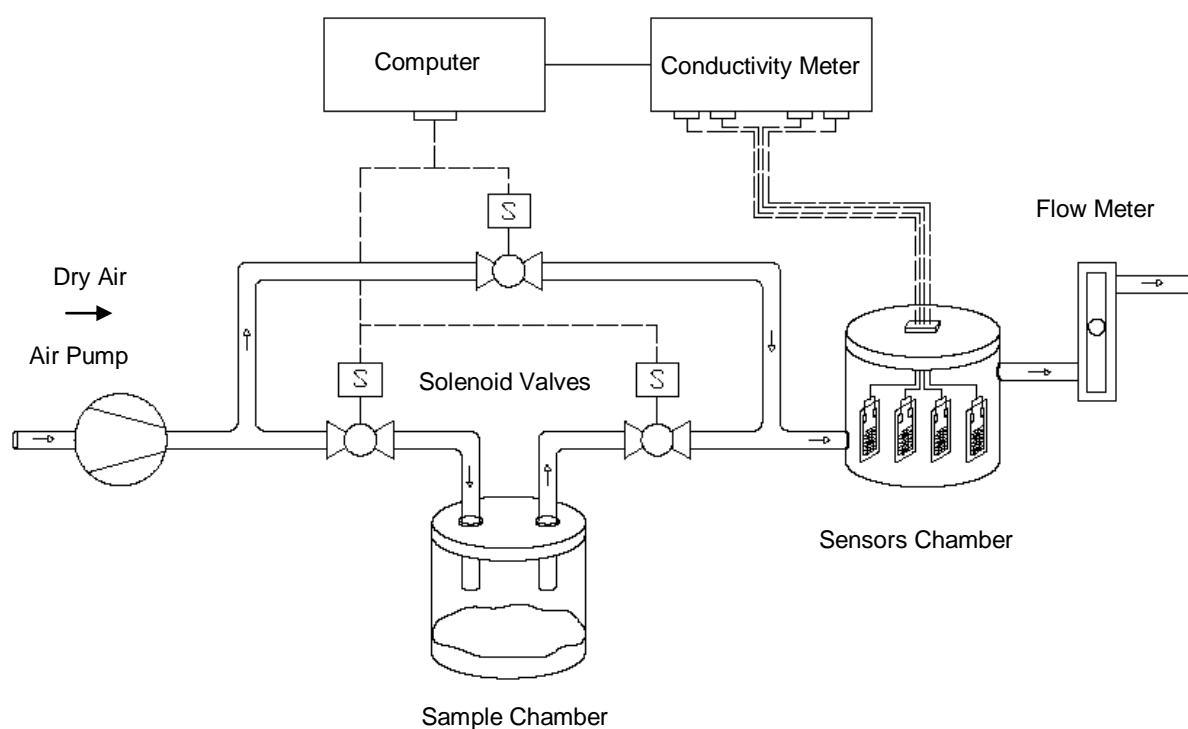
Figure 2.6 – Setup of the e-nose measuring systems.

2.4. Bibliography

[1]   C. P. Fredlake, J. M. Crosthwaite, D. G. Hert, S. N. V. K. Aki, and J. F. Brennecke, "Thermophysical Properties of Imidazolium-Based Ionic Liquids," *Journal of Chemical & Engineering Data*, vol. 49, no. 4, pp. 954–964, 2004.

[2]   G. Williams and D. K. Thomas, "Phenomenological and Molecular Theories of Dielectric and Electrical Relaxation of Materials, APPLICATION NOTE DIELECTRICS 3, NOVOCONTROL GMBH.," 2008.

[3]   J. Mijovic and B. D. Fitz, "Dielectric Spectroscopy of Reactive Polymers," *APPLICATION NOTE DIELECTRICS 2, NOVOCONTROL GMBH.*, no. Section 5, 1998.

[4]   M. Dionísio and J. F. Mano, "Handbook of Thermal Analysis and Calorimetry. Recent Advances Techniques and Applications. Vol5," in in *Electric Techniques*, Elsevier., M. E. Brown and P. K. Gallangher, Eds. 2008, pp. 209–268.

[5]   Novocontrol, "'Alpha high resolution dielectric/impedance anlayzer'."2003.

[6]   T. Carvalho, V. Augusto, a R. Brás, N. M. T. Lourenço, C. a M. Afonso, S. Barreiros, N. T. Correia, P. Vidinha, E. J. Cabrita, C. J. Dias, M. Dionísio, and B. Roling, "Understanding the ion jelly conductivity mechanism.," *The journal of physical chemistry. B*, vol. 116, no. 9, pp. 2664–76, Mar. 2012.

[7]   S. Havriliak and S. Negami, "A Complex Plane Representation of Processes in Some Polymers," *Polymer*, vol. 8, no. 4, p. 16–&, 1967.

[8]   Menczel and R. Bruce Prime, *Thermal Analysis of Polymers, Fundamentals and Applications.*, John While. Hoboken, New Jersey, 2009.

[9]   D. Wu, A. Chen, and C. S. Johnson Jr, "An Improved Diffusion-Ordered Spectroscopy Experiment Incorporating Bipolar-Gradient Pulses," *Journal of Magnetic Ressonance*, vol. A115, no. 2, pp. 260–264, 1995.

[10]   "Http://sourceforge.net/projects/dimreduction/," 2011. .

Chapter 3

UNDERSTANDING THE ION JELLY CONDUCTIVITY MECHANISM

3. UNDERSTANDING THE ION JELLY CONDUCTIVITY MECHANISM

The results reported in this chapter were published in the Journal of Physical Chemistry B (DOI: 10.1021/jp2108768).

3.1. Thermal Characterization

To obtain a proper understanding of the transport properties of IJs and BMIMDCA, the thermal transitions were first investigated by DSC. The respective thermograms, recorded in heating mode, are represented in Figure 3.1.
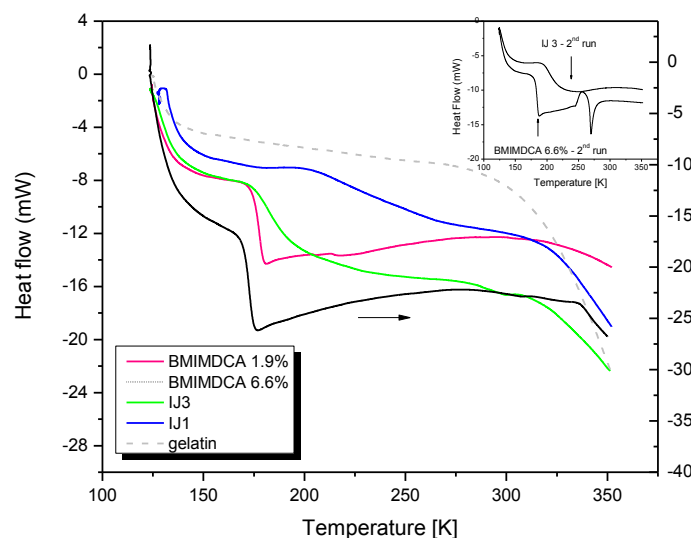
Figure 3.1 - DSC scans obtained in heating mode at 20 K.min^{-1} for BMIMDCA$_{1.9\%water}$, BMIMDCA$_{6.6\%water}$ and both Ion Jelly showing the heat flow jump at the glass transition; in the studied temperature range no transitions are detected for gelatin. The inset shows the second heating scan for BMIMDCA$_{6.6\%water}$ and IJ3, where cold crystallization and melt are observed for the IL and avoided for the Ion Jelly (see text).

For BMIMDCA$_{1.9\%water}$, BMIMDCA$_{6.6\%water}$, and IJ3, it is clear the heat flow jump, which is the characteristic signature of the glass to supercooled liquid transition; although, not so clear, the same transition is also observed for IJ1. Therefore, all the materials tested in this work are classified as glass formers. In this temperature range, no transition was detected for gelatine (see dashed line in figure 3.1).

The width of the transition is higher for both IJ materials, in particular for IJ1, which covers an extremely wide temperature range, relative to BMIMDCA either with 1.9 and 6.6% of water. As a result, the glass transition temperature determined from the onset (see *Introduction*) of the calorimetric signal will be taken for comparison being 174.2 K (-99.0 °C), 169.8K (-100.5 °C), 174.4 K (-98.8 °C), and 203.9 K (-69.2 °C) for respectively, BMIMDCA$_{1.9\%water}$, BMIMDCA$_{6.6\%water}$, IJ3 and IJ1 (see Table 3.1).

Table 3.1- Glass Transition Temperatures Taken at the Onset (on), Midpoint (mid) and Endset (end) of the Heat Flow Jump for both BMIMDCA and both IJs, Obtained during a First Heating Ramp at 20 K/min, and Heat Capacity Associated with the Glass Transition

System	$T_{g,on}$/K	$T_{g,mid}$/K	$T_{g,end}$/K	ΔC_p(J.g^{-1}.K^{-1})
BMIMDCA$_{1.9\%water}$	174.2	177.6	179.7	0.68
BMIMDCA$_{6.6\%water}$	169.8	172.5	177.8	0.72
IJ3	174.4	181.8	193.3	0.47
IJ1	203.9	220.6	256.0	0.30

The values extracted from the midpoint and endset are also included in Table 3.1, as well as the heat capacity jump. While the onset of the glass transition detected for IJ3 occurs near to the onset of the bulk ionic liquid, the temperature of the glass transition increases significantly in IJ1. This will be confirmed later by DRS. For the IL, it is observed a decrease of the glass transition with the water content. This is consistent with the data provided by Fredlake et al.[1] for BMIMDCA with lower water content (0.515%) for which a higher T_g value is reported: 183 K (-90 °C) taken at the midpoint; in this work, the T_g values taken at the midpoint were estimated as, respectively, 177.6 K (-95.6 °C) and 172.5 K (-100.65 °C) for BMIMDCA$_{1.9\%water}$, BMIMDCA$_{6.6\%water}$. Therefore, a plasticizing effect of water at these relative low water contents can be inferred. The shift of the position of the glass transition tower lower temperatures was also observed for another IL, 1-ethl-3-methylimidazolium acetate, for water contents from 0 up to 40% w/w.[2]

In addition to the glass transition, Fredlake et al.[1] report the occurrence of cold crystallization at 244 K (-29 °C) followed by melting at 267 K (-6 °C) for BMIMDCA. This was investigated here for both BMIMDCA, and indeed, cold crystallization of the supercooled liquid and subsequent melt are detected at temperatures close those reported in [1] but only in a second heating run (see the illustrative thermogram for BMIMDCA$_{6.6\%water}$ in the inset of Figure 3.1). It is worth noting that prior to the second heating run during which crystallization was observed, the sample was heated up to 363 K in the first heating scan and kept 5 min at this temperature. This assures the water removal, which seems to be a condition to occur further crystallization. In the second heating scan, the glass transition temperature increased to 184.6 K for both BMIMDCA$_{1.9\%water}$ and BMIMDCA$_{6.6\%water}$ (taken at the midpoint), confirming the shift to higher temperatures upon dehydration, and the water content remaining in both samples is similar and probably negligible (at least below 0.5% according to the previous discussion). Moreover, no crystallization was observed in subsequent runs for both IJs (see the second heating scan for IJ3 in the inset of Figure 3.1). This can be taken as an indication that, upon thermal treatments, the supramolecular structure of gelatine stabilizes to some extent (i) the disordered amorphous state of the IL and (ii) the water retention. This can be seen as a plus concerning the potential applications and performance of these materials.

The first scan is the one taken for all samples since it reproduces the conditions followed in the dielectric measurements.

3.2. Dielectric Characterization

3.2.1. Conductivity

Figure 3.2 shows the real (a-d) and imaginary (e-h) components of the complex conductivity, $\sigma^*(\omega) = \sigma'(\omega) + i\sigma''(\omega)$, from 10^{-1} to 10^{-6} Hz covering different temperatures ranges for each material: $BMIMDCA_{1.9\%water}$ and $BMIMDCA_{6.6\%water}$, IJ3 and IJ1 from top to bottom. The insets shows the respective components of the dielectric complex function $\varepsilon^*(\omega) = \varepsilon'(\omega) + i\,\varepsilon''(\omega)$ associated with reorientational motions of dipoles. The relationship between both is given by[3] $\sigma^*(\omega) = i\omega\varepsilon_0.\varepsilon^*(\omega)$. As it becomes clear from the permittivity and loss curves, conductivity strongly affects the dipolar spectra mainly at the low frequency side and at the highest temperatures. This conductivity contribution can be analyzed to extract information on the charge transport mechanism for each material, which will be carried out in the next section.

To evaluate the influence of gelatin itself in the IJ conductivity, a film of gelatin with 22% of water was also measured at 298 K; this was the minimal water content that allowed preparing self-supported gelatin films. Figure 3.2 shows the real conductivity for this material. It is evident that the dielectric response for $gelatin_{22\%water}$ is significantly lower relative to any of the tested materials of either IL or IJ. Even at the highest frequencies, the real conductivity of $gelatin_{22\%water}$ is around 4 decades inferior to that of IJ3; at the lowest frequencies, the response differs around 8 decades! The role of water will be analyzed in the end of this section.

It is worthy to mention that while the dielectric measurements for the IL (either with 1.9 and 6.6% water) were affected by electrical anomalies at temperatures close to room temperature and at the highest frequencies (that persist even reducing the length of the BNC connecting cables), no such instabilities were felt while measuring the ion jelly materials. This can be taken as another advantage of the performance of these devices.
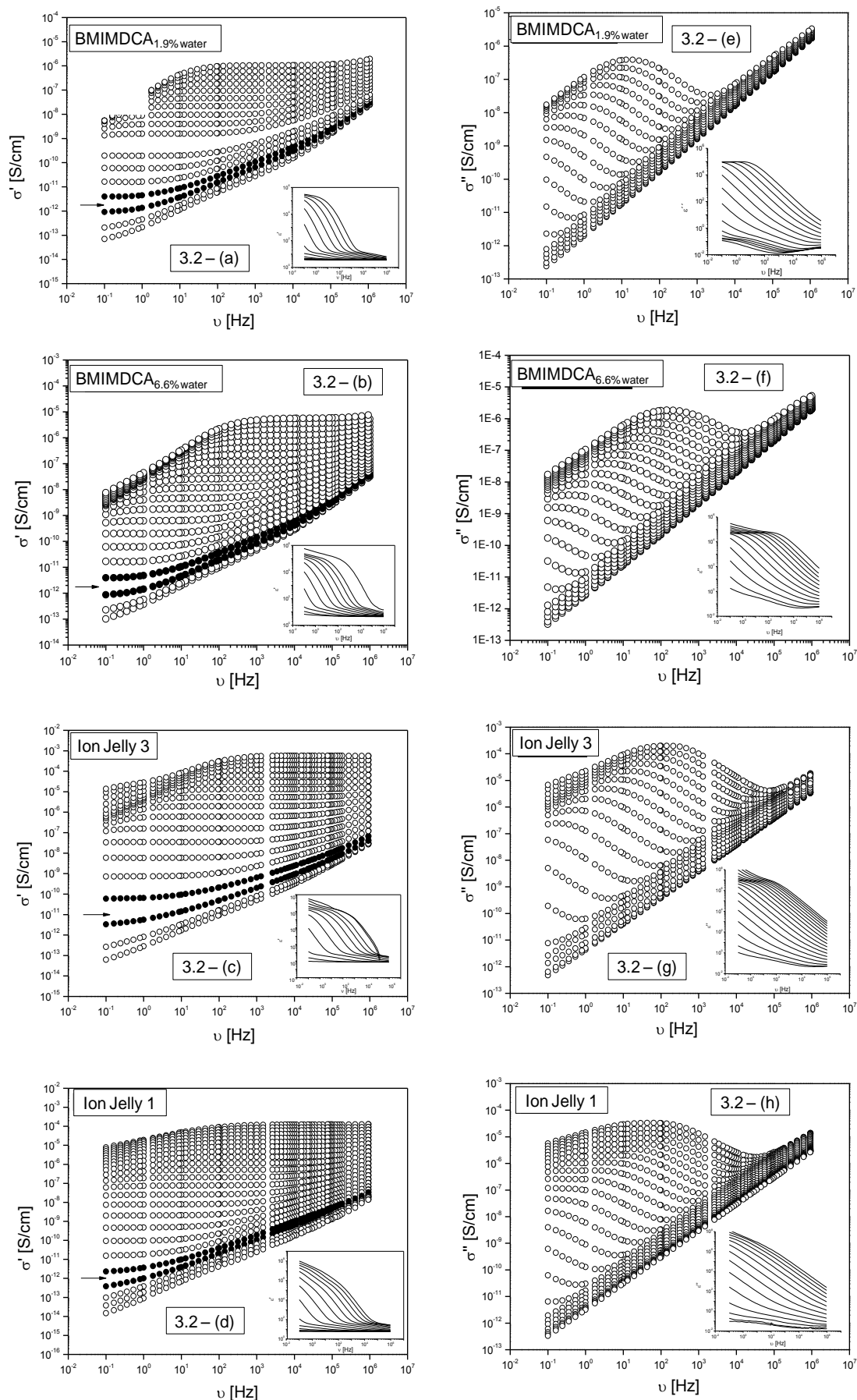
Figure 3.2 – (a-g) - Complex conductivity measured at different temperatures of BMIMDCA$_{1.9\%water}$ and BMIMDCA$_{6.6\%water}$ (in steps of 2 K from 163 K to 213 K) and Ion Jelly (in steps of 5 K starting at 163K (IJ3) and

188K (IJ1)): (a-d) real, σ', and (d-g) imaginary, σ'', components; the onset of the calorimetric T_g occurs at a temperature in between the isotherms represented in filled symbols (indicated by the arrow). The insets display the respective real ε' (a-d) and imaginary ε'' (e-h) parts of the complex dielectric function.
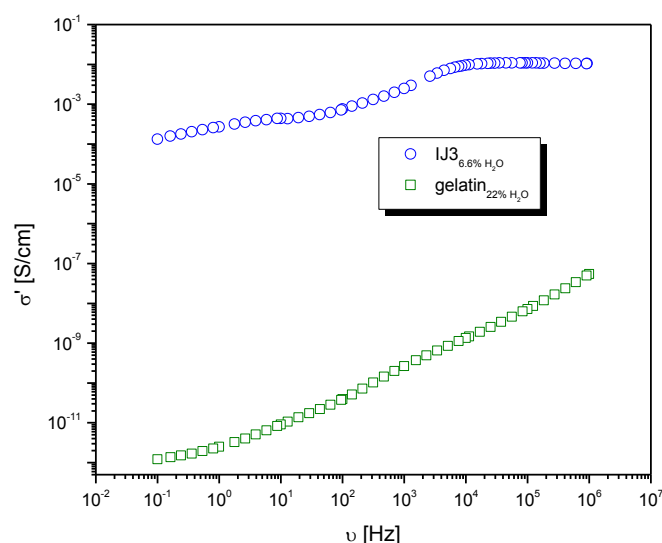
Figure 3.3. Frequency dependence of real conductivity at 298 K for IJ3 (which has 6.6% (w/w) water content) compared with a blank of a gelatine film with 22% (w/w) of water.

The plot of the real part of the complex conductivity (Figure 3.2 – (a-d)) presents a profile similar to the one found for a variety of quite different materials[4–6]: a plateau at low frequencies that bends off at same critical frequency, crossover frequency, into a dispersive regime, with a strong increase of the conductivity with increasing frequency following a power law dependence (a.c. conductivity) as proposed by Jonscher [7] (see Introduction section 1.2.5).

The emergence of a ω_{cross} in the real conductivity spectrum provides a way to get a rough estimate of the glass transition temperature as found for both BMIMDCA materials and IJ3 from which unequivocal calorimetric determination of T_g was possible (the arrow in Figure 3.2 - (a-d) indicates the two temperatures that lie immediately below and above the onset of the T_g detected by DSC). In the case of IJ1, an identical behaviour is observed between the isotherms collected at 203 K and 208 K giving further evidence that the glass transition temperature is closer to the value hardly estimated from DSC measurements ($T_{g, on}$ = 204 K).

The plateau region corresponds to a linear dependence of slope 1 in the plots of log($\varepsilon''(\omega)$) and gives the value of σ_0, the conductivity in the dc limit. At the highest temperatures in each collection of $\sigma'(\omega)$ spectra, instead of an extend plateau in the conductivity plot in the low frequency region, a decrease is observed, due to electrode polarization as found in similar materials[8]. This means that ionic conduction becomes blocked, i.e., ions accumulate in the sample/electrode interface without discharging. In the same frequency region, the loss curves ($\varepsilon''(\omega)$) present a linear dependence with a slope < 1, and the real permittivity ($\varepsilon'(\omega)$) exhibits a tail with several orders of magnitude higher than the values measured at the lowest temperatures and highest frequencies. Additionally, when electrode polarization occurs, a peak is observed in the imaginary part of the conductivity, $\sigma''(\omega)$, as depicted in Figure 3.2 – (e-h). A more detailed analysis will be provided in section 3.2.1.

Jonscher equation was fitted to the real part of conductivity to obtain ω_{cross} and σ_0; the later compares very well with values taken from the plateau region in each isotherm. Figure 3.4 shows for IJ3 the obtained fit as solid lines at temperatures for which data are not influenced by electrode polarization (an effect that in not taken into account in the proposed law).
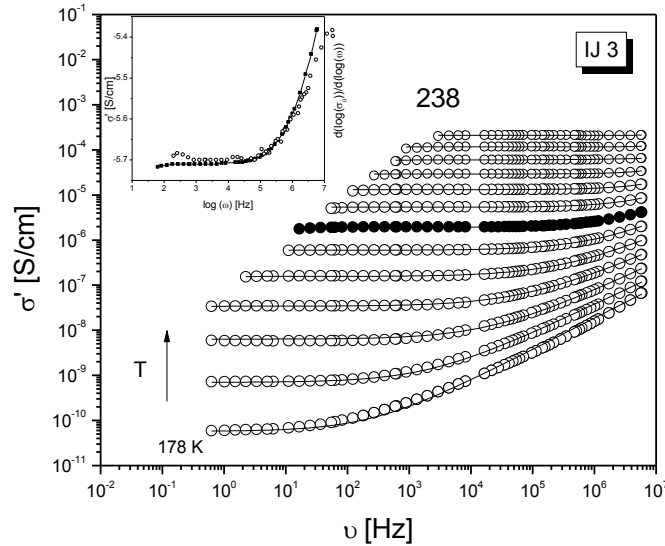
Figure 3.4 – Real part of conductivity for IJ3 from 178 to 238 K in steps of 5K. The solid lines are the obtained fits by the Jonscher law (eq. (2)). Data collected at 208 K are plotted in full circles being the same spectrum presented in the inset together with the respective derivative d(logσ'(ω))/d(log(ω)) (open circles); the continuous increase of the derivative value with the frequency increasing, confirms the sub-diffusive dynamics (see text).

The curve taken at 208 K is plotted in full symbols being the same presented in the inset that also includes its respective derivative plot d(logσ'(ω))/d(log(ω)) (open circles). This is a way to verify if ion transport at short times (high frequency side of the spectrum) is governed by subdiffusive dynamics. In fact, if dipolar relaxation dominates, a different profile for the a. c. contribution would be obtained.[9], [10] Moreover, subdiffusive bulk ion dynamics usually leads to an apparent slope d(logσ'(ω))/d(log(ω)), which increase continuously with increasing frequency. In contrast, reorientational motions of dipoles lead to a ε'' peak, which implies that in the low-frequency of the peak, the slope d(logσ'(ω))/d(log(ω)) is larger than unity, and in the high-frequency flank, it is smaller than unity. So, in the case of reorientational motions, one does not expect a continuous increase of the slope with increasing frequency as we obtained. Therefore, there is strong evidence that subdiffusive dynamics dominate at short times allowing to extract transport properties.

The temperature dependence of the σ_0 values is plotted in Figure 3.5 for the four materials.
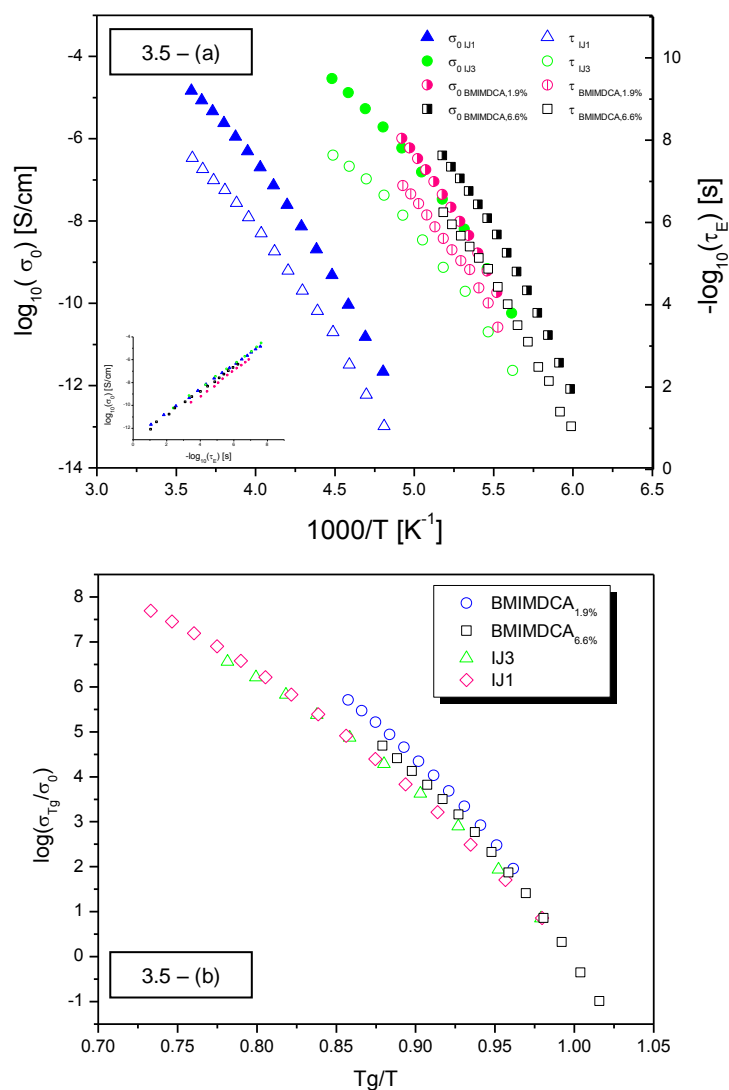
Figure 3.5 – (a).Temperature dependence of the dc conductivity, σ_0, and of the relaxation time, τ_e, taken from the crossover frequency. The correlation between both is displayed in the inset (BNN plot) for which a slope near 1 and a r^2=0.99 was found: $\log(\sigma_0)=(1.06\pm0.02)\log(\tau_e) -(12{,}95\pm0{,}09)$. (b) Temperature dependence of conductivity normalized for the value measured at the calorimetric glass transition temperature (σ_{Tg}); the temperature axis is scaled to the glass transition temperature, T_g.

The empirical Vogel Fülcher Tammann-Hesse (VFT) equation [11–13] was fitted to the conductivity data, which usually describes the temperature dependence of the dynamic glass transition relaxation time (eq. 3.1 – (a)) and the electrical conductivity (eq. 3.1 – (b)) of supercooled liquids including ionic liquids,[10], [14–18] quite well

$$\tau(T) = \tau_\infty \exp\left(\frac{B}{T - T_0}\right) \qquad (3.1 - (a))$$

$$\sigma_0(T) = \sigma_\infty \exp\left(-\frac{B}{T-T_0}\right) \quad (3.1-(b))$$

where τ_∞ and σ_∞ are the values of the relaxation time and conductivity in the high temperature limit, B is an empirical parameter characteristic of the material accounting for the deviation of linearity (roughly B is lower with the more curve dependence), and T_0 is the Vogel temperature interpreted as the glass transition temperature of an ideal glass, i. e., a glass obtained with an infinitely slow cooling rate[19].

The crossover frequency can be used[16] to derive the attempt rate, $\omega_e = 1/\tau_e = (2\pi f_e)$.

The frequency f_e, which characterizes the onset of the dc conductivity, is related to it by the empirical relationship known as the BNN relationship, σ_0 - $1/\tau_e$ (see *Introduction* section 1.2.5), that predicts similar temperature dependencies for σ_0 and τ_e^{-1}. In Figure 3.5 – (a), the $-\log(\tau_e)$ plot against the reciprocal of temperature was included for all materials, running parallel to the VFT-like temperature dependence of $\sigma_0(T)$. Table 3.2 presents the estimated parameters of the VFT fit to the $\sigma_0(T)$ and $\tau_e(T)$, where it can be seen the similarity between the B and T_0 parameters obtained from both kind of representations, indicating the parallelism of $\sigma_0(T)$ and $\tau_e(T)$ for all materials. To analyze better the origin of such dependence, the log $\sigma_0(T)$ is represented versus $-\log \tau_e(T)$ in the inset of Figure 3.5 – (a), this proves that the BNN relationship holds in the studied frequency/temperature range for the four materials as reported for a variety of ion conducting disordered systems.[16], [20–22].

Figure 3.5 – (b) shows the plot of the normalized conductivity for the value measured at the glass transition temperature, σ_{Tg}, of each system and scaled to T_g. From this plot, it is possible to conclude that relative similar temperature dependencies are observed for the different systems. However, the plots do not follow in a single chart as observed for a series of ionic liquids (inset of Figure 2a in ref 37). The temperature dependence of BMIMDCA$_{1.9\%water}$ conductivity exhibits a relatively higher curvature, meaning that its conductivity changes more with the temperature while approaching T_g. This can be due to the temperature evolution of the type of motion to which the conductivity seems to be correlated with (as it will be analyzed in the last section of this chapter), and it is usually quantified by the fragility index; this quantity measures the degree of deviation from Arrhenius-type temperature dependence near T_g,[24]; its determination and analysis will be carried out in the next chapter.

Table 3.2. Fit Parameters Obtained According to the VFT Law for the Conductivity (eq. 3.1 – (b)) and the Relaxation Times (eq. 3.1 – (a))[a]

Sample	VFT fit parameters of σ_0[b)]			VFT fit parameters of τ_e[c)]		
	σ_∞/ S.cm^{-1}	B/ K	T_0 / K	τ_∞/ s	B / K	T_0/ K
BMIMDCA$_{1.9\%water}$	37±21	1167±91	136±2	(2.2±0.3)X10-14	1048±346	136±9
BMIMDCA$_{6.6\%water}$	229±100	1328±58	127±1	(1.3±1.2)x10^{-16}	1610±374	120±4
Ion Jelly (IJ3)	59±15	1375±39	128±1	(4.0±2.7)x10^{-14}	1224±156	130±4
Ion Jelly (IJ1)	376±116	2453±76	133±1	(1.2±0.6)x10^{-15}	2508±154	130±3

[a]The uncertainties are the statistical errors given by the fitting program. For each material, the similarity between B and T_0 estimated through σ_0(T) and τ_e(T) indicates a parallelism between these two quantities (see text for details). [b]According to the VFT law for conductivity. [c]According to the VFT law for relaxation time.

Since it was proved that no dipolar relaxation is affecting conductivity data and that the BNN relation holds, it is possible to go further on data treatment to estimating transport properties. For the determination of diffusion coefficients (equation 1.20(a) and 1.20(b) in *Introduction*) the mean square displacement $<\Delta r^2(t^*)>$ is needed. An good estimate is to take the square of the van der Waals (vdW) diameter.[25] The vdW value used for BMIM was the one reported in the literature, 0.66 nm.[26] This value is in reasonable agreement with the value of 0.76 nm estimated by using an Hartree-Fock ab initio method provided by a commercially available software;[27] therefore, the vdW diameter estimated by using Spartan[27] for the DCA anion (0.424 nm) was adopted since no value was provide in the literature, as far as we know.

Taking the vdW diameter, the individual diffusion coefficients were estimated from equations 1.20-a and 1.20-b (se *Introduction*). The mobility, µ, was then readily determined (equation 1.15 – (b) by taking D=D$_+$ + D$_-$). In figure 6 the obtained D$_+$ and D$_-$ diffusion coefficients (Figure 3.6 – (a)) and µ (Figure 3.6 – (b)) are displayed for BMIMDCA$_{1.9\%water}$ and BMIMDCA$_{6.6\%water}$ and both IJs. The estimated self-diffusion coefficients of the cation are slightly higher than those of the anion as generally observed (see ref 39 and references therein), being a consequence of a higher vdW diameter of the former.

Figure 3.6 – (c) includes the cation diffusion coefficient determined from Pulse Field Gradient (PFG) Nuclear Magnetic Ressonance (NMR) measurements for BMIMDCA$_{6.6\%water}$ and IJ3, the IJ containing the water content; because of the absence of protons or high sensitive NMR nuclei in the anion structure, its diffusion coefficients were not able to be determined by NMR.

For IJ3, it was possible to estimate the cation diffusion coefficients from DRS data over a large temperature range up to the temperature interval covered by PFG NMR measurements. From 213 to 298 K, the crossover frequency was estimated from the dc conductivity values taken at the high frequency plateau through the BNN relationship (stars in Figure 3.6 – (c)). Interesting enough is the fact that the cation diffusion coefficients estimated for IJ3 from dielectric data agree so well with the values directly measured by PFG NMR. Since an average diffusion coefficient is extracted from DRS measurements, this offers a way to validate the deconvolution of this quantity in its individual D_+ and D_- contributions. Concerning the $BMIMDCA_{6.6\%water}$ it was not possible to obtain either crossover frequency or dc conductivity values in the high temperature range due to the influence of electrical anomalies affecting the measurements at the highest frequencies as mentioned before. However, a single VFT equation describes both DRS and PFG NMR data.
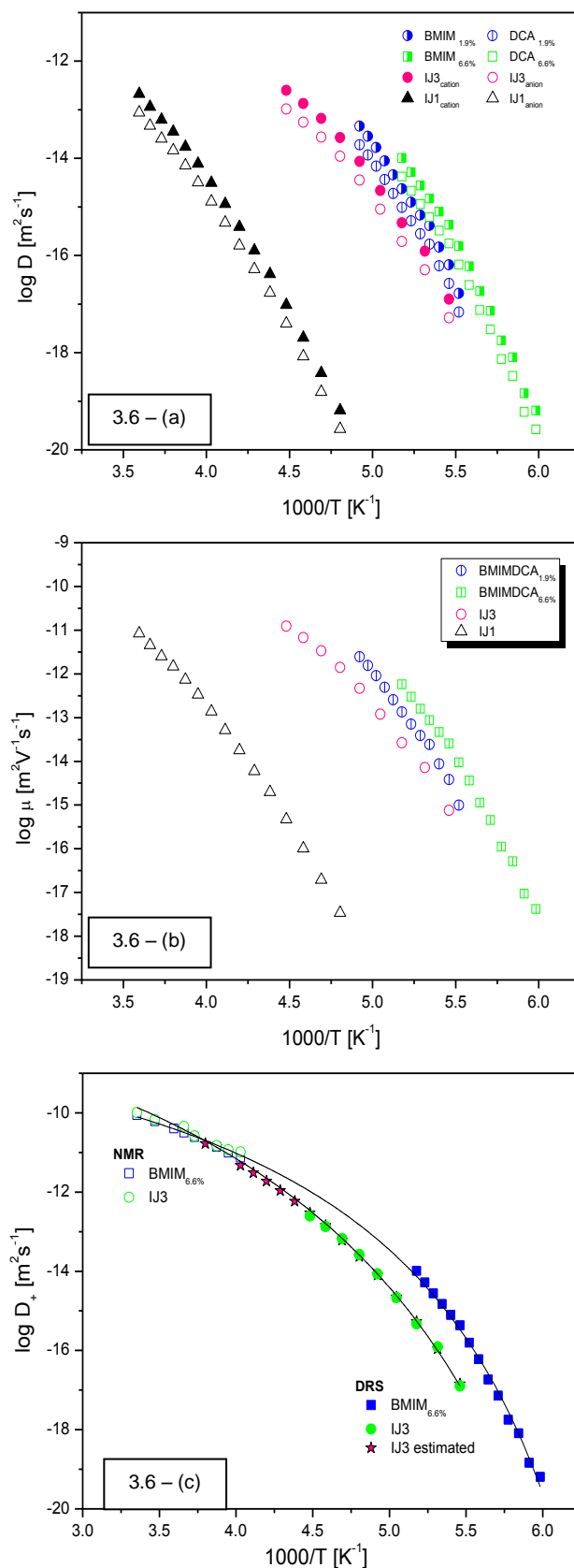
Figure 3.6 – (a-c) – Thermal activation plot for a) diffusion coefficients of BMIM (cation) and DCA (anion) (equations 1.20-a and 1.20-b), replacing the mean-square displacement by the vdW diameters, and b) mobilities, μ, (equation 1.15-b) by taking $D = D_+ + D_-$ for the four materials. (c) Values of the cation diffusion coefficients (D_+) determined from PFG NMR and the VFT fit (solid lines); data represented by stars for IJ3 were estimated also through equation 10a but using the BNN relationship to obtain the crossover frequency from σ_0 (see text).

From the diffusion coefficients and σ_0 values, the mobility is readily obtained through equation 1.15-b (*Introduction*). The respective temperature dependence is included in figure 6, becoming clear that the nonlinear temperature dependence of conductivity is originated by a VFT behaviour of the mobility as found in related materials.[10], [16-17]

From the comparison of the transport properties of the IL with two different water contents, it becomes obvious that water enhances the mobility and increases the value of the ionic diffusion coefficients. The influence of water on the transport properties of several ILs was recently investigated by Spohr and Patey[28] by molecular dynamical simulations that conclude that the dominant effect of water is dynamical in origin. For room temperature ionic liquid-water mixtures for which the ion size disparity is not to large (as in the actual IL), it was demonstrated that the lighter water molecules tend to displace much heavier counterions from the ion coordination shells, which reduces caging and increases the diffusivity, leading to higher conductivities and lower viscosities. The results here reported corroborate their conclusions as found also for another IL (*N,N*-diethyl-*N*-methylammoniumtriflate), where it was observed that water facilitates the translational motion of both ions increasing mobility[29]. Moreover water molecules weaken the contact ion pair since it shields the electrostatic attractions between ions, promoting ion dissociation[29].

The diffusion coefficients and mobility of charge carriers in IJ3 are close to those of the bulk BMIMDCA. This means that the solid-like material retains a similar ability for charge transport as the IL. As observed earlier, the gelatine conductivity (even containing a large water amount, 22%) is rather low compared with IJ3 (remember Figure 3.3). Nevertheless, in IJ3, the gelatine matrix should promote charge separation in large charge clusters, which are known to exist in ILs[30–32]. Increasing the number of charge carriers resulting in a material with conductivity and mobility comparable to those of the pure. The same is not true in IJ1. This is probably due to a rather low ratio BMIMDCA/gelatine, pointing to the existence of a critical composition, which leads to those properties. The difference in the temperature range where these quantities are able to be estimated is determined by the glass transition temperature that, as above-reported, is nearly the same for IJ3 and BMIMDCA and ~ 30 K higher for IJ1.

Moreover, it is relevant to observe that the diffusion coefficients at higher temperatures, including room temperature, as observed by PFG NMR, are the same for IJ3 and BMIMDCA$_{6.6\%water}$. Therefore, the presence of the gelatine matrix does not impair the diffusion of the IL ions.

3.2.2. Analysis of Real Permittivity ε'

The effect of electrode and interfacial polarization can be also analysed trough the real permittivity spectra, $\varepsilon'(\omega)$, that, oppositely to the dielectric loss, is insensitive to pure dc conductivity; the extremely high values of conductivity made impossible the analysis of any relaxation process including the cooperative motion behind the process associated with the dynamical glass transition. Through ε'' data. $\varepsilon'(\omega)$ presents a multimodal character, and therefore, a sum of HN equations (see eq. 1.13 in *Introduction*) was used to fit the raw data.[1] An adequate simulation of the experimental data

---

[1] The fitting of a sum of HN equations to the ε´data was made by Professor Carlos Mariano Dias (Materials Science Department of FCT/UNL; nevertheless the analysis is kept on this chapter since the further data treatment was carried out by Tânia Carvalho.

was only possible considering four individual processes (designated from I to IV in decreasing order of frequency at the same T). Figure 3.7 – (a-d) shows the obtained results as solid lines illustrating how well data were described by the fit.
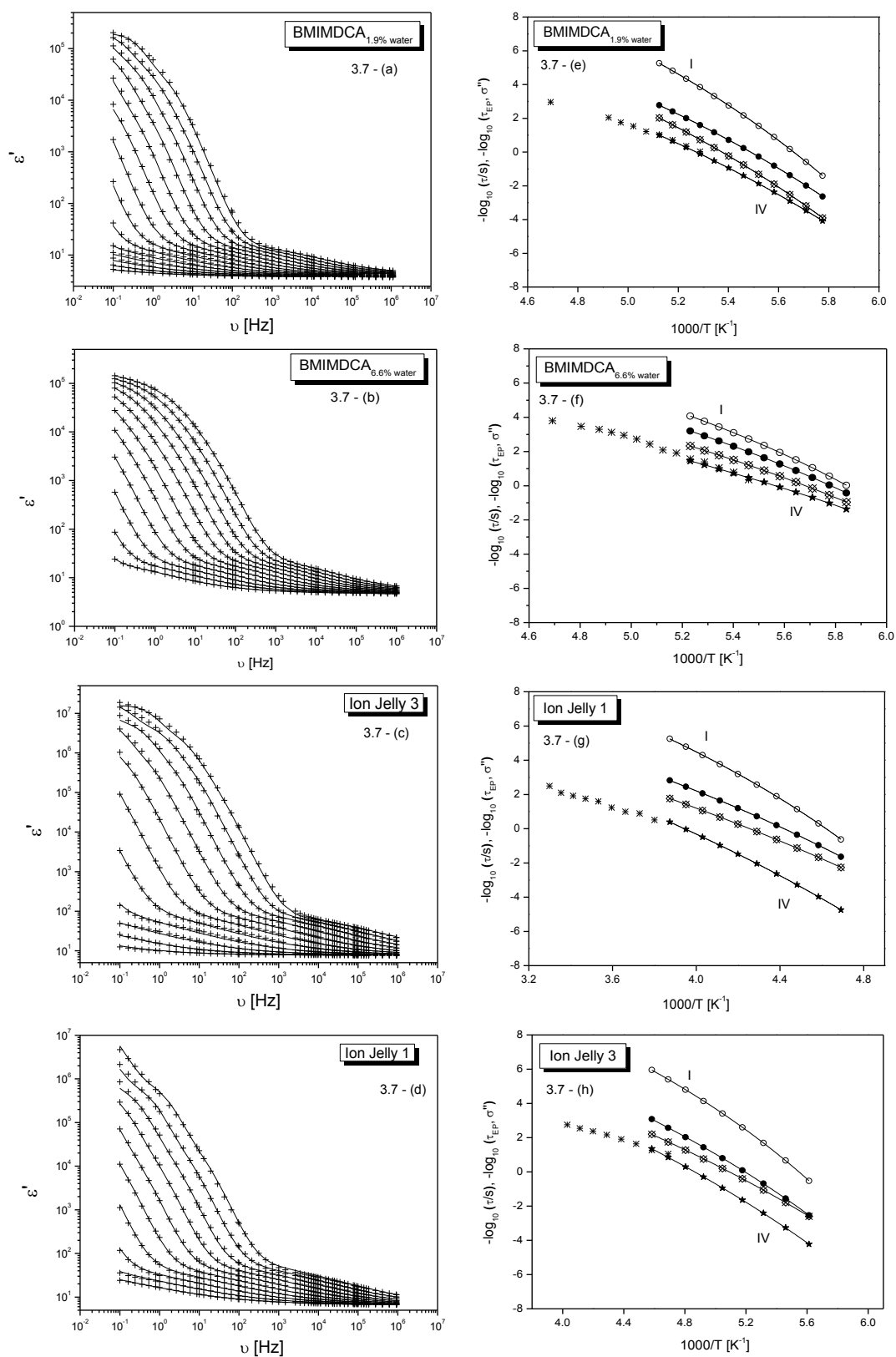
Figure 3.7 - (a-d) Real permittivity spectra, ε', of $BMIMDCA_{1.9\%water}$, $BMIMDCA_{6.6\%water}$, and both IJs; the solid lines are the overall fit of a sum of four individual HN functions to the raw data. (e-h) Respective relaxation maps

are presented (solid lines are the VFT fit). The asterisks in the relaxation maps are the relaxation times taken from the maximum of $\sigma''(\omega)$ in excellent agreement for all systems with the values estimated from the fit to process IV. Note a different scale in the X-axis for IJ1 due to its higher glass transition temperature.

In Figure 3.7 – (e-h), the relaxation maps for all considered processes are displayed. The temperature dependence of the maximum observed in σ'' (ω) was included in each relaxation map revealing an excellent agreement with the activation plot of process IV for all systems. This is a way to confirm the accuracy of the fitting procedure and the assignment of this process to electrode polarization.

It should be noted that in spite of expecting a multimodal nature of the dielectric processed due to the simultaneous contribution, in order of increasing frequency, (i) electrode polarization, (ii) interfacial polarization, and (iii) reorientational dipolar motions, it is not straightforward the reason why four processes were needed to simulate the raw data. This can have real physical meaning due to polarization processes usually found in inhomogeneous materials where internal phase boundaries develop at which charges can be blocked giving rise to different interfacial polarizations of the Maxwell-Wagner-Sillars type;[33] these interfaces in the here-tested materials could be ionic liquid/gelatine, water/ionic liquid, or gelatine/water. Even within the bulk ionic liquid, interfacial polarization can emerge. Indeed, for alkyl-MIM ILs, it was demonstrated by molecular simulation the existence of nanometer –scale structuring with aggregation of the alkyl chains in nonpolar domains, which permeate a tridimensional network of ionic channels formed by anions and by the imidazolium rings of the cations in such a way that microphase segregation exists between polar and nonpolar domains,[30], [31] strengthening the existence of interfacial polarization in the pure IL itself. However, the need of using four processes could alternatively arise from an inadequacy of a single HN relaxation function to describe the totality of the interfacial processes taking place inside the material. It is not clear up to now what is the actual cause of this behaviour.

In Figure 3.7 - (e-h), it becomes obvious that all considered processes follow VFT dependencies of the respective relaxation times; the VFT parameters are presented in Table 3.3

Table 3.3 – VFT parameters estimated for each process used in the HN fit to the ε' data

	I			II		
	τ_∞/s	B /K	T_0 / K	τ_∞/s	B /K	T_0 / K
BMIMDCA$_{1.9\%}$	6.18×10^{-17}	3078.8	107.2	2.32×10^{-19}	3202.2	111.4
BMIMDCA$_{6.6\%}$	3.45×10^{-13}	2493.2	92.8	1.88×10^{-14}	2349.4	101.7
IonJelly 3	5.57×10^{-15}	3942.0	85.5	1.53×10^{-14}	3671.1	81.0
IonJelly 1	3.69×10^{-14}	4798.1	98.5	9.12×10^{-14}	4447.9	86.9
	III			IV		
BMIMDCA$_{1.9\%}$	τ_∞/s	B /K	T_0 / K	τ_∞/s	B /K	T_0/ K
BMIMDCA$_{6.6\%}$	9.60×10^{-19}	2953.5	111.0	3.58×10^{-23}	3118.7	116.3
IonJelly 3	1.24×10^{-15}	2285.5	106.4	2.06×10^{-16}	2071.7	113.7
IonJelly 1	7.40×10^{-17}	3497.6	92.1	2.20×10^{-18}	3031.4	105.7
BMIMDCA$_{1.9\%}$	1.70×10^{-14}	3932.5	102.3	9.69×10^{-18}	3669.9	122.8

The relaxation process detected at the highest frequencies, i.e., process I, is related to the dipolar relaxation associated with the dynamic glass transition (impossible to analyze from the ε'' data, as previous mentioned). From the VFT parameters obtained from process I, it is possible to estimate the glass transition temperature at $\tau = 100$ s,[34] as 171.7 K (-101.5 °C), 164.6 K (-108.6 °C), 172.7 K (-101.0 °C), and 206.6 K (-66.6 °C), respectively, for BMIMDCA$_{1.9\%water}$, BMIMDCA$_{6.6\%water}$, IJ3, and IJ1. Having in mind that the estimated parameters are being taken from a process that is really weak compared with process II and III, the obtained T_g values are in excellent agreement with those determined calorimetrically (see Table 3.1). Roughly, the magnitude of each process decrease a decade from IV to I, the first having values of the order of $10^6 - 10^7$, while process I has a dielectric strength of the order of hundreds. This is the reason why the frequency dependent real conductivity can be taken as mostly due to subdiffusive transport. The low intensity of the cooperative motion associated with the dynamical glass transition compared with conductivity contribution leaves $\sigma'(\omega)$ unaffected, and therefore, meaningful values of crossover frequency, and consequently of τ_e, were estimated.

3.3. Decoupling Index

The VFT dependence obeyed by the relation times of process I was also observed for the dc conductivity. This could point to a correlation between the dynamics of the structural relaxation and the ion motion. To test this, the decoupling index, $R_\tau (T_g)$, was determined for each material, which is the ratio of the structural relaxation time to the conductivity relaxation time[35-36] giving a physical idea of the relationship between the conductivity and structural relaxation processes.[37] This factor conveniently describes the extent to which the ion conducting motions in a given glass can be considered decoupled from the viscous motions of the glassy matrix.[38] An approximate relationship between the logarithm of the decoupling index and the conductivity (in S cm^{-1}) measured at T_g was proposed by Angell[39]

$$\log(R_t\left(T_g\right)) = \log\left(10^{15}\sigma_0\left(T_g\right)\right) \qquad \text{Eq. 3.2}$$

giving the orders of magnitude of the mobility of the charge carriers relative to the mobility driven by the cooperative dynamics. The σ_0 values obtained at the calorimetric T_g were $\sigma_0(T_g)_{BMIMDCA1.9\%water} = 2$ x 10^{-12}, $\sigma_0(T_g)_{BMIMDCA6.6\%water} = 8$ x 10^{-12}, $\sigma_0(T_g)_{IJ3} = 8$ x 10^{-12}, and $\sigma_0(T_g)_{IJ1} = 3$ x 10^{-13} S cm^{-1} given as log decoupling indexes, respectively, 3.3, 3.9, 3.9, and 2.5. In superionic conductors, this value is very large (~7[40] or 9[37]), meaning that the species responsible for conductivity are more mobile 10^7 to 10^9 times than that of the species becoming jammed at the glass transition; it was proposed that the excess mobility was unlikely attributed to any ionic species, instead it should be probably due to the motion of protons themselves[37]. Also, in fast ion conducting AgI-Ag$_2$O-V$_2$O$_5$ glasses, very large values of $R_\tau (T_g)$ were estimated (from 11 to 14) pointing to a decoupling between the motion of the Ag$^+$ ion and the matrix[41]. Also in ion gels, the ion transport is found to be decoupled from the

segmental motion of the polymers, leading to relatively high ionic conductivities even at their glass transition temperatures ($\sim 10^{-7}$ S cm^{-1}) with R_τ (T_g) ≈ 7 in PMMA/[C$_2$mim][NTf$_2$] electrolytes[42].

In the present case, not so high decoupling indexes were estimated meaning by one side that no significant protonic conduction is involved and by other side the the cooperative motion associated with the dynamical glass transition and conductivity are correlated, which points to a dynamic glass transition assisted hopping mechanism of charge transport as found for related systems[23].

In a few words to finalize this section, the dc conductivity of IJ3 follows closely the behaviour of BMIMDCA. At a fixed temperature, the ionic liquid with the highest water amount, BMIMDCA$_{6.6\%water}$, exhibits the highest conductivity, while IJ1 presents the lowest values highly determined by its high glass transition temperature.

Summarizing this section on transport properties, it was observed for the four systems here investigated that the mobility and diffusion coefficients follow a VFT like temperature dependence. Water enhances ion mobility in the bulk ionic liquid; however, in the ion jelly material, the gelatine amount is significant in determining the transport properties since the composite having the higher water content (IJ1) exhibits the lower diffusion coefficients and mobility. Therefore, a critical composition IL/gelatine should exist above which a self-supported material can exhibit ionic liquid-like properties as found here for IJ3.

3.4. Bibliography

[1]   C. P. Fredlake, J. M. Crosthwaite, D. G. Hert, S. N. V. K. Aki, and J. F. Brennecke, "Thermophysical Properties of Imidazolium-Based Ionic Liquids," *Journal of Chemical & Engineering Data*, vol. 49, no. 4, pp. 954–964, Jul. 2004.

[2]   S. V. Troshenkova, E. S. Sashina, N. P. Novoselov, K. F. Arndt, and S. Jankowsky, "Structure of ionic liquids on the basis of imidazole and their mixtures with water," *Russian Journal of General Chemistry*, vol. 80, no. 1, pp. 106–111, Feb. 2010.

[3]   F. Kremer and S. A. Rozanski, "The Dielectric Properties of Semiconducting Disordered Materials," in *Broadband Dielectric Spectroscopy*, Springer-V., Berlin, Germany: , 2003, pp. 475–494.

[4]   E. Neagu; P. Pissis; L. Apekis; J. L. Gomez Ribelles, "Dielectric relaxation spectroscopy of polyethylene terephthalate (PET) films," *Journal of Physics D: Applied Physics*, vol. 30, no. 11, pp. 1551–1560, 1997.

[5]   M. Sun, S. Pejanovic, and J. Mijovic, "Dynamics of Deoxyribonucleic Acid Solutions As Studied by Dielectric Relaxation Spectroscopy and Dynamic Mechanical Spectroscopy," *Macromolecules*, vol. 38, no. 23, pp. 9854–9864, 2005.

[6]   H. Lu, X. Zhang, and H. Zhang, "Influence of the relaxation of Maxwell-Wagner-Sillars polarization and dc conductivity on the dielectric behaviors of nylon 1010," *Journal of Applied Physics*, vol. 100, no. 5, p. 054104, 2006.

[7]   A. K. Jonscher, "Universal Dielectric Response," *Nature*, vol. 267, no. 5613, pp. 673–679, 1977.

[8]   J. R. Sangoro, C. Iacob, S. Naumov, R. Valiullin, H. Rexhausen, J. Hunger, R. Buchner, V. Strehmel, J. Kärger, and F. Kremer, "Diffusion in ionic liquids: the interplay between molecular structure and dynamics," *Soft Matter*, vol. 7, no. 5, p. 1678, 2011.

[9]   M. T. Viciosa, M. Dionísio, and J. L. Gómez Ribelles, "Kinetics of free radical polymerization probed by dielectric relaxation spectroscopy under high conductivity conditions," *Polymer*, vol. 52, no. 9, pp. 1944–1953, Apr. 2011.

[10]   C. Iacob, J. R. Sangoro, a Serghei, S. Naumov, Y. Korth, J. Kärger, C. Friedrich, and F. Kremer, "Charge transport and glassy dynamics in imidazole-based liquids.," *The Journal of chemical physics*, vol. 129, no. 23, p. 234511, Dec. 2008.

[11]   G. Tammann and W. Hesse, "The dependancy of viscosity on temperature in hypothermic liquids," *Zeitschrift für anorganische und allgemeine Chemie*, vol. 156, no. 4, pp. 245–257, 1925.

[12]   G. S. Fulcher, "Analysis of recent measurements of the viscosity of glasses," *Journal of the American Ceramic Society*, vol. 8, no. 6, pp. 339–355, 1925.

[13]   H. Vogel, "The temperature dependence law of the viscosity of fluids," *Physikalische Zeitschrift*, vol. 22, pp. 645–646, 1921.

[14]   O. Zech, A. Stoppa, R. Buchner, and W. Kunz, "The Conductivity of Imidazolium-Based Ionic Liquids from (248 to 468) K. B. Variation of the Anion," *Journal of Chemical & Engineering Data*, vol. 55, no. 5, pp. 1774–1778, May 2010.

[15]   N. Ito, W. Huang, and R. Richert, "Dynamics of a supercooled ionic liquid studied by optical and dielectric spectroscopy.," *The journal of physical chemistry. B*, vol. 110, no. 9, pp. 4371–7, Mar. 2006.

[16]   J. Sangoro, C. Iacob, a Serghei, S. Naumov, P. Galvosas, J. Kärger, C. Wespe, F. Bordusa, a Stoppa, J. Hunger, R. Buchner, and F. Kremer, "Electrical conductivity and translational diffusion in the 1-butyl-3-methylimidazolium tetrafluoroborate ionic liquid.," *The Journal of chemical physics*, vol. 128, no. 21, p. 214509, Jun. 2008.

[17]   J. R. Sangoro, a. Serghei, S. Naumov, P. Galvosas, J. Kärger, C. Wespe, F. Bordusa, and F. Kremer, "Charge transport and mass transport in imidazolium-based ionic liquids," *Physical Review E*, vol. 77, no. 5, pp. 4–7, May 2008.

[18]   J. Leys, M. Wübbenhorst, C. Preethy Menon, R. Rajesh, J. Thoen, C. Glorieux, P. Nockemann, B. Thijs, K. Binnemans, and S. Longuemart, "Temperature dependence of the electrical conductivity of imidazolium ionic liquids.," *The Journal of chemical physics*, vol. 128, no. 6, p. 064509, Feb. 2008.

[19]   M. Dionísio and J. F. Mano, "Electrical Techniques," in *Handbook of Thermal Analysis and Calorimetry*, 5th ed., Elsevier, 2008, pp. 209–268.

[20]   B. Roling, C. Martiny, and S. Murugavel, "Ionic Conduction in Glass: New Information on the Interrelation between the 'Jonscher Behavior' and the 'Nearly Constant-Loss Behavior' from Broadband Conductivity Spectra," *Physical Review Letters*, vol. 87, no. 8, pp. 1–4, Aug. 2001.

[21]   J. Dyre and T. Schrøder, "Universality of ac conduction in disordered solids," *Reviews of Modern Physics*, vol. 72, no. 3, pp. 873–892, Jul. 2000.

[22] C. Aliaga and S. Baldelli, "Sum frequency generation spectroscopy of dicyanamide based room-temperature ionic liquids. Orientation of the cation and the anion at the gas-liquid interface.," *The journal of physical chemistry. B*, vol. 111, no. 33, pp. 9733–40, Aug. 2007.

[23] J. R. Sangoro, C. Iacob, A. Serghei, C. Friedrich, and F. Kremer, "Universal scaling of charge transport in glass-forming ionic liquids.," *Physical chemistry chemical physics : PCCP*, vol. 11, no. 6, pp. 913–916, Feb. 2009.

[24] R. Böhmer, K. L. Ngai, C. a. Angell, and D. J. Plazek, "Nonexponential relaxations in strong and fragile glass formers," *The Journal of Chemical Physics*, vol. 99, no. 5, pp. 4201–4209, 1993.

[25] "In ions, the Pauling diameter is often taken as an estimate of the mean square displacement (as mentioned in ref 26,) while the vdW diameter refers to neutral atoms/molecules; however, ions in ionic liquids interact via both electrostatic interactions and." .

[26] T. Frömling, M. Kunze, M. Schönhoff, J. Sundermeyer, and B. Roling, "Enhanced lithium transference numbers in ionic liquid electrolytes.," *The journal of physical chemistry. B*, vol. 112, no. 41, pp. 12985–90, Oct. 2008.

[27] "Spartan Student V4.1.2, Wavefunction Inc., Irvine, California." .

[28] H. V Spohr and G. N. Patey, "The influence of water on the structural and transport properties of model ionic liquids.," *The Journal of chemical physics*, vol. 132, no. 23, p. 234510, Jun. 2010.

[29] T. M. Chang, L. X. Dang, R. Devanathan, and M. Dupuis, "Structure and dynamics of N,N-diethyl-N-methylammonium triflate ionic liquid, neat and with water, from molecular dynamics simulations.," *The journal of physical chemistry. A*, vol. 114, no. 48, pp. 12764–74, Dec. 2010.

[30] J. N. A. Canongia Lopes and A. a H. Pádua, "Nanostructural organization in ionic liquids.," *The journal of physical chemistry. B*, vol. 110, no. 7, pp. 3330–5, Feb. 2006.

[31] A. Triolo, O. Russina, H. J. Bleif, and E. Di Cola, "Nanoscale segregation in room temperature ionic liquids.," *The journal of physical chemistry. B*, vol. 111, no. 18, pp. 4641–4, May 2007.

[32] J. N. Canongia Lopes, M. F. Costa Gomes, and A. A. H. Pádua, "Nonpolar, polar, and associating solutes in ionic liquids.," *The journal of physical chemistry. B*, vol. 110, no. 34, pp. 16816–8, Aug. 2006.

[33] P. A. M. Steeman and J. van Turnhout, "Dielectric Properties of inhomogeneous Media," in *Broadband Dielectric Spectroscopy*, Springer-V., Berlim, Germany: , 2003.

[34] R. R and B. A, *Disorder Effects on Relaxational Processes*, Springer. Berlin, Germany: , 1994.

[35] Angell. C. A, "Fast Ion Motion in Glassy and Amorphous Materials," *Solid State Ionics*, vol. 9/10, no. DEC, pp. 3–16, 1983.

[36] C. T. Moynihan, N. Balitactac; L. Boone; T. A. Litovitz, "Comparison of Shear and Conductivity Relaxation Times for Concentrated Lithium Chloride Solutions," *The Journal of Chemical Physics*, vol. 55, no. 6, p. 3013, 1971.

[37] F. Mizuno, J. P. Belieres, N. Kuwata, a. Pradel, M. Ribes, and C. a. Angell, "Highly decoupled ionic and protonic solid electrolyte systems, in relation to other relaxing systems and their energy landscapes," *Journal of Non-Crystalline Solids*, vol. 352, no. 42–49, pp. 5147–5155, Nov. 2006.

[38] K. L. Ngai, "Structural relaxation and conductivity relaxation in glassy ionics," *Le Journal de Physique IV*, vol. 02, no. C2, pp. C2–61–C2–73, Oct. 1992.

[39] Angell. C. A., "Mobile Ions in Amourphous Solids," *Annual Review of Physical Chemistry*, vol. 43, pp. 693–717, 1992.

[40] J. R. Sangoro, G. Turky, M. A. Rehim, C. Iacob, S. Naumov, A. Ghoneim, J. Ka, and F. Kremer, "Charge Transport and Dipolar Relaxations in Hyperbranched Polyamide Amines," pp. 1648–1651, 2009.

[41] S. Bhattacharya, "Conductivity relaxation in some fast ion-conducting AgI–Ag2O–V2O5 glasses," *Solid State Ionics*, vol. 161, no. 1–2, pp. 61–65, Jul. 2003.

[42] T. Ueki and M. Watanabe, "Macromolecules in Ionic Liquids: Progress, Challenges, and Opportunities," *Macromolecules*, vol. 41, no. 11, pp. 3739–3749, Jun. 2008.

Chapter 4

IMPROVING AND UNDERSTANDING IJ CONDUCTIVE PROPERTIES USING DCA BASED ILS

4. IMPROVING AND UNDERSTANDING IJ CONDUCTIVE PROPERTIES USING DCA BASED ILS

In the present chapter we have tried to evaluate the impact of different IL cations on IJ physical chemical properties, namely: BPyDCA, BMPyrDCA and EMIMDCA.

Previously [1-2] we found that IJs based on ILs that contains DCA anion have led to stable and transparent materials. This result can be partially explained by the fact that DCA anion is a strong ligand [3-4].

In this work we have also studied the impact of water on both IL and IJ physical chemical properties. In our previous study [2] we have observed that water plays an essential role on the ionic diffusion, mobility and conductivity. The idea here was to test if this effect could be correlated in any extension with the change on IL cation, since different cations establish different interactions with water, gelatine or even with the DCA anion.

Moreover, the physical properties as conductivity are strongly temperature dependent. In such glass former systems, the glass transition temperature (T_g) gains a particular relevance since it can determine, when over passed, the onset of diffusive behaviour (see chapter 1) as it was previously shown in chapter 3 and reported in reference [2]. Therefore, the T_g determination and the evaluation of the conductivity and dynamical behaviour below in the glass region, and above T_g in the supercooled regime, is important for the understanding of the IJ performance, being the reason why the calorimetric and dielectric experiments were done covering a wide range of temperatures. Thus, besides the T_g estimate, it was also possible to evaluate the dynamic fragility, i.e., the temperature resistance of flow properties for the IJ systems and correlate both parameters with the obtained conductivity.

To simplify the discussion, the materials characterization is presented in two parts according the used experimental technique, calorimetry and dielectric spectroscopy.

4.1. Thermal Characterization

A liquid below its melting point should crystallize, however, a pre-requisite is needed: the formation of a nucleus on which a crystal can subsequently grow.

Thus crystallization is a two-step process: nucleation and crystal growth, which are both dependent on kinetic and thermodynamic factors [5]. For instance, nucleation is thermodynamically favored at low temperatures where molecules aggregate in the liquid phase forming structured clusters inside which crystalline nucleus start to appear. The nucleation of crystals inside such "metastable dense liquid clusters" [6] was demonstrated for glucose isomerase in poly ethyleneglycol using confocal scanning laser fluorescence microscopy [6-7]. On the other hand an increase in temperature kinetically favors the nucleation step due to a viscosity decrease. Thus during the temperature decrease the nucleation rate slows down which led to a decrease on nucleus concentration which promotes the reduction of cluster volume [6]; it is important to note that the authors go further sustaining that nucleation is also a two-step mechanism where the formation of mesoscopic clusters of dense liquid is the first step followed by nucleation, however a detailed discussion on nucleation theories is out of the scope of this thesis.

Basically, the crystallization exothermic process always occurs between the glass transition and melting, since at low temperature the nucleus diffusion is to low which makes the crystal growth "kinetically impractical" [5], [8].

The displacement of crystallization processes between glass transition and melting depends not only on the material nature [5] but also on the temperature rate at which the processes takes place.

In summary, crystallization results from the interplay between nucleation and crystal growth. Nevertheless nucleation cannot be followed by calorimetry since the heat effects produced during the process are below the DSC detection limit. On the other hand, the crystal growth can be clearly identified on the thermogram through the appearance of an exothermal peak. The use on DSC is extremely important to understand and characterize the crystallization process. Thus, through this technique, is possible to find the conditions where crystallization occurs. This is very useful on pharmaceutical industry to identify the occurrence of polymorphism, which is the formation of different crystalline forms on the same drug substance, meaning that the molecule will have different physical properties [9].

Furthermore the crystallization process can also be avoided during the thermal treatment of the given sample. This can be attained by performing the thermal treatment using ultra fast temperature scan. A good example of this fact was given by Evgeny Zhuravlev *et al* [8] for the poly (ε-caprolactone) (PCL) thermal analysis. In this case the author shows that the PCL crystallization could be avoided using a cooling rate of 500 K/s. Moreover the same authors also showed that was also possible to suppress nucleation when a cooling rate of nearly 7000K/s was used.

Crystallization and the characteristics of the formed crystals, as size, perfection and polymorphism, are largely determined by nucleation. But crystallization can depend also on the sample composition, namely the hydration level. In fact the impact of water content on both IJ and ILs physical properties was one of the majors issues studied on this chapter. In this particular we have showed on BMIMDCA, BMPyrDCA and EMIMDCA ILs that the crystallization process could be only observed after water removal. This fact clarifies why *Tc* and *Tm* are present only in the second run of DSC measurement. This subject will be discussed below.

Additionally, the liquid and further on, the supercooled liquid, could fail crystallization at all and vitrify in an out of equilibrium condition, becoming a glass. The temperature at which a liquid-like system changes to glass (solid-like material), is called glass transition temperature, T_g. The glass transition establishes a boundary below which the substance is no longer in a metastable equilibrium state [10-11]. The motion that allows the sample above its T_g to be pliable is a long range motion, which is frozen in the glass, below T_g. The glass lacks any structure; is a solid like material that arrested the disorder of the original supercooled liquid being only strewn around the space surrounded. As the glass transition is over passed by temperature increasing, the material changes from hard and brittle to soft and pliable.

Although glasses form by avoiding crystallization upon cooling the liquid, it can also crystallize by a process designated by some authors as devitrification. The mechanism that allows devitrification to occur, in this sense, was elucidated by Sanz *et al.* [12] through computer simulation studies for

monodisperse hard-sphere glasses. This process was observed for a anti-inflammatory drug, indomethacin [13].

From the established above, it is clear that phase transformations are complex phenomena, where crystallization and vitrification could be either driven or avoided by different thermal treatments. We found that ILs are suitable models to understand these physical changes.

The thermal transitions studied on the present work where performed through DSC analysis. The respective thermograms, recorded in the first heating scan, are presented in Figure 4.1 (a-d); the insets of figures 4.1 (b), 4.1 (c) and 4.1 (d) include the termograms collected in a second heating scan.

In the present work we have studied twelve systems that includes neat ILs and their respective IJs, which the respective thermograms are presented in Figure 4.1: a) $BPyDCA_{0.4\%}$, $BPyDCA_{9\%}$, $BPyDCA_{IJ}$, b) $BMIMDCA_{0.4\%}$, $BMIMDCA_{9\%}$, $BMIMDCA_{IJ}$, c) $BMPyrDCA_{0.4\%}$, $BMPyrDCA_{9\%}$, $BMPyrDCA_{IJ}$ and d) $EMIMDCA_{0.4\%}$, $EMIMDCA_{9\%}$ and $EMIMDCA_{IJ}$. It is clear in the low temperature region of the thermograms, the heat flow jump. Nonetheless, this jump is not so pronounced on the IJs which exhibit a broader transition width.

The presence in each system of a glass transition from which a Tg can be determined, allow us to classify all the tested materials as glass formers.

The temperature values extracted from the onset, the midpoint, and the endset of the glass transition are presented in Table 4.1. When we compare the T_g values, while the onset of the two ILs, either with 0.4% and 9% water, are quite similar, for IJs this value is always higher; this will be later confirmed by DRS. Since the IJ has 9% of water content, the higher T_g value may indicate that water in these composites is not interacting directly with the IL, instead is assuring the gelatine structure, otherwise a lower T_g should be determined since water has a plasticizing effect decreasing the glass transition temperature; this will be explored in more detail in chapter 5.

In Figures 4.1 (a-d), at higher temperatures a broad and endothermic peak which onset is located around 300 K is detected for all systems, corresponding to water evaporation. The insets of Figure 4.1 (b), Figure 4.1 (c) and Figure 4.1 (d), present the thermograms of the indicated systems taken in a second heating scan after water removal. It is possible to see three distinct transitions: the glass transition, an exothermic peak indicating crystallization, and an endothermic peak corresponding to melting. The arrows in each figure indicate the respective scale, in order to be noted more clearly the T_g in the sample.

The temperatures of the minimum/maximum of melting and crystallization peaks, in the cases where it are observed, were also included in Table 4.1.

For $EMIMDCA_{0.4\%}$ and $EMIMDCA_{9\%}$ the temperature values of melting and crystallization are 264.5 K (-8.7 °C), 237.3 K (-35.9 °C), 263.2 K (-9.9 °C) and 225.7(-47.5 °C), respectively, which are in agreement with the values reported by Fletcher *et al* [14]. For $BMIMDCA_{0.4\%}$ the temperature values of melting and crystallization are 268.2 K (-4.8 °C) and 247.8 K (-25.2 °C), respectively, which are in excellent agreement with the values reported by Fredlake *et al* [15]. For BMPyrDCA, to our knowledge, there are no reported values of melting or crystallization temperature. On each sample mentioned above, melting and crystallization are only possible on the second run, since it is needed the water removal for both phenomena take place. To ensure this, the sample was heated to 423 K in

the first heating and maintained 5 min at this temperature. Melting happens when the structure of the ILs is no longer a crystalline structure, but became a disordered liquid.

The detection upon heating of a glass transition followed by crystallization in dry BMPyrDCA and EMIMDCA ILs, reveals that these materials are completely amorphous below T_g. Above T_g, they enter into a supercooled regime, crystallizing later at T_c exhibiting a three dimensional structure. However there are conditions and or/materials where amorphous regions coexist with a crystalline phase as is well known in semi-crystalline polymers and other ILs [15-17]. For the respective IJs, only the glass transition is detected, which means that these materials are completely amorphous.
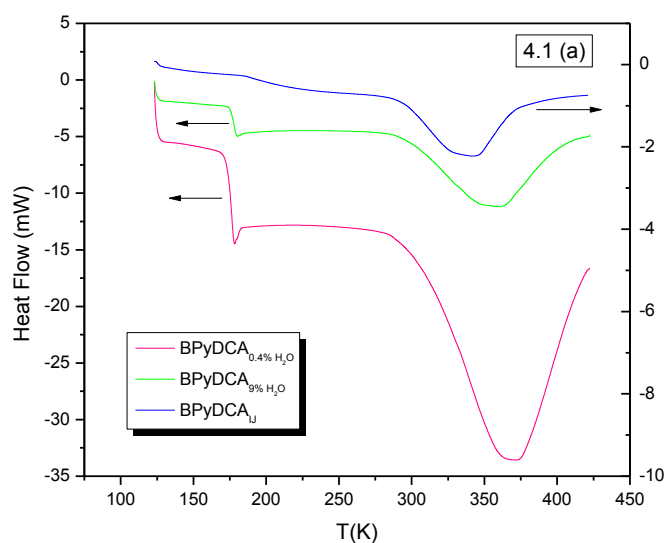
Figure 4.1 (a) - DSC scans obtained in heating mode at 20 K.min^{-1} for BPyDCA$_{0.4\%water}$, BPyDCA$_{9\%water}$, and BPyDCA$_{IJ}$ showing the heat flow jump at the glass transition.
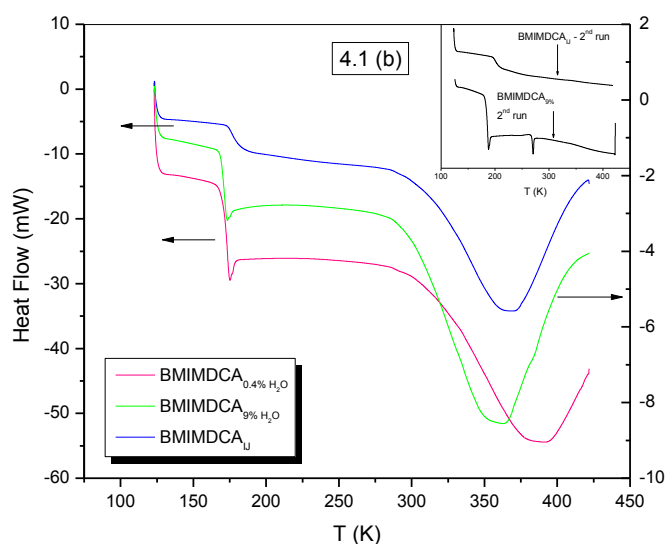
Figure 4.1 (b) - DSC scans obtained in heating mode at 20 K.min^{-1} for BMIMDCA$_{0.4\%water}$, BMIMDCA$_{9\%water}$, and BMIMDCA$_{IJ}$ showing the heat flow jump at the glass transition. The inset shows the second heating scan for BMIMDCA$_{9\%water}$ and BMIMDCA$_{IJ}$, where cold crystallization and melt are observed for the IL and avoided for the IJ (see text).
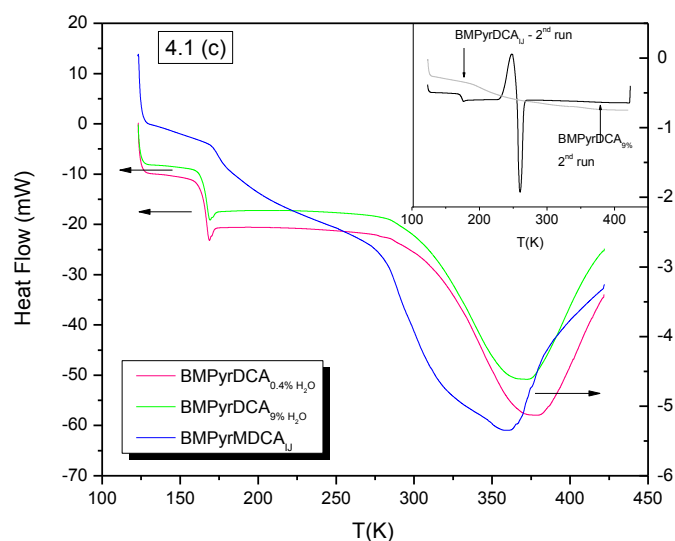
Figure 4.1 (c) - DSC scans obtained in heating mode at 20 K.min^{-1} for BMPyrDCA$_{0.4\%water}$, BMPyrDCA$_{9\%water}$, and BMPyrDCA$_{IJ}$ showing the heat flow jump at the glass transition. The inset shows the second heating scan for BMIPyrDCA$_{9\%water}$ and BMPyrDCA$_{IJ}$, where cold crystallization and melt are observed for the IL and avoided for the IJ (see text).
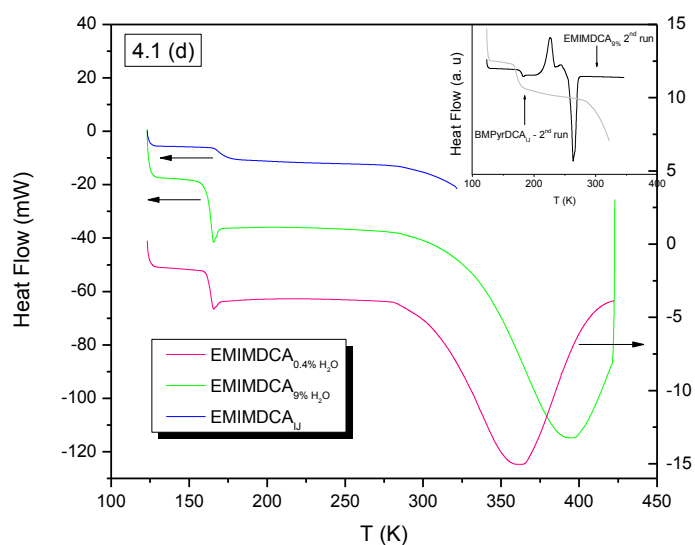
Figure 4.1 (d) - DSC scans obtained in heating mode at 20 K.min^{-1} for EMIMDCA$_{0.4\%water}$, EMIMDCA$_{9\%water}$, and EMIMDCA$_{IJ}$ showing the heat flow jump at the glass transition. The inset shows the second heating scan for EMIMDCA$_{9\%water}$ and EMIMDCA$_{IJ}$, where cold crystallization and melt are observed for the IL and avoided for the IJ (see text).

Table 4.1 - Glass Transition Temperatures Taken at the Onset (on), Midpoint (mid) and Endset (end) of the Heat Flow Jump for both BPyDCA, BMIMDCA, BMPyrDCA, EMIMDCA and respective IJ, obtained during a First Heating Run at 20 K/min; melting and crystallization temperatures obtained from a second heating run.

System		$T_{g,on}$/K	$T_{g,mid}$/K	$T_{g,end}$/K	T_c/K	T_m/K	T_0/T_g
BPyDCA$_{0.4\%water}$	1st heating run	173.5	176.5	176.9	----	----	0.80
	2nd heating run	193.1	195.7	196.0	----	----	
BPyDCA$_{9\%water}$	1st heating run	175.4	177.8	179.0	----	----	0.78
	2nd heating run	194.9	197.2	197.9	----	----	
BPyDCA$_{IJ}$	1st heating run	185.4	189.6	213.4	----	----	0.71
	2nd heating run	213.9	227.1	249.8	----	----	
BMIMDCA$_{0.4\%water}$	1st heating run	170.6	173.4	173.7	----	----	0.76
	2nd heating run	183.5	186.2	186.4	247.8	268.2	
BMIMDCA$_{9\%water}$	1st heating run	169.0	171.5	172.3	----	----	0.76
	2nd heating run	185.4	187.4	188.1	----	----	
BMIMDCA$_{IJ}$	1st heating run	174.2	176.5	182.3	----	----	0.73
	2nd heating run	196.8	200.4	206.4	----	----	
BMPyrDCA$_{0.4\%water}$	1st heating run	164.6	167.2	167.6	----	----	0.82
	2nd heating run	171.1	173.9	174.2	----	----	
BMPyrDCA$_{9\%water}$	1st heating run	164.4	167.5	168.2	----	----	0.74
	2nd heating run	171.7	174.6	171.5	247.9	260.0	
BMPyrDCA$_{IJ}$	1st heating run	170.5	173.9	180.1	----	----	0.65
	2nd heating run	188.0	198.7	220.5	----	----	
EMIMDCA$_{0.4\%water}$	1st heating run	161.6	164.1	164.6	----	----	0.46
	2nd heating run	180.6	182.6	183.6	237.3	264.5	
EMIMDCA$_{9\%water}$	1st heating run	161.9	164.2	164.5	----	----	0.71
	2nd heating run	180.1	182.6	182.8	225.7	263.2	
EMIMDCA$_{IJ}$	1st heating run	166.2	168.4	174.8	----	----	0.73
	2nd heating run	191.1	195.1	203.0	----	----	

In general, two types of behaviour are observed for the studied ILs and the respective IJs. The first group, which includes BPyDCA , Figure 4.1 – (a), corresponds to materials which are 100% amorphous, since only the glass transition is detected upon thermal analysis; this behaviour accounts for the hydrated and dry ILs, and the respective IJs as well. However, the shape of the respective heat flux steps is much broader that the observed for the other systems. Here, it is very important the analysis of the DRS results, since we can predict a range of temperatures for the T_g value (see next section).

The second group of ILs, include the ones presented in Figure 4.1 – (b), Figure 4.1 – (c) and Figure 4.1 – (d), BMIMDCA, BMPyrDCA and EMIMDCA. As observed for the previous group, a glass transition is detected for the hydrated materials. Nonetheless, in the second heating run after water removal, the samples undergo crystallization, i. e., the samples change from a glass to a supercooled liquid occurring subsequently crystallization, followed by melting. In other words, at temperatures above T_g, the supercooled liquid crystallizes, melting upon further heating at T_m.

Under the tested conditions, BPyDCA IL and IJ are completely amorphous, while the other materials are crystallisable.

4.2. Dielectric Characterization

For dielectric characterization we have also studied the twelve systems mentioned previously which include neat ILs and their respective IJs, $BPyDCA_{0.4\%}$, $BPyDCA_{9\%}$, $BPyDCA_{IJ}$, $BMIMDCA_{0.4\%}$, $BMIMDCA_{9\%}$, $BMIMDCA_{IJ}$, $BMPyrDCA_{0.4\%}$, $BMPyrDCA_{9\%}$, $BMPyrDCA_{IJ}$, $EMIMDCA_{0.4\%}$, $EMIMDCA_{9\%}$ and $EMIMDCA_{IJ}$. Since the studied ILs presented different physical chemical characteristics we have grouped according some common particularities.

4.2.1. Conductivity

4.2.1.1. BMIMDCA and BPyDCA

Since BMIMDCA and BPyDCA present same similarities in terms of conductivity, their conductive properties will be discussed together.

As previously mentioned, the different materials were also submitted to dielectric analysis. In Figure 4.2, the real (ε') and imaginary (ε'') parts of the complex permittivity measured for BMIMDCA as a function of frequency (ν) at 175.15 K are presented; the dependency for the conductivity is included in the inset. In the medium frequency range, the spectrum is dominated by the direct conductivity, also called pure conductivity, σ_0, indicated in the figure, which is a frequency independent conductivity value. Some authors refer the pure conductivity as direct conductivity (σ_{dc}). In this spectral region, the $\log (\varepsilon'')$ vs $\log_{10}\nu$ representation should give a straight line with a slope of -1; for $BMIMDCA_{0.4\%water}$ at 175.15 K the obtained slope is -0.98.

The real part is dominated by the blocking effect of the charge carriers at the electrodes at the lower frequencies. This phenomenon is called electrode polarization (EP). In $BMIMDCA_{0.4\%water}$ at 175.15 K EP is observed for frequencies below around 10 Hz which is a temperature dependent

phenomenon. The inset shows the frequency dependence of the real conductivity. In this representation three distinct regions are identified: the region corresponding to EP, the region where the pure conductivity should be extracted (σ_0), and the region of sub-diffusive conductivity (SD); the increase in ε' is due to electrode polarization. This behaviour is common for all studied materials, except for BMPyrDCA that will be analyzed separately. The extremely high values of conductivity masked any possible analysis of relaxation process for this system.
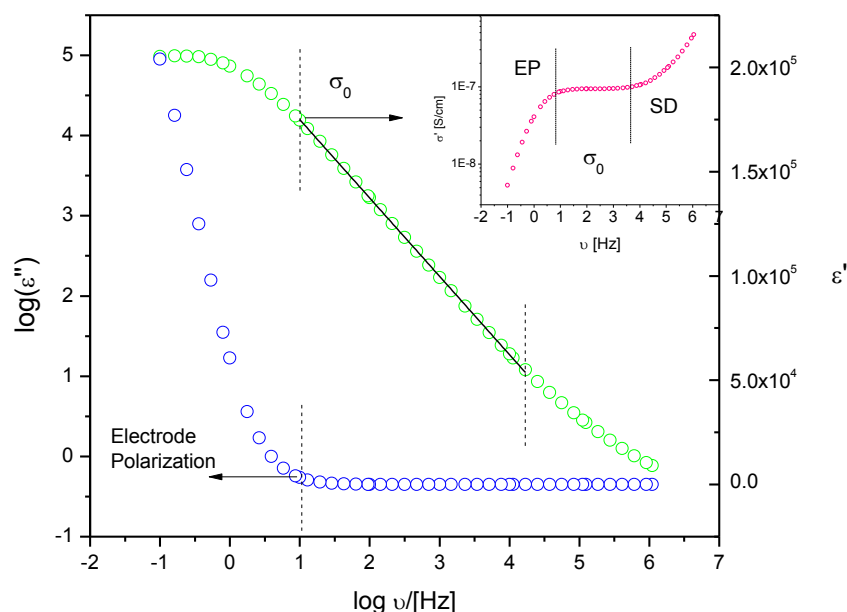
Figure 4.2 - Real (o) and imaginary (o) parts of the complex permittivity of BMIMDCA$_{0.4\%water}$, as a function of the frequency at 175.15 K. Inset: The conductivity as a function of frequency. See text for the meanings of the abbreviations.

In order to study the transport mechanism of charge carriers the analysis was taken over the broadest accessible range of temperatures and frequencies. We determined the conductivity of the twelve materials, looking for tendencies in this property and in its temperature dependence. Figure 4.3 (a-f), shows the real components of the complex conductivity, $\sigma^*(\omega) = \sigma'(\omega) + i\sigma''(\omega)$, from 10^{-1} Hz to 10^6 Hz covering a range of temperatures from 163 to 313K for each material: BPyDCA$_{0.4\%}$, BPyDCA$_{9\%}$ and BPyDCA$_{IJ}$; BMIMDCA$_{0.4\%}$, BMIMDCA$_{9\%}$ and BMIMDCA$_{IJ}$ from top to bottom.

An important feature in this spectral region is the plateau in σ' (corresponding to a linear dependence of slope -1 in the plots of ε'' versus frequency as above mentioned), which gives σ_0. At lower temperatures, or high frequencies, the $\sigma'(\nu)$ plot presents a pronounced increase. The overall conductivity behaviour follows a power law dependence (a. c. conductivity) against the angular frequency ω according the equation proposed by Jonscher [18] (equation 1.14 in *Introduction*).

The characteristic crossover frequency is the frequency at which the plateau bends off to the frequency dependent region, separating the two regimes.

At very low temperatures, the regime is permanently sub-diffusive (see *Introduction*) and no crossover is observed.

It is interesting to observe that there is some correlation between the temperature at which occurs the emergence of a crossover frequency in the conductivity measurements and the glass transition temperature, as determined from DSC analysis ($T_{g,DSC}$), like we already observed on chapter 3. In the real conductivity spectra collected for each system presented in figure 4.3 (a-f), the $T_{g,DSC}$ value is indicated by an arrow; it always lies between two temperatures at which a plateau start to emerge.

Therefore, it is possible for each system to go the other way around defining a range of temperatures within which a bending to a plateau occurs in the conductivity spectra and correlate it with the glass transition. For almost the studied systems, it is observed that the temperature range thus defined includes the T_g value extracted from the DSC measurements, providing a mean to roughly estimated the glass transition. The major error in this prediction was found for $BPyDCA_{IJ}$ and is in the order of 10%.
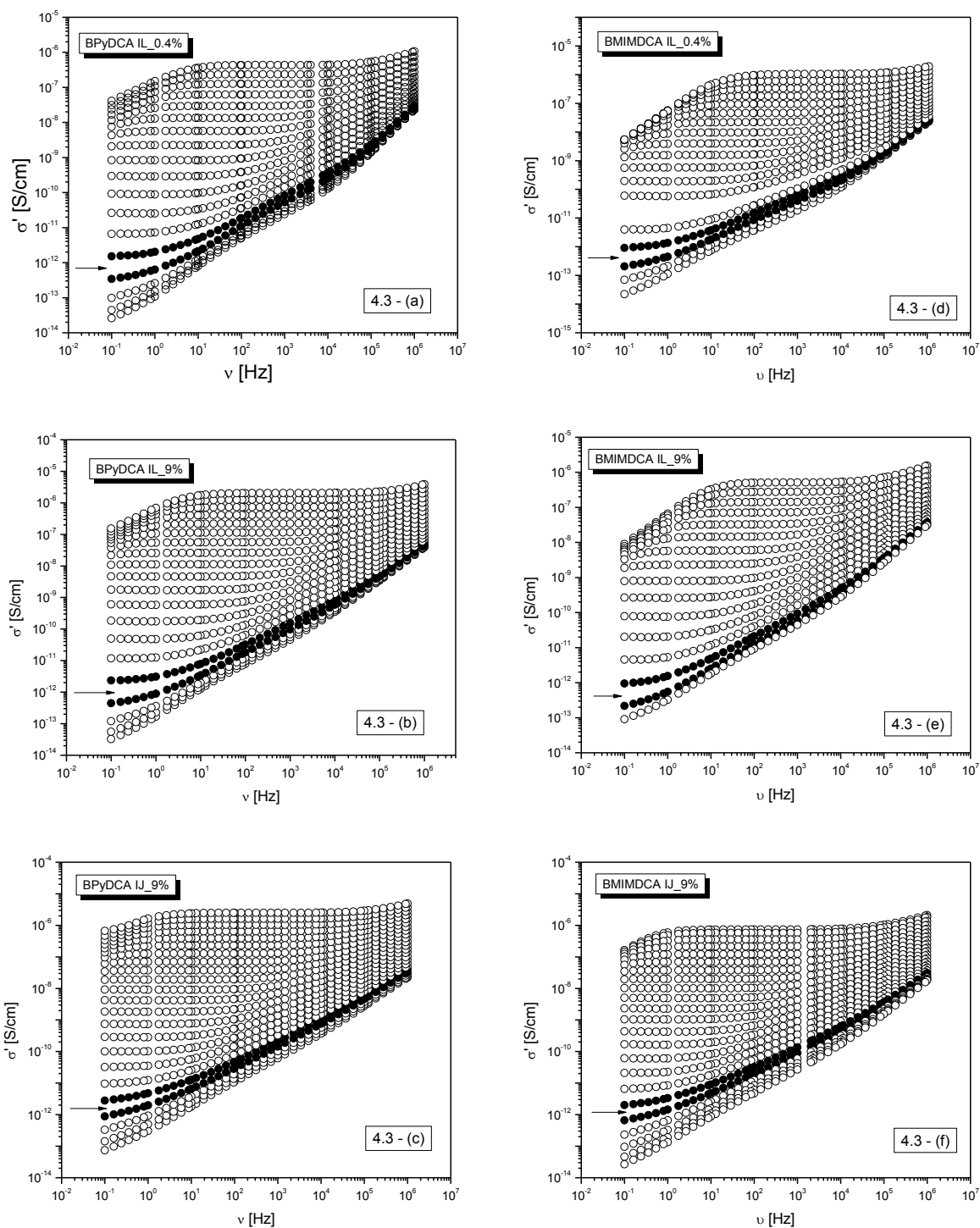
Figure 4.3 (a – f) - Complex conductivity measured at different temperatures of: (a) BPyDCA$_{0.4\%water}$, (b) BPyDCA$_{9\%water}$ and (c) BPyDCA$_{Ion\ Jelly}$; (d) BMIMDCA$_{0.4\%water}$, (e) BMIMDCA$_{9\%water}$ and (f), BMIMDCA $_{Ion\ Jelly}$ (in steps of 2 K from 163 K to 103 K): (a-f) real, σ', components; the estimated onset of the calorimetric T$_g$ occurs at a temperature in between the isotherms represented in filled symbols (indicated by the arrow).

Figure 4.4 (a-f) below presents a comparison between the T_g extracted from the DSC measurements and the one predicted through the plot of conductivity versus frequency, showing a relatively good agreement.

This behaviour leads to us to assume that some motional mechanism as the one underlying the process associated with the dynamical glass transition needs to be settled in order to enable the diffusive movement of ions.
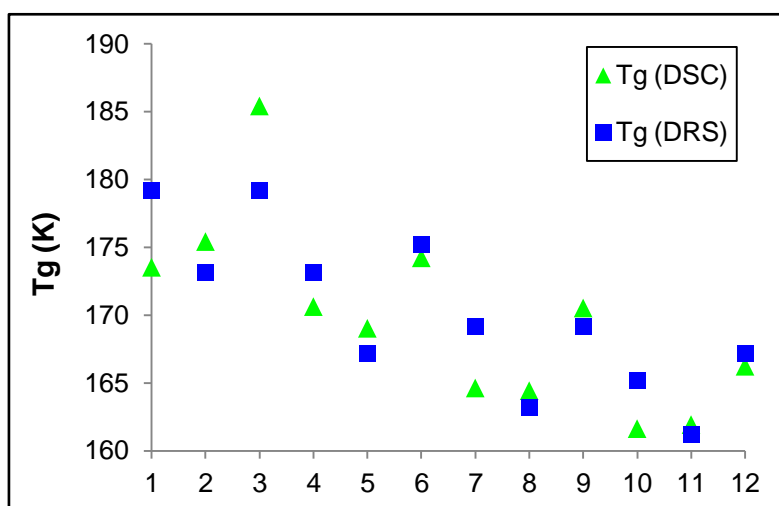
Figure 4.4 – Correlation between the T_g extracted from DSC (in green) and predicted from the change in the profile of the conductivity plot taken by DRS (in blue), in which of the studied samples: 1-BPyDCA$_{0.4\%}$, 2-BPyDCA$_{9\%}$, 3-BPyDCA$_{IJ}$; 4-BMIMDCA$_{0.4\%}$, 5-BMIMDCA$_{9\%}$, 6-BMIMDCA$_{IJ}$; 7-BMPyrDCA$_{0.4\%}$, 8-BMPyrDCA$_{9\%}$, 9-BMPyrDCA$_{IJ}$; 10-EMIMDCA$_{0.4\%}$, 11-EMIMDCA$_{9\%}$, 12-EMIMDCA$_{IJ}$.

4.2.1.2. 1-Buthyl-1-Methyl Pyrrolidinium Dicyanamide (BMPyrDCA)

As mentioned previously in *Introduction*, for the dielectric response of a material not only charge transport processes contribute as mainly analyzed in this section, but also interfacial polarizations and reorientational motions of dipoles. The latter give rise to relaxational processes, which manifest spectrally as a peak in the imaginary part of permittivity ε'' and a sigmoidal curve in the real part ε' of the complex dielectric function against frequency. This is quite different from the permittivity spectrum depicted earlier in figure 4.2 for BMIMDCA, from which no information of relaxation process was possible to extract due to the conductivity contribution. Oppositely, for BMPyrDCA as shown in Figure 4.5, the conductivity contribution at lower temperatures is relatively small and the imaginary part of the complex permittivity, ε'', exhibit a well-defined peak, which shifts to higher frequencies with increasing temperatures, being this behaviour similar to another ones related in previous studies [19]. The $\varepsilon''(\nu)$ curves were collected at low temperatures, even below the calorimetric glass transiton of BMPyrDCA. Therefore, the relaxation process is a secondary one, very local in nature probably due to intra-ionic motions. The low frequency tail that increases significantly with the tempeature increase, denounces the incoming of the relaxation process asscociated with the dynamical glass transition involving larger scale motions. The observation of dipolar relaxation in BMPyrDCA means that under the influence of the external electrical field this IL behaves mainly as a single dipole instead of behaving as an anion

plus a cation; the dipolar behavior was recently observed by NMR experiments for another IL [20]; we will return to this discussion later on this capter.
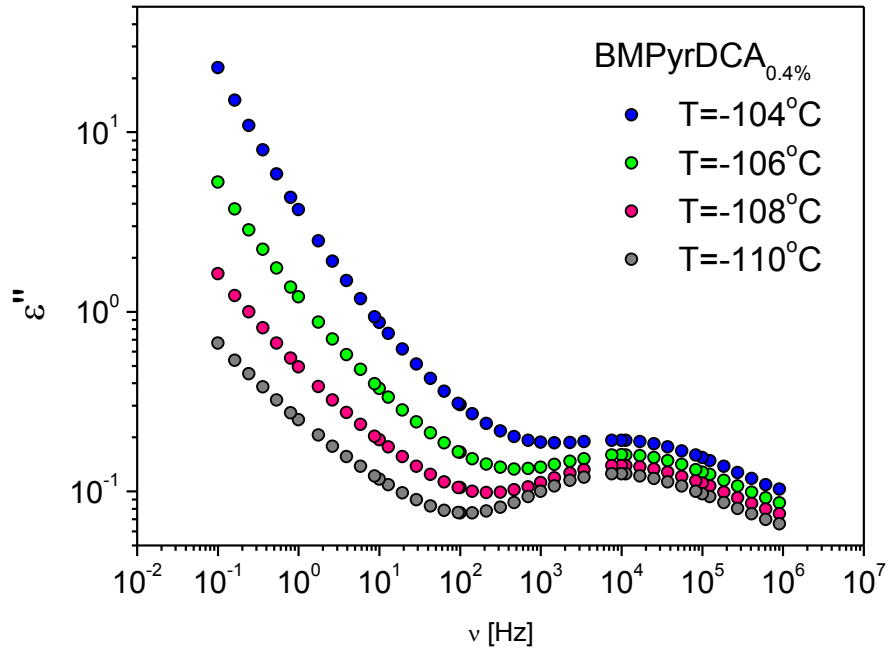
Figure 4.5 - Imaginary part of the complex dielectric function for a relaxation process in BMPyrDCA$_{0.4\%}$.

The type of cooperative mobility that sets in with the temperature increase, which is behind the process associated with the dynamical glass transition, enables the translational motion of charge carriers, increasing conductivity which later on masks the relaxation processes; i.e., the number of species that behave as a separate cation-anion pair start to dominate over those that respond to the applied filed as a single dipole. The real conductivity plot in figure 4.6 – (a) for BMPyrDCA$_{0.4\%}$ reflects the dipolar behaviour at the lowest temperatures making impossible to extract transport properties from the spectra. For BMPyrDCA$_{9\%}$ and BMPyrDCA$_{IJ}$ the usual profile of conducting disordered systems is recovered. This should not be interpreted as an absence of the relaxation(s) process(es) in these systems, but simply that it are submerged by the conductivity response or, by other words, that the dielectric response in these ILs is dominated by the conductivity behaviour of two separate ions, anion and cation, rather than by dipolar reorientation.
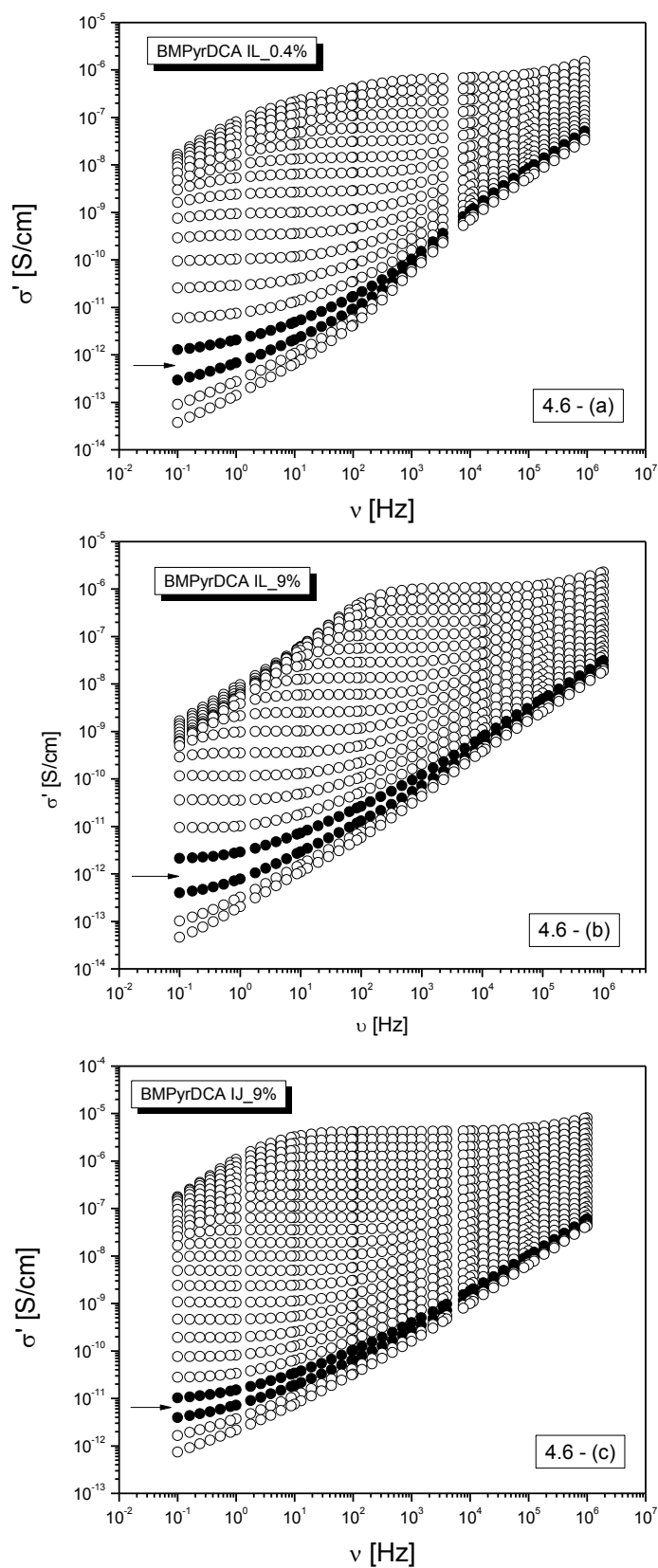
Figure 4.6 - (a – c) - Complex conductivity measured at different temperatures of BMPyrDCA$_{0.4\%water}$, BMPyrDCA$_{9\%water}$ and BMPyrDCA$_{Ion\ Jelly}$ (in steps of 2 K from 163 K to 103 K): (a-c) real, σ´, components; the estimated onset of the calorimetric T$_g$ occurs at a temperature in between the isotherms represented in filled symbols (indicated by the arrow).

4.2.1.3. EMIMDCA

In Figure 4.7 – (a-c), the isotherms behaviour follows the same trend as verified for the systems above, with exception for $BMPyrDCA_{0.4\%}$, like we already discuss.
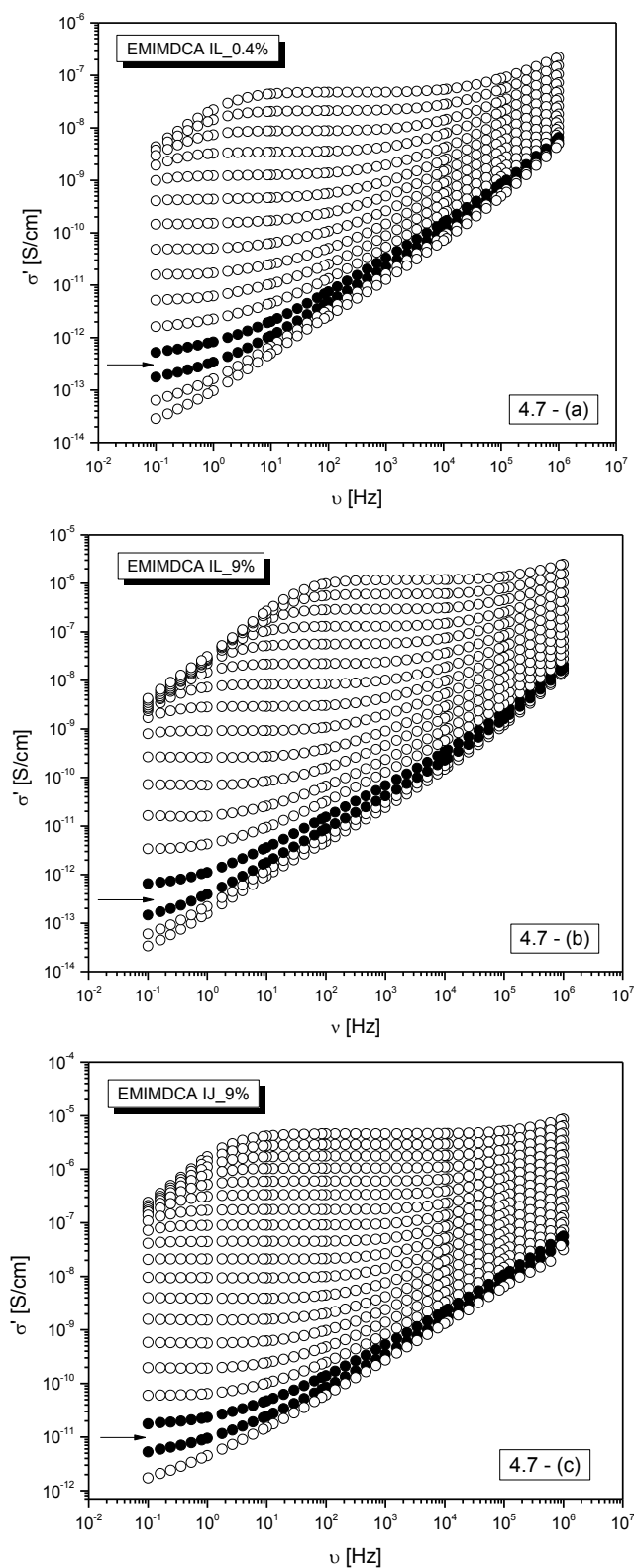
Figure 4.7 - (a-c) - Complex conductivity measured at different temperatures of $EMIMDCA_{0.4\%water}$, $EMIMDCA_{9\%water}$ and $EMIMDCA_{Ion\ Jelly}$ (in steps of 2 K from 163 K to 313 K): (a-c) real, σ', components; the onset of the calorimetric T_g occurs at a temperature in between the isotherms represented in filled symbols (indicated by the arrow).

In Figure 4.8 (a-f) and Figure 4.9 (a-f), for each system, it is shown the isotherms fitted by Jonscher equation. Figure 4.8 presents the conductivity spectra of non-crystallisable systems under the tested conditions, while figure 4.9 presents the corresponding spectra for the crystallisable ones.

The complex conductivity, σ^*, is similar to other materials in terms of frequency and temperature dependence, for example [21-25]. In all cases the real part of conductivity, σ', has a plateau on the low frequency side. So, we choose these isotherms since they are not influenced by electrode polarization. The curve that is presented as full circles, was collected at 211K for $BPyDCA_{0.4\%}$, 197K for $BPyDCA_{9\%}$, 201K for $BPyDCA_{IJ}$; 191K for $BMIMDCA_{0.4\%}$, 189K for $BMIMDCA_{9\%}$ and 199K for $BMIMDCA_{IJ}$; 187K for $BMPyrDCA_{0.4\%}$, 185K for $BMPyrDCA_{9\%}$ and 195K for $BMPyrDCA_{IJ}$; 189K for $EMIMDCA_{0.4\%}$, 177K for $EMIMDCA_{9\%}$ and 193 for $EMIMDCA_{IJ}$, being the same presented in the inset that also includes its respective derivative plot $d(log\sigma'(\omega))/d(log(\omega))$ (open circles). From the analysis that was done in the previous chapter, we are able to conclude that there is strong evidence that sub-diffusive dynamics dominate at short times, in all the twelve systems; for $BMPyrDCA_{0.4\%}$ the derivative analysis was performed in a isotherm taken well above the glass transition i.e. at a temperature at which the conductivity overwhelms the dipolar contribution.
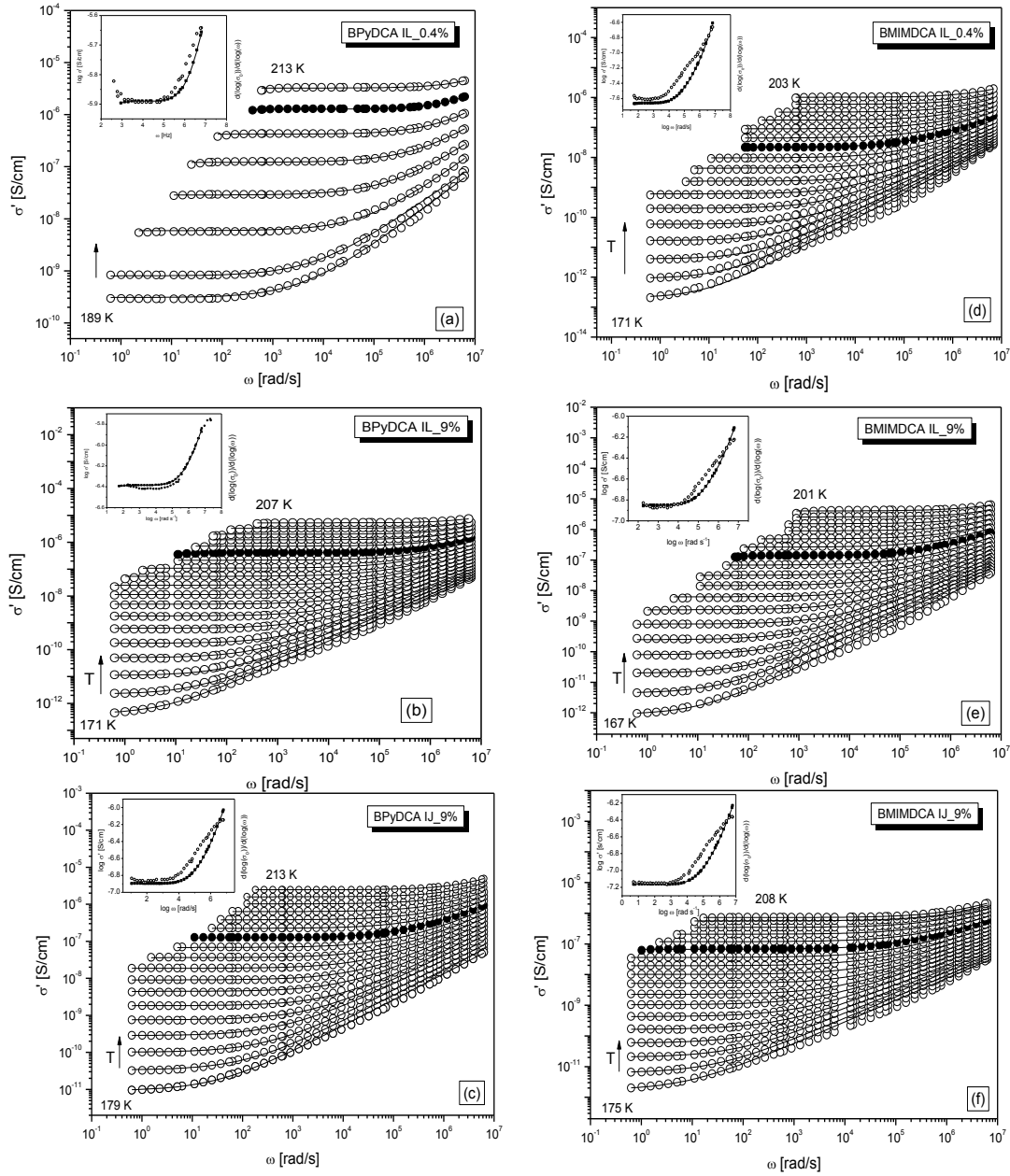
Figure 4.8 (a-f) – Real part of conductivity for BPyDCA$_{0.4\%}$, BPyDCA$_{9\%}$ and BPyDCA$_{IJ}$ from 189 to 213 K, 171to 207K and 179 to 213K, respectively, in steps of 2K and for BMIMDCA$_{0.4\%}$, BMIMDCA$_{9\%}$ and BMIMDCA$_{IJ}$ from 171 to 203 K, 167to 201K and 175 to 208K, respectively. The solid lines are the obtained fits by the Jonscher law (eq. 1.14, see Introduction). Data collected at 211 K for BPyDCA$_{0.4\%}$, 197K for BPyDCA$_{9\%}$, 201 K for BPyDCA$_{IJ}$, 191 K for BMIMDCA$_{0.4\%}$, 189K for both BMIMDCA$_{9\%}$ and 199K for BMIMDCA$_{IJ}$, are plotted in full circles being the same spectrum presented in the inset together with the respective derivative d(logσ'(ω))/d(log(ω)) (open circles); the continuous increase of the derivative value with the frequency increasing, confirms the sub-diffusive dynamics (see text).
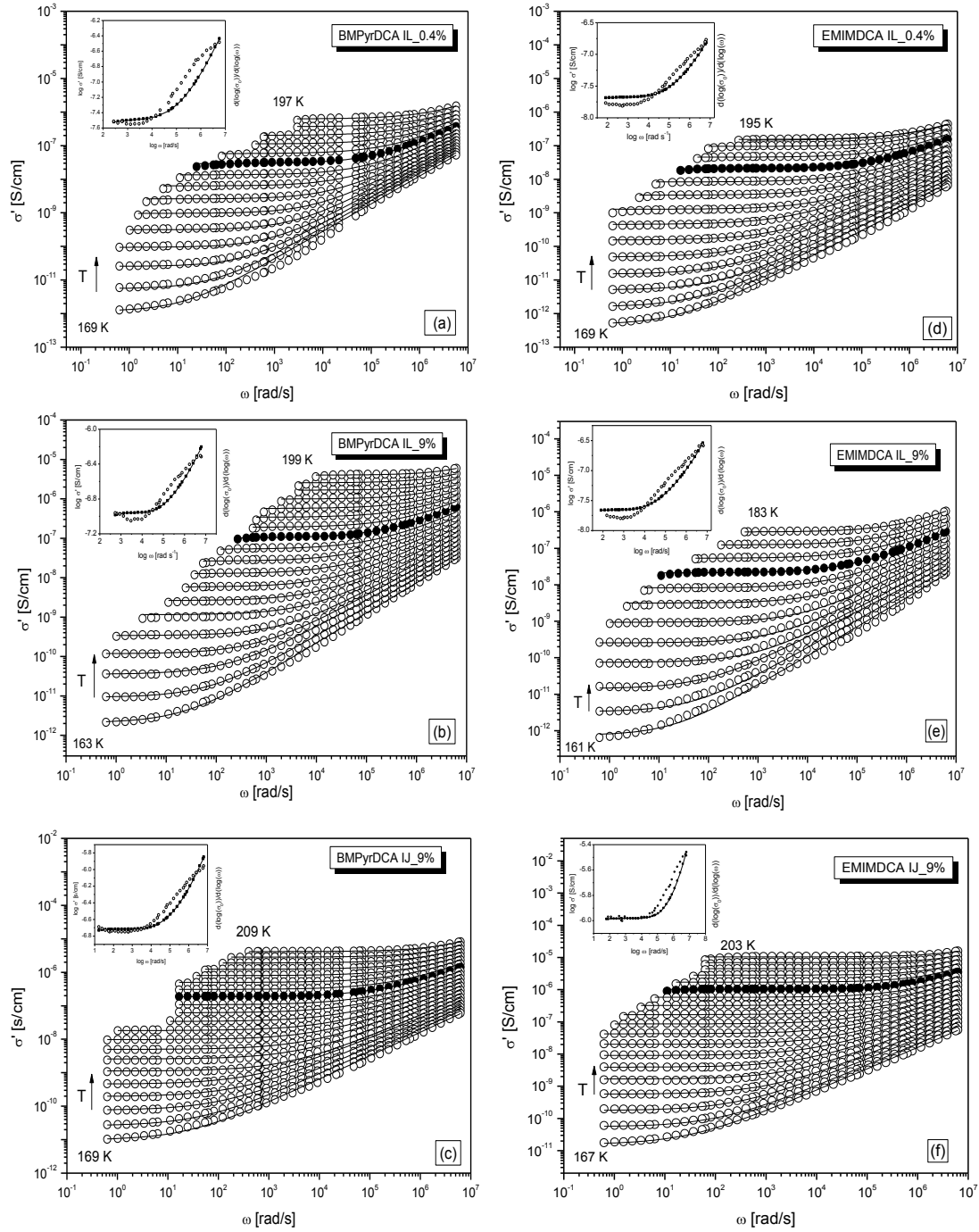
Figure 4.9 (a-f) – Real part of conductivity for BMPyrDCA$_{0.4\%}$, BMPyrDCA$_{9\%}$ and BMPyrDCA$_{IJ}$ from 169 to 197 K, 163 to 199K and 169 to 209 K, respectively, in steps of 2 K and for EMIMDCA$_{0.4\%}$, EMIMDCA$_{9\%}$ and EMIMDCA$_{IJ}$ from 169 to 195 K, 161 to 283 K and 167 to 203 K, respectively. The solid lines in the figures in the right side are the obtained fits by the Jonscher law (eq. 1.14) being the reason why the plots are in function of the angular frequency, ω. Data collected at 187 K for BMPyrDCA$_{0.4\%}$, 185K for BMPyrDCA$_{9\%}$, 195 K for BMPyrDCA$_{IJ}$, 189 K for EMIMDCA$_{0.4\%}$, 177K for EMIMDCA$_{9\%}$ and 193 K for EMIMDCA$_{IJ}$, are plotted in full circles being the same spectrum presented in the inset together with the respective derivative d(log$\sigma'(\omega)$)/d(log(ω)) (open circles); the continuous increase of the derivative value with the frequency increasing, confirms the sub-diffusive dynamics (see text).

In Figure 4.10 (a-d), an overview of the conductivity values obtained for the twelve systems, is shown. The inset shows the BNN relationship, σ_0 - $1/\tau_e$, meaning that analogous temperature dependence for σ_0 and $1/\tau_e$ is predictable. The values of σ_0 increase from the IJ to IL with lower amount of water and then, the higher value is achieved on ILs with higher amount of water. As the conductivity is related to the mobility of the charge carriers, this can be explained by the higher viscosity induced by gelatine in the case of the IJ film, and the lower water content in ILs with 0.4% water content. Like we had the possibility to observe through the DSC analysis, each material considered in this study, is a glass forming system. Therefore, the empirical VFT equation was fitted to the conductivity data, which usually describe the temperature dependence of the structural relaxation time and the conductivity of supercooled liquids quite well. The results of the fitting are summarized in table 4.2. The VFT law has been fitted through the data points in its linearized form:

$$\ln \tau = ln\tau_\infty + \frac{B}{T-T_0} \qquad (4.1)$$

$$\ln \sigma = ln\sigma_\infty - \frac{B}{T-T_0} \qquad (4.2)$$

where B is an empirical parameter characteristic of the material accounting for the deviation of linearity (roughly the lower B the more curved is the 1/T plot), the σ_∞ is the high temperature limit of the conductivity and T_0 is the Vogel temperature, interpreted as the glass transition temperature of an ideal glass, i. e., a glass obtained with an infinitely slow cooling rate [26]. The glass transition temperature is always higer than the ideal glass transition temperature ($T_g > T_0$), according to an empirical approximation: $T_0/T_g \approx 0.75$. T_0 is adjusted arbitrarily by subtracting ca. 50 K from the experimental T_g value [27]. The relation between T_g and T_0 for BMIMDCA$_{0.4\%water}$, BMIMDCA$_{9\%water}$ and BMIMDCA$_{Ion\ Jelly,}$ gives, respectively: $T_0/T_g \approx 0.75$, $T_0/T_g \approx 0.76$ and $T_0/T_g \approx 0.73$. All the other systems follow this trend with a break down for EMIMDCA$_{0.4\%}$ for which $T_0/T_g \approx 0.49$; this arises from an overestimation of T_g due to a low curvature in the activation plot.

Vogel-Fulcher-Tammann (VFT) parameters have been extracted from these data.

Table 4.2 - Fit Parameters Obtained According to the VFT Law for the Relaxation Times (eq. 4.1) and the Conductivity (eq. 4.2)[a]

	VFT fit parameters of σ_0[b]			VFT fit parameters of τ_e[c]		
Sample	σ_∞/ S.cm^{-1}	B/ K	T_0 / K	τ_∞/ s	B / K	T_0 / K
BPyDCA$_{0.4\%water}$	120.3±26.3	1294±26.7	140.7±0.5	(3.1±1.9)x10^{-15}	1240.6±103.4	139.8±2.2
BPyDCA$_{9\%water}$	14.7±2.8	1022.0±19.6	138.5±0.4	(5.8±2.4)x10^{-14}	966.4±49.9	137.7±1.2
BPyDCA$_{Ion Jelly}$	36.6±6.5	1307.3±23.2	134.0±0.5	(1.1±0.7)x10^{-14}	1334.4±147.4	132.5±3.2

	VFT fit parameters of σ_0[b]			VFT fit parameters of τ_e[c]		
Sample	σ_∞/ S.cm^{-1}	B/ K	T_0 / K	τ_∞/ s	B / K	T_0 / K
BMIMDCA$_{0.4\%water}$	325±115	1413±46	131±1	(2.6±2.1)x10^{-15}	1278±170	131±3
BMIMDCA$_{9\%water}$	68±13	1176±21	131±0	(9.7±6.8)x10^{-15}	1124±124	130±3
BMIMDCA$_{Ion Jelly}$	67±6	1469±15	128±0	(1.5±0.7)x10^{-15}	1355±70	130±2

	VFT fit parameters of σ_0[b]			VFT fit parameters of τ_e[c]		
Sample	σ_∞/ S.cm^{-1}	B/ K	T_0 / K	τ_∞/ s	B / K	T_0 / K
BMPyrDCA$_{0.4\%water}$	20.5±0.7	918.7±27.9	136.7±0.6	(4.1±1.9)x10^{-13}	804.6±53.2	138.0±1.3
BMPyrDCA$_{9\%water}$	24.7±7.7	1180.2±40.4	123.7±0.9	(6.7±4.8)x10^{-15}	1269.3±147.9	120.0±3.2
BMPyrDCA$_{Ion Jelly}$	276.3±75.0	1721.8±45.8	113.5±0.9	(9.9±8.7)x10^{-17}	2265.3±357.2	101.9±6.5

	VFT fit parameters of σ_0[b]			VFT fit parameters of τ_e[c]		
Sample	σ_∞/ S.cm^{-1}	B/ K	T_0 / K	τ_∞/ s	B / K	T_0 / K
EMIMDCA$_{0.4\%water}$	(7.9±7.8)x10^{13}	5629.2±1018.2	76.0±9.3	(9.9±9.9)x10^{-29}	6337.0±5444.3	67.4±48.2
EMIMDCA$_{9\%water}$	47611.3±40162.8	1700.6±197.4	117.3±3.0	(2.1±2.1)x10^{-17}	1668.4±860.4	114.6±14.1
EMIMDCA$_{Ion Jelly}$	174.1±41.8	1338.5±32.5	122.6±0.7	(1.3 ±0.9)x10^{-16}	1484.2±150.2	118.8±3.1

[a]The uncertainties are the statistical errors given by the fitting program. For each material, the similarity between B and T_0 estimated through σ_0(T) and τ_e(T) indicates a parallelism between these two quantities (see text for details). [b]According to the VFT law for conductivity. [c]According to the VFT law for relaxation time.

The figure below shows that all the four compounds have a relatively pronounced curvature, so called fragile behaviour, as seen in many glass forming substances[28-32].
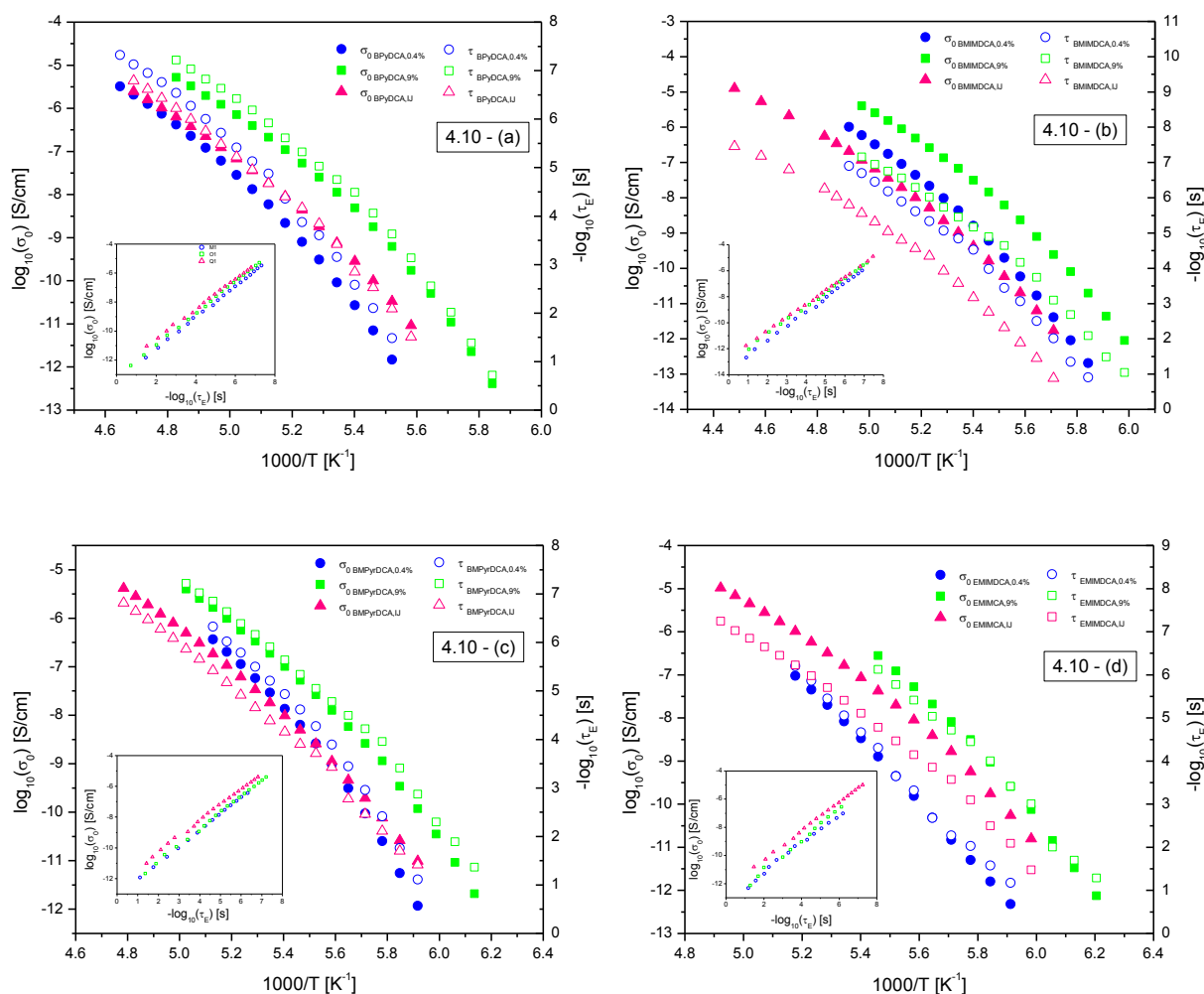
Figure 4.10 (a-d) - Temperature dependence of the dc conductivity, σ_0, and of the relaxation time, τ_e, taken from the crossover frequency. The correlation between both is displayed in the inset (BNN plot) for which a slope near 1 is found (the lowest correlation factor found is $r^2=0.994$).

Table 4.2 shows the similarity between B and T_0 parameters obtained from equations 4.1 and 4.2, indicating the parallelism between $\sigma_0(T)$ and $\tau_e(T)$ for all systems, corroborating what was predicted in the analysis of the BNN relationship.

Several authors have discussed the influence of different properties as the size of the IL cation and molecular volume on the VFT behaviour [33-37]: according to Leys *et al.* [38] and Rivera [39], T_g decreases with the increasing of anion radius while Sangoro *et al.* [37] reports a non-uniform dependence of T_0 with the size of the cation alkyl chain; a non-universal behaviour is found in literature for σ_∞ , while an increase with the species size, either anion [38] or cation [37] is reported, a decrease of both σ_∞ and conductivity at room temperature with the cation size is observed for imidazolium ILs with BF4 anion [40].

Nevertheless, the variation of factors as radius and volume is almost negligible in the tested ILs (see Table 2.1 in the *Experimental* section); for instance, from the smallest ionic cation, EMIM, to the largest, BPy, the radius changes less than 1 Å. In the following T_0 and calorimetric T_g (figure 4.11-a) and the conductivity and diffusion coefficient both at room temperature, respectively σ_{RT} and D_{RT} (figure 4.11- b) will be analyzed for the different cations using the respective van der Waals radii only with the purpose of getting a clearer picture of the different data. The change in these properties should be discussed based more on structural details of the cation rather than on dimensional ones, as mentioned before.
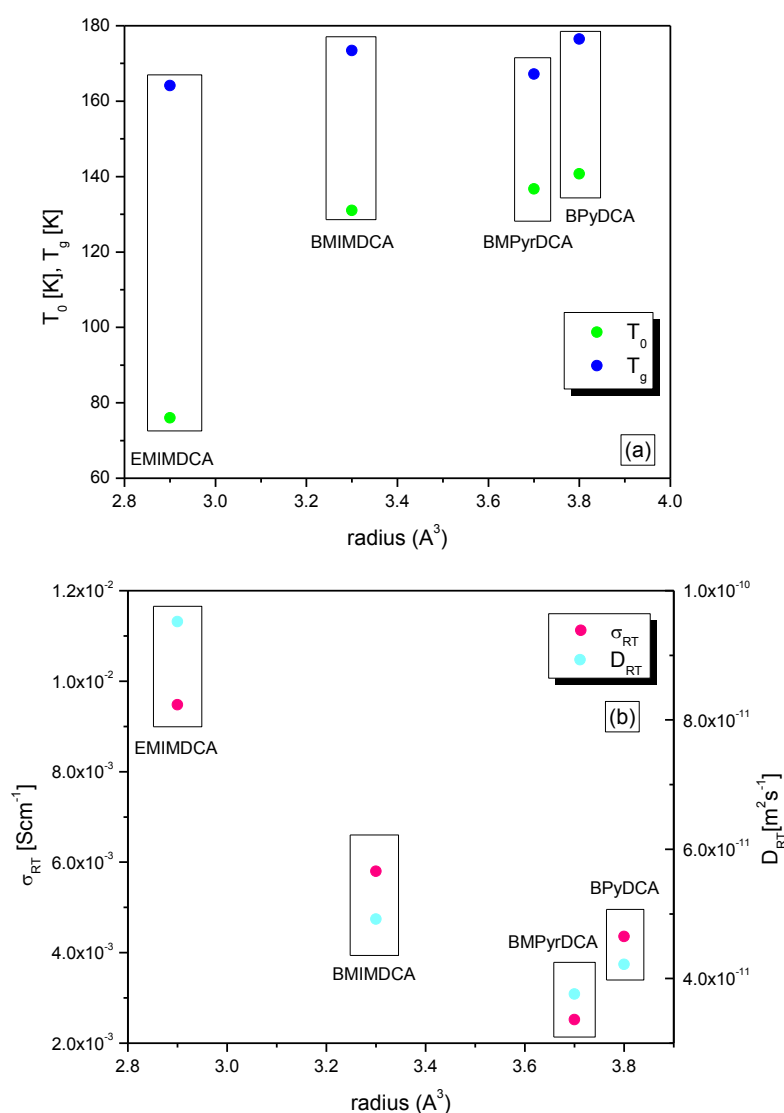
Figure 4.11 - T_o and calorimetric T_g (figure 4.11 – (a)); conductivity and diffusion coefficient both at room temperature, respectively σ_{rT} and D_{rT}, (figure 4.11 – (b)) versus van der Waals radii.

It is important to recall here the structure of the different cations, given that all the ILs under study have the same DCA anion (see scheme below).
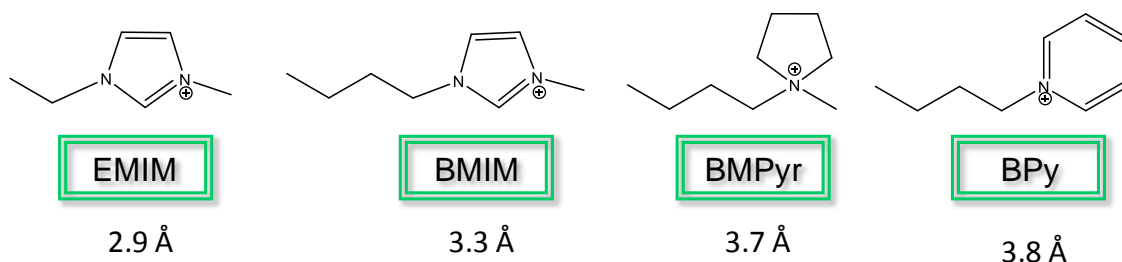
Scheme 4.1- ILs cations structures and respective van-der-Walls ratios

Some considerations can be done regarding the different structures: while BMPyr has a saturated ring (pyrrolidinium), the other cations have an aromatic ring and consequently a greater extent of positive charge delocalization; in BMPyr the positive charge is more localized over the nitrogen atom making more important the electrostatic charge interaction with the DCA anion, which could originate a behaviour closer to a single dipole as observed from the dielectric measurements for the BMPyr sample containing less water.

Two opposite effects are manifest in BMIM, by one side, the charge delocalization which dilutes the electrostatic interaction and by other, the directionality in the interaction due to the ability to form H-bonds. The latter could originate some peculiarities in the IL behaviour as reported for IL containing fluorinated anions, where the observed strong deviations of experimental conductivities, as compared to which is predicted by Nernst-Einstein equation, are attributed to a nanoscale organization of the anions due to the preferential orientation adopted by their perfluorinated moieties [41].

This makes difficult the task to find a correlation between the transport properties and glass transition with structural details in the studied ILs that doesn't vary monotonically. An alternative discussion could be done based in the dependence of the glass transition on the type of interionic interactions. Some authors [40], [42-43] associate this behaviour with the cohesive force between the ions, which is substantially determined by the molecular volume. Once, two possibilities emerge, i. e., when the molecular volume is low (or equivalent molar), the cohesive force is mainly determined by attractive Coulomb forces between ions, which decrease with increasing molar volume. Nevertheless, if the molar volume is to large (> 250 cm^3/mol), the interactions are dominated by van der Waals forces, which lead to an increasing value of T_g with molar volume or cation radius [43] (see figure 4.12 retrieved from ref [43]). The tested ILs have *molecular* volumes from 184.5 to 214.5 cm^3.mol (see *Experimental* section), falling close to the critical *molecular* volume that corresponds to the lower T_g values of the proposed correlation, revealing relatively good agreement to which is predicted (see colored circles in figure 4.12). This is due to a counterbalance between Coulombic and van der Waals interactions in the ILs under study.
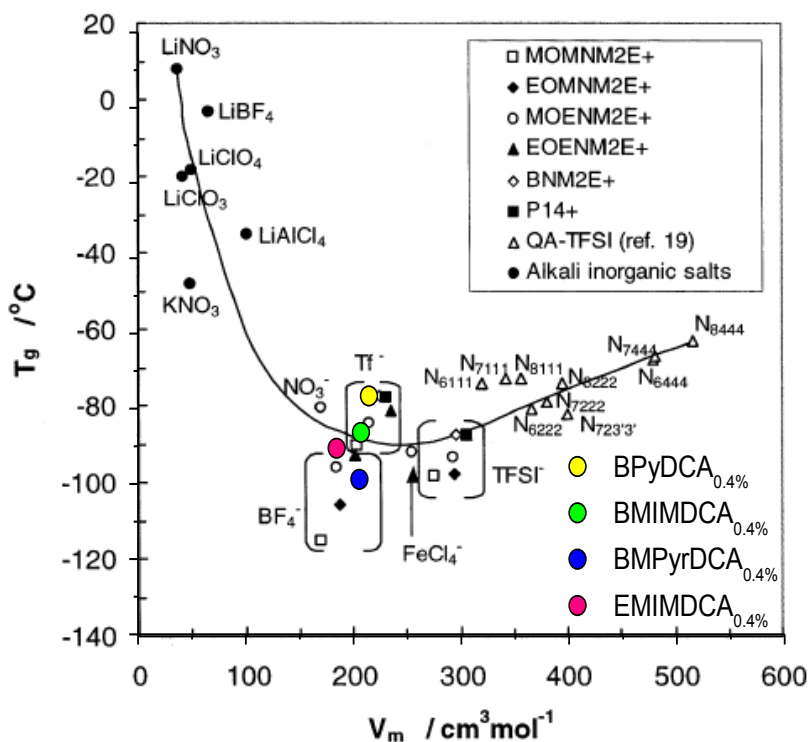
Figure 4.12 - Dependence of the cohesion of salts of weakly polarisable cations and anions, assessed by the T_g value, on the ambient-temperature molar volume, V_m, and, hence, on the interionic spacing $[(r^+ + r^-) \approx V_m1/3]$. A broad minimum in the ionic liquid cohesive energy is seen at a molar volume of 250 cm^3 mol^{-1}, which corresponds to an interionic separation of ~0.6 nm, assuming a face-centered cubic packing of anions about the cations. The lowest T_g value in the plot should probably be excluded from consideration, because of the nonideal Walden behaviour for this IL (MOMNM$_2$E$^+$BF$_4^-$). The line through the points is a guide to the eye. (background figure retrieved from ref [43])

For the respective IJs and ILs with 9% water, the change in T_g is similar to the IL$_{0.4\%}$; it should be remember that for the IJs an higher T_g value is always found (discussed previously in the calorimetric section). If we look for the values of the parameter T_0 (K), with the exception of the abnormally low value for EMIM$_{0.4\%}$ (67 K) due to a close Arrhenian behaviour (the same doesn't happen with 9% or IJ, presenting a value close to 117 K), no significant changes are found for the other IL's; also, no general tendency is observed when we compare the ILs or the respective IJs. The value of B (not shown) doesn't reveal also a clear tendency; this will be better discussed in the next section in terms of fragility.

When we analyze the parameter σ_∞, a parallelism between the values of this parameter and the conductivity measured at room temperature (σ_{RT}) is found, i. e., the higher the conductivity, the higher the value of σ_∞; since a greater uncertainty affects σ_∞, the comparison in figure 4.11 b) is made through (σ_{RT}). Nevertheless, is worth to mention the uncommon and quite higher σ_∞ value, and completely unrealistic error value, for EMIMDCA with both 0.4% and 9% water content due to its almost linear temperature dependence as mentioned above. It is observed in figure 4.11 b) that conductivity at room temperature decrease on going from EMIM to BMPyr; the value for BMPyr approaches close to the one of BMIM. The lowest conductivity value for BMPyr agrees with the dipolar

behaviour found for BMPyrDCA, which could meant that a significant fraction of ion pairs behave as dipoles decreasing the contribution to conductivity.

If we analyse $BMIMDCA_{0.4\%}$ and $EMIMDCA_{0.4\%}$ separately, since that in terms of structure they are the most similar, we verify that $BMIMDCA_{0.4\%}$ has higher volume and, consequently, higher van der Waals radius, due the fact that in this case is present a butyl group instead a ethyl group. Hence, the analysis of the conductivity values and their VFT fits shows a decreasing conductivity with the chain length increasing in agreement with which is reported by Leys *et al* [40]. This reflects in a decreasing in the diffusion and mobility of the ions, as it will be shown below. Thus, it is possible to conclude that the alkyl chain plays an important role in the mobility of charge carriers and, thus, in the conductivity, as previously studied by another groups [19]. Nevertheless, it is important to note, that the reported decrease with cation chain length [19] is only a general trend for the first members of the imidazolium series, going from C_2 to C_4, for C_6 an increase is observed as also reported in [40] and [30].

In the same route as we did on our previous studies, we have performed fits of the conductivity data to the VFT equation, like we saw in Figure 4.10 – (a-d). This equation is used to describe data of glassforming systems since it can reproduce the curvature in the activation plot which is characteristic for many glass formers. Structural variation lead to differences which exceed three orders of magnitude in both cases, BPyDCA and BMIMDCA, exceding twoorders of magnitude in the case of BMPyrDCA and five orders of magnitude regarding to EMIMDCA in σ_0 (between the sample with 0.4% and 9% water content). The Figure above shows a ilustrative compilation of these results.

The experimental curves presented in Figure 4.6 and Figure 4.7 – (a-c) are normalized with respect to frequency and conductivity, when the last starts the plateau, i. e., when the subdiffusive and diffusive regimes are observed at the same time. All the curves fall into one chart, meaning that all the systems are governed by the same mechanism (Figure 4.13).

The coefficient diffusion, *D*, is a property associated with the random motion of elementary constituents of matter, basically atoms, molecules and ions, owing to their thermal energy.
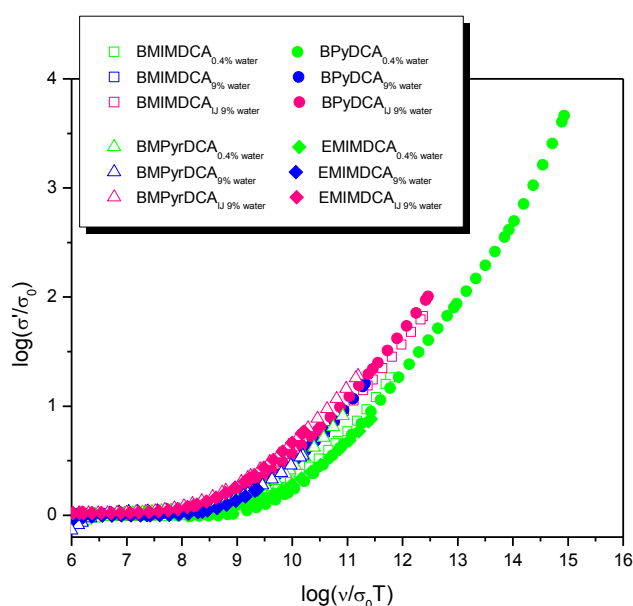
Figure 4.13 – Normalized conductivity with pure conductivity in function of frequency.

Consequently, from previous equations, the mobility as well as their type of temperature dependence can be determined, as we can see in plot of Figure 4.14. The diffusion coefficients presented in Figure 4.14 are related with the mobilities, μ, through the Nernst-Einstein equation:

$$\mu = \frac{qD}{K_B T} \qquad (4.3)$$

where q and K_B corresponds to elementary charge and Boltzmann constant, respectively. Like we say earlier, since the systems can be decomposed by their cations and anions, the overall coefficient diffusion, can be decomposed in the follow equations:

$$D_+ = \frac{\langle \Delta r_+^{\,2}(t*) \rangle}{6\gamma} v_{cross} \quad (4.4\ a) \qquad\qquad and \qquad\qquad D_- = \frac{\langle \Delta r_-^{\,2}(t*) \rangle}{6\gamma} v_{cross} \quad (4.4\ b)$$

where $<\Delta r_+^2(t^*)>$ and $<\Delta r_-^2(t^*)>$ are the mean-square displacements for the cation and anion, respectively, and were estimate by taken the square of the van der Waals (vdW) diameter.

Some authors [21] calculate the mean jump length by combining PFG NMR and DRS. However they need temperatures where the measurement windows of both techniques coincide. Since we do not have this pre-requisite, we calculate this feature by estimating the van der Waals diameter. The same authors also refer that the diffusion coefficients decrease with increasing molecular volume, Vm, of the IL, which is in reasonable agreement to our results. Nevertheless, this may be due the fact that both ILs have very similar Vm values.

It becomes clear for all the twelve systems can be monitored by dielectric spectroscopy.
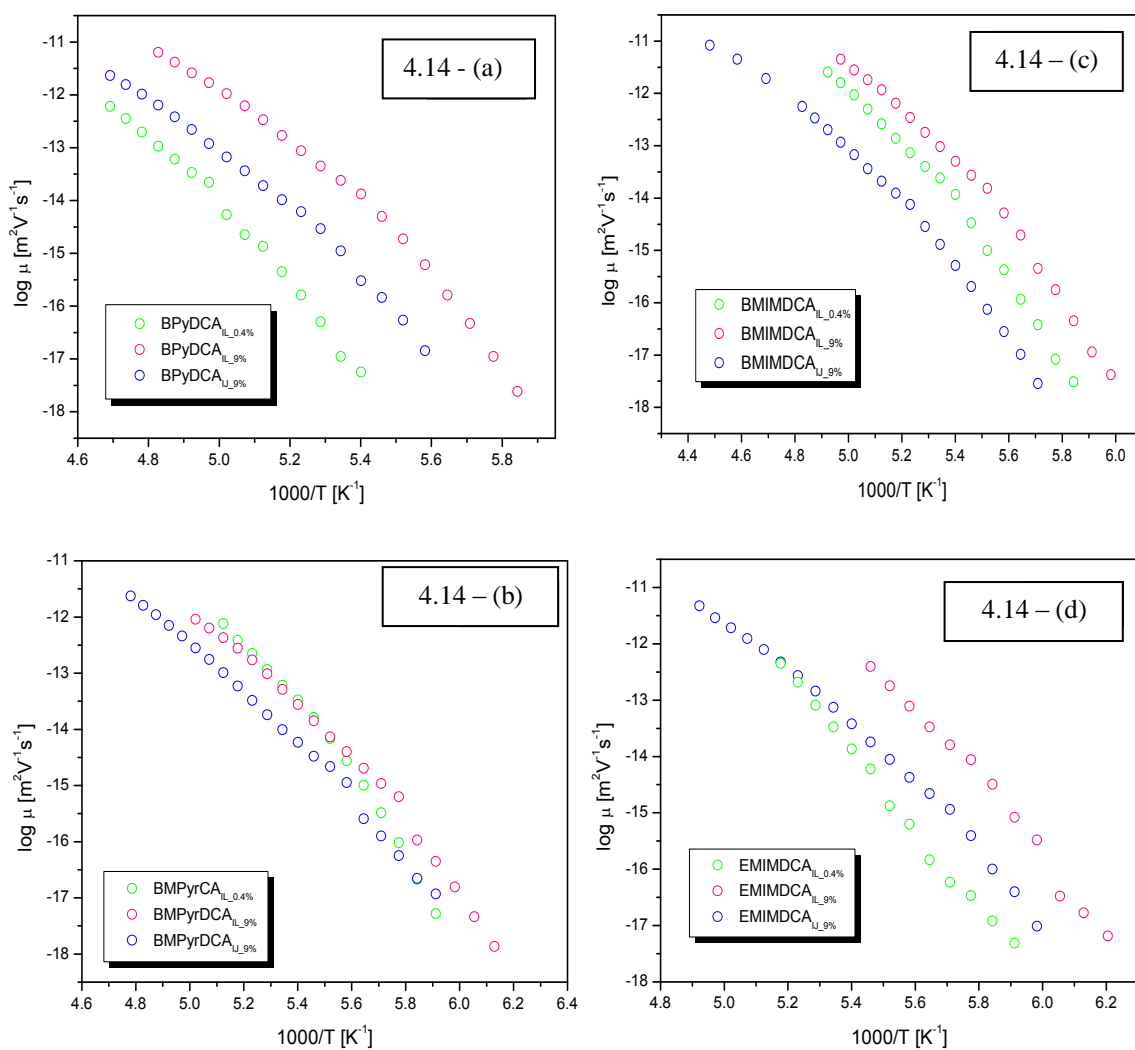
Figure 4.14 – (a-d) –Mobilities, μ, (equation 4.3) by taking $D = D_+ + D_-$ for the four ILs.
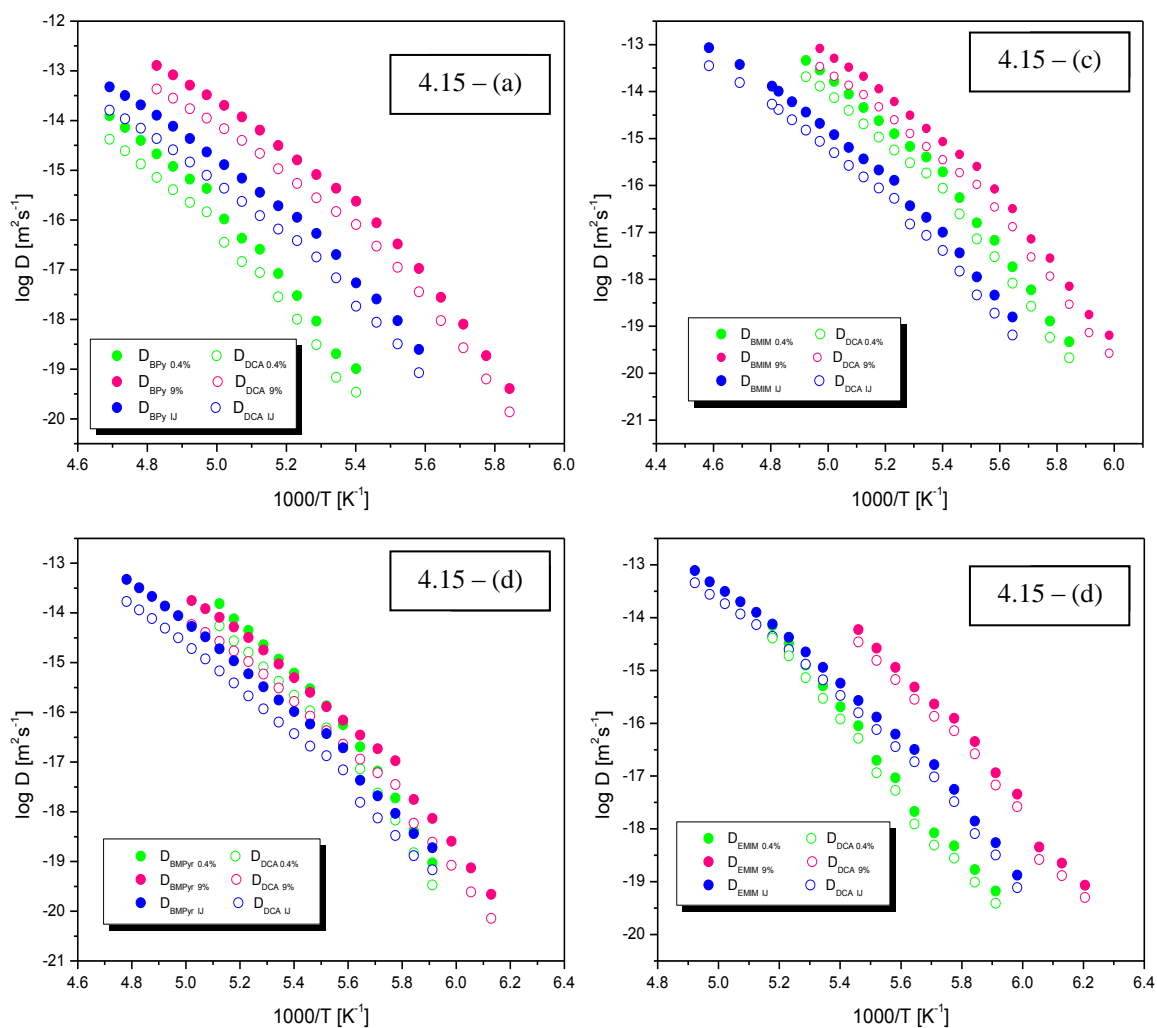
Figure 4.15 - (a – d) - Thermal activation plot for diffusion coefficients of BPy, BMIM, BMPyr and EMIM (cation) and DCA (anion) (equations 4.4 – (a) and 4.4 – (b)), replacing the mean-square displacement by the vdW diameters.

PFG NMR technique emerges as a good strategy to overcome the problem of electrode polarization that dramatically affects the IL's conductivity measurements at high temperatures. The measurements performed by PFG NMR (which measures the diffusion coefficient directly), jointly with the diffusion coefficients measured by DRS, are shown in Figure 4.16.

Through the equation 4.4 – (a-b) it is possible to access diffusion coefficients in a broad range comprising over 10 orders of magnitude by employing both techniques DRS and PG NMR, which shows the excellent agreement for each system, through the VFT fitting.
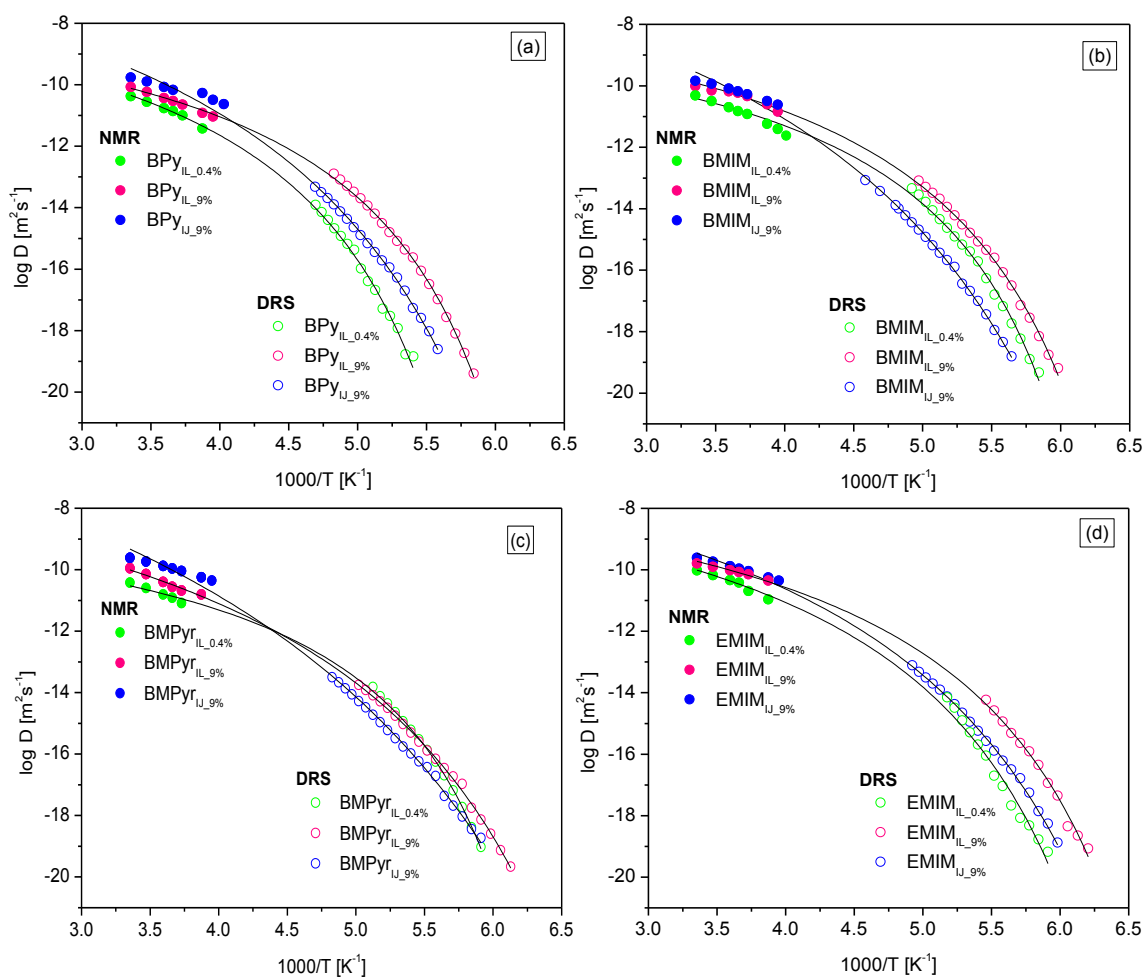
Figure 4.16 - (a-d) – Values of the cation diffusion coefficients (D_+) determined from PFG NMR and the VFT fit (solid lines).

The reason why the diffusion coefficient decreases with the temperature is related with the dramatic increase of viscosity with the temperature decrease making more and more difficult the motion of charge carriers; when the material is at a temperature below its T_g, large-scale molecular motion is not possible since the sample is essentially frozen. If it is at a temperature above its T_g, molecular motions take place, allowing the increasing of the free movements of the ions.

Earlier the diffusion coefficients at room temperature of the different materials were compared in figure 4.11 b). Now, in figure 4.17 a-c) the diffusion coefficients are compared for the 4 ILs for each condition (water content and supported in IJ). At the lowest temperatures, the samples with a higher diffusion coefficient are those having a lower T_g, since the more easily a material can move, the less heat it takes for the structure to initiate wiggling and break out of the rigid glassy state

So, comparing the T_g values, for the samples with 0.4% of water, we can see that this is the decreasing order of T_g: BPyDCA > BMIMDCA > EMIMDCA > BMPyrDCA. Which means that the inverse order give us the increasing order of the diffusion coefficient, i. e., BPyDCA is the IL with higher Tg and lower D, which it is possible to verify in the Figure 4.17a). Doing the same reasoning for the ILs with 9% water content, we conclude that: BPyDCA > BMIMDCA > BMPyrDCA > EMIMDCA, that is exactly the sequence of the IJ films, which means that, if the EMIMDCA$_{9\%}$ and BMIMDCA$_{9\%}$ have the lower T_g, they have the higher D, that it is possible to prove, one more time, through figure 4.17b).
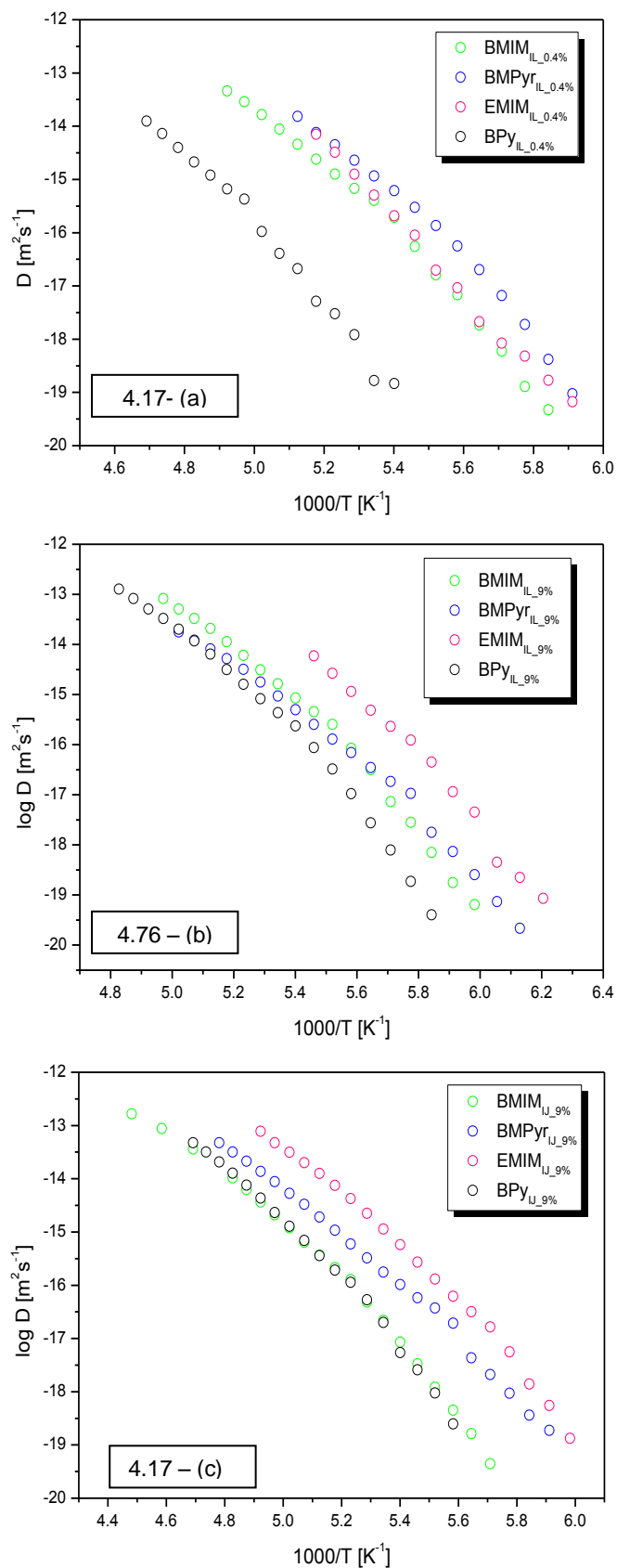
Figure 4.17 - (a-c) - Thermal activation plot for diffusion coefficients of BPy, BMIM, BMPyr and EMIM (cation) (equation 5a) with 0.4% water content, b) with 9% water content and c) the IJ correspondent of each IL, replacing the mean-square displacement by the vdW diameters

Nevertheless, the comparison at room temperature does not give the same hierarchy as the one now obtained when D is compared at low temperatures. For instance, while BMPyr$_{0.4\%}$ has a lower T$_g$ relatively to BMIM$_{0.4\%}$ having a higher D at low temperatures, at 298 K BMIM$_{0.4\%}$ is the one that has the highest D between the two ILs. This has to do with the way how their properties vary with the temperature, which is analysed in the next section through fragility.

4.3. Fragility

Once the behaviour of all investigated systems could be fitted with a single VFT curve, all compounds could be characterized through a set of parameters, σ_∞, B and T_0, like we had the opportunity to mention previously. This allows the determination of fragility.

In ILs there is the possibility to exist two types of glass formers: "fragile" or strong" liquid [44], with possibility of a fragile to strong transition. Both types of liquids shows qualitatively different temperature dependency of the viscosity: strong liquids nearly behave according to the Arrhenius law, while the fragile liquids show a non-Arrhenius dependence. In other words, fragility is a quantitative measure of the degree of deviation from Arrhenius-type temperature dependence near T_g, providing a useful classification of glass formers in terms of fragility. Materials are called "strong" if show a strong resistance against structural degradation when heated through their supercooled regime [45]revealing a$\tau(T)$ dependence close to an Arrhenius-type behavior and "fragile" if their $\tau(T)$ significantly deviates from linearity, induced by high cooperative molecular rearrangements[46]. Furthermore, from the VFT parameters and the glass transition temperature extracted from the DSC, T_g^{DSC}, it is possible also to estimate the fragility index, m, Fragility values typically range between m = 16 for strong systems and m = 200 for fragile ones, being estimated according to the following equation[19]:

$$m = \frac{BT_g}{\ln 10(T_g - T_0)^2} \qquad (4.5)$$

The thus obtained values for BMIMDCA$_{0.4\%water}$, BMIMDCA$_{9\%water}$ and BMIMDCA$_{Ion\ Jelly}$ were, respectively, 56, 52 and 48, reflecting the deeper temperature dependence of relaxation times for the pure IL. Likewise, it was found experimentally that the fragility could be related to the interactions between the system elementary units like van der Waals forces and hydrogen-bonding [47]. Strong liquids (e.g., SiO2) typically have three-dimensional network structures of covalent bonds while fragile liquids (e.g., o-terphenyl) typically consist of molecules interacting through nondirectional, noncovalent interactions (e.g., dispersion forces)[47]. The three materials seem to fall closer in the first category. It is known for ILs that the fragility depends very strongly on local interionic Coulomb forces[19] and when these increase over van der Waals attractions, fragility decreases[31]. Therefore, the lower value of m estimated for IJ could be interpreted in terms of an increasing importance of Coulomb interactions occurring between the small DCA anion and the imidazolium part of the cation. Indeed gelatin helps to hold closer the ion-pairs promoting the Coulombic attractions of oppositely charged ions and decreasing the van der Waals repulsions of the alkyl chains on the imidazolium cation.

Comparing BMIM and EMIM, we observe a decreasing of fragility with chain length, which can be explained from the fact that the van der Waals forces between the molecules of the ILs increase with the chain length.

By other side, in BMIMDCA, an additional effect influences its fragility: the ability of the hydrogen atoms of the imidazolium cation to form hydrogen bonds with the anion. This was evidenced by Fourier transform infrared spectroscopy (FTIR) for the homologous 1-ethyl-3-methylimidazolium cation[48] and by using ab initio and Density Functional Theory (DFT) methods for 1-methyl-3-methyl imidazolium (MMIM), EMIM, 1-propyl-3-methyl imidazolium (PMIM) and BMIM[49].

For single atomic anion dialkylimidazolium ILs as chlorides and bromides it was found that hydrogen-bonded networks exist in both solid and liquid phases and an effort is being carried to simulate H-Bonds in multiple atom anions[50]. Nevertheless it is important to note that some ambiguity exits in this matter: since each cation can display different conformers as in DCA, this gives rise to different co-conformations where the ion contact can be mediated via hydrogen bond or not. In [BMIM][DCA], the ion contact in-plane co-conformers is mediated via the hydrogen atom while the on-top co-conformation is not [49-50]; therefore it is important to know how strongly the different co-conformations are contributing.

Although the fragility for BMIMDCA either neat ionic liquid or ion jelly are relatively similar, the small difference could be originated by the ability to establish H-Bonds in neat BMIMDCA, since it is known that liquids forming H-Bonds are moderately fragile[43]. If a hydrogen-bonded network is conceived in BMIMDCA, in the IJ's composites its extent would be smaller due to the interference of gelatine impairing the establishment of a so extended HB network, and consequently decreasing the m parameter. Recalling the heat capacity determined calorimetrically, its higher value could be taken as an indication of higher extent in HBs in BMIMDCA given that the hydrogen bond-breaking is an additional source of degree's of freedom, contributing to enlarge the ΔCp jump [51]. The fragility index of BMIMDCA is close to the value found for C_9mimBF_4 and C_6mimTf_2N (m=55 and m=57, respectively) [48]. IJ have m values of the order of those obtained by calorimetry from the influence of the heating rate on the temperature location of the glass transition signal for other ILs: C_5O_2ImCl ($m=49$) [52]. Nevertheless, some care must be done in this comparison because the values are too close.

Table 4.3 – Fragilities of the twelve samples, according to Eq. 4.5

Samples	Fragility
$BPyDCA_{0.4\%}$	71.6
$BPyDCA_{9\%}$	46.3
$BPyDCA_{IJ}$	33.4
$BMIMDCA_{0.4\%}$	50.8
$BMIMDCA_{9\%}$	48.4
$BMIMDCA_{IJ}$	47.6
$BMPyrDCA_{0.4\%}$	69.0
$BMPyrDCA_{9\%}$	41.0
$BMPyrDCA_{IJ}$	32.6
$EMIMDCA_{0.4\%}$	48.4
$EMIMDCA_{9\%}$	48.3
$EMIMDCA_{IJ}$	43.4

It is possible to reanalyze now in terms of fragility the change in the coefficient diffusion observed for BMPyr and BMIM commented in the end of the previous section. If both ILs had the same *m* parameter, the respective D(1/T) plots should evolve in parallel. Since BMPyr is more fragile, its diffusion coefficient varies more with the temperature then BMIM, and the respective D plots cross at a given temperature varying the order expected for the D values based simply on the T_g values.

In overall, the results presented in this chapter, suggest that EMIMDCA is an excellent candidate for the development of IJ films with high room temperature conductivity.

4.4. Bibliography

[1]   P. Vidinha, N. M. T. Lourenço, C. Pinheiro, A. R. Brás, T. Carvalho, T. Santos-Silva, A. Mukhopadhyay, M. J. Romão, J. Parola, M. Dionisio, J. M. S. Cabral, C. a M. Afonso, and S. Barreiros, "Ion jelly: a tailor-made conducting material for smart electrochemical devices.," *Chemical communications (Cambridge, England)*, no. 44, pp. 5842–4, Nov. 2008.

[2]   T. Carvalho, V. Augusto, a R. Brás, N. M. T. Lourenço, C. a M. Afonso, S. Barreiros, N. T. Correia, P. Vidinha, E. J. Cabrita, C. J. Dias, M. Dionísio, and B. Roling, "Understanding the ion jelly conductivity mechanism.," *The journal of physical chemistry. B*, vol. 116, no. 9, pp. 2664–76, Mar. 2012.

[3]   D. R. MacFarlane, J. Golding, S. Forsyth, M. Forsyth, and G. B. Deacon, "Low viscosity ionic liquids based on organic salts of the dicyanamide anion," *Chemical Communications*, no. 16, pp. 1430–1431, 2001.

[4]   M. Zavrel, D. Bross, M. Funke, J. Büchs, and A. C. Spiess, "High-throughput screening for ionic liquids dissolving (ligno-)cellulose.," *Bioresource technology*, vol. 100, no. 9, pp. 2580–7, May 2009.

[5]   J. J. Moura Ramos and H. P. Diogo, "Are Crystallization and Melting the Reverse Transformation of Each Other?," *Journal of Chemical Education*, vol. 83, no. 9, p. 1389, Sep. 2006.

[6]   P. G. Vekilov, "Nucleation.," *Crystal growth & design*, vol. 10, no. 12, pp. 5007–5019, Nov. 2010.

[7]   D. Vivarès, E. W. Kaler, and A. M. Lenhoff, "Quantitative imaging by confocal scanning fluorescence microscopy of protein crystallization via liquid-liquid phase separation.," *Acta crystallographica. Section D, Biological crystallography*, vol. 61, no. Pt 6, pp. 819–25, Jun. 2005.

[8]   E. Zhuravlev, J. W. P. Schmelzer, B. Wunderlich, and C. Schick, "Kinetics of nucleation and crystallization in poly(ε-caprolactone) (PCL)," *Polymer*, vol. 52, no. 9, pp. 1983–1997, Apr. 2011.

[9]   R. Purohit and P. Venugopalan, "Polymorphism : An Overview," *Resonance*, no. September, pp. 882–893, 2009.

[10]   C. A. Angell, "On Importance of Metastable Liquid State and Glass Transition Phenomenon to Transport and Structure Studies in Ionic Liquids .I. Transport Properties.," *Journal of Physical Chemistry*, vol. 70, no. 9, pp. 2793–2803, 1966.

[11] S. Sastry, "Liquid limits: glass transition and liquid-gas spinodal boundaries of metastable liquids.," *Physical review letters*, vol. 85, no. 3, pp. 590–3, Jul. 2000.

[12] E. Sanz, C. Valeriani, E. Zaccarelli, W. C. K. Poon, P. N. Pusey, and M. E. Cates, "Crystallization Mechanism of Hard Sphere Glasses," *Physical Review Letters*, vol. 106, no. 21, p. 215701, May 2011.

[13] Y. Sun, L. Zhu, K. L. Kearns, M. D. Ediger, and L. Yu, "Glasses crystallize rapidly at free surfaces by growing crystals upward," *Proceedings of the National Academy of Sciences*, vol. 108, no. 15, pp. 5990–5995, Mar. 2011.

[14] S. I. Fletcher, F. B. Sillars, N. E. Hudson, and P. J. Hall, "Physical Properties of Selected Ionic Liquids for Use as Electrolytes and Other Industrial Applications," *Journal of Chemical & Engineering Data*, vol. 55, no. 2, pp. 778–782, Feb. 2010.

[15] C. P. Fredlake, J. M. Crosthwaite, D. G. Hert, S. N. V. K. Aki, and J. F. Brennecke, "Thermophysical Properties of Imidazolium-Based Ionic Liquids," *Journal of Chemical & Engineering Data*, vol. 49, no. 4, pp. 954–964, Jul. 2004.

[16] M. Yang, J.-N. Zhao, Q.-S. Liu, L.-X. Sun, P.-F. Yan, Z.-C. Tan, and U. Welz-Biermann, "Low-temperature heat capacities of 1-alkyl-3-methylimidazolium bis(oxalato)borate ionic liquids and the influence of anion structural characteristics on thermodynamic properties.," *Physical chemistry chemical physics : PCCP*, vol. 13, no. 1, pp. 199–206, Jan. 2011.

[17] A. L. Saroj and R. K. Singh, "Thermal, dielectric and conductivity studies on PVA/Ionic liquid [EMIM][EtSO4] based polymer electrolytes," *Journal of Physics and Chemistry of Solids*, vol. 73, no. 2, pp. 162–168, Feb. 2012.

[18] A. K. Jonscher, "Universal Dielectric Response," *Nature*, vol. 267, no. 5613, pp. 673–679, 1977.

[19] J. Leys, M. Wübbenhorst, C. Preethy Menon, R. Rajesh, J. Thoen, C. Glorieux, P. Nockemann, B. Thijs, K. Binnemans, and S. Longuemart, "Temperature dependence of the electrical conductivity of imidazolium ionic liquids.," *The Journal of chemical physics*, vol. 128, no. 6, p. 064509, Feb. 2008.

[20] E. J. Cabrita, "FCT/UNL, private communication."

[21] J. R. Sangoro, C. Iacob, S. Naumov, R. Valiullin, H. Rexhausen, J. Hunger, R. Buchner, V. Strehmel, J. Kärger, and F. Kremer, "Diffusion in ionic liquids: the interplay between molecular structure and dynamics," *Soft Matter*, vol. 7, no. 5, p. 1678, 2011.

[22] J. Sangoro, C. Iacob, a Serghei, S. Naumov, P. Galvosas, J. Kärger, C. Wespe, F. Bordusa, a Stoppa, J. Hunger, R. Buchner, and F. Kremer, "Electrical conductivity and translational diffusion in the 1-butyl-3-methylimidazolium tetrafluoroborate ionic liquid.," *The Journal of chemical physics*, vol. 128, no. 21, p. 214509, Jun. 2008.

[23] J. R. Sangoro, a. Serghei, S. Naumov, P. Galvosas, J. Kärger, C. Wespe, F. Bordusa, and F. Kremer, "Charge transport and mass transport in imidazolium-based ionic liquids," *Physical Review E*, vol. 77, no. 5, pp. 4–7, May 2008.

[24] M. Sun, S. Pejanovic, and J. Mijovic, "Dynamics of Deoxyribonucleic Acid Solutions As Studied by Dielectric Relaxation Spectroscopy and Dynamic Mechanical Spectroscopy," *Macromolecules*, vol. 38, no. 23, pp. 9854–9864, 2005.

[25] H. Search, C. Journals, A. Contact, M. Iopscience, and I. P. Address, "Dielectric relaxation spectroscopy of polyethylene terephthalate (PET) films," *Journal of Physics D: Applied Physics*, vol. 30, pp. 1551–1560, 1997.

[26] M. Dionisio and J. F. Mano, "Electrical Techniques," in in *Handbook of Thermal Analysis and Calorimetry*, 5th ed., Elsevier, 2008, pp. 209–268.

[27] M. Galiński, A. Lewandowski, and I. Stępniak, "Ionic liquids as electrolytes," *Electrochimica Acta*, vol. 51, no. 26, pp. 5567–5580, Aug. 2006.

[28] C. A. Angell, "Entropy and Fragility in Supercooling Liquids," vol. 102, no. 2, 1997.

[29] W. Xu, L.-M. Wang, R. a. Nieman, and C. A. Angell, "Ionic Liquids of Chelated Orthoborates as Model Ionic Glassformers," *The Journal of Physical Chemistry B*, vol. 107, no. 42, pp. 11749–11756, Oct. 2003.

[30] J. Leys, R. N. Rajesh, P. C. Menon, C. Glorieux, S. Longuemart, P. Nockemann, M. Pellens, and K. Binnemans, "Influence of the anion on the electrical conductivity and glass formation of 1-butyl-3-methylimidazolium ionic liquids.," *The Journal of chemical physics*, vol. 133, no. 3, p. 034503, Jul. 2010.

[31] W. Xu, L.M. Wang, R. a. Nieman, and C. A. Angell, "Ionic Liquids of Chelated Orthoborates as Model Ionic Glassformers," *The Journal of Physical Chemistry B*, vol. 107, no. 42, pp. 11749–11756, Oct. 2003.

[32] C. A. Angell., "Mobile Ions in Amourphous Solids," *Annual Review of Physical Chemistry*, vol. 43, pp. 693–717, 1992.

[33] J. R. Sangoro, a. Serghei, S. Naumov, P. Galvosas, J. Kärger, C. Wespe, F. Bordusa, and F. Kremer, "Charge transport and mass transport in imidazolium-based ionic liquids," *Physical Review E*, vol. 77, no. 5, pp. 4–7, May 2008.

[34] J. R. Sangoro, G. Turky, M. A. Rehim, C. Iacob, S. Naumov, A. Ghoneim, J. Ka, and F. Kremer, "Charge Transport and Dipolar Relaxations in Hyperbranched Polyamide Amines," pp. 1648–1651, 2009.

[35] M. Tress, M. Erber, E. U. Mapesa, H. Huth, J. Müller, A. Serghei, C. Schick, K.-J. Eichhorn, B. Voit, and F. Kremer, "Glassy Dynamics and Glass Transition in Nanometric Thin Layers of Polystyrene," *Macromolecules*, vol. 43, no. 23, pp. 9937–9944, Dec. 2010.

[36] C. Krause, J. R. Sangoro, C. Iacob, and F. Kremer, "Charge transport and dipolar relaxations in imidazolium-based ionic liquids.," *The journal of physical chemistry. B*, vol. 114, no. 1, pp. 382–6, Jan. 2010.

[37] C. Iacob, J. R. Sangoro, a Serghei, S. Naumov, Y. Korth, J. Kärger, C. Friedrich, and F. Kremer, "Charge transport and glassy dynamics in imidazole-based liquids.," *The Journal of chemical physics*, vol. 129, no. 23, p. 234511, Dec. 2008.

[38] J. Leys, R. N. Rajesh, P. C. Menon, C. Glorieux, S. Longuemart, P. Nockemann, M. Pellens, and K. Binnemans, "Influence of the anion on the electrical conductivity and glass formation of 1-butyl-3-methylimidazolium ionic liquids.," *The Journal of chemical physics*, vol. 133, no. 3, p. 034503, Jul. 2010.

[39] A. Rivera and A. R. Ernst, "Evidence of secondary relaxations in the dielectric spectra of ionic liquids," *Physical Review B*, vol. 73, no. 21, pp. 1–5, 2006.

[40] J. Leys, M. Wübbenhorst, C. Preethy Menon, R. Rajesh, J. Thoen, C. Glorieux, P. Nockemann, B. Thijs, K. Binnemans, and S. Longuemart, "Temperature dependence of the electrical conductivity of imidazolium ionic liquids.," *The Journal of chemical physics*, vol. 128, no. 6, p. 064509, Feb. 2008.

[41] F. Castiglione, M. Moreno, G. Raos, A. Famulari, A. Mele, G. B. Appetecchi, and S. Passerini, "Structural organization and transport properties of novel pyrrolidinium-based ionic liquids with perfluoroalkyl sulfonylimide anions.," *The journal of physical chemistry. B*, vol. 113, no. 31, pp. 10750–9, Aug. 2009.

[42] J. R. Sangoro, C. Iacob, S. Naumov, R. Valiullin, H. Rexhausen, J. Hunger, R. Buchner, V. Strehmel, J. Kärger, and F. Kremer, "Diffusion in ionic liquids: the interplay between molecular structure and dynamics," *Soft Matter*, vol. 7, no. 5, p. 1678, 2011.

[43]   W. Xu, E. I. Cooper, and C. A. Angell, "Ionic Liquids: Ion Mobilities, Glass Temperatures, and Fragilities," *The Journal of Physical Chemistry B*, vol. 107, no. 25, pp. 6170–6178, Jun. 2003.

[44]   C. A. Angell, "Formation of Glasses from Liquids and Biopolymers," *Science*, vol. 267, no. 5206, pp. 1924–1935, 1995.

[45]   R. Böhmer, K. L. Ngai, C. a. Angell, and D. J. Plazek, "Nonexponential relaxations in strong and fragile glass formers," *The Journal of Chemical Physics*, vol. 99, no. 5, p. 4201, 1993.

[46]   J. C. Dyre, "A phenomenological model for the Meyer-Neldel rule," *Journal of physics. C. Solid state physics*, vol. 19, no. 28, pp. 5655–5664, Oct. 1986.

[47]   M. D. Ediger and S. R. Nagel, "Supercooled Liquids and Glasses," *The Journal of Phisical Chemistry*, vol. 100, no. 95, pp. 13200–13212, 1996.

[48]   Y. Yoshida, K. Muroi, A. Otsuka, G. Saito, M. Takahashi, and T. Yoko, "1-Ethyl-3-Methylimidazolium Based Ionic Liquids Containing Cyano Groups: Synthesis, Characterization, and Crystal Structure.," *Inorganic chemistry*, vol. 43, no. 4, pp. 1458–62, Feb. 2004.

[49]   K. Dong, S. Zhang, D. Wang, and X. Yao, "Hydrogen bonds in imidazolium ionic liquids.," *The journal of physical chemistry. A*, vol. 110, no. 31, pp. 9775–82, Aug. 2006.

[50]   V. Kempter and B. Kirchner, "The role of hydrogen atoms in interactions involving imidazolium-based ionic liquids," *Journal of Molecular Structure*, vol. 972, no. 1–3, pp. 22–34, May 2010.

[51]   N. Lebrun and J. . van Miltenburg, "Calorimetric study of maltitol: correlation between fragility and thermodynamic properties," *Journal of Alloys and Compounds*, vol. 320, no. 2, pp. 320–325, May 2001.

[52]   J. J. M. Ramos, C. A. M. Afonso, and L. C. Branco, "Glass transition relaxation and fragility in two room temperature ionic liquids," *Journal of Thermal Analysis and Calorimetry*, vol. 71, pp. 659–666, 2003.

Chapter 5

UNDERSTANDING THE IMPACT OF WATER ON THE GLASS TRANSITION TEMPERATURE AND TRANSPORT PROPERTIES OF IONIC LIQUIDS

5. Understanding the impact of water on the glass transition temperature and transport properties of ionic liquids

The present study has been initiated to present reliable data for the physic-chemical properties of a series of aqueous solutions of ILs, which includes thermal behaviour, diffusion coefficient of the cation and the anion, mobility of the ions and ionic conductivity over a wide range of temperature.

It is known that water influences several properties of ILs. Aiming to understand the molecular interactions between the IL and water, this chapter focuses on the study of the impact of water on the transport properties and glass transition temperature of different ILs. In particular, seeks to establish a correlation between T_g and the amount of water in an IL, since sometimes in high hydrophilic materials, it is not easy to know the water content immediately before the start of the measurements due to the Karl Fischer uncertain.

Since we aim to apply the IJ materials in electrochemical devices, the principal feature requested from the IL is high conductivity. Initially it was thought that the IL with the higher conductivity would lead to the IJ with higher conductivity also. This condition was observed for the IL EMIMDCA. Furthermore, it was realized that an EMIMDCA-based IJ with 9% water content had a higher conductivity than the IL EMIMDCA with the same water percentage. This led us to conclude on chapter 4 that EMIMDCA was a suitable IL for the development of IJ films with high room temperature conductivity.

To extend our approach we set out to evaluate the impact of water on the physic - chemical properties of different ILs, namely: BMIMDCA, BMPyrDCA, EMIMSO$_4$, and complemented our data for EMIMDCA. For that purpose, three samples with different water contents, 9%, 12% and 30%, in addition to the neat IL were prepared: EMIMDCA$_{0.4\%}$, EMIMDCA$_{9\%}$, EMIMDCA$_{12\%}$ and EMIMDCA$_{30\%}$; BMIMDCA$_{0.4\%}$, BMIMDCA$_{9\%}$, BMIMDCA$_{12\%}$ and BMIMDCA$_{30\%}$; BMPyrDCA$_{0.4\%}$, BMPyrDCA$_{9\%}$, BMPyrDCA$_{12\%}$ and BMPyrDCA$_{30\%}$; EMIMSO$_{4,\ 0.4\%}$, EMIMSO$_{4,\ 9\%}$, EMIMSO$_{4,\ 12\%}$ and EMIMSO$_{4,\ 30\%}$; the water contents were determined by Karl-Fischer titration (see *Experimental*).

Due to their unique and largely studied properties, ILs are very suitable to use as electrolytes[1]. In IL/water mixtures, ion solvation and ion association are very important aspects to consider when looking at ion-solvent interactions. The main idea in this chapter is to clarify these interactions by using DRS and DSC. In the case of ion association, it is possible to find in the literature case studies reporting very different situations. For instance, no ion associations are detected for most of the aqueous electrolytes [2]. Nonetheless, in the case of sodium chloride, all ions are in the form of hydrated clusters and "these clusters behave as strongly bound units where the cation and anion in each cluster are inseparable" [3]. Yet, this type of behaviours is not totally understood and same questions remain [4-5].

5.1. EMIMDCA

5.1.1. Thermal Characterization

As was done in the previous chapters, DSC was used to probe phase transformations and estimate T_g for the cases where the glass transition is detected. We initiated our study with the thermal characterization of EMIMDCA $_{9\%}$, which has a considerable amount of water.

To achieve the conditions of total water removal and observe the shift on the T_g, melting and crystallization, differential scanning calorimetry was carried out in eighteen successive scans, nine on cooling and the other nine on heating. The final temperature in each heating scan is progressively increased from an initial value of 50 ºC to a final value of 130ºC (illustrated in scheme 5.1).
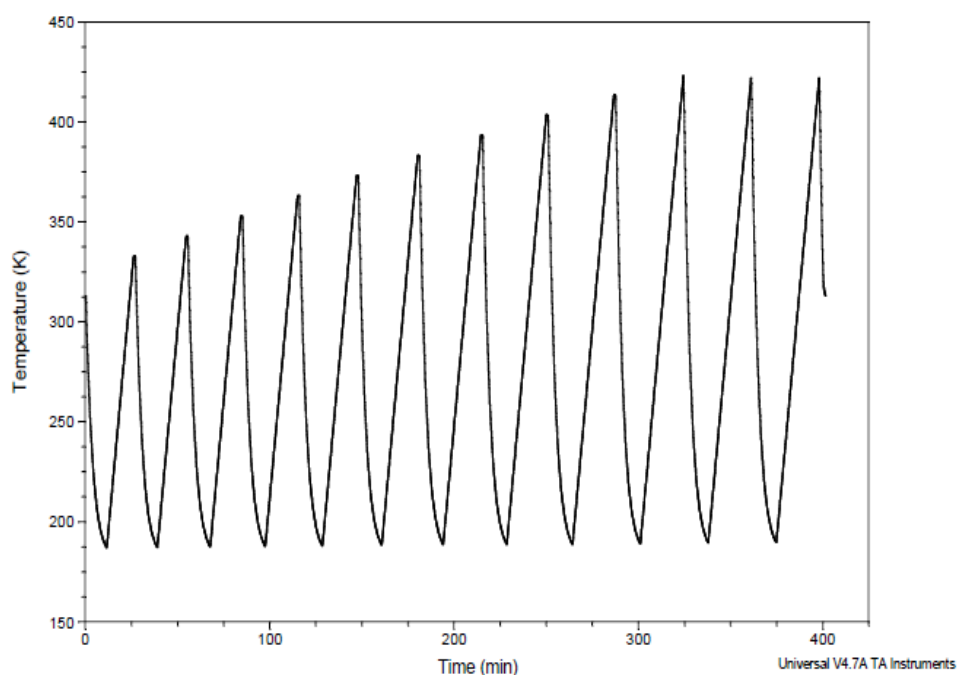
Scheme 5.1 – Cyclic thermal treatment for water removal.

No phase transitions were observed on cooling (not shown). Each cooling/heating scan was made at a scan rate of 20ºC min^{-1}; the T_g was not detected since it lies at very low temperatures, in a temperature region where the linearity of the temperature change is lost.
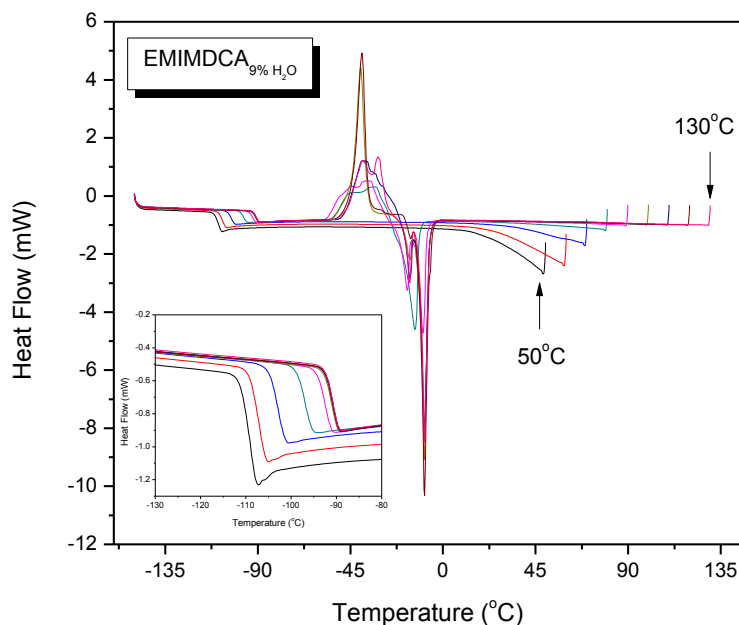
Figure 5.1 - DSC thermograms obtained for EMIMDCA $_{9\%}$ showing the heat flow jump at the glass transition as well as the crystallization and melting phase transitions, from the fourth scan. The inset shows in more detail the evolution of the glass transition with sample dehydration. All the scans were obtained in successive sweeps with increasing final temperature.

From Figure 5.1 it is possible to infer that all scans exhibits a heat flux change in the DSC thermogram, corresponding to the glass transition temperature, T_g. No endothermic peak, corresponding to a melting point, or an exothermic peak, corresponding to crystallization, are observed on the first four scans, which is due to the presence of a higher water quantity.

As we showed in chapter 4, a two step-process for the crystallization process is needed: nucleation and crystal growth. It was also mentioned that a temperature increase favors the nucleation step due a decrease in viscosity. Thus, at higher temperatures relatively to the glass transition temperature range, and for a lower amount of water, it is possible to observe crystallization; at even higher temperatures the endothermic peak due to melting is detected.

The crystallization and melting temperature are taken to be the maximum value on the observed exothermic and endothermic peak on heating, respectively. The glass transition temperature is taken from the onset ($T_{g, on}$), midpoint ($T_{g, mid}$) and endpoint ($T_{g, end}$) of a small heat capacity change on heating from the amorphous glass state to the liquid state.

The inset of Figure 5.1 is a scale-up of the temperature region for which the glass transition is detected. It nicely illustrates the shift towards higher temperatures with dehydration upon thermal treatment. The estimated glass transition temperatures are presented in table 5.1 and shown in more detail in Figure 5.2. It is interesting to note that a shift of T_g close to 20 K is observed between the dry and hydrated sample, evidencing the strong plasticizing effect of water in this IL. This observed decrease is in agreement with the results of several authors [6-7].

Table 5.1 - Glass transition temperatures taken at the onset (on), midpoint (mid) and endset (end) of the heat flow jump for EMIMDCA$_{9\%}$, obtained during a first heating run at 20 K/min; melting and crystallization temperatures obtained from the fourth heating run.

System		$T_{g,on}$/K	$T_{g,mid}$/K	$T_{g,end}$/K	T_c/K	T_m/K
EMIMDCA$_{9\%}$	1st heating run	162.2	164.4	165.1	----	----
	2nd heating run	164.3	166.3	167.5	----	----
	3rd heating run	168.6	169.8	171.7	----	----
	4th heating run	174.6	176.0	177.7	240.2	259.5
	5th heating run	179.0	180.7	181.9	235.3	263.4
	6th heating run	180.6	182.0	183.3	233.1	264.0
	7th heating run	180.7	182.2	183.5	234.7	264.1
	8th heating run	181.0	182.7	183.5	233.8	264.2
	9th heating run	180.9	182.2	183.6	235.4	264.1

From Figure 5.2 it is possible to see that from the fifth scan (after heating up the sample to 363.15 K), the changes in T_g, T_c and T_m are negligible.
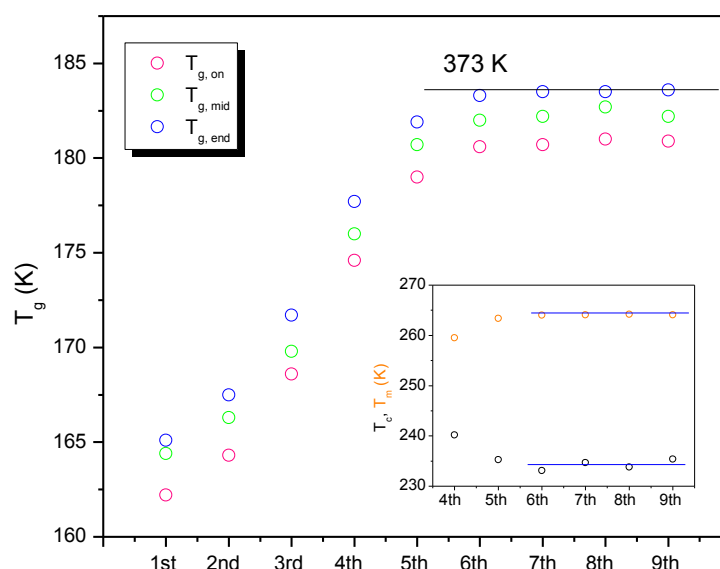
Figure 5.2 – Plot of the glass transition temperatures for EMIMDCA$_{9\%}$ for each cycle. The inset shows the two phase transformations, crystallization and melting. It was used a 20 K.min^{-1} rate scan.

The EMIMDCA$_{9\%}$ sample was also measured by DRS but only two scans were carried out. It is not possible to monitor melting or crystallization through DRS since these phenomena only occur after the fourth run and the DRS data are taken from the first run. Aiming to observe these phase

transformations through this technique, a second run was carried out. However, no conclusions could be reached.

The sample with 0.4% water amount is the neat IL, used as received. From the plasticizing water effect illustrated in Figure 5.1 it was expected that the sample with lower water amount would show the highest T_g. The glass transition located at a higher temperature is the one relative to the sample containing 9% of water. For the other three samples, the temperature location remains almost unchanged. This may seem an unexpected result. However, some care should be taken when doing this comparison: the endothermic event centered around 373 K (100°C) in the thermograms depicted in Figure 5.3 is due to water evaporation. It is evident that this endothermic peak has a smaller area in the case of the sample labeled 9%; samples labeled 12 and 30% have almost the same water amount and therefore the glass transition occurs at the same temperature. Surprisingly, the "as received" EMIMDCA, which supposedly should contain 0.4% water, is the IL that exhibits water evaporation to a higher extent. This means that above critical water content value the glass transition remains unaltered. Some discrepancies could also arise due to the fact that, initially, for equilibration, all the samples remain a few minutes at 40°C, a temperature at which some water could evaporate (from the thermograms, it is clear that water evaporation starts just above ~10°C).
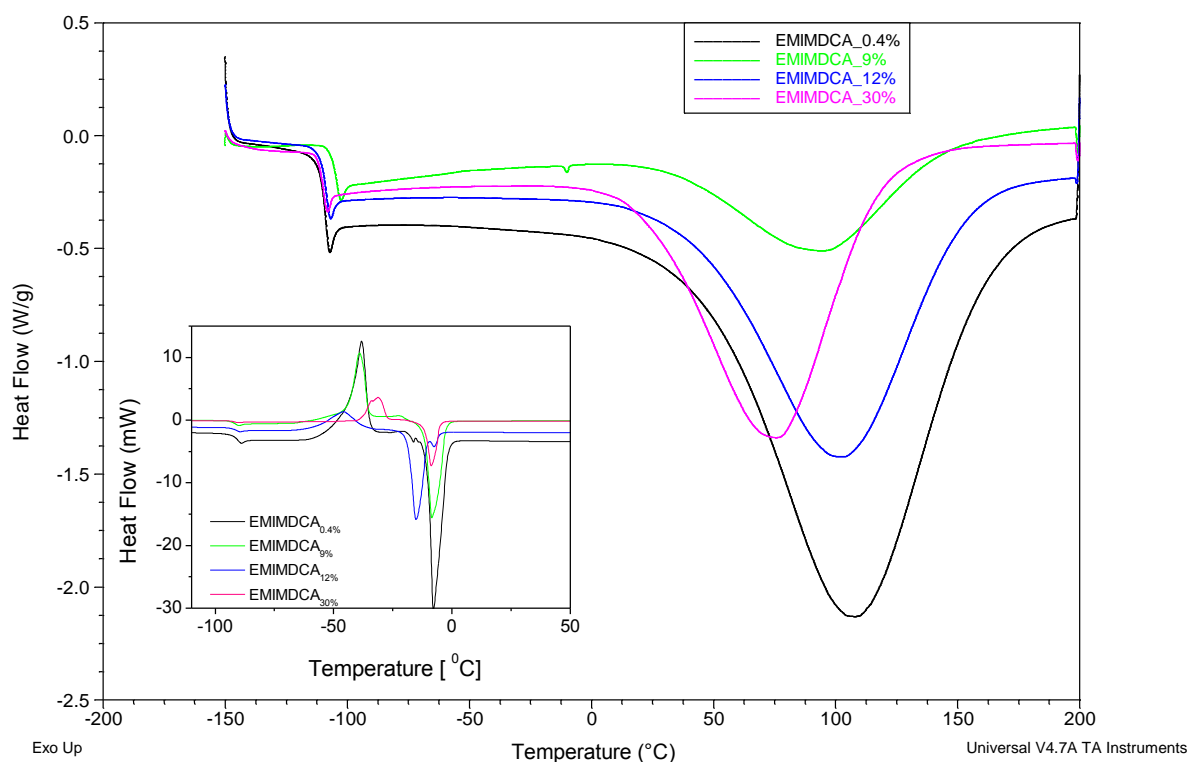
Figure 5.3- DSC scans obtained for EMIMDCA with 0.4%, 9%, 12% and 30% water content, showing the heat flow jump at the glass transition temperature during the first cycle. The curves were vertically shifted to allow a better comparison of both heat flux discontinuity in the glass transition region and endothermal water evaporation. The inset shows the second heating run in which crystallization and melting are observed.

Table 5.2 shows the estimated T_g values and the peak temperatures for crystallization and melting, which are present only in the second run. In the second cycle, the T_g for all systems is almost the same and therefore the value of 180.1$\pm$0.4 K could be taken as the T_g for dry EMIMDCA.

Table 5.2 - Glass transition temperatures taken at the onset (on), midpoint (mid) and endset (end) of the heat flow jump for EMIMDCA$_{0.4\%}$, EMIMDCA$_{9\%}$, EMIMDCA$_{12\%}$ and EMIMDCA$_{30\%}$ obtained during a first and a second heating run at 20 K/min; melting and crystallization temperatures obtained from the minimum and maximum of the peak, respectively.

System		$T_{g,on}$/K	$T_{g,mid}$/K	$T_{g,end}$/K	T_c/K	T_m/K
EMIMDCA$_{0.4\%}$	1st heating run	162.14	164.26	164.61	------	------
	2nd heating run	180.59	182.95	183.09	235.41	265.06
EMIMDCA$_{9\%}$	1st heating run	166.47	168.88	169.19	------	------
	2nd heating run	179.79	181.49	182.03	234.00	264.85
EMIMDCA$_{12\%}$	1st heating run	162.20	164.77	164.93	------	------
	2nd heating run	180.10	182.30	182.41	233.78	265.24
EMIMDCA$_{30\%}$	1st heating run	161.31	163.39	163.64	------	------
	2nd heating run	179.78	181.27	181.76	240.68	264.23

5.1.2. Dielectric Relaxation Spectroscopy Characterization

5.1.2.1. Conductivity

DRS is a very sensitive technique to polarization and conductivity changes when an oscillating electric field is applied to a wide range of substances. Given that in electrolyte solutions polarization arises from orientational fluctuations of permanent dipoles, both of solvent molecules and of ion pairs, from intramolecular polarizability and ion motion [8]. Therefore, it seemed advantageous to characterize our samples with this method.

The electric response for the ILs with different water percentages was probed by DRS measurements covering 7 orders of magnitude ($10^{-1} - 10^{6}$ Hz). The IL aqueous solutions and the neat IL were cooled from room temperature to 153 K and 163 K, respectively, and then heated to 313 K. Measurements were taken isothermally every 2 K to 213 K and every 5 K in the remaining temperature range, as it is shown in Table 5.3.

Table 5.3 – Temperature range covered in the DRS measurements and temperature domain where electrical anomalies were registered for EMIMDCA with different water contents.

IL	Temperature range [ºC]	
	Measurements	Electrical anomalies
EMIMDCA 0.4%	-110 to 40	-20 to -15
EMIMDCA 9%	-120 to 40	-55 to -40
EMIMDCA 12%	-120 to 40	-70 to -55
EMIMDCA 30%	-120 to 40	-70 to -55

Figure 5.4 shows the conductivity, σ', versus frequency plot, obtained previously for all the studied systems. Conductivity spectra are characterized by a plateau, which is associated with the pure conductivity, σ_0, and is quite visible at temperatures above 171 K (-102ºC). The electrode polarization effect starts to be evident at 187 K (-86°C) (decrease in conductivity at the lowest frequencies; see *Introduction*).

Also, in Figure 5.4, in the inset a), a discontinuity is observed between 195 K (-78ºC) and 263 K (-10ºC), which is illustrated by the isochronal plot of the conductivity measured at 4×10^{5} Hz. If we take into account the DSC results, this behaviour may be related with the crystallization (drop in σ') and at higher temperatures with melting (further increase in σ'). This behaviour was already observed by Viciosa *et al*[9].

In the temperature range 171 K (-102ºC) to 195 K (-78ºC), the pure conductivity was obtained from the fitting with Jonscher's equation (see equation 1.14 from chapter I); red solid lines in the main figure. From 263 K (-10ºC) to 313 K (40ºC) the values were estimated by directing extraction of the pure conductivity from the plateau. The dependence with the temperature reciprocal is shown in the inset of Figure 5.4; the lack of points in the intermediate temperature region is due to the occurrence of crystallization. The Vogel-Fulcher-Tamman-Hesse (VFTH) [10-12] equation, was fitted to the remaining data:

$$\sigma_0(T) = \sigma_\infty \exp\left(\frac{-B}{T-T_0}\right) \qquad \text{(Equation 5.1)}$$

It should be noted that in the lower temperature range the material is in the supercooled state and in the high temperature region is in the molten state. Therefore, the plotted relaxation times refer to equilibrium states. Clearly, the conductivity follows a non-Arrhenian temperature dependence, in agreement with the behaviour reported by Rivera *et al* [13]. An identical VFTH temperature dependence is observed for the relaxation process that is assumed to be responsible for dynamical glass transition (designated α-process) being cooperative in nature [14-15]. Therefore, for ILs based on imidazolium cations, for which the temperature dependence of the pure conductivity obeys a VFTH law, it is assumed that the conductivity mechanism is coupled with the α-process, i.e., to the dynamical behaviour of the cooperative molecular motions driving the glass transition [9].
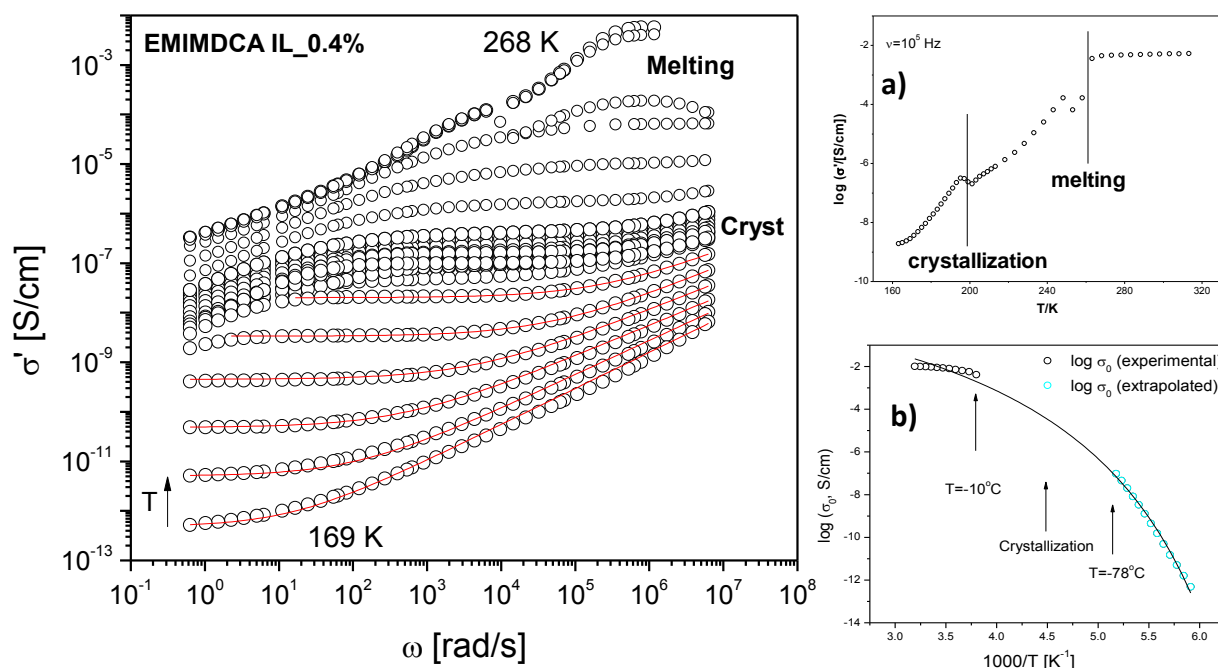
Figure 5.4 - Real part of conductivity of EMIMDCA IL_0.4%. The solid lines are the fits obtained by the Jonscher law (eq 1.14), for isotherms in steps of 4K between 169 K and 189 K for EMIMDCA IL_0.4%. The isotherms for the highest temperatures were taken between 258K and 268 K in steps of 5 K; the isotherms between 201 K and 211 K in steps of 2 K, were included to illustrate the crystallization effect. The inset a) shows the isochronal plot of the conductivity at 4×10^5 Hz, illustrating the effect of crystallization and melting. The inset b) displays the conductivity as a function of the inverse of temperature (1000/K). The blue symbols show the σ_0 values obtained from Jonscher's fit to the data while the black circles represent the values directly extracted from the plateau; the lack

of points in the intermediate temperature region is due to the occurrence of crystallization. The solid line is the VFTH fitting curve.

Figure 5.5 shows the frequency dependence of the conductivity of EMIMDCA, both neat and with different water contents at 175 K (-98ºC). This temperature was chosen since it was less affected by electrode polarization when compared with higher temperatures. From this figure it is possible to infer that conductivity increases with the water percentage increase. Hence, the conductivity of neat IL is affected by water addition. Differences in conductivity for different water contents are due to the dissociation of the IL into ions. It was expected that increasing the water percentage would lead to an increase in conductivity. This means that somewhere between 9 and 12% a water amount that confers the highest conductivity is achieved, and beyond that critical value a plateau is reached. However, we see that EMIMDCA$_{12\%}$ and EMIMDCA$_{30\%}$ have the same conductivity, which could be related to the fact that above 12% of water probably the maximum extent of solvated ions is attained. This seems to be corroborated by the DSC results that show an invariance of the glass transition temperatures above 12%. Below this water percentage, not all the ions are saturated and the observed conductivity increase with hydration, maybe attributed to a disruption of IL-IL interactions, concomitant with the establishment of water-IL cation and water-IL anion interactions and a consequent increase of charge transport. This could be explained by assuming that the water-anion and water-cation interactions are stronger than cation-anion interactions. This was demonstrated for several hydrophilic ILs, including EMIMEtSO$_4$, whose water mixtures exhibit negative excess enthalpies up to 0.8 molar fraction of water [16]; for this IL, 12% and 30% of water correspond, respectively, to 0.64 and 0.85 mole fraction of water.
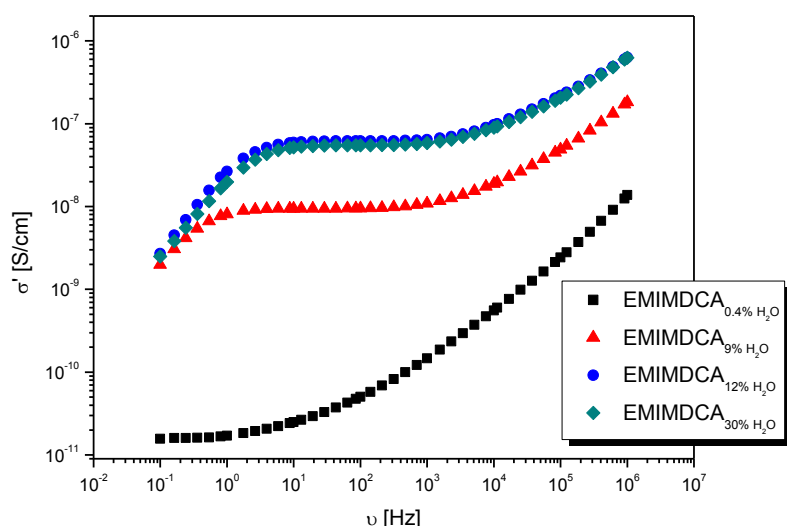
Figure 5.5 - Real part of complex conductivity (σ') of EMIMDCA with 0.4%, 9%, 12% and 30% water contents versus frequency (υ) (from 10^{-1} to 10^{6} Hz) at -98ºC.

5.1.2.2. Transport properties

It is known that IL viscosity will decrease significantly with the addition of a few solvents, such as water [17], which will increase ion dissociation in more dilute solutions. Also, as reported by Tshibangu *et al* [16], viscosity strongly depends on the interaction between the cation and the anion, the possibilities to form hydrogen bonding and the symmetry of the ions, which will affect the diffusion of the ions. Furthermore, other author studied some factors that control the diffusion of ions in ILs, namely, the effects of ion size, shape of the ions, magnitude of interactions between the cation and the anion, effects of conformational flexibility, effects of molecular mass and nanostructure of the IL mixtures with neutral molecules (for example, water) and salts [17].

Figure 5.6 shows the temperature dependence of the diffusion coefficient of the anion EMIM and the cation DCA estimated by equations 1.20 (a) and 1.20 (b) in chapter 1. The sample corresponding to the neat IL shows an Arrhenian behaviour whereas the aqueous IL solutions show a non-Arrhenian behaviour.
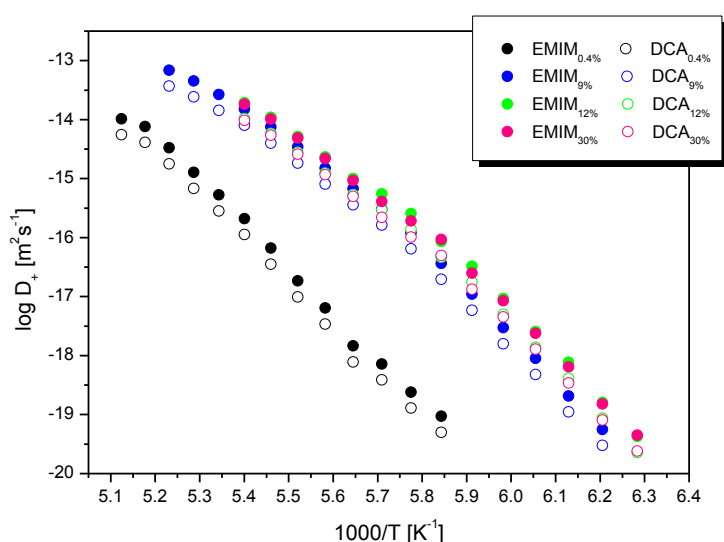
Figure 5.6 - Diffusion coefficient of EMIM (given as log D_+) in EMIMDCA with 0.4%, 9%, 12% and 30% water content, as a function of inverse temperature.

Some factors such as exchange-repulsion, dispersion, charge-charge interaction and the effect of polarization are considered as the main factors that contribute to the intermolecular interactions in ion pairs, which are composed by cations and anions. Studies show that the charge-charge interaction is the major source of the attraction between the cation and the anion of an IL [17-18]. Also, the polarization of the ions produced by the surrounding ions has a significant effect on the motion of ions in ILs. The strong attraction between the anion and the cation could be at the origin of the slow diffusion of ions in ILs [17]. In Figure 5.6 it is possible to observe that for the aqueous solutions the anion-cation interactions have the same impact since there are no significant discrepancies between the diffusion coefficients.
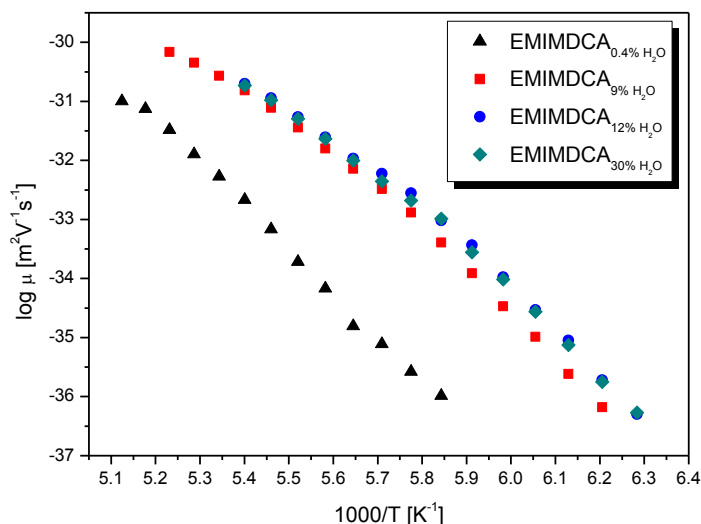
Figure 5.7 Mobility (given as μ) for EMIMDCA with 0.4%, 9%, 12% and 30% water content as a function of inverse temperature.

Also, in Figure 5.7, no discrepancies are observed since the mobility depends directly from the diffusion coefficients (see equation 1.15 (b) in chapter I).

A phenomena observed previously was the electrode polarization. This is known to happen at lower frequencies (and high temperatures) due to the accumulation of mobile charges on the interface of the electrode. Since polarization depends on the geometry of the electrode and on the electrode material [19], we carried out measurements on both gold and stainless steel electrodes. In Figure 5.8, it is possible to see that no significant differences between the two electrodes were detected, except that for lower frequencies, electrode polarization is slightly smaller for the gold electrodes. However, since, unlike gold electrodes, stainless steel electrodes do not undergo oxidation, we chose to use the later.
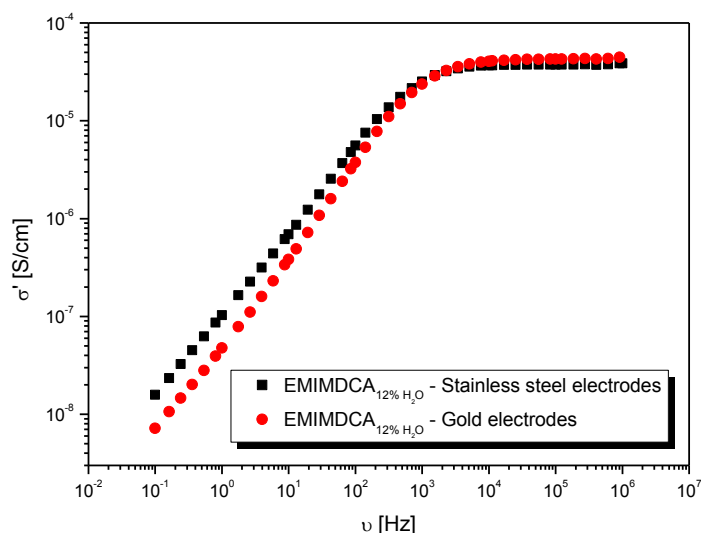
Figure 5.8 – Real part of conductivity, at -74ºC, as a function of frequency using two different electrode materials, keeping the same geometry.

5.2. BMPyrDCA

5.2.1. Thermal Characterization

The thermal behaviour of the neat IL and the IL with different water contents was investigated in the temperature range -150 to 200ºC, for which only the glass transition was detected.

Figure 5.9 presents the first cycle of the DSC thermograms collected on heating at a rate of 20 ºC min^{-1}. The values of the glass transition temperature taken at the midpoint are very similar, and do not follow a monotonic trend with the water content. Therefore, BMPyrDCA is must less sensitive to water than EMIMDCA. The average value for the T_g of the hydrated IL is 167.5±0.5 K, taken at the midpoint of the first cycle, whereas T_g for the dry material is 175.1±0.1 K (Table 5.4).
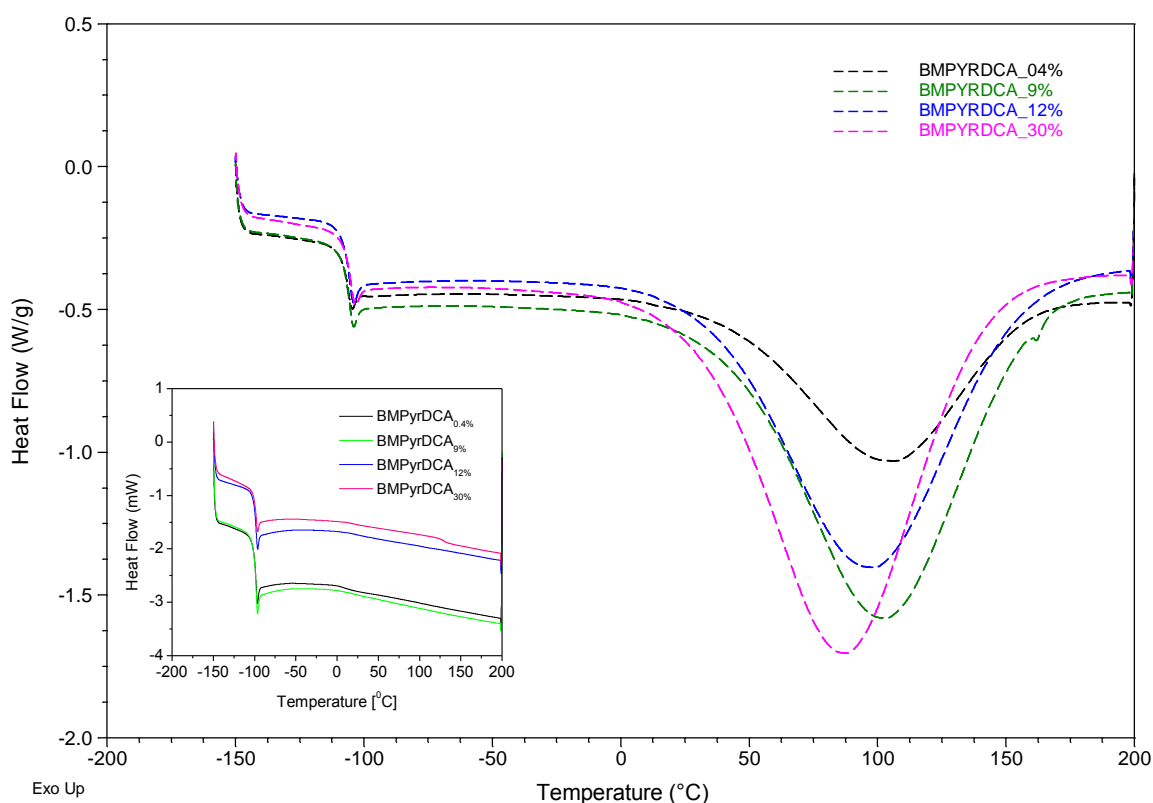
Figure 5.9 - DSC thermograms normalized by mass obtained for BMPyrDCA with 0.4%, 9%, 12% and 30% water content showing the heat flow jump at the glass transition during the first cycle. The inset displays the thermograms collected during a second heating run, after water removal, showing that the glass transition of all systems remains invariant.

Table 5.4 - Glass transition temperatures taken at the onset (on), midpoint (mid) and endset (end) of the heat flow jump for BMPyrDCA$_{0.4\%}$, BMPyrDCA$_{9\%}$, BMPyrDCA$_{12\%}$ and BMPyrDCA$_{30\%}$ obtained during a first and second heating run at 20 K/min; melting and crystallization temperatures were not observed.

System		$T_{g,on}$/K	$T_{g,mid}$/K	$T_{g,end}$/K	T_c/K	T_m/K
BMPyrDCA$_{0.4\%}$	1st heating run	164.25	166.80	167.30	___	___
	2nd heating run	172.87	175.19	175.34	___	___
BMPyrDCA$_{9\%}$	1st heating run	165.01	167.45	167.75	___	___
	2nd heating run	172.57	175.00	175.43	___	___
BMPyrDCA$_{12\%}$	1st heating run	165.08	167.53	167.85	___	___
	2nd heating run	172.93	174.91	175.68	___	___
BMPyrDCA$_{30\%}$	1st heating run	165.51	168.02	168.46	___	___
	2nd heating run	172.72	175.22	175.67	___	___

5.2.2. DRS Characterization

5.2.2.1. Conductivity

DRS has been demonstrated to be the suitable technique to show and characterize different type of relaxations processes due to different molecular motions. Both, main relaxation (α - process) and secondary relaxations [13], the main relaxation appearing at low frequencies than the secondary relaxations, are detected simultaneously for a variety of ILs. However, the origin of secondary relaxations is an issue that still raises many scientific discussions, mainly concern with whether they are inter or intramolecular in nature [4-7].

As for the other systems studied, the dielectric response for BMPyrDCA was probed by DRS measurements covering 7 orders of magnitude (10^{-1} – 10^6 Hz). In this frequency range the main relaxation (α – relaxation) is observed, as well as secondary relaxations at a temperature below T_g. This behaviour can also be observed through the electric modulus representation (Figure 5.10), which is frequently used to evaluate molecular mobility and conductivity in ILs. It is well known that from the mixture of an ionic substance with solvents capable to form H-bonds, such as ILs and water, respectively, there could result additional relaxation processes, due to ion solvations, i. e., *direct ion - solvent interactions* [8].

As mentioned in previous chapters, the complex dielectric function is dependent of both angular frequency and temperature, which leads to several relaxation processes such as microscopic fluctuations of molecular dipoles, translation of mobile charge carriers and electrode polarization. Each one of these processes will have a distinct impact on the frequency and temperature dependence of the real and imaginary part of the complex dielectric function [24].

As we can see from Figure 5.10, the conductivity of the BMPyrDCA sample with 30% water content shows a quite different behaviour. This atypical behaviour is related with the relaxations mentioned above which are not detected in either of the other systems. For this reason, the data analysis for this aqueous solution was carried out differently from the previous ones.
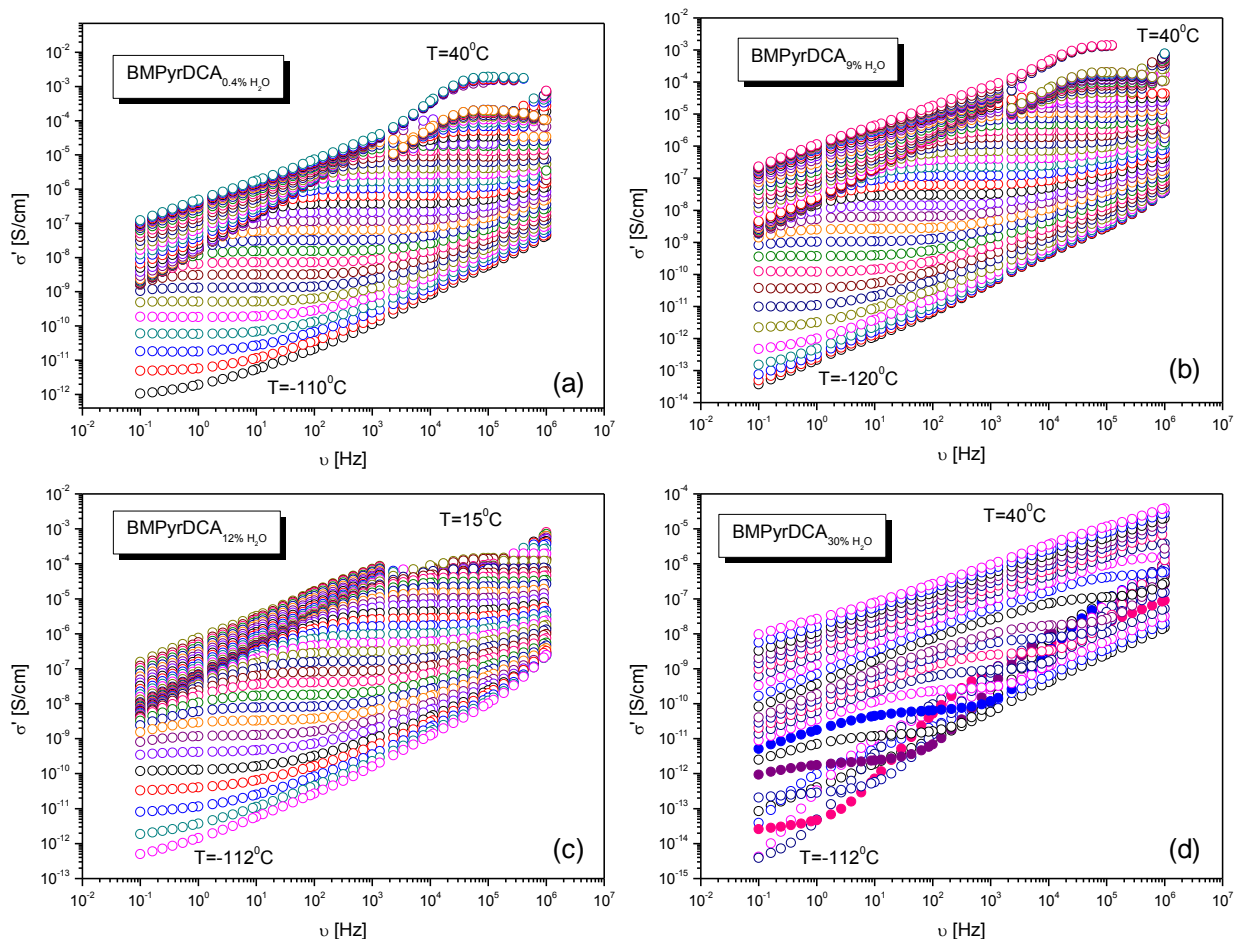
Figure 5.10 Real part of complex conductivity (σ') of BMPyrDCA with 0.4%, 9%, 12% and 30% water content versus frequency (υ) (from 10^{-1} to 10^6 Hz) measured at temperatures from -120ºC to 40ºC.

A relaxation process appears as a peak in the plot of ε'' vs frequency, shown in Figure 5.11. This peak is shifting to higher frequencies (and higher temperatures), indicated by the pink arrows. At low frequencies (high temperatures), an increase in the imaginary part of the complex dielectric function is observed, showing a slope < -1, indicated by the yellow arrow, which is due to electrode polarization. This type of behavior is designated as non–ohmic conductivity [24].

In the mixture of the IL with water two types of interactions should be considered: ion – ion and ion – water interactions. Since the relaxation processes are present only in the sample with higher water content, it is possible to infer that the latter interactions are responsible for the peaks presented in the ε'' plot. Another reason why the relaxation process appears only in the IL with 30% water is maybe an increase in the segmental mobility. It is known that pure water has some relaxation processes [25], although not at these temperatures. However, the relaxation processes present in this IL sample are not from the pure water, but the mixture, since the IL and the water are miscible. In

other words, for substances highly hydrophobic, the *shielding effect* is so pronounced that the characteristic relaxation processes of water are clearly evident. Nevertheless, because the IL is hydrophilic, this phenomenon is due to mixture as a whole [18 - 21].

Some authors also showed that in aqueous solutions, the attractive forces between the cation and water are strongly dominated by electrostatic forces [8]. Depending on the surface-charge density of the cations they could align perfectly with the water molecule. In Figure 5.12 – a), the water molecule is very well aligned with the cation due to its high surface-charge density. However, with a decrease of the surface-charge density, a deviation from this alignment is observed (Figure 5.12- b). Keeping in mind the structure of BMPyrDCA, it is possible to know that this cation is the one with less polarizability due to the inexistence of π – bonds, contrarily to what happens with the other cations studied. In Figure 5.12 – c) it is observed the preference of the water molecules orientation towards the anion. However, as it was already mentioned in chapter 3, water can form H-bonds with the anion DCA and, since the anion is the same for all the ILs, except for the IL EMIMEtSO$_4$ (see section 5.4), this argument does not apply.
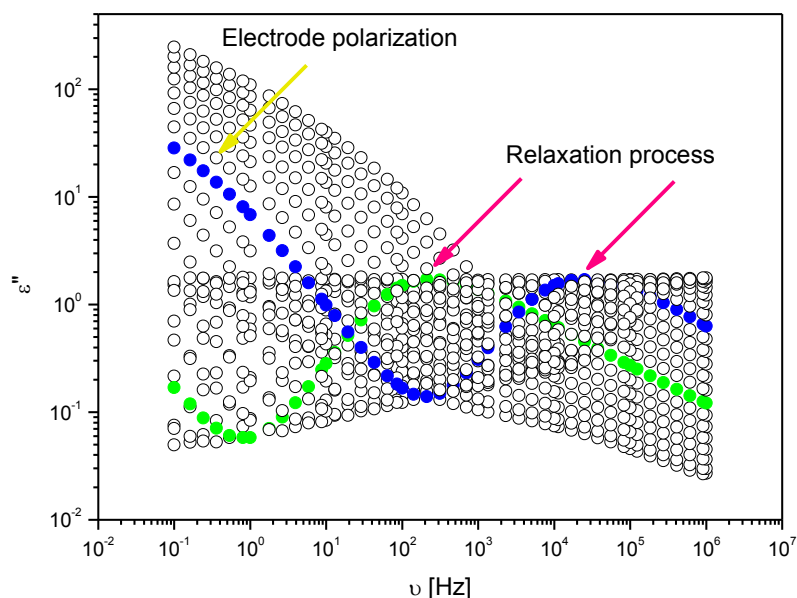
Figure 5.11 Imaginary part of complex permittivity of BMPyrDCA with water content as a function as frequency (ν) (from 10^{-1} to 10^6 Hz) for temperatures from -112ºC to -60 ºC. The -98 ºC and -86 ºC isotherms are in solid circles to emphasize the dielectric loss peak.
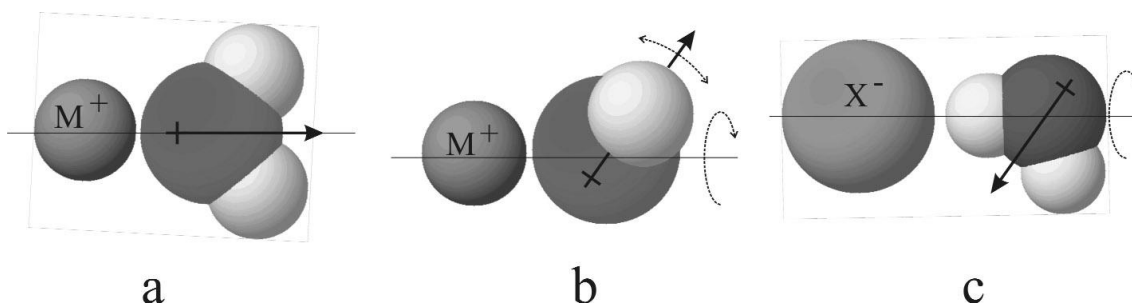
Figure 5.12 – Preferred orientation of water molecules towards (a) a cation with high surface-charge density, (b) a cation with low surface-charge density and (c) an anion. The arrow indicates the direction of the water dipole moment. (Retrieved from [8]).

Some authors have been discussed how to best represent ac data, via the conductivity or the electric modulus [29-32]. We chose the latter one to represent dielectric properties due to the suppression of the electrode polarization effect, which facilitates the identification of dipolar relaxations [33] and its analysis.

The electric modulus is related to the complex permittivity by the following equation:

$$M^*(\omega) = 1/\varepsilon^* = i\omega\varepsilon_0/\sigma^* \quad [24]$$ (Equation 5.2)

In order to get an accurate understanding of dipolar polarization due to reorientational motions of permanent dipoles, the imaginary part of the complex electric modulus, M*(ω)

$$M^*(\omega) = M'(\omega) + iM''(\omega)$$ (Equation 5.3)

will be analyzed based on the real and imaginary components of the complex dielectric permittivity, by the following expression:

$$M''(\omega) = \frac{\varepsilon'}{[(\varepsilon')^2 + (\varepsilon'')^2]}$$ (Equation 5.4)

The relaxation time, determined from the modulus, is correlated to the Debye relaxation (which means that the *x* and *y* from equation 1.13 in chapter I are equal to unity, the peak showing a completely symmetrical form), through the following equation:

$$\tau_{M''} = \frac{\varepsilon_\infty}{\varepsilon_0}\tau_{\varepsilon''}$$ (Equation 5.5)

$\tau_{M''}$ is smaller than $\tau_{\varepsilon''}$ since $\varepsilon_\infty < \varepsilon_0$. As a consequence, a Debye-like relaxation process appears at a higher frequency in the modulus plot [34].

In Figure 5.13 the imaginary part of the spectra of the electric modulus of the sample with 30% water, BMPyrDCA$_{30\%}$, is plotted. This electrical modulus plot shows a typical ionic conductor behaviour [35], where it is possible to see the ionic conduction as a relaxation process represented as a relaxation peak. In the case where conductivity, σ_{dc}, is frequency dependent, it was expected a peak with a symmetric Debye shape, corresponding to a normal diffusion. However, due to the dispersion of the conductivity curves of ionic conductors at high frequencies, where it is present a sub-diffusive diffusion, the shape of the peak is distorted [13]. In the electric modulus the dipolar contribution emerges at the lower temperatures while conductivity is felt at the higher temperatures (corresponding to the lowest frequencies in the isothermal dielectric spectra). At temperatures below T$_g$ another peak in *M"* can be detected due to a secondary relaxation.

$\alpha \qquad condc$
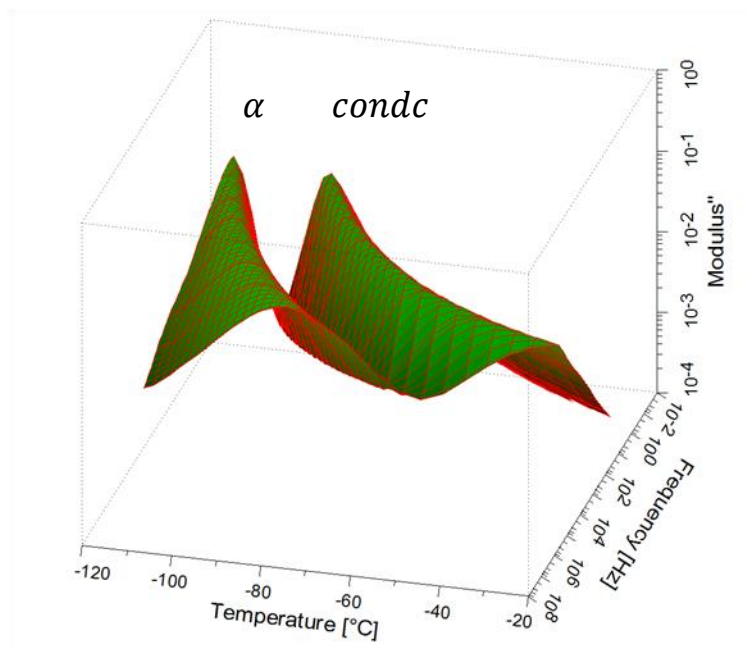
Figure 5.13 – 3-D Spectra of the imaginary part of the electric modulus spectra *M"* as a function of temperature and frequency for BMPyrDCA$_{30\%}$ in the temperature range -110 ºC to -78 ºC.

In figure 5.13 the peaks that are observed in the temperature range 163 K (-110 ^{0}C) to 195 K (-78 ^{0}C) are due to dipolar relaxation, from which it is possible to infer about the molecular mobility that originates the dynamical glass transition, allowing to go further in the analysis compared to DSC. From Figure 5.14 it is possible to infer that multiple relaxation processes take place in BMPyrDCA$_{30\%}$. To gain insight into the mobility the electric modulus peak, associated with reorientational polarization, was analyzed and compared with the one observed in ε'', Figure 5.11. The characteristic relaxation time is extracted from the frequency dependence of ε'' through the HN equation (equation 1.13 in chapter I). Identical data treatment was carried out for the electrical modulus peak. The temperature dependence of the respective relaxation times, is plotted in figure 5.14.

While the main relaxation exhibits a non-Arrhenian behaviour, the secondary relaxation, β, shows an Arrhenian linear temperature dependence (E$_a$= 68.3 kJ.mol^{-1}), although only a few spectra allowed to extract the respective relaxation times.
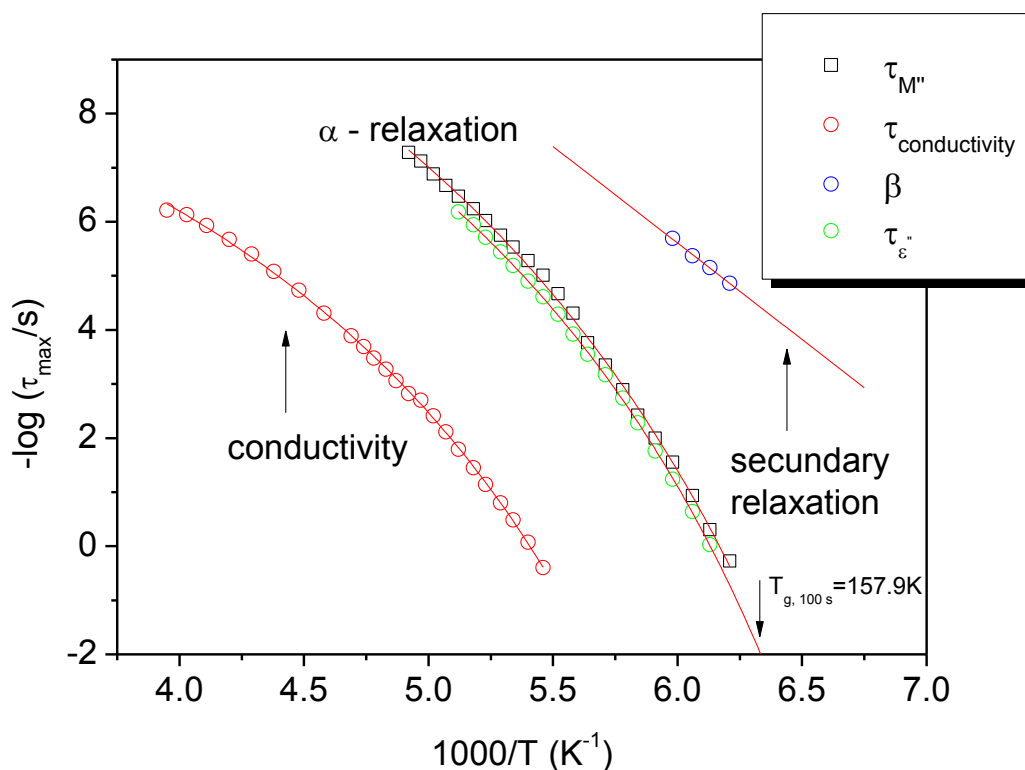
Figure 5.14 – Relaxation times, τ_{max}, as a function of inverse temperature obtained by DRS for different processes: $\square$ – α-relaxation obtained from M'', $\circ$ - α-relaxation obtained from ε'', $\circ$ - β - relaxation process and $\circ$ - the relaxation process that results from conductivity, through the M''; solid lines are the fitting by VFTH.

Table 5.5 presents the VFTH parameters used to simulate the temperature dependence of the diferent non-linear processes. From the VFTH equation obtained from the $\varepsilon''(1/K)$ fit, a glass transition temperature of 157.9 K (-115.3 ^{o}C) is estimated for τ= 100 s [36-37].

The proximity to the value estimated by DSC for BMPyrDCA$_{30\%}$, 165.5 K (-107.6^{0}C), seems to confirm that this process is associated with the dynamic glass transition (usually designated as α-relaxation). Although the proposed criterion refers to $\tau_{\varepsilon''}$, if applied to $\tau_{M''}$ it allows obtaining a T$_g$ value of 156.9 K (-116.3^{0}C), also close to the calorimetric value. The reason why this process was detected only in the mixture with 30% of water probably means that the water molecules take part in the process facilitating the underlying motions and enhancing its intensity due to the high dipolar moment of water. As previously mentioned, for the dilectric response both reorientational dipolar motions and charge transport contribute. If the conductivity higly dominates it is not possible to unravel relaxational processess. It seems that in this particular system, with so low glass transition temperature, the water molecules interact with the ion pair and only at higher temperatures will start to contribute more effctively for conductivity, which allows in this temperature region, near T$_g$, the detection and characterization of the relaxation processes.   Nevertheless more studies should be carry out to clarify this.

Table 5.5 – Summary of the VFTH parameters for the detected processes in the ε'' and M'' representations.

VFTH parameters	α-process		$M''_{Conductivity}$
	ε''	M''	
τ_∞ / s	3.4×10^{-15}	3.0×10^{-16}	4.4×10^{-12}
B / K	1434.7	1647.3	1416.0
T_0 / K	120.1	116.1	130.8
T_g (τ=100s) / K	157.9	165.5	----

5.2.2.2. Transport Properties

As is possible to observe in section 5.2.2.1, due to the relaxations processes present in the sample BMPyrDCA$_{30\%}$, it is not possible to proceed with the fitting of the curves in the plot of conductivity versus frequency, i. e., the characterisc plateau is not observed, which prevents to extracting any information about pure conductivity or the crossover frequency. For these reasons, only the neat IL and the samples with 9% and 12% water content are shown in Figure 5.15. This plot was collected at a temperature of -104 ºC where no electrode polarization is observed. In the aqueous solutions (BMPyrDCA with 9% and 12% water content) the water effect appears to be "invisible".
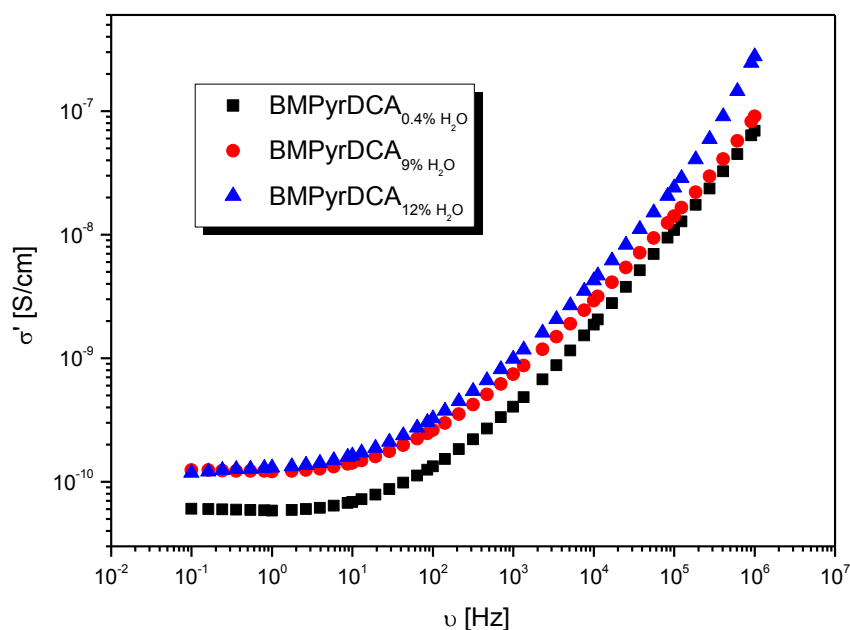
Figure 5.15 Real part of complex conductivity (σ') of BMPyrDCA with 0.4%, 9% and 12% water content as a function of frequency (υ) (from 10^{-1} to 10^6 Hz) at -104ºC.

Figure 5.16 shows the temperature dependence of the diffusion coefficient of the anion BMPyr estimated by equation 1.20 (a) in chapter I, for the samples containing water from 0.4 to 12 %, all exhibiting a non-Arrhenius behaviour. Identical behaviour is observed for the mobility as shown in figure 5.17 (estimated according to equation 1.15 b) in chapter I).
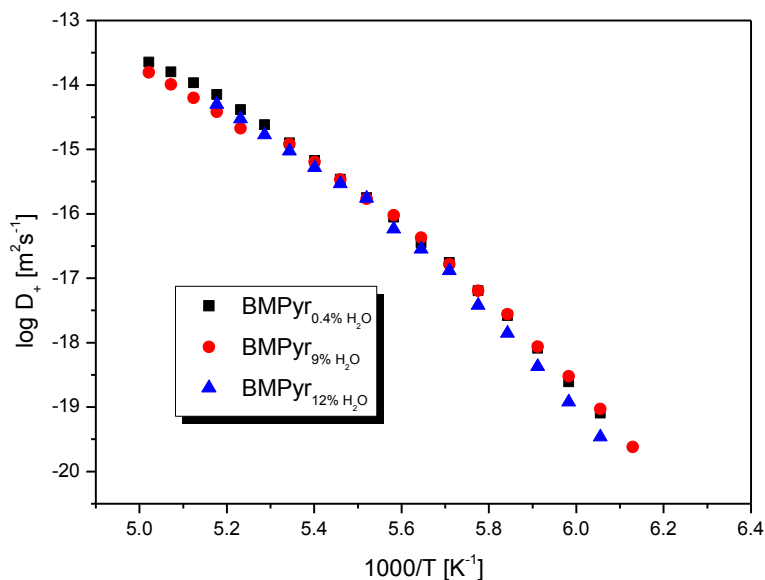
Figure 5.16 Diffusion coefficient of BMPyr (given as log D_+) in BMPyrDCA with 0.4%, 9% and 12% water content as a function of inverse temperature.
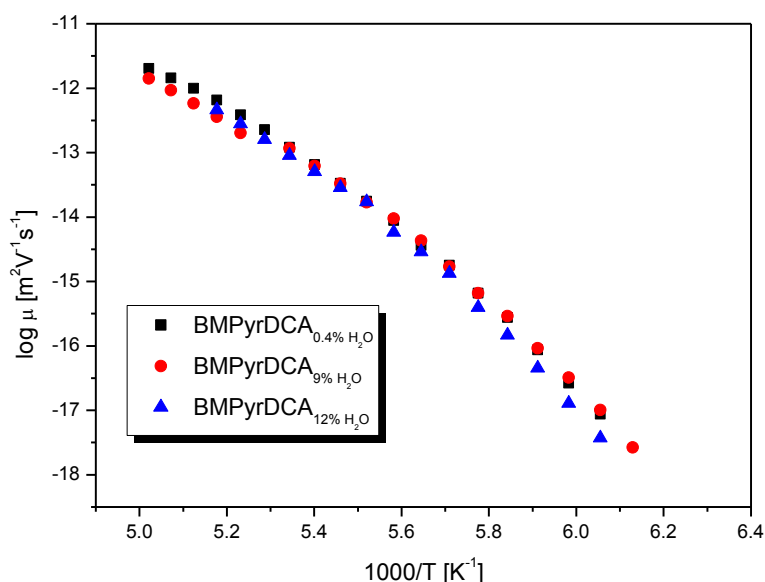
Figure 5.17 Mobility (given as log μ) of BMPyrDCA with 0.4%, 9% and 12% water content as a function of inverse temperature.

A summary of the glass transitions detected for 1-buthyl – 3 – methyl imidazolium dicyanamide and 1-ethyl – 3 – methyl imidazolium ethylsulfate is presented in tables 5.6 and 5.7. Those systems were submitted to the same type of experimental measurements and data treatment as done for the

other two ILs. However no significant effects were observed between the different hydrated samples.

This means that the estimated transport properties are similar to the ones presented in chapter IV.

Table 5.6 - Glass transition temperatures taken at the onset (on), midpoint (mid) and endset (end) of the heat flow jump for $BMIMDCA_{0.4\%}$, $BMIMDCA_{9\%}$, $BMIMDCA_{12\%}$ and $BMIMDCA_{30\%}$ obtained during a first and second heating run at 20 K/min; melting and crystallization temperatures obtained from the minimum/maximum of the respectively peak.

System		$T_{g,on}$/K	$T_{g,mid}$/K	$T_{g,end}$/K	T_c/K	T_m/K
$BMIMDCA_{0.4\%}$	1st heating run	169.18	171.77	172.09	___	___
	2nd heating run	185.29	187.73	187.85	257.57	271.15
$BMIMDCA_{9\%}$	1st heating run	173.15	175.39	176.22	___	___
	2nd heating run	185.48	187.77	187.99	___	___
$BMIMDCA_{12\%}$	1st heating run	168.13	170.40	170.58	___	___
	2nd heating run	185.50	187.50	187.70	___	___
$BMIMDCA_{30\%}$	1st heating run	167.88	170.39	170.58	___	___
	2nd heating run	185.24	187.64	187.74	___	___

Table 5.7 - Glass transition temperatures taken at the onset (on), midpoint (mid) and endset (end) of the heat flow jump for $EMIMEtSO_{4\_0.4\%}$, $EMIMEtSO_{4\_9\%}$, $EMIMEtSO_{4\_12\%}$ and $EMIMEtSO_{4\_30\%}$ obtained during a first and second heating run at 20 K/min; melting or crystallization temperatures were not observed.

System		$T_{g,on}$/K	$T_{g,mid}$/K	$T_{g,end}$/K	T_c/K	T_m/K
$EMIMEtSO_{4\_0.4\%}$	1st heating run	164.48	166.80	167.21	___	___
	2nd heating run	172.51	174.91	175.18	___	___
$EMIMEtSO_{4\_9\%}$	1st heating run	166.95	169.88	170.44	___	___
	2nd heating run	192.09	194.97	195.11	___	___
$EMIMEtSO_{4\_12\%}$	1st heating run	167.63	170.02	170.31	___	___
	2nd heating run	192.67	194.73	195.26	___	___
$EMIMEtSO_{4\_30\%}$	1st heating run	167.17	169.88	169.91	___	___
	2nd heating run	192.02	195.01	195.10	___	___

5.3. Conclusion

The thermal properties neat ILs and ILs with different amounts of water were evaluated.

With the exception of BMPyrDCA which only undergoes a 7 K increase of T_g upon dehydration, the other tested ILs show a significant shift of the glass transition temperature to higher temperatures with the water removal: BMIMDCA – 18 K; EMIMDCA – 18 K and EMIMEtSO$_4$ – 25 K. This illustrates the plasticizing effect of water in these materials and, at the same time, it shows the greater interaction of water with these ILs relatively to BMPyrDCA, the complete water removal being only assured after an heating treatment up to 473 K (200°C).

The transport properties, conductivity, diffusion coefficients and mobility of charge carriers are also influenced by the presence of water, decreasing a few orders of magnitude upon dehydration. Almost all systems exhibit a temperature dependence of these properties following a VFTH law. This points to a correlation between the conductivity mechanism and the cooperative molecular motion that originates the glass transition. This can also be seen by the emergence of the plateau due to dc conductivity that only occurs at temperatures near the glass transition temperature, meaning that the translational motion of charge carriers does not occur at temperatures where the cooperative mechanism is frozen; this reinforces what was observed in chapters 3 and 4 for these ILs and for BPyDCA.

Unfortunately, the expected correlation between both the glass transition temperature and the transport properties with the water added to the IL was not observed, preventing deeper conclusions.

Interestingly, dipolar relaxation was observed for BMPyrDCA$_{30\%}$, allowing to go further in the data treatment. The electric modulus representation was used advantageously relative to the $\varepsilon''(f)$ spectra since is not affected by electrode polarization Multiple processes were identified: a secondary relaxation process and two intense processes that only emerge at temperatures above the calorimetric glass transition. The Havriliak Negami equation was fitted to both $\varepsilon''(f)$ and $M''(f)$ spectra allowing to estimate the respective relaxation times. An Arrhenian temperature dependence (although only over a very restricted temperature range) was observed for the secondary relaxation while for the other processes a VFTH law is obeyed. From the extrapolation to 100 s of the relaxation times, a glass transition temperature was estimated in good agreement with the calorimetric value, helping to assign the respective relaxation to the cooperative α-process observed for a variety of glass formers. Once again, the process located at the lower frequencies and higher temperatures in the modulus representation, which is associated with the conductivity, follows a VFTH dependence. It exhibits a curvature (quantified by the B parameter) very close to the α-process, corroborating, as previously found, a correlation between the charge carriers motion and the cooperative motion of the ionic liquid as a single dipole.

5.4. Bibliography

[1]   M. Galiński, A. Lewandowski, and I. Stępniak, "Ionic liquids as electrolytes," *Electrochimica Acta*, vol. 51, no. 26, pp. 5567–5580, Aug. 2006.

[2]   A. A. Zavitsas, "Properties of Water Solutions of Electrolytes and Nonelectrolytes," *The Journal of Physical Chemistry B*, vol. 105, no. 32, pp. 7805–7817, Aug. 2001.

[3]   J. J. Max and C. Chapados, "IR spectroscopy of aqueous alkali halide solutions: Pure salt-solvated water spectra and hydration numbers," *The Journal of Chemical Physics*, vol. 115, no. 6, p. 2664, 2001.

[4]   Y. Marcus and G. Hefter, "Ion pairing.," *Chemical reviews*, vol. 106, no. 11, pp. 4585–621, Nov. 2006.

[5]   G. Hefter, "When spectroscopy fails: The measurement of ion pairing," *Pure and Applied Chemistry*, vol. 78, no. 8, pp. 1571–1586, 2006.

[6]   C. P. Fredlake, J. M. Crosthwaite, D. G. Hert, S. N. V. K. Aki, and J. F. Brennecke, "Thermophysical Properties of Imidazolium-Based Ionic Liquids," *Journal of Chemical & Engineering Data*, vol. 49, no. 4, pp. 954–964, Jul. 2004.

[7]   C. A. Angell, "Formation of Glasses from Liquids and Biopolymers," *Science*, vol. 267, no. 5206, pp. 1924–1935, 1995.

[8]   R. Buchner, "What can be learnt from dielectric relaxation spectroscopy about ion solvation and association?," *Pure and Applied Chemistry*, vol. 80, no. 6, pp. 1239–1252, 2008.

[9]   M. T. Viciosa, H. P. Diogo, and J. J. Moura Ramos, "The Ionic Liquid BmimBr: a dielectric and thermal characterization," *The Royal Society of Chemistry Advances*, vol. 3, no. 16, pp. 5663–5672, 2013.

[10]   H. Vogel, "The temperature dependence law of the viscosity of fluids," *Physikalische Zeitschrift*, vol. 22, pp. 645–646, 1921.

[11]   G. S. Fulcher, "Analysis of recent measurements of the viscosity of glasses," *Journal of the American Ceramic Society*, vol. 8, no. 6, pp. 339–355, 1925.

[12]   G. Tammann and W. Hesse, "The dependancy of viscosity on temperature in hypothermic liquids," *Zeitschrift für anorganische und allgemeine Chemie*, vol. 156, no. 4, pp. 245–257, 1925.

[13]   A. Rivera and A. R. Ernst, "Evidence of secondary relaxations in the dielectric spectra of ionic liquids," *Physical Review B*, vol. 73, no. 21, pp. 1–5, 2006.

[14]   P. Lunkenheimer and A. Loidl, "Glassy Dynamics Beyond the α-Relaxation," in in *Broadband Dielectric Spectroscopy*, F. Kremer and A. Schönhals, Eds. Berlin, Germany, 2002, pp. 131–165.

[15]   F. Kremer and A. Schonalds, "The Scaling of the Dynamics of Glasses and Supercooled Liquids," in in *Broadband Dielectric Spectroscopy*, F. Kremer and A. Schonalds, Eds. Berlin, Germany, 2002, pp. 99–127.

[16]   L. E. Ficke and J. F. Brennecke, "Interactions of Ionic Liquids and Water,"*The Journal of Physical Chemistry B"*, vol. 114, pp. 10496-10501, 2010.

[17]   S. Tsuzuki, "Factors controlling the diffusion of ions in ionic liquids.," *Chemphyschem : a European journal of chemical physics and physical chemistry*, vol. 13, no. 7, pp. 1664–70, May 2012.

[18]   S. Tsuzuki, H. Tokuda, K. Hayamizu, and M. Watanabe, "Magnitude and directionality of interaction in ion pairs of ionic liquids: relationship with ionic conductivity.," *The journal of physical chemistry. B*, vol. 109, no. 34, pp. 16474–81, Sep. 2005.

[19]   J. R. Sangoro, a. Serghei, S. Naumov, P. Galvosas, J. Kärger, C. Wespe, F. Bordusa, and F. Kremer, "Charge transport and mass transport in imidazolium-based ionic liquids," *Physical Review E*, vol. 77, no. 5, pp. 4–7, May 2008.

[20]   U. Schneider, R. Brand, P. Lunkenheimer, and A. Loidl, "The Excess Wing in the Dielectric Loss of Glass-Formers: A Johari-Goldstein β -Relaxation?," *Physical Review Letters*, vol. 84, no. 24, pp. 5560–5563, 2000.

[21]   B. Th, C. Tschirwitz, S. Benkhof, and E. A. Rossler, "Susceptibility functions for slow relaxation processes in supercooled liquids and the search for universal relaxation patterns," *Journal of Chemical Physics*, vol. 118, no. 16, pp. 7544–7555, 2003.

[22]   K. Duvvuri and R. Richert, "Dielectric hole burning in the high frequency wing of supercooled glycerol," *The Journal of Chemical Physics*, vol. 118, no. 3, p. 1356, 2003.

[23]   K. L. Ngai and M. Paluch, "Classification of secondary relaxation in glass-formers based on dynamic properties.," *The Journal of chemical physics*, vol. 120, no. 2, pp. 857–73, Jan. 2004.

[24]   A. Schönhals and F. Kremer, "Analysis of Dielectric Spectra," in in *Broadband Dielectric Spectroscopy*, Springer V., A. Schönhals and F. Kremer, Eds. Berlin, Germany, 2003, pp. 59–98.

[25]   U. Kaatze, "Bound water: Evidence from and implications for the dielectric properties of aqueous solutions," *Journal of Molecular Liquids*, vol. 162, no. 3, pp. 105–112, Aug. 2011.

[26]   W. Wachter, R. Buchner, and G. Hefter, "Hydration of tetraphenylphosphonium and tetraphenylborate ions by dielectric relaxation spectroscopy.," *The journal of physical chemistry. B*, vol. 110, no. 10, pp. 5147–54, Mar. 2006.

[27]   A. Tromans, P. M. May, G. Hefter, and M. U. V, "Ion Pairing and Solvent Relaxation Processes in Aqueous Solutions of Sodium Malonate and Sodium Succinate," *Jounal of Physical Chemistry B*, vol. 108, pp. 13789–13795, 2004.

[28]   R. Buchner, C. Hölzl, J. Stauber, and J. Barthel, "Dielectric spectroscopy of ion-pairing and hydration in aqueous tetra-n-alkylammonium halide solutionsElectronic supplementary information (ESI) available: Relaxation parameters and relevant solution properties. See http://www.rsc.org/suppdata/cp/b1/b1103," *Physical Chemistry Chemical Physics*, vol. 4, no. 11, pp. 2169–2179, May 2002.

[29]   D. P. Almond, "Impedance and Modulus Spectroscopy of 'Real' Dispersive Conductors," *Solid State Ionics*, vol. 11, no. 1, pp. 57–64, 1983.

[30]   J. C. Dyre, "S o m e remarks on ac c o n d u c t i o n in disordered solids," *Journal of Non-Crystalline Solids*, vol. 135, pp. 219–226, 1991.

[31]   S. Elliott, "Use of the modulus formalism in the analysis of ac conductivity data for ionic glasses," *Journal of Non-Crystalline Solids*, vol. 170, no. 1, pp. 97–100, 1994.

[32]   C. T. Moynihan, "Analysis of electril relaxation in glasses and melts with large concentrations of mobile ions," *Journal of non*, vol. 172–174, pp. 1395–1407, 1994.

[33]   S. Ramesh, C.-W. Liew, and a. K. Arof, "Ion conducting corn starch biopolymer electrolytes doped with ionic liquid 1-butyl-3-methylimidazolium hexafluorophosphate," *Journal of Non-Crystalline Solids*, vol. 357, no. 21, pp. 3654–3660, Nov. 2011.

[34]   M. Dionísio and J. F. Mano, "Electric Techniques," in in *Handbook of Thermal Analysis and Calorimetry*, Elsevier., M. E. Brown and P. K. Gallagher, Eds. 2008, pp. 209–268.

[35]   J. Dyre and T. Schrøder, "Universality of ac conduction in disordered solids," *Reviews of Modern Physics*, vol. 72, no. 3, pp. 873–892, Jul. 2000.

[36]   R. Böhmer, K. L. Ngai, C. a. Angell, and D. J. Plazek, "Nonexponential relaxations in strong and fragile glass formers," *The Journal of Chemical Physics*, vol. 99, no. 5, p. 4201, 1993.

[37]   C. T. Moynihan, P. B. Macedo, C. J. Montrose, C. J. Montrose, P. K. Gupta, M. a. DeBolt, J. F. Dill, B. E. Dom, P. W. Drake, a. J. Easteal, P. B. Elterman, R. P. Moeller, H. Sasabe, and J. a. Wilder, "Structural Relaxation in Vitreous Materials," *Annals of the New York Academy of Sciences*, vol. 279, no. 1 The Glass Tra, pp. 15–35, Oct. 1976.

Chapter 6

ELECTRONIC NOSE (E-NOSE) BASED ON ION JELLY MATERIALS

6. ELECTRONIC NOSE (E-NOSE) BASED ON ION JELLY MATERIALS

6.1 Introduction

This chapter describes chemiresistive gas sensors based on conductive polymer composites (IJ films) prepared from ILs and gelatine, as well as an electronic nose, formed by an array of four gas sensors, capable of detecting and identifying various polar and nonpolar volatile compounds.

Gelatine is a low-cost widely available biopolymer, with excellent features as gelling agent and viscoelastic properties. Its different properties give rise to a wide range of applications such as in cosmetics, pharmacy, photography, food industries and in gelatine-based electrolyte [1-12]. It is prepared through partial hydrolysis of collagen, which is the main component of bones, cartilages and skin [13], after undergoing acid or alkaline pre-treatment [14-18]. By this process, gelatine becomes water soluble once its hydrogen and covalent bonds were cleaved. Depending on the acid or alkaline pre-treatment, two different types of gelatine are produced, type A-gelatine and type B-gelatine, with isoelectric points at ~ 4-5 or ~ 8-9, respectively [13]. The gelatine used in this work was the type A-gelatine.

The component that confers conductivity to IJ films is the IL. Lately, ILs have attracted, enormously, the scientific community, due to their unique physical-chemical properties. The most important feature for this work are ionic conductivity, chemical and electrochemical stabilities[19-21]. However, their application as active layer in gas sensors is somehow limited due to their physical state (liquid). The combination of gelatine and an IL forms IJ. Since IJ is a solid matrix, does not flow along the electrode, has a higher dimensional stability, i. e., IJ is auto sustainable, and it can be applied in chemiresisitive sensors.

The aim of this work is to use IJ films as active layers in gas sensors for e-noses. The mostly used commercial sensors are based on metal oxide semi conductors (MOS), which operate at high temperatures. Composite conductive polymer based sensors have gained large importance since they work at room temperature, hence have lower power consumption. The use of different IJs, containing different ILs, makes it possible to form a wide range of highly selective sensor arrays.

An e-nose is an array of gas sensors attached to a pattern recognition system that can detect and recognize odours [22]. The first gas sensor device was described in 1954 by Hartman, with the aim to detect flavours in vegetables [23]. These sensors were originally used for quality control applications in food, drinks and cosmetics industries. Nevertheless, current applications include detection of human body odours, classification of beverages, volatile halogenated organic compounds (VHOC), detection of methanol in sugar cane spirit and diagnosing respiratory diseases [24, 30], among many others.

Thus, depending on the specific need, there are different types of sensors employed in e-nose systems, as shown in Figure 6.1, adapted from reference [31], by adding a novel type of sensor, i.e., Composite Polymer (Ion Jelly), which will be focused in this thesis. The design of the first gas multisensor array was described by Persaud and Dodd in 1982 [32], aiming to mimic the mammalian olfactory system .
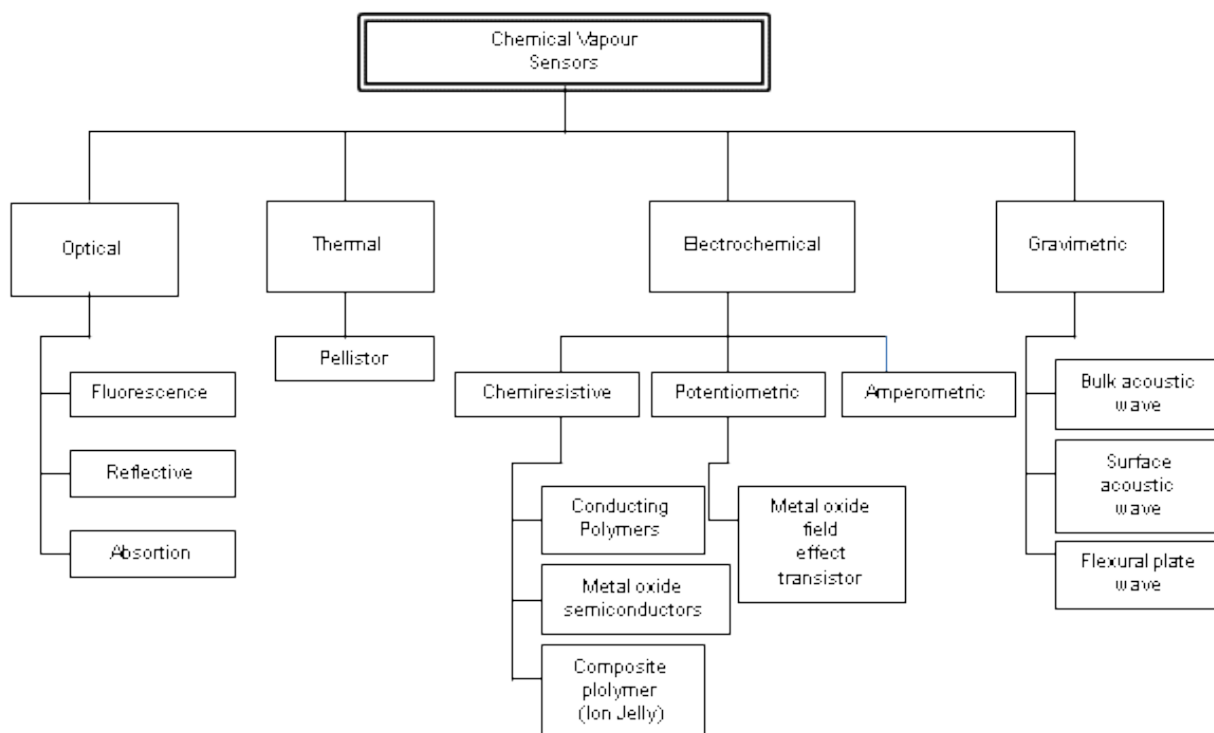
Figure 6.1 – Types of sensors utilized in e-noses (adapted from [31])

Basically, a gas sensor is composed by a sensing material that eventually converts a chemical or physical interaction into an electrical signal that reflects an optical, thermal, electrochemical or gravimetric change. The great advantages of these devices are related with the fact that they are inexpensive and reusable. The above mentioned interaction can occur through four distinct pathways: adsorption, which is the adhesion from the gas sample constituents (atoms, molecules or ions) to the chemical surface; absorption, which is the passage of the constituents through the chemical layer; co-ordination chemistry, which is related with the interactions between the organic and inorganic ligands with metal centers; and chemisorptions. All these mechanisms will influence the selectivity and reversibility of the system. Chemisorption is a sub-class of adsorption. This phenomenon happens when a chemical reaction occurs in the layer deposited under the sensor, in which new chemical species are held (e. g. corrosion and metal oxidation). Depending on the chemical identity of the vapour and of the sensing material, different types of electronic bonds are created, such as ionic or covalent bonds. For this reason, chemisorption is the suitable mechanism when a high selective system in needed. However, it is not possible to have both features, selectivity and reversibility [31]. In order to overcame this drawback Persaud and Dodd [32] proceeded to the manufacture of an array of reversible and semi-selective sensors with different chemical properties.

As said before, e-nose systems are based on arrays of sensors which give a unique response for a certain odour, i. e., a fingerprint for each sample, mimicking the mammalian nose. A schematic comparison between the human nose and an e-nose is shown Figure 6.2.
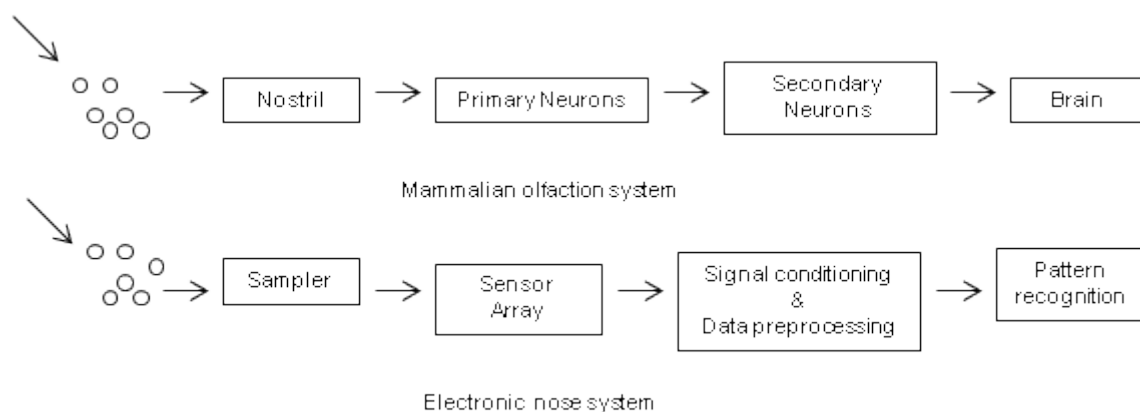
Figure 6.2 – Comparison of the mammalian olfactory system and the e-nose system (adapted from [33])

As shown above, the sample is vapourised over the sensors that are made of specific materials (as, for instance, IJ) which suffer reversible changes in a particular physical/chemical property, such as the electrical conductance [34]. Sensors that change their electrical conductance upon exposure to vapours are called chemoresistive sensors. These changes depend mainly on the nature of the sensing material, the nature of the analyte and its concentration. Since the array of sensors is formed by different sensing materials, a pattern is generated which is unique for this e-nose-analyte set.

A specific type of chemiresistive sensors are conductive polymer based whose performance could be enhanced adding, for example, ILs and gelatine. IL will increase the conductivity and gelatin will confer dimensional stability to the material. This combination leads to IJ films. A wide range of methods are applied on the fabrication of composite conductive polymers (CCP), such as hot pressing (compression molding) [35], simple dissolution followed by sonication and evaporation [36], polymer grafting by γ-radiation [37], [38] and reactive polymers [39]. The great advantage of the composite conductive polymer is the ease of manufacture of the IJ films, since they are a direct mixture of an IL and gelatine (see Chapter 2). In general, the main advantage of CCP is the fact that they demonstrate a higher selectivity, more reproducibility and easier preparation procedure than CP [40].

In a typical experiment, a reference gas (e.g. dry air) passes through the sensors in order to obtain a baseline. This step is a pre-treatment. Then, the sensors are exposed to the headspace of a volatile sample for a given period (exposure time) and finally to the reference gas again (recovery time) in order to recover and prepare the sensor array for the next cycle. Several such cycles can be performed for the same sample generating data to be statistically treated afterwards. In general, the response of the sensor is given as a first order time response, since it obey a first order differential equation. Figure 6.3 shows a typical conductance *versus* time plot for a single chemoresistive sensor during one complete analysis cycle.
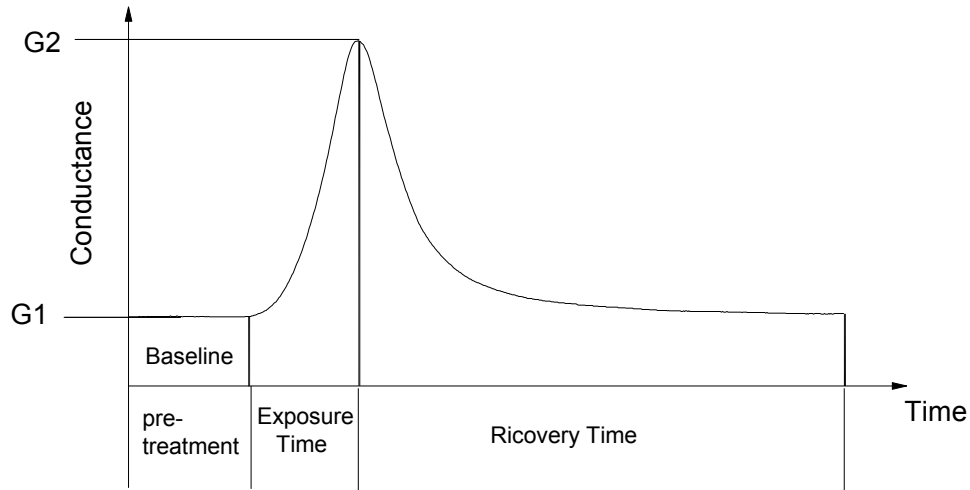
Figure 6.3 – Typical chemoresistive gas sensor response. G1 is the conductance before the exposure period and G2 is the conductance at the end of the exposure period.

Several methods for treating data have been described [33] as, for instance:

1. Differential: where the baseline, G1, is subtracted from the sensor response, G2, in order to minimize the noise, δ_A, present. The relative response, Ra, is given by:

$$Ra = (G2 + \delta_A) - (G1 + \delta_A) = G2 - G1 \qquad \text{Eq. 6.1}$$

2. Relative: this method is obtained by the quotient between the sensor response and the baseline, in order to reduce the multiplicative drift, δ_M. The relative response is obtained through the follow equation:

$$Ra = \frac{G2(1+\delta_M)}{G1(1+\delta_M)} = \frac{G2}{G1} \qquad \text{Eq. 6.2}$$

3. Fractional: the relative response is calculated by the quotient between the sensor response minus the baseline, divided by the baseline. Usually, from Figure 6.3, the relative response (Ra), defined in Equation 6.3, is calculated and then used as input variable for multivariate methods.
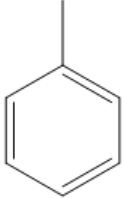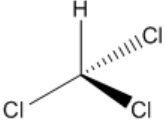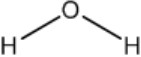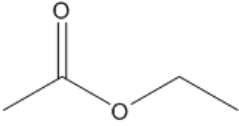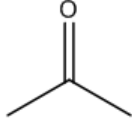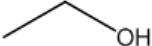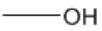
$$Ra = \frac{G2-G1}{G1} \qquad \text{Eq. 6.3}$$

In order to obtain a reliable pattern recognition it is essential to treat the data by statistical methods as, for instance, principal components analysis (PCA), discriminant function analysis (DFA), partial least squares (PLS), multiple linear regression (MLR), and cluster analysis (CA). PCA is the most commonly used method in e-nose systems, because it is simple and reduces the variables to two or three (principal components), which can be plotted as bi or three-dimensional graphs.

6.2. Results and Discussion

The electronic nose was formed by an array of four sensors (S1, S2, S3 and S4). Each sensor was formed by a distinct IJ film based on a different IL: BMIMDCA, EMIMDCA, BMPyrDCA and 1-butyl-3-methyl imidazolium bromide (BMIMBr). Each sensor individually responds to vapours and produces a distinguishable response pattern for the eight separate types of solvents tested (Table 6.1): ethyl acetate, acetone, chloroform, ethanol, hexane, methanol, toluene and water as can be seen in Figures 6.7-6.10. The changes in conductance of the sensors were monitored during fifteen reproducible cycles of exposure to the gas vapour samples inside the sample chamber (Figure 6.4), followed by exposure to atmospheric air in order to achieve the total recovery of the sensors. From Figure 6.4 we conclude that it was possible to achieve an excellent reproducibility for methanol. The same approach and the same results were verified for the others solvents.

Table 6.1 – Chemical structures of the eight solvents used in this experiment

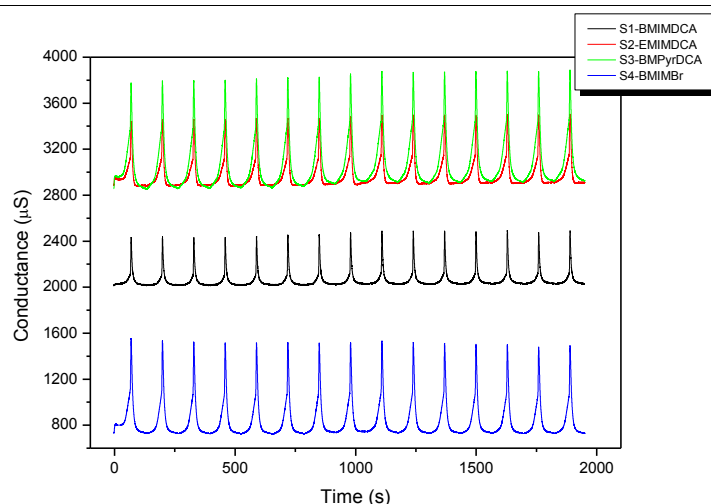| Solvent	Chemical structure
Toluene	
Chloroform	
Water	
Ethyl acetate	
Acetone	
Hexane	
Ethanol	
Methanol	

Figure 6.4 - Response of the sensors to a sequence of 15 exposures/recoveries. Exposure periods of 65 s to air saturated with methanol at 30° C and recovery periods of 65 were employed. Sensor 1 – BMIMDCA$_{IJ}$; sensor 2 - EMIMDCA$_{IJ}$; sensor 3 - BMPyrDCA$_{IJ}$ and sensor 4 – BMIMBr.

As said before, the matrix used in the present work is a conducting polymer composite. This type of sensor is usually formed by conducting particles like polypyrrole, carbon black and an insulating polymer matrix [33]. Nevertheless, our material is composed by an IL which confers conductivity to the material and gelatine which confers the dimensional stability. Depending on the IL, the response of the system is different.

Conformational changes in the polymer chains, as recently observed by means of polarization-modulation infrared reflection absorption spectroscopy (PM-IRRAS) [43], in conducting polymer gas sensors, after exposure to volatile organic compounds, may also play an important role on electrical conductivity. The choice of IJ films instead of the usual polypyrrole or carbon black is related with two main factors: the manufacture of IJ is quite easy and they are completely amorphous. This is a main advantage since, as it is known, the transport properties of polymers and composite polymers depend on the mobility. If a composite is crystalline, the mobility will decrease, since the crystalline domains are normally impermeable to vapours at room temperature and can lead to the crosslinking between the vapour molecules and the matrix.

The transducer device is composed by two parallel interdigitated electrodes, where the IJ film is deposited onto the substrate surface as shown in Figure 6.5.
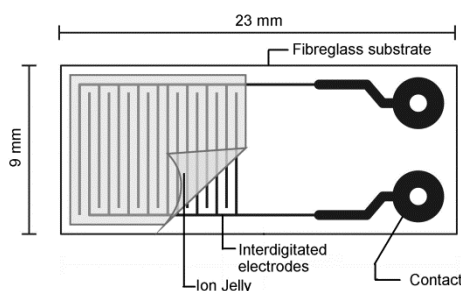
Figure 6.5 – Typical structure of a conductive polymer composite sensor.

Such sensors show conductivity changes in response to the exposure to vapours. It could be observed that they respond to a wide range of volatile compounds as shown in Figures 6.6 – 6.9.

The response time depends on the rate of diffusion of the vapour into the IJ composite polymer. As verified by George, S. C. *et al.* [44], the diffusion rate depends on many factors such as: the nature of the polymer and the gaseous material, the crosslinking between them, the concentration of the gas sample, the thickness of the polymer, the effect of fillers, plasticizers, and the temperature. As a result, the diffusion coefficient and, consequently, the conductance of the penetrating molecule depend on the rate of absorption of the vapour by the polymer. As higher the size of the molecule the lower is the diffusion coefficient. Also, compacted or elongated molecules have faster diffusion coefficients when compared with spherical-shaped molecules [44]. This explains the fact that the change in conductance achieved after exposure to toluene is much lower than after exposure to methanol.
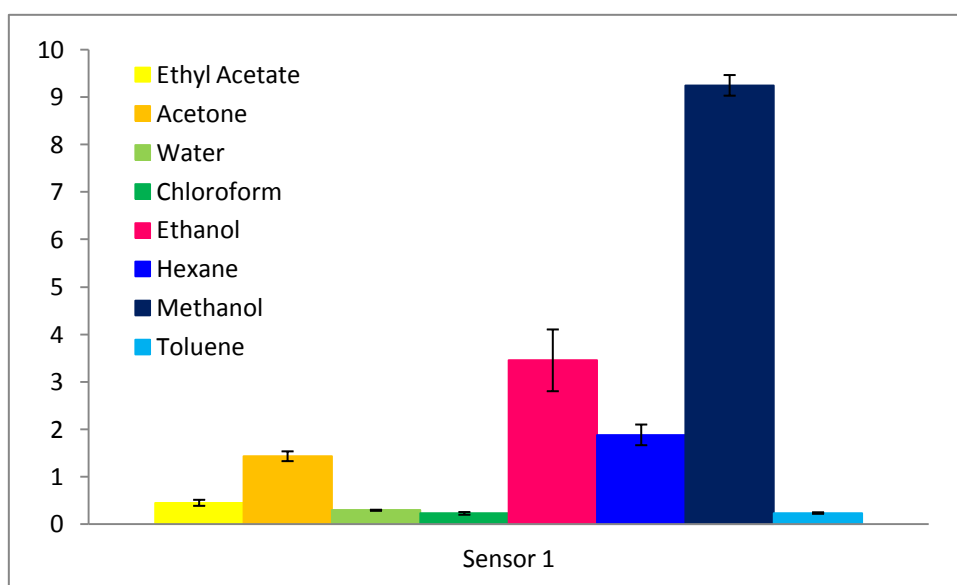
Figure 6.6 – Relative response for sensor 1: BMIMDCA$_{IJ}$.
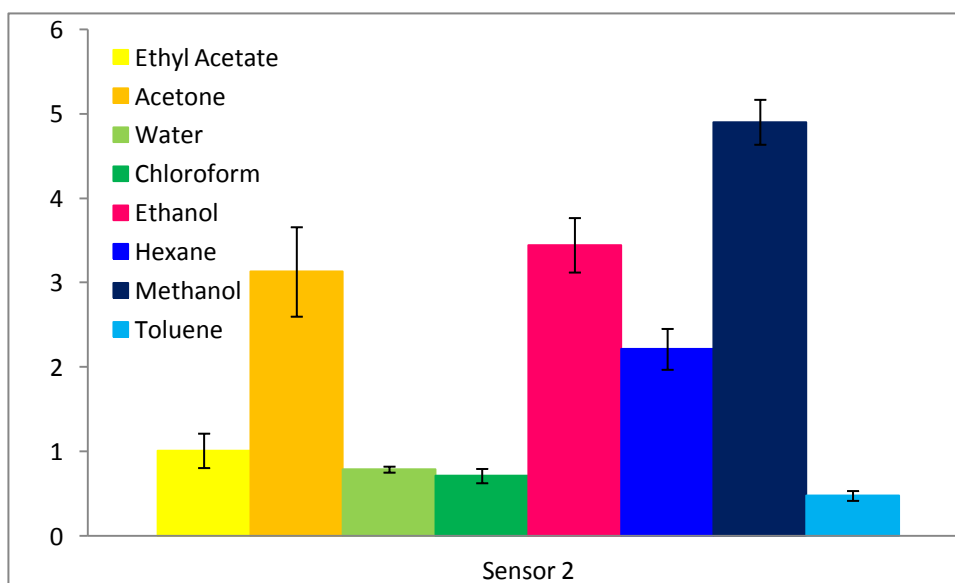
Figure 6.7 – Relative response for sensor 2: EMIMDCA$_{IJ}$.
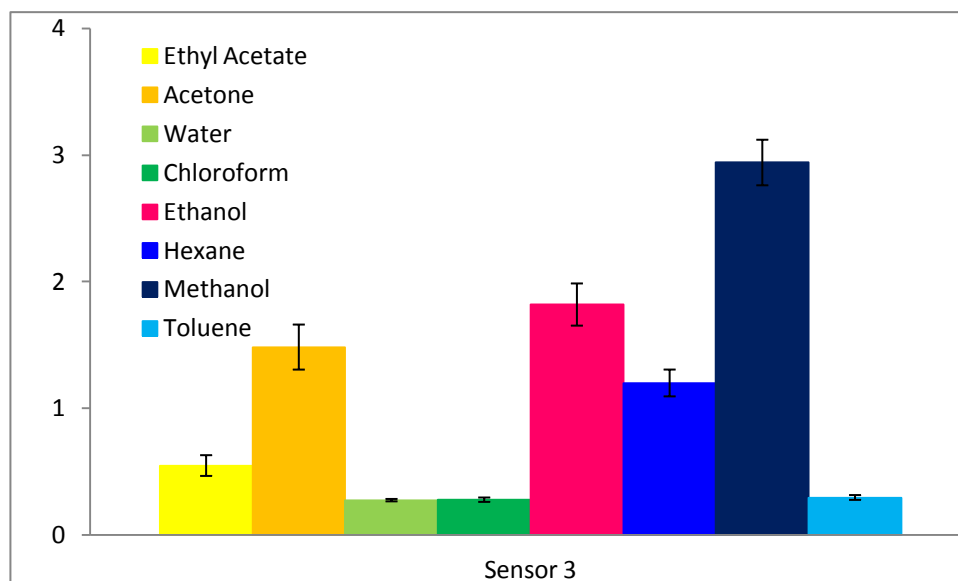
Figure 6.8 – Relative response for sensor 3: BMPyrDCA$_{IJ}$.
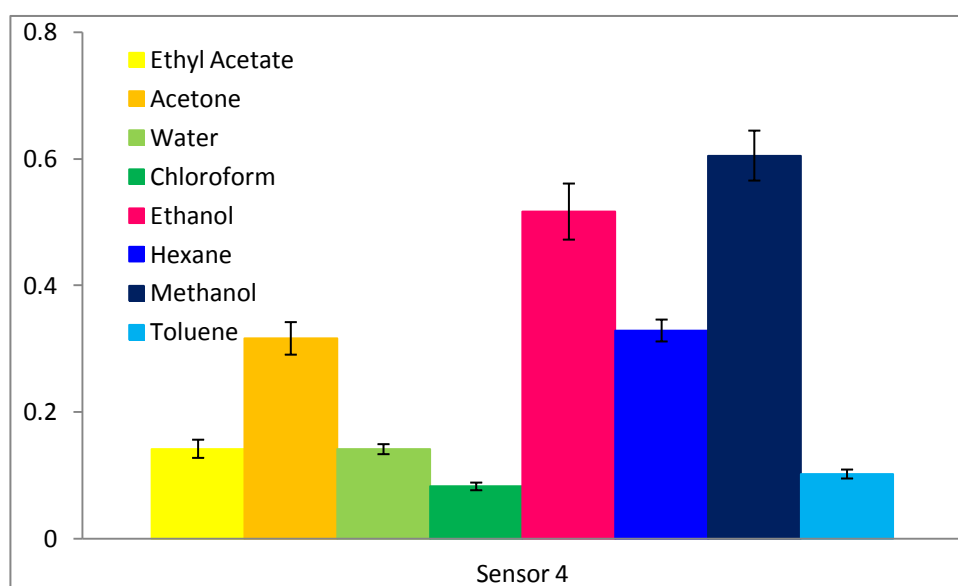
Figure 6.9 – Relative response for sensor 4: BMIMBr$_{IJ}$.

The relative responses (Ra) of the four gas sensors to the eight volatile compounds were used as input variables for a PCA. A three dimensional plot of the three first components, which accounted for 99.9 % of the variance, is shown in Figure 6.10. As can be seen, the data for each of the volatile compounds were grouped in separate clusters, indicating a perfect classification of the compounds according to their nature. Leave-one-out validation analysis gave a hit rate > 95 % for all the available data, showing the high reliability of this e-nose.
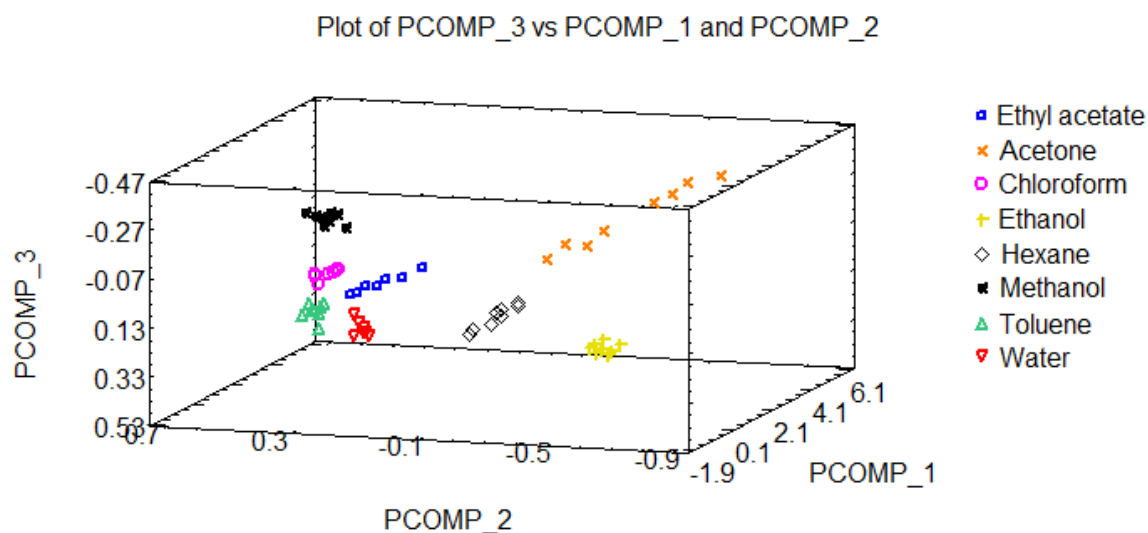
Figure 6.10 – PCA plot for the array of four IJ gas sensors.

It is worth to mention that: (a) all the IJs show a good response to the eight volatile compounds and have fast response and recovery times, i. e., all the compounds could be easily distinguished; (b) IJ films show very good repeatability after several exposures; (c) IJ films offer numerous advantages over other materials since they have high sensibility, fast response and short recovery time; (d) IJ films are inexpensive and easy to prepare; (e) the four sensors have been studied along three months and still respond perfectly well to the volatile compounds. Hence they are not disposable; (f) since these materials work at room temperature, no heater is required and hence the power consumption is low, which is interesting if portability is desired; (g) the e-nose was tested with eight different solvents (volatile compounds) of different natures (organic and inorganic, polar and non-polar) just to prove the concept, i.e. that IJs can be successfully applied to gas sensors and e-noses. Nevertheless, the system is not limited for solvent analysis but may be applied in countless other much more complex analyses as, for instance, food and beverage quality control, environmental analyses, etc.

6.3 Conclusion

Four IJs based on different ILs, BMIMDCA, EMIMDCA, BMPyrDCA and BMIMBr, were prepared and deposited onto interdigitated electrodes forming chemiresistive gas sensors. The three most sensitive sensors were grouped in an array assembling an electronic nose, which was able to detect and to perfectly classify eight distinct solvents: ethyl acetate, acetone, chloroform, ethanol, hexane, methanol, toluene and water. This is a spectacular result considering the small number of sensors and the nature of the tested volatile compounds. For instance, ethanol and methanol are very similar in their chemical structures and yet could be correctly identified. Furthermore, these IJ based sensors are very easy to prepare, fairly cheap, operate at room temperature, and show very good repeatability. They had been tested regularly during three months without any failure.

6.4. Bibliography

[1]   P. Vidinha, N. M. T. Lourenço, C. Pinheiro, A. R. Brás, T. Carvalho, T. Santos-Silva, A. Mukhopadhyay, M. J. Romão, J. Parola, M. Dionisio, J. M. S. Cabral, C. a M. Afonso, and S. Barreiros, "Ion jelly: a tailor-made conducting material for smart electrochemical devices.," *Chemical communications (Cambridge, England)*, no. 44, pp. 5842–4, Nov. 2008.

[2]   M. M. Silva, P. C. Barbosa, L. C. Rodrigues, a. Gonçalves, C. Costa, and E. Fortunato, "Gelatin in electrochromic devices," *Optical Materials*, vol. 32, no. 6, pp. 719–722, Apr. 2010.

[3]   T. L. Greaves and C. J. Drummond, "Protic ionic liquids: properties and applications.," *Chemical reviews*, vol. 108, no. 1, pp. 206–37, Jan. 2008.

[4]   L. Kulisiewicz and A. Delgado, "Network structure of gelatin gel at high pressure determined by rheological measurements," *High Pressure Research*, vol. 29, no. 1, pp. 67–71, Mar. 2009.

[5]   R. S. G. Silva and L. a. a. Pinto, "Physical Cross-linkers: Alternatives to Improve the Mechanical Properties of Fish Gelatin," *Food Engineering Reviews*, vol. 4, no. 3, pp. 165–170, Jul. 2012.

[6]   I. Kołodziejska, K. Kaczorowski, B. Piotrowska, and M. Sadowska, "Modification of the properties of gelatin from skins of Baltic cod (Gadus morhua) with transglutaminase," *Food Chemistry*, vol. 86, no. 2, pp. 203–209, Jun. 2004.

[7]   S. Keim and J. Hinrichs, "Influence of stabilizing bonds on the texture properties of high-pressure-induced whey protein gels," *International Dairy Journal*, vol. 14, no. 4, pp. 355–363, Apr. 2004.

[8]   C. Jo, H. Kang, N. Y. Lee, J. H. Kwon, and M. W. Byun, "Pectin- and gelatin-based film: effect of gamma irradiation on the mechanical properties and biodegradation," *Radiation Physics and Chemistry*, vol. 72, no. 6, pp. 745–750, Apr. 2005.

[9]   H. Y. Liu, D. Li, and S. D. Guo, "Extraction and properties of gelatin from channel catfish (Ietalurus punetaus) skin," *LWT - Food Science and Technology*, vol. 41, no. 3, pp. 414–419, Apr. 2008.

[10]   J. M. Koli, S. Basu, B. B. Nayak, N. Kannuchamy, and V. Gudipati, "Improvement of gel strength and melting point of fish gelatin by addition of coenhancers using response surface methodology.," *Journal of food science*, vol. 76, no. 6, pp. E503–9, Aug. 2011.

[11]   L. Kulisiewicz, A. Baars, and A. Delgado, "Effect of high hydrostatic pressure on structure of gelatin gels," *Bulletin of the Polish Academy of Sciences Technical Sciences*, vol. 55, no. 2, pp. 239–244, 2007.

[12]   A. Jongjareonrak, S. Rawdkuen, M. Chaijan, S. Benjakul, K. Osako, and M. Tanaka, "Chemical compositions and characterisation of skin gelatin from farmed giant catfish (Pangasianodon gigas)," *LWT - Food Science and Technology*, vol. 43, no. 1, pp. 161–165, Jan. 2010.

[13]   M. C. Gómez-Guillén, B. Guiménez, M. E. López-Caballero, and M. Montero, "Functional and bioactive properties of collagen and gelatin from alternative sources: A review," *Food Hydrocolloids*, vol. 25, pp. 1813–1827, 2011.

[14]   L. Ghasemi-mobarakeh, M. P. Prabhakaran, and M. Morshed, "Application of conductive polymers , scaffolds and electrical stimulation for nerve tissue engineering," *Journal of Tissue Engineering and Regenerative Medicine*, vol. 5, no. January, pp. E17–E35, 2011.

[15]   S. Panzavolta, M. Gioffrè, M. L. Focarete, C. Gualandi, L. Foroni, and A. Bigi, "Electrospun gelatin nanofibers: optimization of genipin cross-linking to preserve fiber morphology after exposure to water.," *Acta biomaterialia*, vol. 7, no. 4, pp. 1702–9, Apr. 2011.

[16]   S. H. Nezhadi, P. F. M. Choong, F. Lotfipour, and C. R. Dass, "Gelatin-based delivery systems for cancer gene therapy.," *Journal of drug targeting*, vol. 17, no. 10, pp. 731–8, Dec. 2009.

[17]   D. Olsen, "Recombinant collagen and gelatin for drug delivery," *Advanced Drug Delivery Reviews*, vol. 55, no. 12, pp. 1547–1567, Nov. 2003.

[18]   a Bigi, S. Panzavolta, and K. Rubini, "Relationship between triple-helix content and mechanical properties of gelatin films.," *Biomaterials*, vol. 25, no. 25, pp. 5675–80, Nov. 2004.

[19]   a. Fernicola, B. Scrosati, and H. Ohno, "Potentialities of ionic liquids as new electrolyte media in advanced electrochemical devices," *Ionics*, vol. 12, no. 2, pp. 95–102, Jun. 2006.

[20]   M. Galiński, A. Lewandowski, and I. Stępniak, "Ionic liquids as electrolytes," *Electrochimica Acta*, vol. 51, no. 26, pp. 5567–5580, Aug. 2006.

[21]   W. Lu, A. G. Fadeev, B. Qi, E. Smela, B. R. Mattes, J. Ding, G. M. Spinks, J. Mazurkiewicz, D. Zhou, G. G. Wallace, D. R. MacFarlane, S. A. Forsyth, and M. Forsyth, "Use of Ionic Liquids for π-Conjugated Polymer Electrochemical Devices.pdf," *Science*, vol. 297, no. 983, 2002.

[22]   J. W. Gardner and P. N. Bartlett, "A brief history of electronic noses," *Sensors and Actuators B*, vol. 18–19, pp. 211–220, 1994.

[23]   J. Hartman, "A possible objective method for the rapid estimation of flavors in vegetables," *Proceedings of the American Society for Horticultural Science*, vol. 64, no. DEC, pp. 335–352, 1954.

[24]   C. Wongchoosuk, M. Lutz, and T. Kerdcharoen, "Detection and classification of human body odor using an electronic nose.," *Sensors (Basel, Switzerland)*, vol. 9, no. 9, pp. 7234–49, Jan. 2009.

[25]   M. Mamat, S. A. Samad, and M. a Hannan, "An electronic nose for reliable measurement and correct classification of beverages.," *Sensors (Basel, Switzerland)*, vol. 11, no. 6, pp. 6435–53, Jan. 2011.

[26]   S. Ampuero and J. O. Bosset, "The electronic nose applied to dairy products: a review," *Sensors and Actuators B: Chemical*, vol. 94, no. 1, pp. 1–12, Aug. 2003.

[27]   R. W. C. Li, L. Ventura, J. Gruber, Y. Kawano, and L. R. F. Carvalho, "A selective conductive polymer-based sensor for volatile halogenated organic compounds (VHOC)," *Sensors and Actuators B: Chemical*, vol. 131, no. 2, pp. 646–651, May 2008.

[28]   L. O. Péres, R. W. C. Li, E. Y. Yamauchi, R. Lippi, and J. Gruber, "Conductive polymer gas sensor for quantitative detection of methanol in Brazilian sugar-cane spirit," *Food Chemistry*, vol. 130, no. 4, pp. 1105–1107, Feb. 2012.

[29]   M. Peris and L. Escuder-Gilabert, "A 21st century technique for food control: electronic noses.," *Analytica chimica acta*, vol. 638, no. 1, pp. 1–15, Apr. 2009.

[30]   J. L. Valera, B. Togores, and B. G. Cosio, "Use of the Electronic Nose for Diagnosing Respiratory Diseases," *Archivos de Bronconeumología (English Edition)*, vol. 48, no. 6, pp. 187–188, Jun. 2012.

[31]   D. James, S. M. Scott, Z. Ali, and W. T. O'Hare, "Chemical Sensors for Electronic Nose Systems," *Microchimica Acta*, vol. 149, no. 1–2, pp. 1–17, Dec. 2004.

[32]   K. Persaud and G. Dodd, "Analysis of discrimination mechanisms in the mammalian olfactory system using a model nose," *Nature*, vol. 299, pp. 352–355, 1982.

[33]   K. Arshak, E. Moore, G. M. Lyons, J. Harris, and S. Clifford, "A review of gas sensors employed in electronic nose applications," *Sensor Review*, vol. 24, no. 2, pp. 181–198, 2004.

[34]   G. Harsányi, "Tutorial Polymer films in sensor applications : a review of present uses and future possibilities Ga," *Current Applied Physics*, vol. 20, no. 2, pp. 98–105, 2000.

[35] A. Pasternak, R. Wycisk, and R. Po, "Conductive polymer materials with low filler content," *Journal of Electrostatics*, vol. 56, pp. 55–66, 2002.

[36] F. Zee and J. W. Judy, "Micromachined polymer-based chemical gas sensor array," *Sensors and Actuators B*, vol. 72, no. August 1999, pp. 120–128, 2001.

[37] J. Chen, H. Iwata, Y. Maekawa, M. Yoshida, and N. Tsubokawa, "Grafting of polyethylene by γ-radiation grafting onto conductive carbon black and application as novel gas and solute sensors," *Radiation Physics and Chemistry*, vol. 67, no. 3–4, pp. 397–401, Jun. 2003.

[38] J. Chen, H. Iwata, N. Tsubokawa, Y. Maekawa, and M. Yoshida, "Novel vapor sensor from polymer-grafted carbon black : effects of heat-treatment and g-ray radiation-treatment on the response of sensor material in cyclohexane vapor," *Polymer*, vol. 43, pp. 2201–2206, 2002.

[39] N. Ando and M. Takeuchi, "Electrical resistivity of the polymer layers with polymer grafted carbon blacks," *Thin Solid Films*, vol. 334, no. 1–2, pp. 182–186, Dec. 1998.

[40] a. . Partridge, M. . Jansen, and W. . Arnold, "Conducting polymer-based sensors," *Materials Science and Engineering: C*, vol. 12, no. 1–2, pp. 37–42, Aug. 2000.

[41] R. T. da Rocha, I. G. R. Gutz, and C. L. do Lago, "A Low-Cost and High-Performance Conductivity Meter," *Journal of Chemical Education*, vol. 74, no. 5, p. 572, May 1997.

[42] "Http://sourceforge.net/projects/dimreduction/," 2011. .

[43] L. Caseli, J. Gruber, R. W. C. Li, and L. O. Péres, "Investigation of the conformational changes of a conducting polymer in gas sensor active layers by means of polarization-modulation infrared reflection absorption spectroscopy (PM-IRRAS).," *Langmuir : the ACS journal of surfaces and colloids*, vol. 29, no. 8, pp. 2640–5, Feb. 2013.

[44] S. C. George and S. Thomas, "Transport phenomena through polymeric systems," *Progress in Polymer Science*, vol. 26, no. 6, pp. 985–1017, Aug. 2001.

Chapter 7

CONCLUSION

7. CONCLUSION

In Chapter III, the ionic conductivity of BMIMDCA with 1.9 and 6.6% of water content (w/w) and ion jellies with two different ratios of BMIMDCA/gelatin/water, IJ1 (41.1/46.7/12.2) and IJ3 (67.8/25.6/6.6) % (w/w), was characterized by using dielectric relation spectroscopy (DRS) complemented with differential scanning calorimetry and PFG NMR. Through this approach, it was possible to illustrate the impact of gelatin and water on IL physicochemical properties, which are ultimately implicated on IJ conductivity.

The calorimetric analysis revealed that all materials undergo glass transition, so they are classified as glass formers. For the ionic liquid BMIMDCA, it was observed that upon hydration, it undergoes a shift of the glass transition toward lower temperatures. The glass transition temperatures for IJs were provided for the first time. Upon dehydration, BMIMDCA undergoes cold crystallization. Contrary, both IJ1 and IJ3, no crystallization was detected under thermal cycling, which can be seen as a structural advantage of these ion jelly materials.

From dielectric data, it was possible to extract information on the transport properties since it was shown that subdiffusive dynamics govern the conductivity spectra at high frequencies. It was found that ion jelly having the higher IL/gelatin ratio (IJ3) exhibits identical conductive properties to BMIMDCA. In fact, the diffusion and mobility of ionic species are identical on IJ3 and BMIMDCA, meaning that the ionic conductivity is not significantly affected by the presence of gelatin. Nevertheless, an increase of the amount of gelatin lead to a decrease on the ion jelly conductivity showing that there is a critical ratio of IL/gelatin that leads to those properties. For bulk BMIMDCA, it was found that water increases the mobility and the diffusion coefficients, probably due to a weakening of ionic pairs interaction facilitating translational motions. Data treatment was carried out in order to deconvolute the average diffusion coefficient estimated from dielectric data in its individual contributions of cations (D_+) and anions (D_-). The D_+ values thus obtained for $BMIM^+$ and IJ3 with the same water content (6.6% w/w) revealed mainly for the latter excellent agreement with direct measurements from PFG NMR, obeying the same VFT equation.

A non-Arrhenius temperature dependence of the dc conductivity was observed that its originated by a VFT dependence of mobility in all systems. The VFT dependence of both conductivity and relaxation processes associated with dipolar reorientation, together with low values of decoupling indexes, point to a correlation between the charge transport mechanism and the cooperative motion behind the process associated with the dynamical glass transition.

A multimodal nature was found in the dynamic behavior as probed by DRS due to simultaneous contributions of dipolar reorientations and interfacial and electrode polarizations. The slowest process was found to be compatible with the electrode polarization process, while the one located at higher frequencies was found to be compatible with the relaxation associated with the dynamic glass transition. From the temperature dependence of relaxation times of the latter process, the glass transition temperatures were estimated in very good agreement with calorimetric data.

The ion jelly derived material with the higher amount of ionic liquid (IJ3) has a glass transition temperature (measured in the first heating run) not far from that of BMIMDCA with 1.9 or 6.6% water,

but closer to the less hydrated. Advantageously, both ion jellies did not undergo further crystallization after water removal contrary to which is observed for BMIMDCA with either 1.9 or 6.6% water content. The ion jelly with the lower IL content, although having the highest water amount (12%), presents the higher glass transition temperature, probably due to the high gelatin:BMIMDCA ratio.

It was previously found that IJs based on ILs that contain dicyanamide (DCA) anion have led to stable and transparent materials. Therefore, in chapter IV, the impact of different cations on the physico-chemical properties of DCA based ionic liquids and respective IJs were evaluated by DRS, DSC and PFG-NMR. BPyDCA, BMPyrDCA and EMIMDCA besides BMIMDCA were studied with 0.4% and 9% w/w water contents: the respective IJs with 9% of water were also investigated. As found previously for BMIMDCA, it was observed that the glass transition temperature decreases with the increase of water content. Crystallization was observed for BMIMDCA, BMPyrDCA and EMIMDCA with negligible water content; it was shown how DRS is a suitable tool to monitor crystallization through the σ' trace. Once more no crystallization was detected for any of the ion jelly materials upon thermal cycling. The real conductivity, σ', was measured for all systems. A correlation between the establishment of a plateau in the frequency dependence due to long-range motion of charge carriers (diffusive regime) and the onset of structural relaxation which is in the origin of the glass transition seems to exist. At the lowest frequencies of the conductivity spectra, electrode polarization highly dominates, but the remaining spectral response was able to be simulated by a Jonscher equation allowing deriving transport properties as mobility and diffusion coefficients. Data treatment was carried out as done in chapter III for the estimate of diffusion coefficients that, for all materials, showed a close agreement with PFG NMR data, following the same VFT equation.

The influence of water on the ILs was studied in more detail in chapter V for BMIMDCA, EMIMDCA, BMPyrDCA and EMIMSO$_4$ where IL/water mixtures were prepared with different hydration levels (0.4%, 9%, 12% and 30% w/w). A distinct behavior was observed for the BMPyrDCA with 30% water, that didn't exhibit the usual conductivity vs frequency profile observed for a variety of disordered conductive systems. This allowed analyzing the reorientational polarization by the complex permittivity and electric modulus representation, from which three different processes were identified: a secondary relaxation with Arrhenian temperature dependence, and two other processes whose temperature dependence obeys to a VFT law. The agreement between the temperature found by extrapolating the VFT equation to to τ=100 s with the glass transition temperature calorimetrically determined, seem to confirm that one of these VFT processes, the one located at the lowest temperatures, is consistent with the attribution to the process whose mobility is behind the dynamic glass transition; the high-T VFT process is originated by the mobility of charge carriers. Both evolve more or less in parallel in the relaxation map indicating, once again, a correlation between the two mechanisms.

For the e-nose measurements, in chapter VI it were prepared four IJs based on gelatin and different ILs: BMIMDCA, EMIMDCA, BMPyrDCA and BMIMBr, and deposited onto interdigitated electrodes forming chemiresistive gas sensors. These were grouped in an array assembling an electronic nose, which was able to detect and to perfectly classify eight distinct solvents: ethyl acetate, acetone, chloroform, ethanol, hexane, methanol, toluene and water. This is an interesting result considering the small number of sensors and the nature of the tested volatile compounds. For

instance, ethanol and methanol are very similar in their chemical structures and yet could be correctly identified. Furthermore, these IJ based sensors are very easy to prepare, fairly cheap, operate at room temperature, and show very good repeatability. They had been tested regularly during three months without any failure.

Lastly, with the obtained results, it was shown that ion jelly could be in fact a very promising solution to design novel electrolytes for different electrochemical devices, being much more stable relative to the bulk ionic liquids concerning electrical anomalies that manifest mainly for the IL at high frequencies, attaining conductivities that are comparable to the ionic liquids from which they derive with the advantage of being self-supported materials.